Numerical and experimental optimization of peak power reduction control strategies

Nikolaos Stathopoulos

▶ **To cite this version:**

Nikolaos Stathopoulos. Numerical and experimental optimization of peak power reduction control strategies. Thermics [physics.class-ph]. École Nationale des Travaux Publics de l'État [ENTPE], 2015. English. NNT : 2015ENTP0001 . tel-01559651

HAL Id: tel-01559651

https://theses.hal.science/tel-01559651v1

Submitted on 10 Jul 2017

HAL is a multi-disciplinary open access archive for the deposit and dissemination of scientific research documents, whether they are published or not. The documents may come from teaching and research institutions in France or abroad, or from public or private research centers.

L'archive ouverte pluridisciplinaire **HAL**, est destinée au dépôt et à la diffusion de documents scientifiques de niveau recherche, publiés ou non, émanant des établissements d'enseignement et de recherche français ou étrangers, des laboratoires publics ou privés.

N° d'ordre *2015-ENTP-0001* Année 2015

THÈSE

pour l'obtention du grade de

Docteur de l'Ecole Nationale des Travaux Publics de l'Etat

Université de Lyon

Ecole doctorale : MEGA (Mécanique, Energétique, Génie Civil, Acoustique)
Spécialité : Génie Civil
Préparée au Laboratoire Génie Civil et Bâtiment (LTDS/UMR 5513)

Présentée et soutenue publiquement par

Nikolaos STATHOPOULOS

Optimisation numérique et expérimentale de stratégies d'effacement énergétique

Soutenue le *27/02/2015* devant le jury composé de :

M. EL MANKIBI	HDR	Directeur de thèse
H. EL QARNIA	Professeur	Examinateur
G. FRAISSE	Professeur	Rapporteur
C. GHIAUS	Professeur	Examinateur
F. HAGHIGHAT	Professeur	Rapporteur
P. MICHEL	HDR	Co-directeur de thèse

Abstract

Numerical and experimental optimization of peak power reduction control strategies
Nikolaos Stathopoulos, 2015

Keywords:
Building, Energy, Peak power reduction, Control strategies, Phase Change Materials, Thermal Storage, Heat exchanger, Thermal Simulation, Thermal Comfort, Indoor Air Quality

Considering the current French energy context, two major challenges are emerging. In the short term, significant peak power consumption has been observed in the past few years during the winter season. These peaks are strongly linked to electrical space heating and have important economic, environmental and social implications. In the long term, ambitious environmental goals have been set at national and European levels, requiring thermal storage technology and efficient management of the built environment. As part of the solution, Phase Change Materials (PCM) and heat exchanger applications offer promising results through thermal storage and load shifting techniques.

Within this framework, the objective of this thesis is to develop load shifting solutions which also take into account the thermal comfort of the occupants and the indoor air quality. To achieve this, two tools were necessary: an experimental heat exchanger unit (prototype) and a numerical model that accurately simulates its behavior.

The exchanger contains macroencapsumated PCM (paraffin) and is conceived in a way that facilitates its integration in a ventilation system. It is aimed to shift space heating electrical consumption from peak to off-peak period. The unit was experimentally characterized, using an important amount of sensors through full thermal cycles (charging and discharging) and was coupled to an experimental test cell, which led to the testing of preliminary control strategies.

The numerical model is based on the heat balance approach and the apparent heat capacity method, using finite differences for differential equation solution under Matlab/Simulink environment. After validation with experimental data, the model was used to optimize the performance of the exchanger. Several parameters were investigated, including heat exchanger dimensions, PCM quantity and properties, seeking the configuration with the optimal compromise between stored heat and the time needed for the charging / discharging process.

The numerical model was coupled to a building simulation model and an 80m2 dwelling was conceived for control strategies implementation and evaluation, by investigating different scenarios over a one-month winter period. The scenarios vary with increasing complexity, first considering load shifting and thermal comfort, then adding the final price of electricity consumption and finally taking into account the indoor air quality with the presence of a four-person family.

This study has been conducted within the framework of a project funded by the French National Research Agency (Stock-Air: ANR-Stock-E) and was also financially supported by the French Ministry of Sustainable Development.

Résumé

Optimisation numérique et expérimentale de stratégies d'effacement énergétique
Nikolaos Stathopoulos, 2015

Mots clés:

Bâtiment, Energie, Effacement énergétique, Stratégies de contrôle, Matériaux à changement de phase, Stockage thermique, Échangeur Thermique, Simulation thermique, Confort thermique, Qualité de l'air intérieur

Dans le contexte énergétique français actuel, deux principaux enjeux émergent. À court terme, des pointes de consommation électrique croissantes sont observées les dernières années pendant la période hivernale. Ces pointes sont fortement liées au chauffage électrique et ont des conséquences économiques, environnementales et sociales importantes. Dans un long terme, des objectifs environnementaux ambitieux ont été fixés au niveau national et européen, nécessitant la technologie de stockage thermique et une gestion efficace de l'environnement bâti. Les Matériaux à Changement de Phase (MCP) ainsi que les dispositifs de type échangeurs thermiques offrent des résultats promettant grâce au stockage thermique et le déplacement des consommations.

Dans ce cadre, l'objectif de cette thèse est de développer des solutions de déplacement des consommations énergétiques qui prennent en compte le confort thermique des occupants et la qualité de l'air intérieur. Pour ce faire, deux outils sont nécessaires: un échangeur thermique expérimental (prototype) et un modèle numérique capable de simuler son comportement.

L'échangeur contient du MCP macroencapsulé (paraffine) et est conçu de manière à faciliter son intégration dans un système de ventilation. Il a comme but de décaler la consommation due au chauffage électrique vers la période hors pointe. Le dispositif a été caractérisé expérimentalement lors des cycles thermiques complets (charge et décharge) en utilisant une quantité importante de capteurs. Il a ensuite été couplé à une cellule expérimentale, afin de tester des stratégies de contrôle préliminaires.

Le modèle numérique est basé sur la discrétisation spatiale et l'établissement du bilan de chaleur des couches considérées, la méthode de la capacité thermique apparente, ainsi que l'utilisation des différences finies. Après validation à l'aide des données expérimentales, le modèle a été utilisé pour optimiser la performance de l'échangeur. Plusieurs paramètres ont été étudiés, y compris les dimensions de l'échangeur, la quantité et les propriétés du MCP, en cherchant la configuration avec le compromis optimal entre la chaleur emmagasinée et le temps nécessaire pour la charge et la décharge.

Le modèle numérique a été couplé à un modèle de simulation du bâtiment et un logement de 80m2 a été conçu pour la mise en œuvre et l'évaluation des stratégies de contrôle, en investiguant différents scénarios sur une période hivernal d'un mois. Les scénarios varient avec une complexité croissante, d'abord en considérant l'effacement énergétique et le confort thermique, ensuite en ajoutant le prix final de la consommation électrique et enfin en prenant compte la qualité de l'air intérieur avec la présence d'une famille de quatre personnes.

Cette étude a été menée dans le cadre d'un projet financé par l'Agence National de la Recherche (Stock-Air: ANR-Stock-E) et a également été soutenu par le ministère de l'Ecologie, du Développement durable et de l'Energie.

Acknowledgments

First, I would like to thank M. El Mankibi for his patient and constant guidance during the last three years and for providing a healthy environment for the accomplishment of this PhD dissertation. I would also like to thank M. Michel for the same reasons. Special thanks to Riccardo Issoglio for his great help and advice on all aspects of the experimental part of the study. I acknowledge the financial support from the French National Research Agency (ANR) and the fruitful collaboration with the members of the research project Stock Air.

I am also grateful to Professors Haghighat and Fraisse for accepting to examine this work and participate in the defense jury. My sincere gratitude also goes to Professors El Qarnia and Ghiaus for their willingness to participate in the jury.

Special credits to Henri Odin for his numerous corrections and advice on the proper English writing of this manuscript.

Thanks are also due to all members of the LGCB laboratory for their support and all the joyous moments I spent around them.

My heartfelt gratitude goes to my father, mother and sister for providing me with excellent education conditions and supporting my choices throughout my life. Without them I would not have come so far.

Lastly, I would like to thank my friends in Athens, Lyon and wherever they may now be living for always being there for me, for their constant positive influence and advice and making the world go round.

Contents

List of figures

List of tables

List of symbols

Upper case

C_p	Specific heat capacity [J/(kg·K)]
E	Energy [J]
H	Enthalpy [J/kg]
R	Thermal resistance [(m²K)/W]
L	Latent heat of fusion (J/kg)
P	Power [W]
P_{atm}	Standard atmospheric pressure [Pa]
P_{sat}	Saturation pressure [Pa]
Q	Heat [J]
S	Surface [m²]
T	Temperature [°C, K]
$\overline{T}$	Average temperature [°C, K]
V	Volume [m³]

Lower case

dx	Length of node [m]
dy	Thickness of node [m]
dz	Height of node [m]
h	Convection coefficient [W/m²·K]
m	Mass [kg]
$\dot{m}$	Airflow rate [kg/s, $m^3.h^{-1}$]
p_s	Static pressure
p_t	Stagnation pressure
t	Time [s]
w	Mixture ratio of water vapor mass and dry air mass

Greek symbols

ε	Efficiency [%]
λ	Thermal conductivity [W/(m·K)]
ρ	Density [kg/m³]
ϕ	Relative humidity [%]

Subscripts

Air, a	Related to air / position in the air stream
Inlet/in	Heat exchanger inlet point

Outlet/out	Heat exchanger outlet point
app	Refers to apparent
exp	Refers to experimental
i	Node position lengthwise
j	Node position crosswise
l	Referring to liquid PCM
m	Referring to PCM layer
n	Total number of nodes lengthwise
p	Referring to aluminum layer
q	Total number of PCM nodes crosswise
s	Referring to solid PCM
sim	Refers to simulation

Acronyms

ADEME	French Environment and Energy Management Agency
ANR	French National Research Agency
CHS	Chemical heat storage
COP	Coefficient of performance
DSC	Differential Scanning Calorimetry
EDF	Electricity of France
EES	Electrical energy storage
ES	Energy storage
EU	European Union
GHG	Greenhouse gas
HVAC	Heating, ventilation and air conditioning
IEA	International Energy Agency
INSEE	French National Institute of Statistics and Economic Studies
LHS	Latent heat storage
MEDDE	French Ministry of Sustainable Development
PCM	Phase change material
PEB	Positive energy building
RT	Thermal regulation Act
RTE	French Electricity Transport Network
SHS	Sensible heat storage
TES	Thermal energy storage
UN	United Nations

General introduction

General introduction

Context

Human-induced global warming, fossil resources rarefaction, oil price shocks, increase in world and urban population constitute an alarming list of issues which require serious debates, rigorous decision making and innovative solutions. Several agreements and policies have already been put into practice at the international and national levels and further initiatives are being prepared for the future, reflecting the rising world concern and the need for action.

Regarding these considerations, the building sector plays a key role, as it is one of the major contributors worldwide concerning energy consumption and greenhouse gas emissions. In view of these facts, European and French policies are considering imposing zero or even positive energy buildings regulations in the near future. Two main problems have to be dealt with regarding those goals: renewable energy intermittence and daily or seasonal variations of energy consumption. A significant amount of research has been performed concerning Energy Storage, proving that this field can provide pertinent applications as an answer to these drawbacks.

In general, France faces the above stated challenges but it also presents a specific particularity: high peak power demands. These peaks are mostly encountered during the late afternoon winter period and are closely related to electrical heating. A project was formulated under the aegis and founding of the French National Research Agency aiming at developing and controlling an active PCM-Air heat exchanger coupled to a heat pump, as a technical solution to the augmented electricity demand during the 18:00-20:00 time slot. The project partners include four research units (LGCB, CETHIL, ARMINES – CEP and EDF R&D) and an industrial one (RIBO).

Objectives and approach

It is within this context that the here presented PhD thesis seeks to investigate the potential of a PCM-Air heat exchanger and proposes control strategies that will perform the needed shift in electrical consumption without degrading thermal comfort and indoor air quality.

The general idea is to develop a heat exchanger unit integrated in a ventilation system, in which a sufficient amount of heat will be stored in order to substitute the use of electrical heating during the peak power demand period. Three major objectives were identified:

- The development of experimental and numerical tools that will enable the elaboration, testing and evaluation of the control strategies;
- The optimization of the heat exchanger's performance;
- The elaboration of load shifting control strategies for different scenarios.

The approach that was followed in order to achieve these goals is a retroactive process based on two tools: an experimental and a numerical one (figure A.1). A PCM-Air heat exchanger was designed, constructed, instrumented, characterized and coupled to an experimental test cell. In parallel, a numerical model was developed using the apparent heat capacity approach and the finite difference method. After calibration and validation with the use of experimental data were conducted, the model

was coupled to a building model. An optimization study was performed focusing on the geometry of the exchanger and the PCM properties in order to obtain faster charging/discharging periods with minimum effect on the stored energy. Finally, the optimized version of the exchanger was used for the elaboration of control strategies.

Chapter contents

The thesis is divided into 5 chapters, presenting the various elements that had to be linked together in order to achieve the established goals.

The first chapter briefly presents the energy and built environment context in an International, European Union and French level. Special focus is given on the French peak power demand issue and its strong association with electrical heating. The implications of the peak power demand are discussed, along with existing load shifting management methods and technologies.

The first part of the second chapter deals with energy storage, presenting different methods through which it can be achieved. It focuses on thermal energy storage processes and targets phase change materials by demonstrating existing applications in buildings, enhancement techniques as well as limitations and barriers to their use. The second part of the chapter describes the main elements, operation principles and design philosophy and methods of active latent heat storage units. Finally, existing applications and studies are discussed.

The third chapter presents the experimental part of the study. The assembly procedure of the experimental platform is demonstrated and all the important choices concerning design are explained including PCM, geometry, instrumentation and data acquisition. In a second phase, characterization results are presented, as well as the coupling with an officelike experimental cell and a preliminary control strategy.

The fourth chapter presents the elaborated numerical model that is used to simulate the heat exchanger's behavior. Experimental results are used for the model's calibration and validation; following that, the model is coupled to an existing building simulation model.

Chapter five presents the optimization study of the heat exchanger, performed through the numerical model. Several parameters are investigated (geometry, PCM properties) in order to obtain an ameliorated performance of the heat exchanger in terms of minimum charging time and augmented power. The optimized versions of the exchanger are then used in realistic scenarios in order to achieve load shifting while maintaining acceptable indoor thermal comfort and air quality conditions.

Finally, the last section of this thesis presents the conclusions of the study and discusses the perspectives that can be tackled in the future.

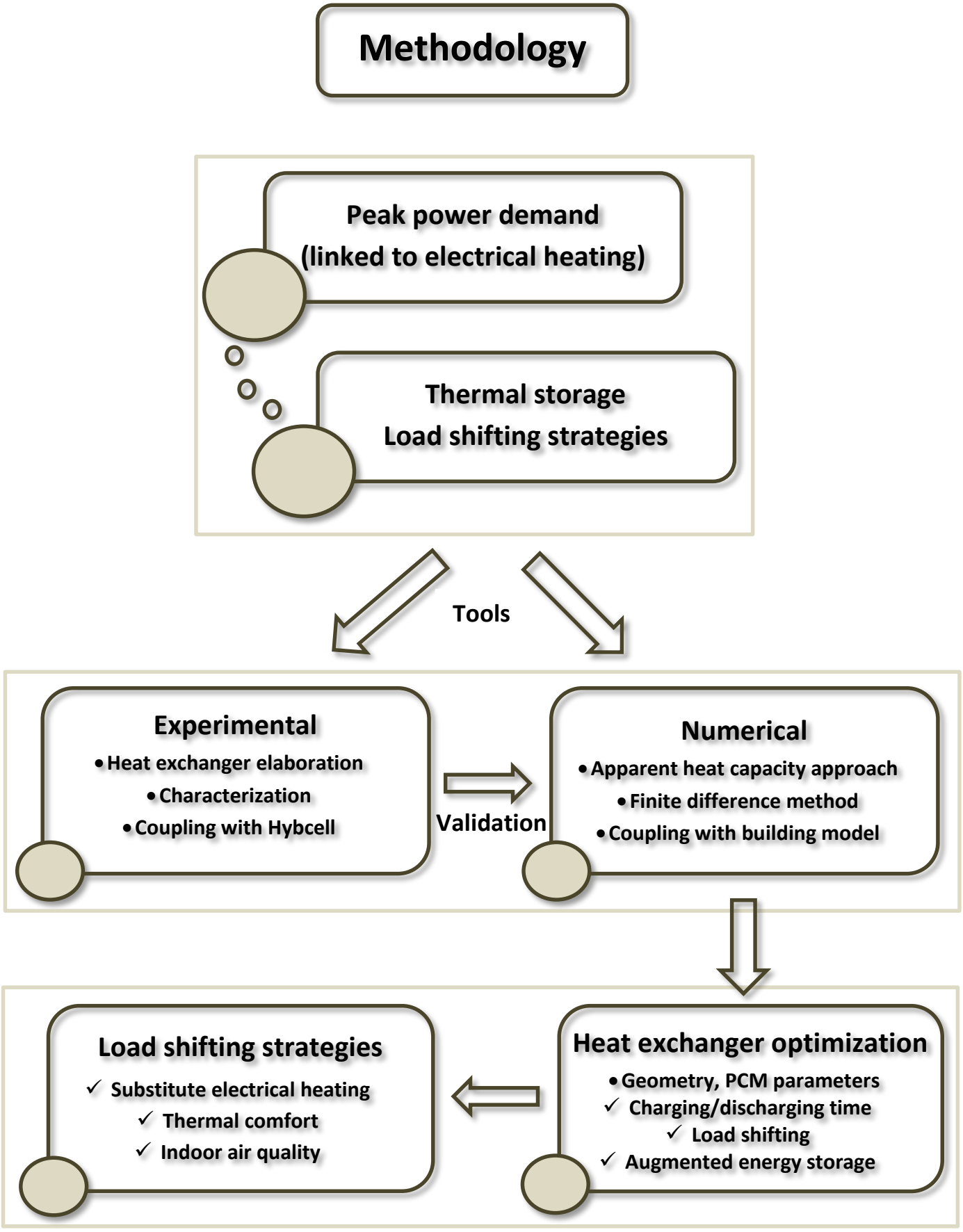

Figure A.1: The methodology followed along this thesis

Chapter 1

Energy context and built environment

Chapter 1 : Energy context and built environment

1.1 Introduction

For almost half a century energy-related issues have gained increasing concern within societies all over the world due to their significant economic and environmental importance. Starting from the oil price shocks in the 70s and until the current awareness about global warming, energy production and management is now a prominent subject in international, national and local debates and policies.

This chapter starts by presenting important international, EU and French policies that reflect the global climate change awareness and sets a significant number of goals for the near and far future. Special focus is then given to the French context and more specifically to the influence of the built environment in energy consumption and greenhouse gas emissions. The considerable share of electrical heating in augmented peak power demand is demonstrated using statistics and figures. Finally, the implications of elevated electricity demand are debated and existing load shifting methods are mentioned as an introduction to energy storage.

Overall, this chapter aims to pass from global energy concerns to the French energy context and the electrical heating-related peak power demand in order to clearly state the problem in question and underline the necessity for efficient solutions.

1.2 At the international and EU levels

Several agreements have been signed between countries worldwide, aiming to reduce energy consumption and greenhouse gases (GHG) emissions. The cornerstone of these efforts was the Kyoto Protocol (United Nations, 1998), an international agreement under the United Nations Framework Convention on Climate Change which sets emissions reduction targets to its participating parties.

Concerning the European Union, the 'Climate and Energy Package' (European Commission, 2008) was adopted in December 2008, focusing on emissions cuts, renewable energy production increase and energy efficiency. The Package sets three key objectives (known as the '20-20-20' targets) for 2020: 20% reductions of GHG emissions comparing to 1990 levels, 20% energy consumption from renewable resources and a 20% improvement in energy efficiency. Before that, the Energy Performance of Buildings Directive (European Commission, 2002) implemented enhanced building regulations and introduced energy certification schemes for buildings in all EU countries. Furthermore, the Communication 'Energy Roadmap 2050' (European Commission, 2011) was adopted in 2011, showing the EU's commitment to reducing GHG emissions to 80-95% below 1990 levels by 2050.

The above agreements and legislations demonstrate the increasing concern for environment friendly policies as well as the demand for more efficient ways of energy utilization.

Built environment: a big energy consumer

One of the most influencing factors when it comes to the energy domain is the built environment: according to the International Energy Agency buildings represent about 40% of primary energy consumption among its 29 member countries. Furthermore, it is estimated (UNEP SBCI, 2009) that

buildings contribute up to 33% of the global GHG emissions, mostly due to fossil fuels utilization during the operational phase. These numbers clearly demonstrate the significant environmental impact of buildings and the key role they can play in reducing energy consumption and GHG emissions.

1.3 At the French level

1.3.1 Energy context and policies

Until 1973, oil constituted the main means of energy production in France, in order to support the industrial development and the declining use of coal. Between that year and the late '80s, the oil price chocks led to a better control of energy consumption and oriented its production to other sources. First the nuclear sector became the dominant producer –it is still so nowadays. An increase of renewable sources production could be observed after the '90s, mostly from hydraulic energy but also from photovoltaic and wind energy (INSEE, 2012). The annual global electricity consumption has tended to stabilize since the '00s, presenting, however, increasing peak power demands, mainly during the winter period. A significant dependence on temperature variation is also observed during winter, mainly due to electrical heating (RTE, 2012a, 2013).

The Kyoto Protocol was implemented through the 'Climate Plan 2004-2012' (MEDDE, 2006) aiming at a 10% reduction of CO_2 emission as well as aiming to raise awareness within society and among public and private actors etc. It was reinforced by the commitments established by the First and Second Grenelle Acts (MEDDE, 2009, 2012) following the 'Grenelle de l'environnement' debate, a multi-party debate launched in 2007. The main commitments include the generalization of standards of low consumption in new housing and public buildings, the renovation of housing and building heating, transportation measures favoring low polluting means, the development of renewable energy, as well as other actions in the health, agricultural and biodiversity domains.

As far as the building sector is concerned, several Thermal Regulations acts have been voted (1974, 1988, 2000, 2005, and 2012), with an increasing interest observed in the last 15 years. They aim to set upper limits on the energy consumption of new buildings for heating, ventilation and air conditioning (HVAC), lighting and hot water consumption and to promulgate the renovation of existing residential and tertiary buildings, with a 38% reduction goal in the consumption of the existing park.

It is worth noting that the new Thermal Regulation Act (RT 2020, currently under discussion) will introduce the concept of positive energy buildings (PEB). It will aim to divide energy consumptions by four and oblige all new buildings to achieve PEB standards.

1.3.2 Built environment and energy consumption

The built environment and energy consumption in France is not an exception compared to the European and international situation, as this sector represents a significant part of energy utilization and GHG emissions (ADEME, 2013, a, b). More specifically, the housing and tertiary sector is to account for 44% of the final energy consumption (figure 1.1), 20% of GHG and 22% of CO_2 emissions (figure 1.2).

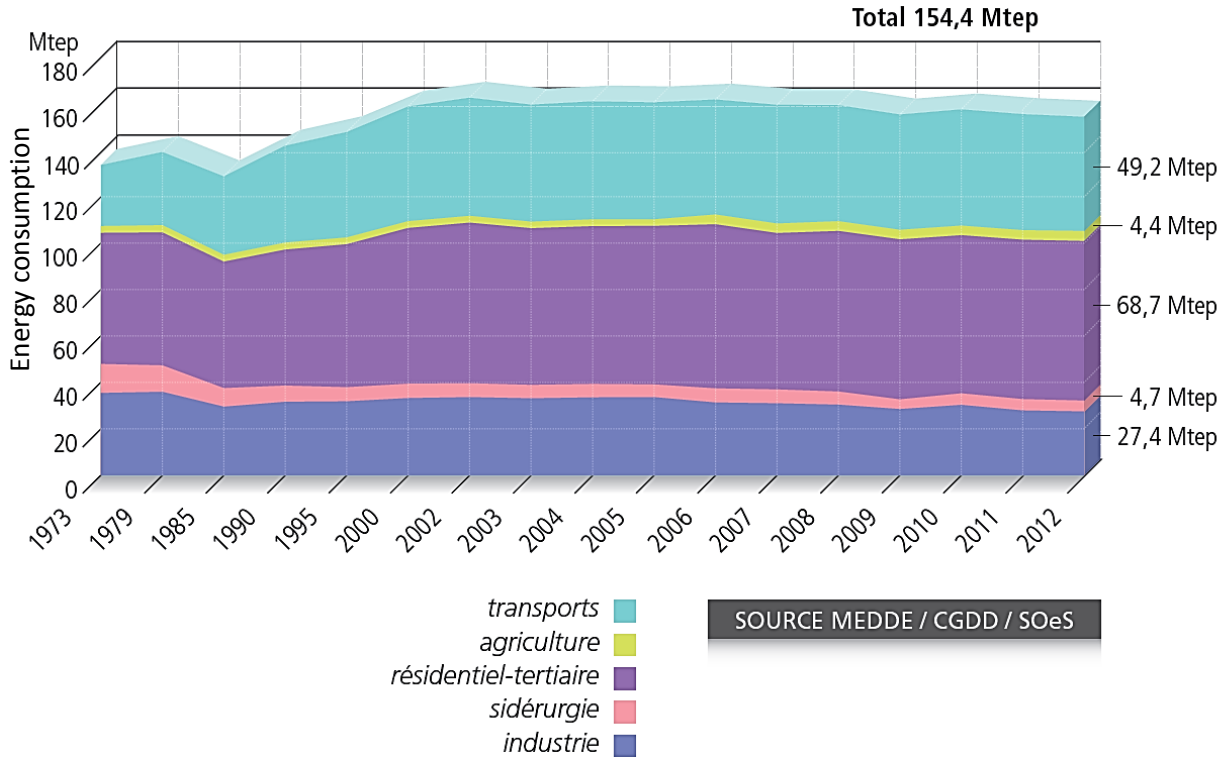

Figure 1.1: Evolution of energy consumption per sector

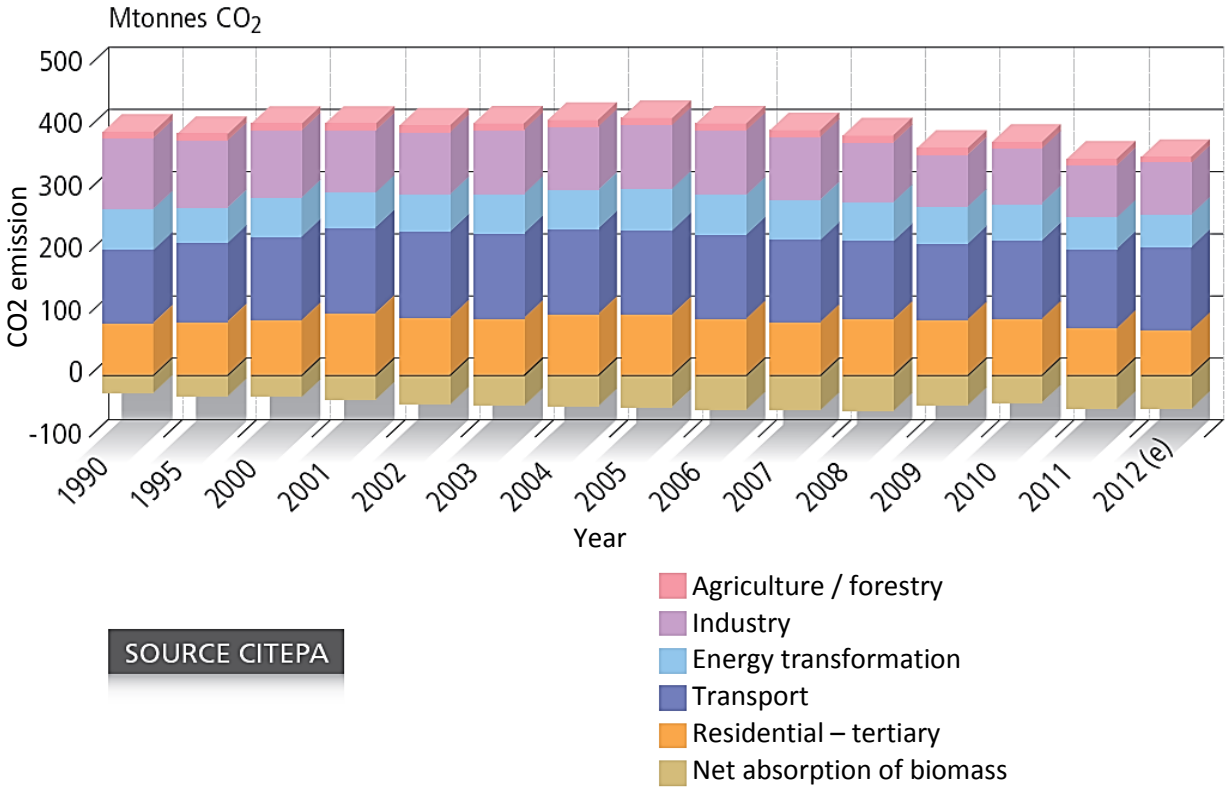

Figure 1.2: Evolution of CO_2 emission per sector

Electricity is the main energy source of French buildings representing 37% of final consumption, followed by gas (32%), oil (16%), renewable/waste (15%) and coal (0,4%) (figure 1.3). It presents a 15% increase since 1973 and along with renewable sources and gas it has contributed to the decrease of coal and oil consumption.

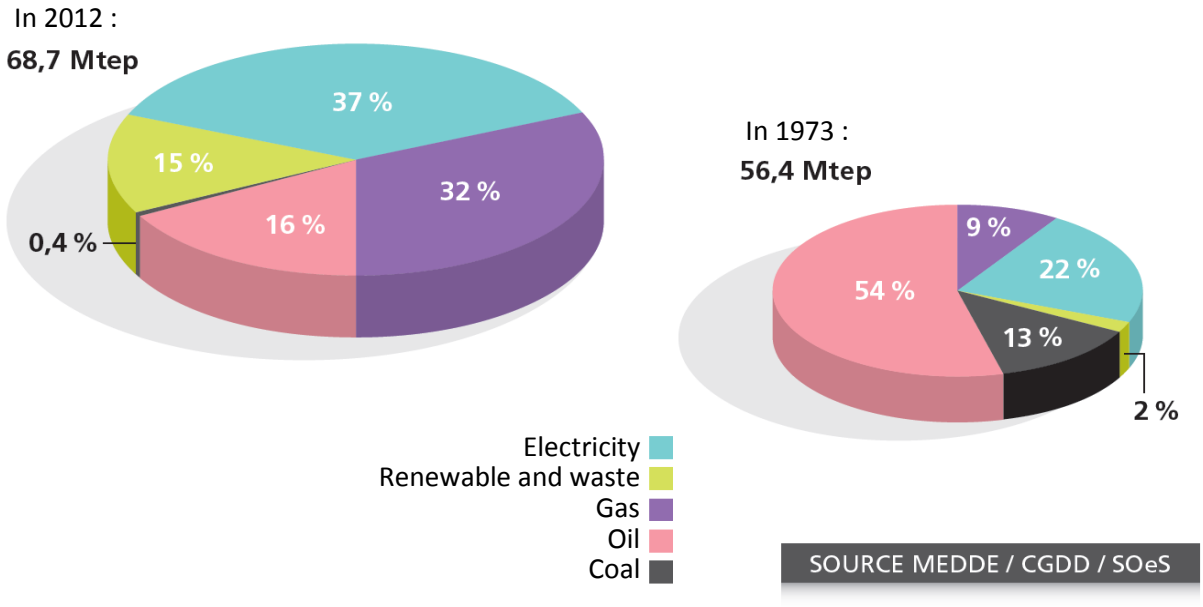

Figure 1.3: Final consumption of the residential/tertiary sector

Furthermore, final electricity consumption in buildings has been increasing with an annual rate of 8% over the past 30 years (figure 1.4, MEDDTL, 2010). This can be explained by the population growth and the subsequent increase of the building stock (+41% of houses in 30 years), the increase of the mean housing surface, the augmented comfort expectations and the apparition of new needs linked to technology advancements. These factors have contributed to a significant increase of electricity consumption for HVAC, household/office appliances, lighting, etc.

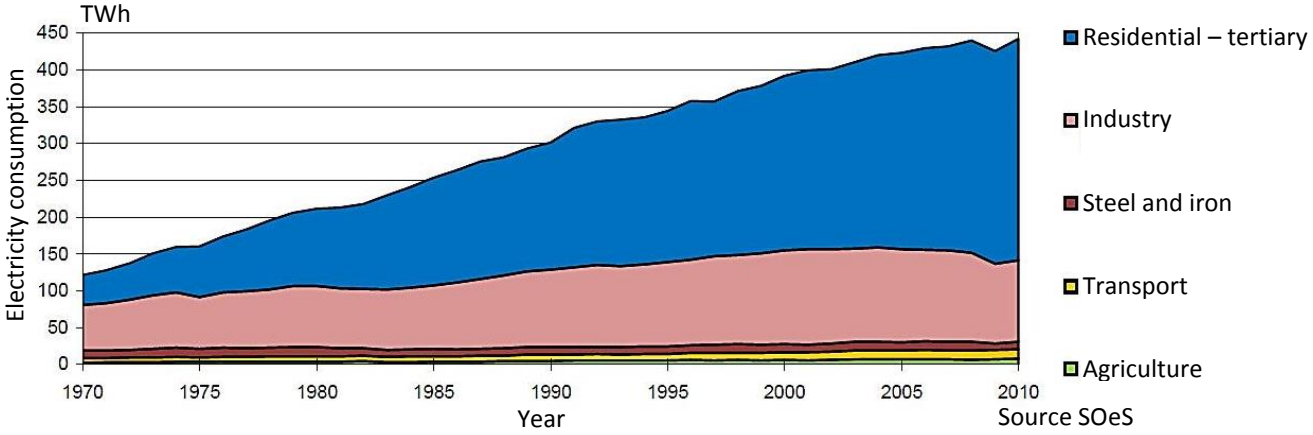

Figure 1.4: Evolution of final electricity consumption per sector

Apart from the performance of the building itself, one also has to consider the related energy and environmental impact on the construction sector (concrete, wood, steel and other components) and on management policies (access to energy sources and networks, transport connection, etc).

1.3.3 Electrical heating

1.3.3.1 Residential sector

In 2012, the residential sector has risen to 33,4 million houses, out of which 27,8 million are main residences. Since 1973, the average unitary consumption (including wood) has shown a significant reduction of 58%, which can be attributed to renovation, new thermal policies and a more energy efficient behavior among occupants (ADEME, 2013, a). Electricity and gas are the two main energy sources of the residential sector. Figure 1.5 illustrates the energy distribution in this sector: almost 2/3 of energy consumption is employed for heating needs, followed by specific usage (PC, drying, TV and other appliances) (19,5%), hot water (12,1%) and cooking (7%).

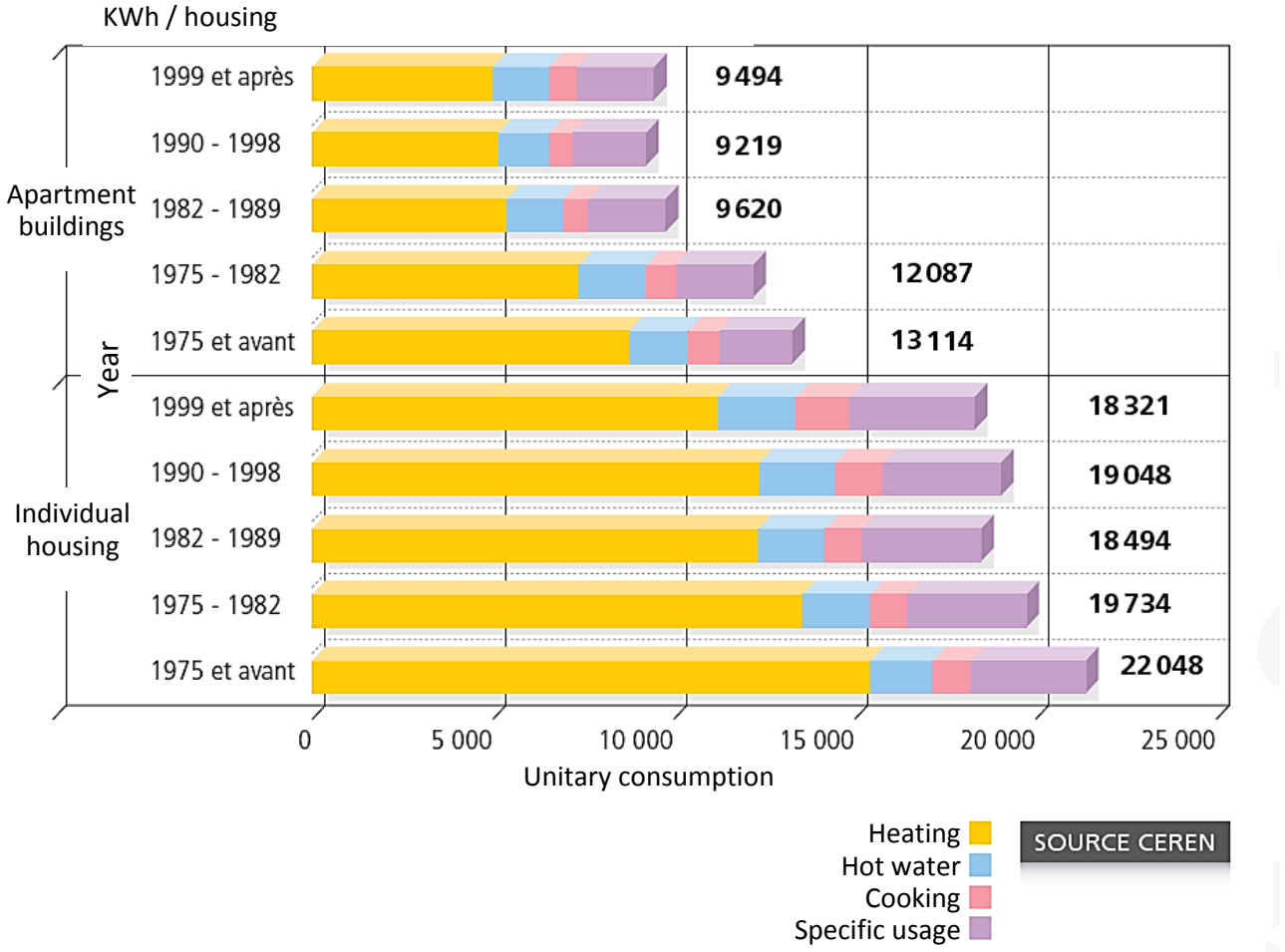

Figure 1.5: Energy distribution within the residential sector

Electrical heating is used in 9,5 million households nationwide, a number that represents 35% of main residences; 44% use gas and 14% fuel (RTE, 2012, b).

Even though the mean unitary housing heating needs have decreased by 44% since 1973, the overall electricity consumption in main residences has increased by 130% in the same period. This can be explained by the strong penetration of specific usage and by the augmenting usage of electrical heating. During the 00's electrical heating was largely preferred in the newly built buildings, mostly because of its advantageous installation and maintenance cost and its moderate price evolution, when compared to other heating means. The percentage of electrical heating use in newly built housing reaches almost 75% of cases in 2008 (figure 1.6). The last Thermal Regulation (RT 2012) resulted in an important decrease of this percentage, as it focuses on primary energy consumption and not on the final one (as was the case with the former regulation RT 2005).

Nevertheless, according to some estimations (NégaWatt 2009), electrical heating reaches an annual consumption of 60 TWh, a number that represents 27% of total electricity consumption of the residential sector and 12,3% of the total annual electricity consumption in France.

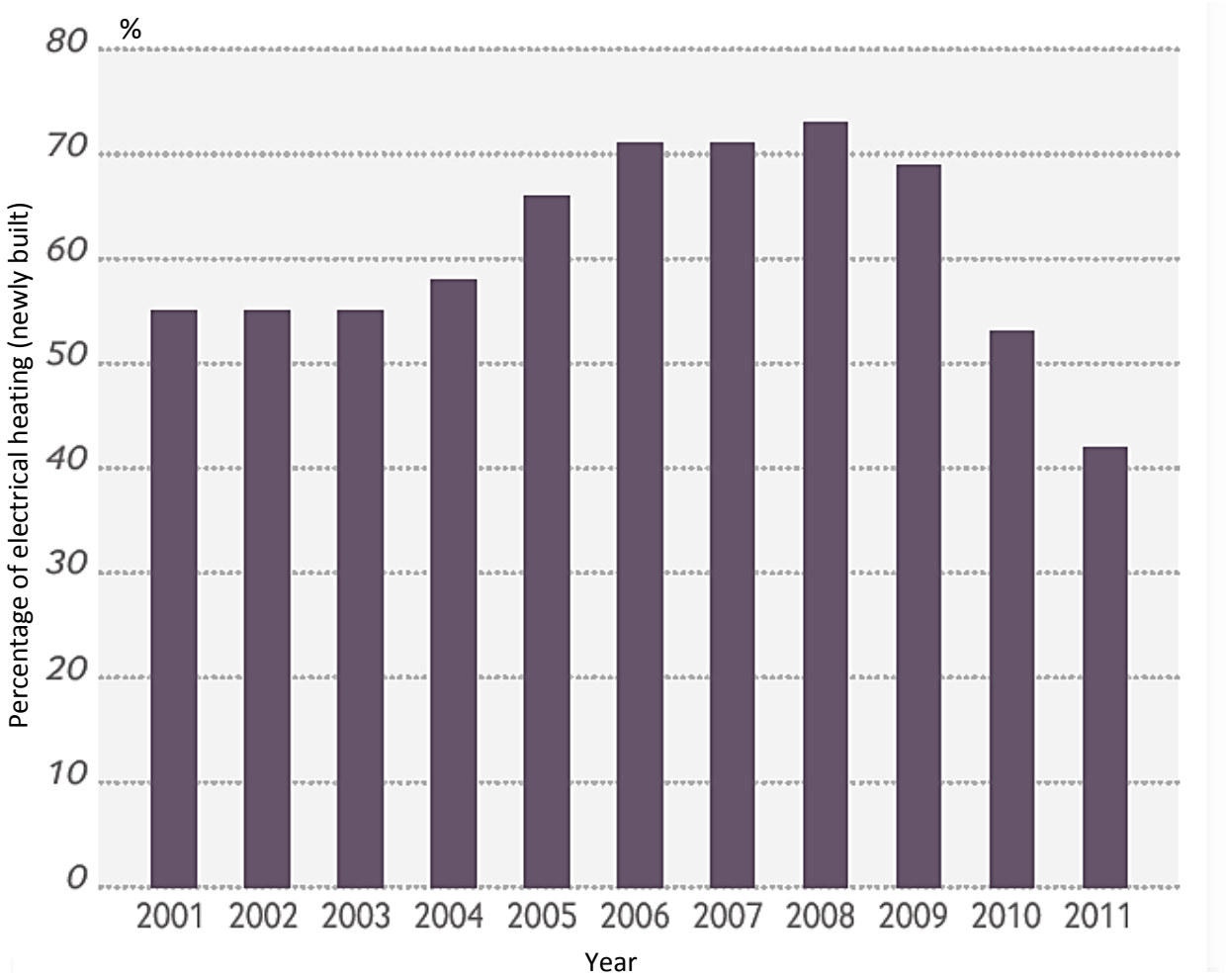

Figure 1.6: Percentage of electrical heating in newly built housing

These figures depend on various factors, one of the most important ones being the weather conditions and the rigorousness of the winter period. For example, throughout the particularly cold winter of 2008/2009 the electrical heating consumption rose to 70 TWh, which corresponds to the total energy consumption of a country like Switzerland. Furthermore, the French electrical Distribution Network (RTE) estimated that during the cold wave of January 7th 2009 electrical heating represented 53% of total residential consumption.

1.3.3.2 Tertiary sector

In 2011, the heating area of the tertiary sector accounts for 931 149 000 m^2 (ADEME, 2013, a). As for the residential sector, gas is the main energy heating source (46%), electricity coming second (25,9%) and fuel last (18,1%). Although the tertiary sector ranks low in the French energy balance, it appears as the most dynamic in terms of energy consumption increase, with an annual growth of 2% for electricity and 0,7% for all energies combined. This fact shows that it can have an increasing impact in the future hence constituting a considerable aspect of energy management policies.

1.3.4 Peak power demand and thermo-sensitivity of French electrical consumption

For the past 15 years electrical consumption in France has shown increasing peaks in electrical consumption (table 1). For the first time, the symbolic threshold of 100.000 MW was surpassed during the cold wave of February 2012. Furthermore, according to RTE (RTE, 2012, a), the increase of these peaks is faster and more dynamic than the increase of the annual electrical consumption. The maximal values are mostly observed during the late afternoon hours of the winter period (19:00) (figure 1.7). They are the result of a decreasing level of tertiary activities, increased public transportation needs and the starting of evening household activities.

Annual electrical consumption peaks	
Thursday 17/01/2013	92 600 MW
Wednesday 08/02/2012	102 100 MW
Tuesday 04/01/2011	91 820 MW
Wednesday 15/12/2010	96 710 MW
Wednesday 07/01/2009	92 400 MW
Monday 15/12/2008	84 420 MW
Monday 17/12/2007	88 960 MW
Friday 27/01/2006	86 280 MW
Monday 28/02/2005	86 020 MW
Wednesday 22/12/2004	81 400 MW

Thursday 09/01/2003	83 540 MW
Tuesday 10/12/2002	79 730 MW
Monday 17/12/2001	79590 MW

Table 1.1: List of annual electrical consumption peaks (RTE, 2012, a)

One of the most influential factors of this phenomenon is electrical heating, as justified by the figures presented in the previous sections. RTE underlines the strong dependence of electrical consumption on outdoor temperature values, particularly during winter. Figure 1.7 also illustrates the increase in power consumption during the cold wave of February 2012.

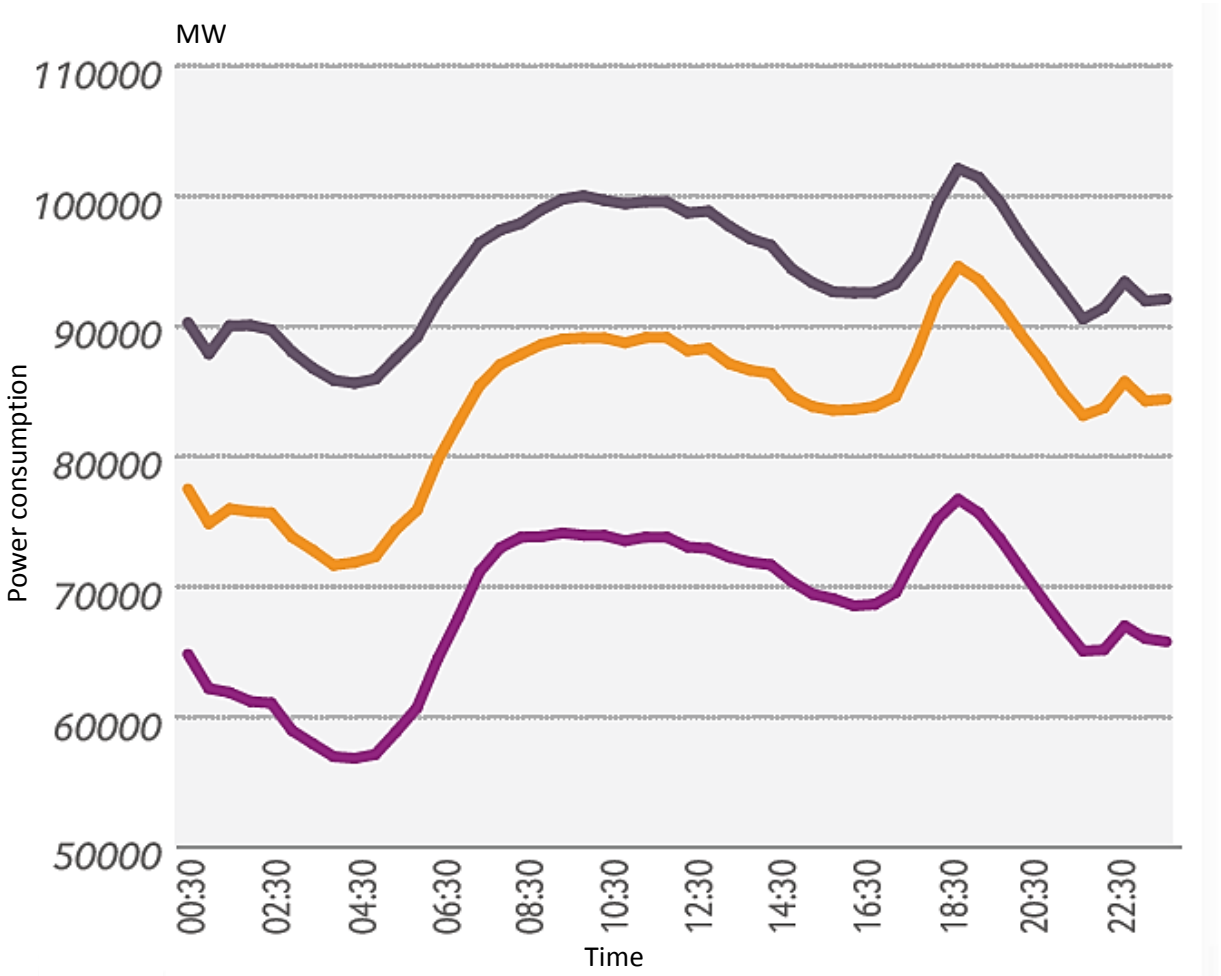

Figure 1.7: Peak power demand around 19:00, before and during the cold wave of February 2012

The term thermo-sensitivity is applied to describe this phenomenon, with a calculated 2300 MW increase in consumption per Celsius degree temperature increase during the 2012 winter. This value presents a growth of 35% when compared to the 2001/2002 one. This phenomenon is much more visible in France than in other European countries as it represents almost half of the total thermo-sensitivity observed in Europe. During periods of great cold, thermo-sensitivity is the predominant factor in electrical consumption. For instance, if we consider the cold wave observed in February 2012, the

thermo-sensitivity part represented on average 40% of the consumption. Figure 1.8 illustrates the electrical consumption and the equivalent thermo-sensitivity part for the first half of February 2012.

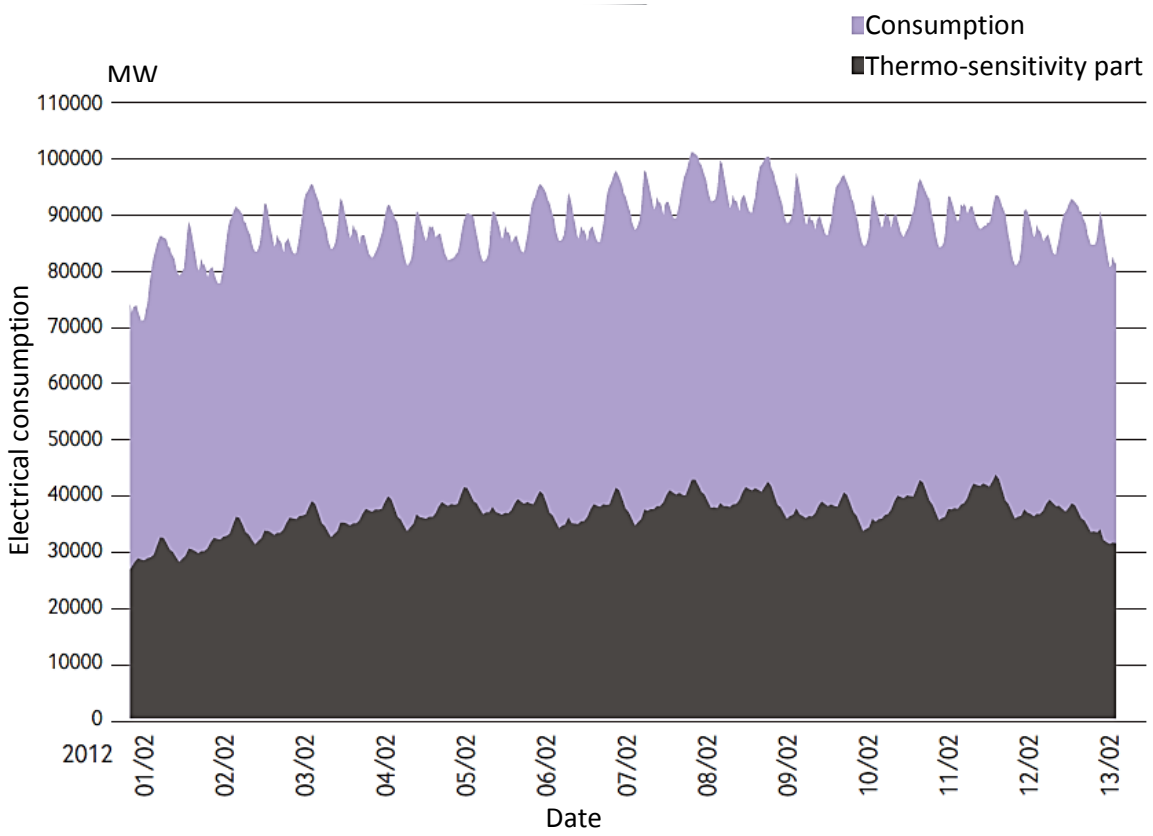

Figure 1.8: Electrical consumption and equivalent thermo-sensitivity part, first half of February 2012

Contrary to the increase in peak power demand over the last 15 year, the annual minimum consumption observed in the summer remains stable during the same period. This results in increasing differences between winter peak demands and summer minimal levels of consumption.

1.3.5 Peak power demand implications

The magnitude of the peak power demand has important economic, environmental and social consequences.

The French energy management system faces increasing difficulties in responding to such events, as it relies in great part on nuclear power plants, presenting mostly constant production rates of 63.130 MW, that cover 77% of total energy consumption (RTE, 2014). As a result, France has to call upon other means of energy production and/or address neighboring countries for importations (figure 1.9). In both cases fossil fuel utilization is usually involved, leading to an increase of CO_2 emission.

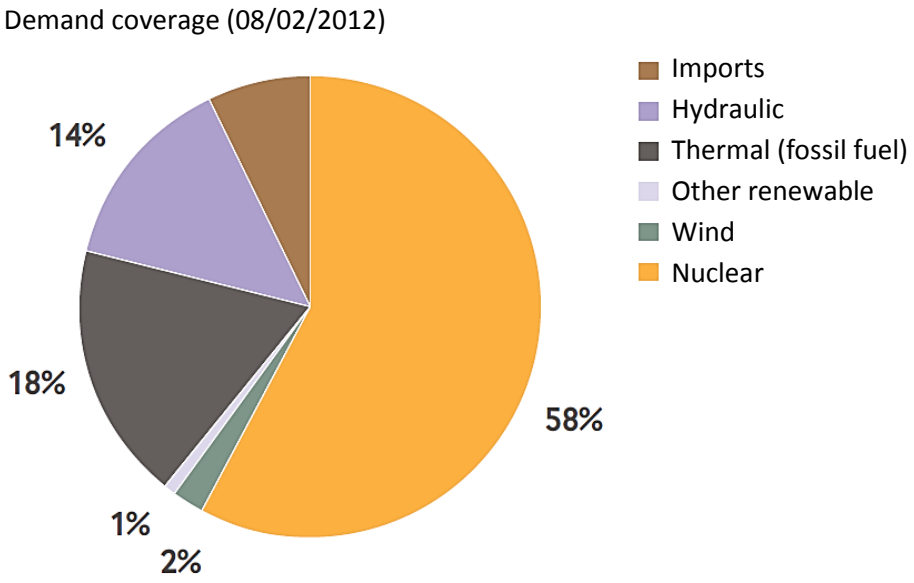

Figure 1.9: Demand coverage during the cold wave of February 8th 2012

According to RTE, CO_2 emissions have been three times higher in winter than in summer over the past six years. Estimations report that a change of electrical heating consumption would result in a change of CO_2 emission by 500-600 g CO_2/kWh (ADEME & RTE, 2007). Furthermore, RTE notes that France has been importing electricity from Germany over the past few years, even though Germany has announced its exit from the nuclear power and closed down seven nuclear sites in 2011.

At the same time, peak power demands lead to the starting of thermal power plants, the reduction of energy exports and the increase of energy importations. In all cases, the energy provider is forced to pay the KWh obtained at price market values, for example two or three times more than the equivalent gas produced energy. The augmented price range is bound to be transferred to the consumer's electrical bill.

In addition, the peak power consumption period represents a relatively small percentage of the total annual consumption. Nevertheless, significant oversizing investments have to be made that are practically not used for the greater part of the year. These costs are also likely to be passed on to the consumers and more specifically to the fixed part of their bill that corresponds to infrastructure development. This outcome penalizes above all small individual consumers, that is to say precarious or energy efficient households.

Increasing bills can contribute to energy precariousness of low income households that cannot afford a well-insulated dwelling or a higher energy budget. Energy precariousness is defined as the difficulty in obtaining the necessary energy supply for the satisfaction of basic needs. This difficulty may occur in conditions of the occupants' insufficient resources or inadequate habitat conditions. According to the French National Institute of Statistics and Economic Studies (INSEE, 2011), 3.8 million households spend more than 10% of their income on energy supply, whereas 3.5 million declare that they suffer from cold in their homes. 621.000 households suffer from both forms of precariousness.

Moreover, according to some assumptions (NégaWatt, 2009), the augmented seasonal demand leads to an increasing concentration of the nuclear units stop in summer in order to obtain maximum power plants operation during the mid-season and winter. Additionally, the French Electricity Company (EDF) performs load-following strategies in some of these plants, resulting in lower production factors. These two management choices differentiate from the original designed operation of the nuclear power plants and may result in a more complicated exploitation, additional costs and degradation of the parc.

Finally, in extreme cases peak electricity demand can lead to partial or total failure in the distribution system (blackout), with severe economic (production deficiency, material damage, etc) and social consequences (transports, discontent among the electricity-depending population, etc).

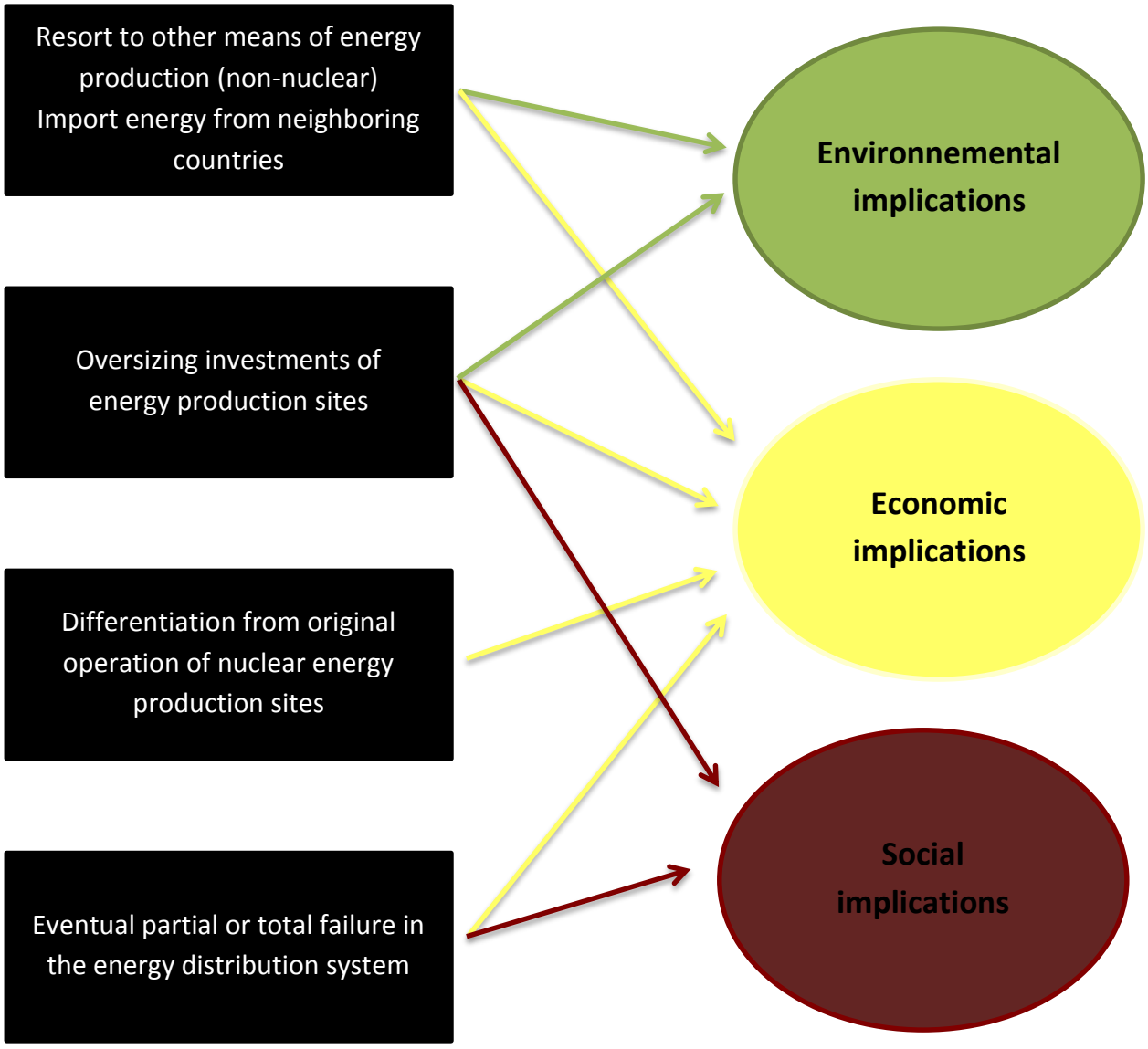

Figure 1.10: Implications of peak power demand

1.3.6 Applied electricity load-shifting methods

Load-shifting management methods and technologies constitute efficient solutions to the increasing electricity peak demands, by storing energy and moving power loads to off-peak times in order to maintain the supply-demand balance and ensure a good operation of the network. Energy storage can be achieved through various processes: electrochemical (batteries, fuel cell), electrical (capacitor, superconducting magnetic field), thermal (sensible, latent, chemical form) and mechanical (hydraulic, flywheel) ones. Some of them provide only short term energy storage and others can achieve very long term storage.

Concerning France, two main peak load shifting categories can be noted:

- The industrial one, that consists in reducing or even stopping the consumption of one or more industrial sites.
- The scattered one that includes the sum of several load shifting application among individuals or professionals.

In both cases, RTE signs contracts with the consumers in question and solicits them in case of important electrical demand, providing advantageous measures in exchange of lower consumption. According to RTE (RTE, 2013), the total load shifting capacity (all features combined) was nearly 900Mw during some days of November 2013. Globally, for the year 2013, the annual activated load shifting volume rose to 20 GWh.

1.4 Conclusion

Throughout this chapter we discussed the increasing concern for energy related subjects, focusing on the French context and the increasing peak power demands. We explained the influence of electrical heating on higher energy needs along with the serious economic, environmental and social problems that may be provoked by this issue. We briefly discussed existing solutions as a transition to the second chapter where energy storage and latent heat storage systems are presented as efficient ways to deal with peak electricity demand.

Chapter 2

Energy storage, PCM and HVAC

Chapter 2 : Energy storage, PCM and HVAC integrated applications

2.1 Introduction

In the previous chapter the international and French energy context was presented, emphasizing on the peak power problem linked to electrical heating. This chapter discusses the benefits of energy storage technology in terms of consumption shifting and more efficient management of the built environment.

At first, the field of application of such technology is presented, along with its different forms, focusing on thermal energy storage. Furthermore, phase change materials are discussed as one of the most frequent ways to achieve thermal storage (classification, properties, containment, applications, enhancement techniques and limitations).

Then several existing studies using PCM integrated in HVAC systems are compared, in order to acquire useful information regarding their development and utilization in the building. Finally, an attempt to summarize the operation principles and design methods is performed, as a guide for the fabrication of a PCM-Air heat exchanger.

2.2 Energy storage: necessity and methods

As discussed earlier, the built environment is one of the major contributors in what concerns energy consumption and GHG emissions. Furthermore, scientific communities have been alerting regarding human-induced climate change and its impact on average earth temperature elevation. At the same time, the world population is increasing and is expected to rise up to 9.6 billion by 2050 (UN, 2013). A growing percentage of the population will be living in cities, indicating that high density urban landscapes will also increase in the future. One of the consequences of this fact will be the intensification of the Urban Heat and Pollution Island effect that can negatively influence mortality rates and heat-related diseases (Haja et al., 2002). Indeed, the 2003 summer heat wave was directly linked to 70.000 deaths in European countries (15.000 deaths in France only) (Robine et al., 2008).

In view of these facts, the need for more efficient energy buildings seems essential, the replacement of conventional energy sources with renewable and waste ones being a highly promising perspective. Nevertheless, implementing renewable sources in the building presents some drawbacks, the main difficulty being the variability and intermittence of their availability (especially concerning wind and solar energy).

In addition, as presented in the previous chapter, daily and seasonal variations in energy consumption lead to peak power usage and tend to become an important issue for energy companies, France being one of the most affected countries in Europe.

In light of these elements, Energy Storage (ES) can play a key role in energy efficient buildings by providing a number of solutions for intermittent resources and mismatching demand, while maintaining comfortable indoor environment. Furthermore, it can contribute to energy supply security, advanced control strategies elaboration (associated with smart grids) and thermal inertia increase.

ES can be performed through various processes, including mechanical, electromagnetic, chemical, biological and thermal ones. Some of them provide only short term energy storage and others can provide very long term storage. This chapter will mainly deal with thermal energy storage, presenting the main methods through which it can be achieved and focusing on phase change materials technology.

2.2.1 Thermal energy storage

Thermal energy storage (TES) allows the stocking of thermal energy in order to reduce indoor air temperature fluctuation or to reinstitute it to the system (building, district, and town) at a later period with an hourly, daily or even seasonal time lag. Excess storable energy can be the result of intermittent power sources (mostly renewable ones) or waste heat from domestic appliances (cooking, ventilation, etc.) (figure 2.1).

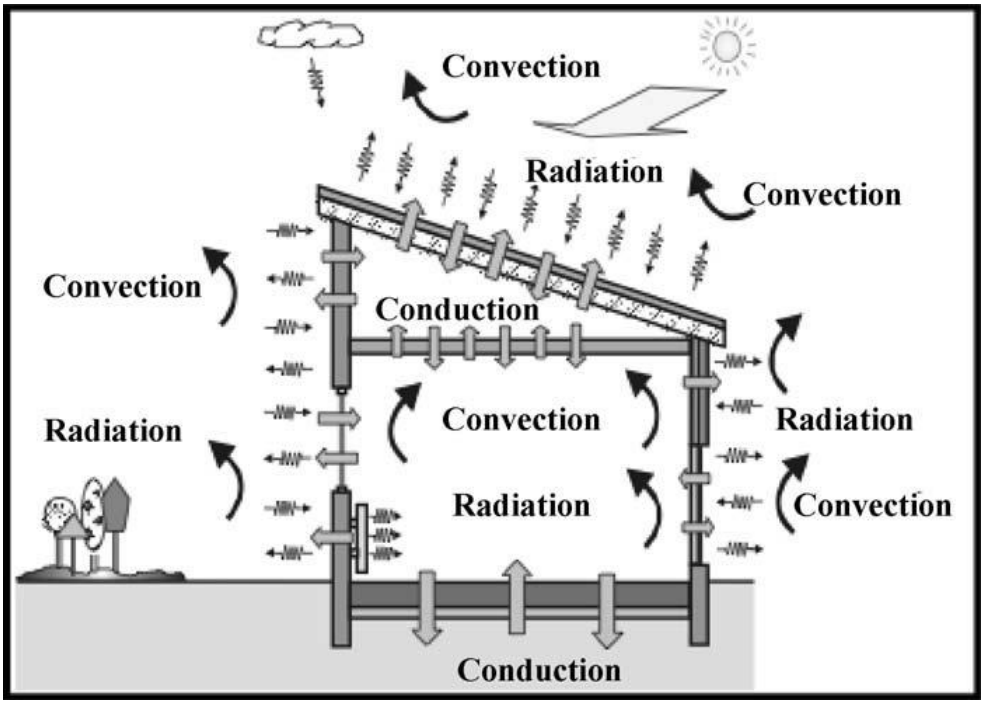

Figure 2.1: Internal and external solicitations in a building, possible heat sources

Depending on the application, the following elements are usually used in TES systems:

- A storage medium where heat or cold is stored.
- A containment component that is used as a reservoir for the storage medium.
- A circuit that allows the flow of the heat/cold transferring fluid (air or water).
- A heat/cold source that is used to heat/cool the circulating fluid.
- A fan or a pump that regulates the flow of the circulating fluid in the system (for some systems).

The operation of TES systems can be divided into three distinct stages: charging, storing and discharging heat or cold. Thermal insulation is needed in order to avoid losses over these processes, as the storage medium is at higher or lower temperatures compared to the surrounding environment. The operational temperature range depends on the applicable case and presents limitations related to the heat source and the storage material.

Parameters that ensure a pertinent implementation of TES systems in the building include:

- high energy density of the storage element
- favorable heat transfer and compatibility between transfer fluids
- container and storage medium compatibility
- stability of the storage material during the charging/discharging process
- long-lasting reversibility of these processes
- limited heat losses, sufficient power load, cost effective system design and storage material

TES can be achieved through three major methods: sensible heat storage, latent heat storage and chemical heat storage.

2.2.1.1 Sensible heat storage and building applications

Sensible heat storage (SHS) occurs in a medium when its temperature changes within a fixed range and without phase change taking place. The storage medium can be a liquid such as water (the most common use) or thermo-oil, a solid such as brick, concrete, sand and soil or even metals such as aluminum and steel. SHS is usually simpler and less expensive to implement than latent heat storage. It presents however lower energy efficiency and storage capacity, which leads to rather large volumes of TES systems. As already explained, in SHS, thermal storage occurs only through an apparent temperature change of the storage medium. Likewise, heat/cold release also manifests at varying temperatures, a fact that can be a drawback if a specific temperature range is sought for.

The capacity of a storage system is defined by the specific heat capacity and the mass of the storage material. The following equation is used to describe the SHS process:

$$Q = mC_p(T_2 - T_1) \qquad \text{equation 2.1}$$

Where Q is the amount of stored sensible heat (J), m is the storage medium mass (kg), C_p is the specific heat of the storage medium at constant pressure (J/Kg.K) and T_1 and T_2 are the temperatures before and after stocking/destocking.

SHS applications can be found in wall insulation, inertia increasing techniques, solar or gas water heaters, load levelling, night cooling etc.

2.2.1.2 Latent heat storage and building applications

Latent heat storage (LHS) occurs when the storage medium undergoes a phase change, from solid to liquid (usually) or liquid to gas or solid to gas, and vice versa. The heat stored or released is used for the phase change, thus allowing to obtain much higher storage capacity and a narrower temperature operating range when compared to SHS systems. This can be demonstrated by considering the melting

of 1kg of ice, a process that requires 333KJ of energy. The same amount is needed to raise the temperature of 1 kg of water from 0°C to 78°C.

The storage media used in such systems are called phase change materials (PCM), the most common being paraffin, hydrated salt and fatty acids. Table 2.1 presents a comparison of SHS (rock bed and water tank) and LHS technology (organic and inorganic PCM) (Farid et al., 2004). The advantages of LHS are evident in terms of storage density and volume.

	Rock	**Water**	**Organic PCM**	**Inorganic PCM**
Density, kg/m3	2240	1000	800	1600
Specific heat, kJ/kg	1.0	4.2	2.0	2.0
Latent heat, kJ/kg	-	-	190	230
Latent heat, kJ/m3	-	-	368	368
Storage mass for 106 J, kg	67,000	16,000	5,300	4,350
Storage volume for 106 J, m^3	30	16	6.6	2.7
Relative storage mass	15	4	1.25	1.0
Relative storage volume	11	6	2.5	1.0

Table 2.1: Comparison between sensible and latent heat storage (Farid et al., 2004)

On the other hand, LHS systems present practical difficulties linked to PCM properties: low thermal conductivity, density (and volume) change, chemical instability and other disadvantages that will be discussed in detail later. In most LHS systems SHS also occurs before and after the phase change. The equation that describes the total heat transfer process is as follows:

$$Q = mC_{p,s}\Delta T\ (s) + mL + mC_{p,l}\Delta T\ (l) \qquad \text{equation 2.2}$$

Where Q is the total amount of stored heat (sensible and latent) (J), m is the storage medium mass (kg), C_{ps} and C_{pl} (J/Kg.K) are the specific heat of the storage medium in solid and liquid form, ΔT is the temperature difference and L is the specific latent heat (J/kg). The first term represents the sensible heat exchanged during the solid phase, the second one the latent heat absorbed or released during the phase change and the last one the sensible heat exchanged during the liquid phase.

Figure 2.2 demonstrates a theoretical temperature profile variation as a function of stored heat during a sensible and a latent heat exchange process. Practically, a small temperature increase is also observed during the latent phase due to the impurity of materials and convective heat transfers.

Concerning the built environment, LHS technology can be introduced into the building structure (wall, ceiling, façade) or in separate heat and cold storage devices usually related to HVAC systems. The first

category constitutes the passive elements of the building, whereas the second one is an active component that can be used on demand.

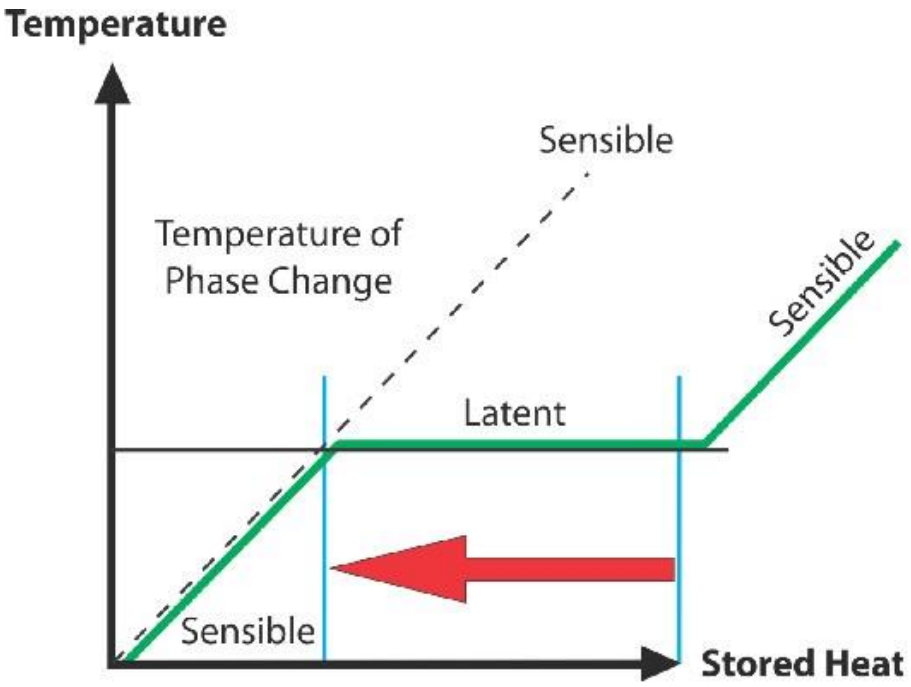

Figure 2.2: Temperature profile variation with stored heat evolution

LHS applications have also been developed in a variety of domains including medical or food transport technologies, spacecraft thermal systems, vehicle thermal comfort, protection of electronic devices, computer cooling, clothing, etc.

2.2.1.3 Chemical heat storage and applications

Chemical heat storage (CHS) can be divided into two categories: thermochemical processes and sorption processes.

The first ones are based on the energy released and absorbed during the breaking and the formation of molecular bonds for completely reversible chemical reactions. Thermal energy can be absorbed when the endothermic dissociation of a material (C) takes place, this constituting the charging procedure. This process leads to the formation of two separate components (A and B), which have different properties and can be stored at ambient temperatures for long periods with few or no thermal losses. Finally, the discharging process occurs when the reversed procedure is performed and the components A and B are mixed through an exothermic reaction that leads to the reformation of the initial material C. The described procedures can be represented by the following equation:

$$C + heat \rightleftarrows A + B \qquad \text{equation 2.3}$$

Where C is the thermochemical material and A and B are the reactants. Reactant A can be a hydroxide, hydrate, carbonate, ammoniate and reactant B can be water, carbon monoxide, ammonia, hydrogen etc. Usually material C is in liquid or solid form, whereas materials A and B can be in any phase.

Sorption systems involve adsorption and absorption processes. The first one takes place when a molecular or atomic layer is shaped, following the accumulation of an adsorptive on the surface of an adsorbent. The adsorptive can be a liquid or gas while the adsorbent can be a solid or liquid. Absorption consists in the formation of a solution which is occurring when a substance is distributed into a liquid or solid.

CHS is an emerging field presenting the advantages of high energy density, with compact and long term storage potential. On the other hand, it is more expensive and technically complex to implement compared with sensible and latent heat storage technology.

Table 2.2 resumes the main parameters of the three TES methods, as well as their advantages and disadvantages (Abedin et al., 2011).

Performance Parameter	**Type of Thermal Energy Storage**		
	Sensible TES	**Latent TES**	**Chemical TES (Sorption and Thermochemical)**
Temperature range	Up to: 110 °C (water tanks) 50 °C (aquifers and ground storage) 400 °C (concrete)	20-40 °C (paraffins) 30-80 °C (salt hydrates)	20-200 °C
Storage density	Low (with high temperature interval): 0.2 GJ/m^3 (for typical water tanks)	Moderate (with low temperature interval): 0.3-0.5 GJ/m^3	Normally high: 0.5-3 GJ/m^3
Lifetime	Long	Often limited due to storage material cycling	Depends on reactant degradation and side reactions
Technology status	Available commercially	Available commercially for some temperatures and materials	Generally not available, but undergoing research and pilot project tests
Advantages	Low cost Reliable Simple application with available materials	Medium storage density Small volumes Short distance transport possibility	High storage density Low heat losses (storage at ambient temperatures) Long storage period Long distance transport possibility Highly compact energy storage
Disadvantages	Significant heat loss over time (depending on level of insulation) Large volume needed	Low heat conductivity Corrosivity of materials Significant heat losses (depending on level of insulation)	High capital costs Technically complex

Table 2.2: Comparison of different types of TES based on various performance parameters, (Abedin et al., 2011)

2.2.2 Electrical energy storage

Electrical energy storage (EES) consists in transforming electrical energy into other forms that facilitate its storage for later use. This can be achieved through a wide range of different technologies, including mechanical, electromagnetic, chemical, biological and thermal ones. Several studies have been performed in the field of EES (Chen et al., 2009), a detailed description of which exceeds the interest of this thesis. Figure 2.3 illustrates a classification of the different forms of EES and the existing applications that derive from them (Fernandes et al., 2012).

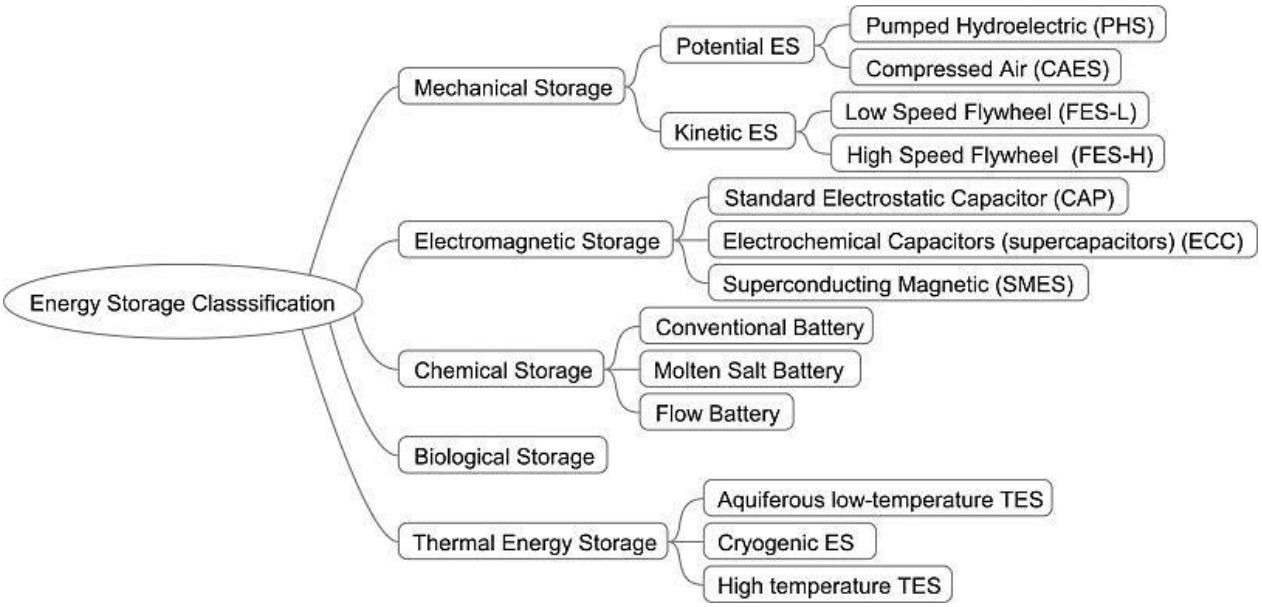

Figure 2.3: Classification and applications of EES (Fernandes et al. 2012)

2.3 Phase Change Materials

Phase change materials (PCM) constitute one of the main elements of latent heat storage systems. The phase change process and the subsequent latent energy storage/release enables them to store significant amounts of heat/cold in small volume and within a certain temperature range. In the majority of PCM building applications, the solid-liquid phase change is preferred because of the small volume change compared to liquid-gas or solid-gas transformations. Pure PCMs have a distinct temperature in which the phase transformation occurs (T_f). When the material is heated to reach this temperature its chemical bonds start to break up through an endothermic process that leads to a solid to liquid transformation and absorption of heat. On the contrary, when the material's temperature decreases again, it regains its solid form during an exothermic process that releases heat. Figure 2.4 (left) shows the cooling process of such a material over time, demonstrating the constant temperature values during the melting phase. Figure 2.4 (right) illustrates the heat flux variation during liquefaction for a fixed temperature difference, with an apparent increase during the phase change. The phase change process of some PCMs is observed within a temperature range, instead of a distinct value. This is due to the mixture of different components that is made in order to acquire PCMs with specific properties.

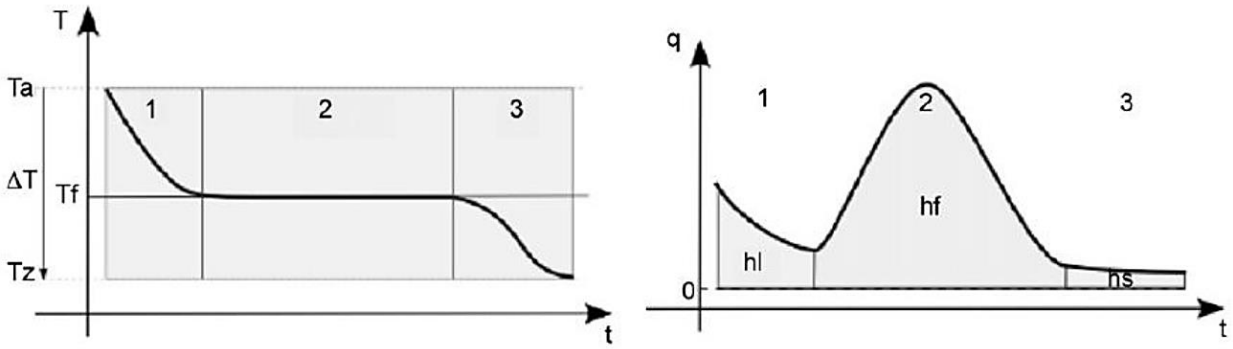

Figure 2.4: PCM temperature and heat flux evolution during solidification, 1: liquid phase 2: melting phase 3: solid phase (Baetens et al., 2010)

Table 2.3 depicts the main desired thermal, physical, chemical and economic properties for an efficient implementation of PCMs in building applications (Hale et al., 1971).

Thermodynamic properties	**Kinetic properties**	**Chemical properties**	**Economic properties**
Phase change temperature meeting application needs	High density	Non-toxic and non-polluting	Cost (cheap)
High thermal conductivity (in liquid and solid phases)+	Low density variation	Compatible with storage containers/no corrosiveness	Availability (abundant and easily available)
High change of enthalpy (near usage temperature)	High rate of crystal growth to meet demands of heat recovery from storage system	Non-flammable /no explosive	
High specific heat and high density	High nucleation rate to avoid super cooling	No phase separation	
Congruent melting		Chemical stability	
High latent heat of fusion per unit volume		Complete reversible freezing and melting cycles	
Small volume changes on phase transformation and small vapor pressure at operating temperatures to reduce containment problem		No degradation after a large number of freezing and melting cycles	
Often not provided for both phases			

Table 2.3: Main desirable characteristics of PCMs (Hale et al., 1971)

2.3.1 Classification

Several criteria exist for the classification of PCMs based on their chemical composition, melting temperature, latent heat of fusion, etc. The most frequent categorization divides them to three groups: organic, inorganic and eutectics (figure 2.5). In fact, the last ones are mixtures of the first two categories but it is now common to be considered as a specific group.

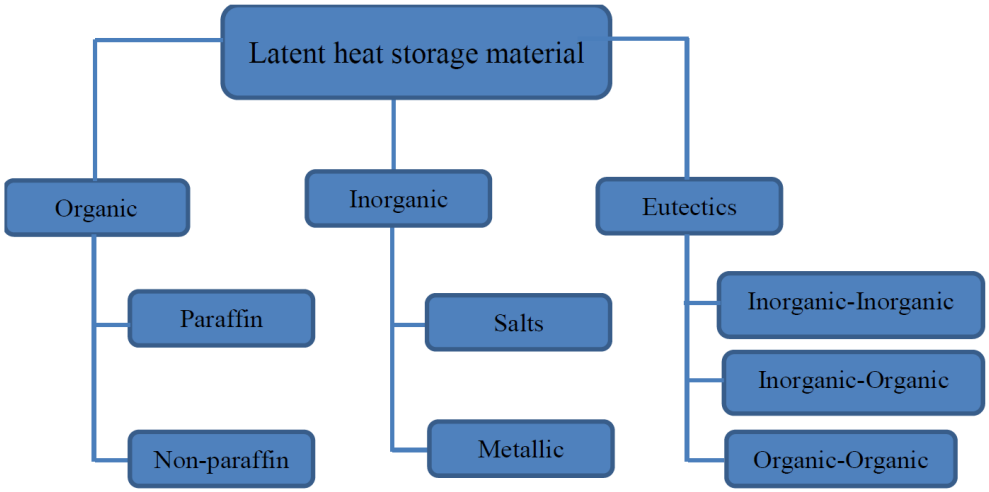

Figure 2.5: Classification of PCMs (IEA, Annex 23, 2013)

A great number of materials have been used and studied as PCMs in TES applications, including hydrated salts, paraffin waxes, fatty acids and eutectics of organic and non-organic compounds. Figure 2.6 illustrates a classification of PCMs according to their melting temperature range and melting enthalpy.

A detailed list of commercially available PCMs can be found in Cabeza et al. (2011) publication.

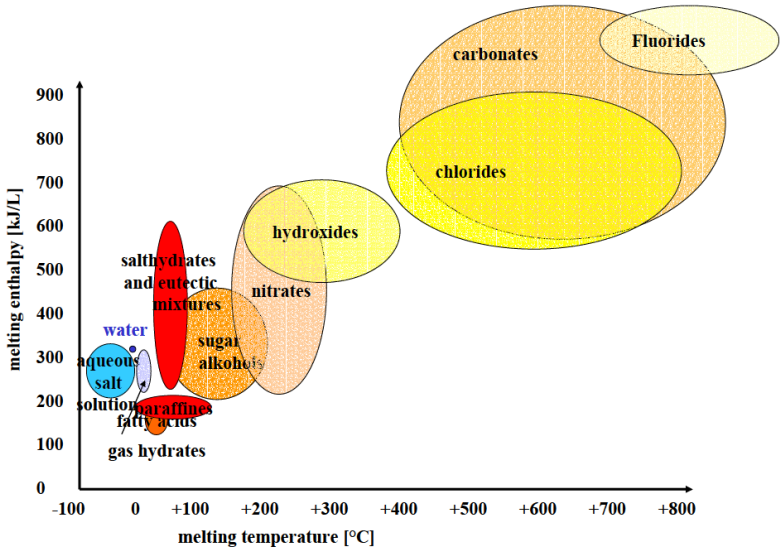

Figure 2.6: Classification of PCMs according to their meting temperature range and enthalpy (IEA, Annex 17, 2005)

2.3.2 Phase change phenomena and properties

Over the years, several problematic phenomena related to PCMs performances have been identified and studied. This section presents the most common ones.

2.3.2.1 The subcooling phenomenon

Subcooling (or supercooling) occurs when the PCM remains in liquid form even when its temperature decreases below the solidification threshold value (Tf). Normally, the solidification process starts with the formation of initial crystals (nucleus) and in a second stage, the propagation of these crystals. In some PCMs however (mostly salt hydrates and some eutectics) it has been observed that the nucleation rate is low, resulting in a reduction of the nucleus. As a consequence, the PCM remains in liquid form, solidification and heat release are delayed, and its temperature increases until it gets back to the solidification value (figure 2.7). Subcooling can have a disrupting effect on the performance of the PCM unit and must be taken into account in the design phase of TES applications. A solution to minimize this phenomenon lies in the addition of suitable nucleating agents to the PCM.

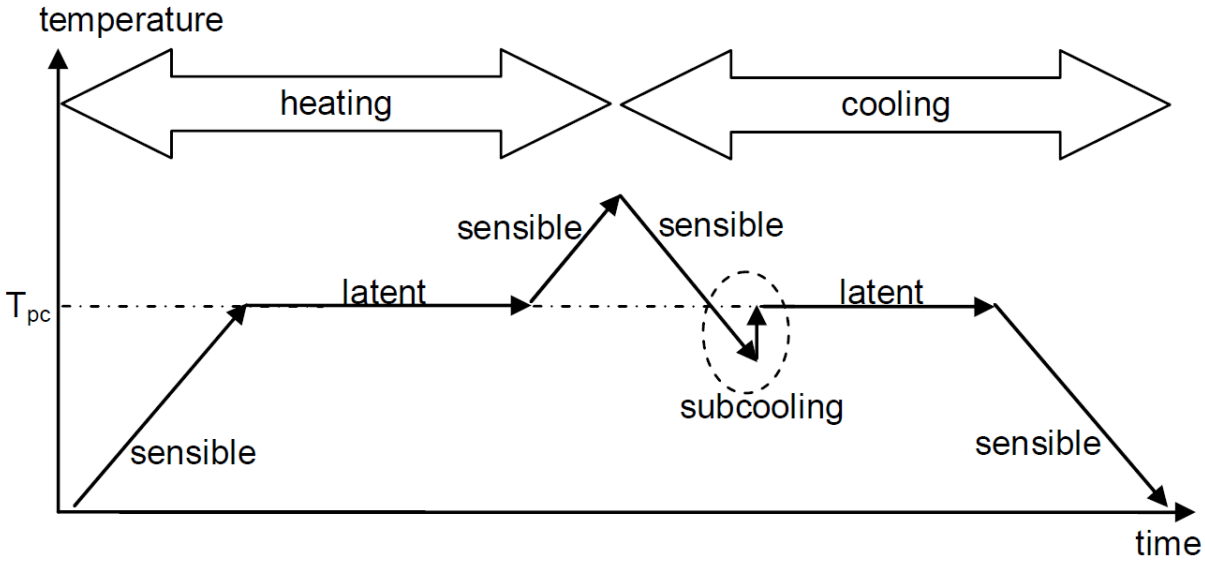

Figure 2.7: Subcooling effect during solidification (Cabeza et al. 2008)

2.3.2.2 The segregation phenomenon

The segregation phenomenon is observed on salt hydrates PCMs and consists in the decrease of the storage density over cycling. It occurs due to the congruent melting of most salt hydrates with the formation of the lower salt hydrate. The effect is non reversible and lowers the thermal properties and performance of the PCM. Solutions can be found in the inclusion of materials that can alter the properties of the salt hydrate by preventing the heavier phases from sinking to the bottom. These materials can be gelling (polymer) or thickening elements and are used to hold the salt hydrate together.

2.3.2.3 Thermal life cycle

Thermal life cycle refers to the number of cyclic phase change repetitions (melting-solidification) before the PCM thermal properties begin to alter (decrease). The thermal life of most PCMs varies between 3000 and 10000 cycles (Hadjieva et al., 1992). Thermal life cycle affects the performance of an LHS unit and can help determining the potential of its use.

2.3.2.4 Incompatibility with storage containers: Corrosion or volume change

Some PCMs present another disadvantage as they may not be compatible with the chosen storage solution. This concerns corrosion and volume changes that could both lead to the degradation of the container and the leakage of the PCM, rendering the application unusable in the long term.

2.3.2.5 Flammability and odor

PCM based materials or applications that are meant to be implemented in the building require respecting building legislation related to fire risks and the occupants' olfactory comfort. Some PCMs present high combustibility values and require special treatment before usage in a real life application. This can include the incorporation of fire retardant additives in the PCM and conducting fire risk tests. However these procedures are bound to increase / raise the final price of the PCM and of its implementation in the building.

Furthermore, some PCMs are not odorless and the inhalation of PCM vapor may cause irritation, both facts being unacceptable by the occupant. Air-tight containment is thus required to overcome these problems.

2.3.3 Containment

PCM containment is a very important issue in an LHS unit as it is related to the heat transfer process and the general rigidity of the application's structure. As PCMs present low thermal conductivity, proper containment can help overpass this disadvantage, for example by providing a high exchange surface to volume ratio or by having a small storage thickness. As discussed earlier, poor containment solutions can lead to corrosion and/or leakage of the PCM and render the equipment non-operational. Several techniques are proposed for the proper containment of PCMs, including macroencapsulation, microencapsulation, direct incorporation, immersion and shaped stabilized PCMs.

2.3.3.1 Macroencaplsuation

Macroencapsualtion is perhaps the most commonly used technique. Containers usually larger than 1 cm in diameter are used to enclose the PCM. The containers can be in the form of tubes, pouches, spheres and panels; they are usually made of high conductivity and rigidity materials such as aluminum, copper etc. Macroencaplusation offers the advantages of small leakage risks and of little affection of the building's structure. On the other hand, it presents poor thermal conductivity and in some cases complicated integration into the building materials.

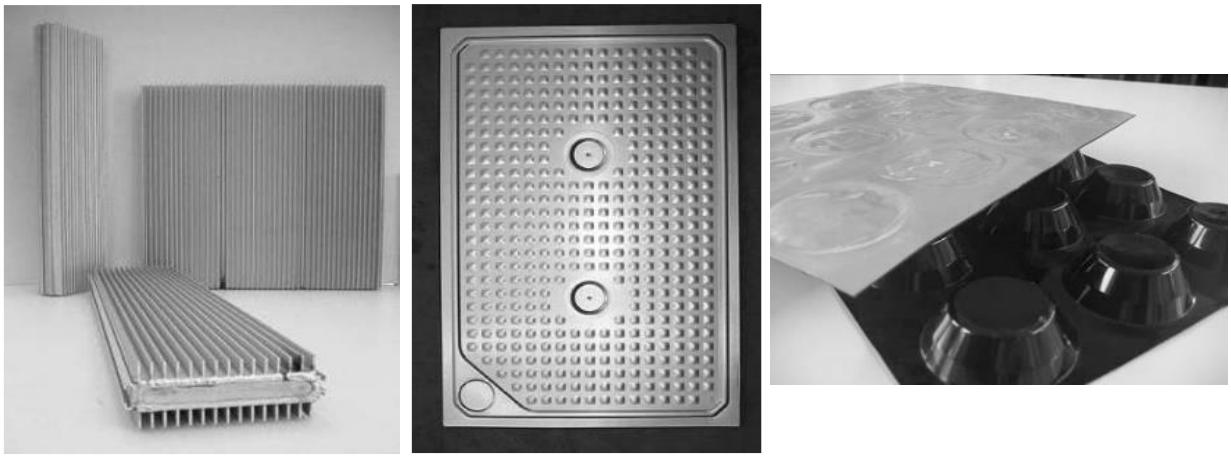

Figure 2.8: Macroencapsulation solutions, from left to right: aluminum profiles with fins, coated aluminum plate, capsule stripes (Cabeza et al., 2008))

2.3.3.2 Microencapsulation

Microencaplsualtion is the technique in which small spherical or rod shaped PCM particles are englobed in a thin molecular polymeric film, obtaining a diameter smaller than 1 mm. The particles are then incorporated in any matrix that is compatible with the film, in order to form a homogenous compound in macro scale. This containment method increases heat transfer as it presents a high surface to volume ratio and improves cycling stability as the phase separation is restricted to microscopic distances. This method facilitates the incorporation of PCM into construction materials.

2.3.3.3 Direct incorporation

Direct incorporation consists in adding liquid or powered PCM to building constructions materials (gypsum, concrete or plaster) during production. It presents the advantage of being the most economical method. Leakage and incompatibility with construction materials are the main disadvantages of this method.

2.3.3.4 Immersion

This technique is based on the sinking of porous building components such as gypsum board, brick, concrete block, wood and plaster into liquid PCM. The PCM is then absorbed into the component's pores by capillary effect. Leakage risk is reported by some researchers. Immersion and direct incorporation both consist in impregnating PCMs directly in typical construction materials.

2.3.3.5 Shape stabilized PCM

Shape- stabilized PCM is the result of a liquid mixture of PCM with a support material, usually high density polyethylene (HDPE) or styrene-butadiene-styrene (SBS). The mixture is then cooled below the glass transition temperature of the supporting material, leading to a solid component that can have up to 80% PCM mass proportion. The observed low thermal conductivity can be increased by adding materials such as ex-foliated graphite into the mixture composition.

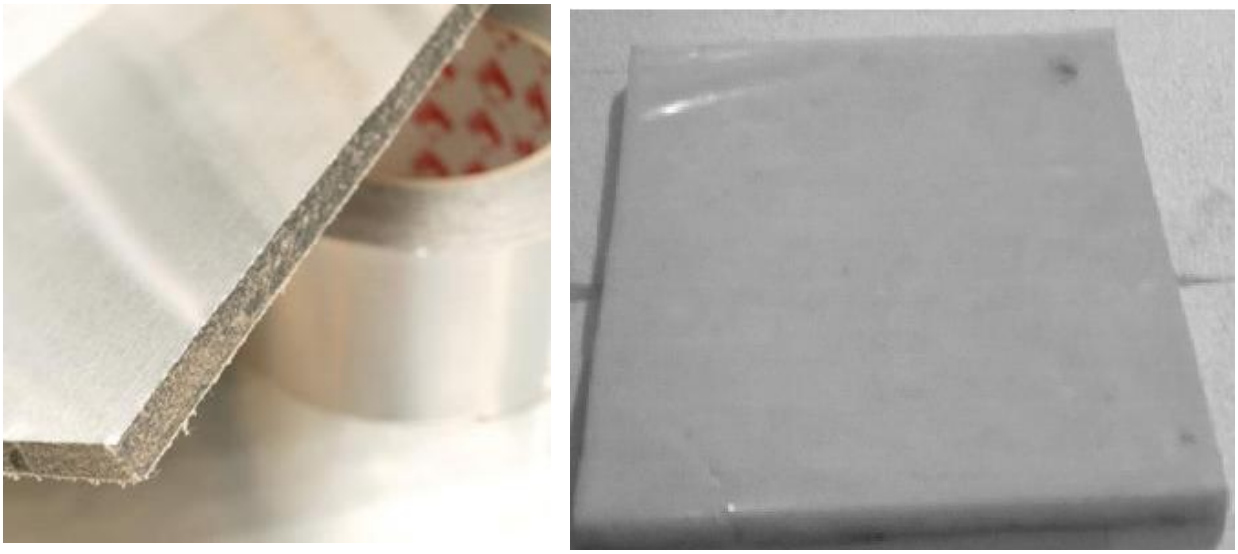

Figure 2.9: PCM construction panels: microencapsulated PCM (left), shape stabilized plate (right) (IEA. Annex 23)

2.3.4 PCM application in buildings

According to L. Cabeza (IEA Task 32, 2005), the first PCM application in the literature appeared in 1975 in a research byTelkes. Since then, several PCM based applications have been proposed and a number of publications has been produced to describe them (Farid et al. 2004, Baetens et al. 2010, IEA Task 32 2005, Pasupathy et al. 2008, Parameshwaran et al. 2012, Pomianowski et al. 2013, Sharma et al. 2009, Soares et al. 2009, Zalba et al. 2003, Zhou et al. 2012, Salyer et al. 1990, Khudair et al. 2004). They can be divided into two large categories: passive and active ones.

2.3.4.1 Passive systems

In passive systems PCM is incorporated into specific components of the building, aiming at several objectives: increasing thermal inertia, minimizing the usage of mechanical heating/cooling devices, lowering the indoor temperature fluctuation and preserving the occupant's comfort. No extra mechanical heating/cooling means are used for the latent heat storage activation of such systems.

The following list presents the main usage of PCM in passive building applications.

PCM in gypsum boards and wallboards

A vast variety of studies and applications has been realized on composites of PCM impregnated gypsum boards and wallboards. Their main goal is to increase the thermal mass of lightweight or existing or renovated buildings, in order to lower indoor temperature fluctuations (figure 2.9).

PCM in concrete

These applications aim to increase heat storage in heavy construction materials by combining the augmented latent heat PCM capacity with the high density of heavy weight concrete.

PCM in bricks

Fewer studies have been performed on PCM-bricks composite constructive applications, showing nevertheless the interest of such technology in decreasing indoor temperature fluctuations. It has been noted that this technology is more suitable for warm climates, such as the Mediterranean one.

Floor and ceiling PCM panels

Floor and ceiling PCM panels have also been developed, aiming to absorb heat (solar related, in roofs for example) and diminish indoor temperature variation.

PCM in glazing and shading shutters

PCM has also been used for optimized glazing and shading components. This technology allows the absorption of a part of the solar heat and can reduce the indoor air temperature fluctuation. Furthermore, some PCMs are translucent and can therefore allow light transmission through them and into the building.

The advantage that emerges from the combination of PCM with the construction materials in question is that the final component offers large areas for heat transfer and LHS potential can therefore be fully exploited.

2.3.4.2 Active systems

Active PCM applications constitute an improved technology for LHS utilization in buildings. Contrary to passive applications, thermal storage can be activated by a supplementary mechanical system (fan, pump, etc), enhancing heat transfer performance and allowing stocking or destocking heat/cold on demand. They can be operated on specific time slots, being able to correlate the needs with the energy supplies and apply in such a way peak power reduction strategies.

In some active PCM systems, the same medium is used both for the heat transfer and storage, whereas in others heat transfer is performed by a first medium (usually air or water) and a second one is used for heat storage (PCM).

Several active PCM applications have been proposed and the main available technologies are briefly presented.

PCM integration with HVAC units

A series of studies has been performed in order to integrate PCM technology in HVAC systems. This is mainly performed in two ways: incorporating either a heat exchanger or a PCM panel board in the HVAC system either PCM. The installation of the PCM technology can be performed in the false ceiling or in the ventilation plenum. This fact usually imposes restrictions in terms of the volume of the unit and the final PCM quantity.

A PCM based heat exchanger usually consists of a set of receptacles that are used to contain the PCM (macro encapsulation); a fluid (air or water) is used as the heat transfer medium. Design considerations include heat transfer optimization between the heat transfer fluid and the PCM. Concerning the PCM panel boards, this consists in the use of passive PCM technology (as presented in the previous section), with the advantage of the coupling with an active mechanical system.

PCM integration in HVAC systems is usually performed to enhance the cooling or heating performance of mechanical ventilation units and for peak power reduction needs.

PCM in construction: ceiling gypsum and radiant floor panels

A thermally activated ceiling gypsum panel has also been developed allowing heat gains of up to 40W/m2 and an increase of the thermal mass of light weight buildings. An incorporated water capillary tube system allows the active control of the thermal storage. Active PCM applications can also be found in radiant floor panels. Granulated PCM was employed together with integrated pipes for heating and cooling. Results demonstrated the benefits of this application in summer conditions.

A table that summarizes passive and active LHS applications in buildings is presented by Parameshwaran et al. (2012), focusing on the applications' potential, integration within the building, and functional aspects.

2.3.5 PCM enhancement techniques

2.3.5.1 Heat transfer

As discussed earlier, one of the main disadvantages of PCMs is their small thermal conductivity values: 0,2 W/(mK) for most paraffins and 0,5 W/(mK) for salt hydrates. These values can be insufficient for rapid charging/discharging phases of LHS systems. For example, it is common in buildings to have daily operation cycles as heat or cold is stored in the night and is released during the day. Low conductivity values can lead to limited charging of the unit and poor performance of the system. Therefore, several enhancement techniques have been proposed in order to increase the heat transfer exchange, mostly aiming to obtain higher PCM conductivity values:

- Microencapsulation of PCMs using a high conductivity material such as graphite, silicon carbide, copper, etc.
- Dispersion of high conductivity material particles (copper, steel, aluminum, etc.) within the PCM
- Addition of high conductivity material into the macroencapsulation container
- Extension of the surface area using fins
- Design optimization to obtain the highest surface to volume ratio possible

Nevertheless, these techniques can have a positive effect on conductivity values but on the other hand they degrade the unit's heat storage capacity due to the replacement of part of the PCM with sensible storage material.

2.3.5.2 Fire retardation

PCM enhancement also concerns fire risks limitation, as building regulations become stricter in this field. Salyer and Sircar (1990) propose the following solutions to fire retard PCM imbibed plasterboard:

- Adding alternate non-flammable surface to the plasterboard (e.g., aluminum foil and rigid polyvinyl chloride film).

- Sequential treatment of plasterboard, first in PCM and then in an insoluble liquid fire retardant (e.g., Fyrol CEF). The insoluble fire retardant displaces part of the PCM and some remains on the surface, thus imparting self-extinguishing characterization to the plasterboard.
- Using brominated hexadecane and octadecane as PCMs. It is anticipated that when these halogenated PCM compounds are combined with antimony oxide in plasterboard, the product will be self-extinguishing.
- Fire retardant surface coatings may be used to prevent effectively the wicking action of the plasterboard paper covers.

2.3.6 Limitations/barriers

Despite the mentioned advantages and the numerous research activities, PCMs have not yet reached large scale commercial usage. Most of the realized studies limit themselves to small laboratory experimental units and few investigations have been performed in actual buildings and real life operation scenarios. Commonly, the developed concepts remain in the prototype stage and in some cases unrealistic scenarios are tested that lead to overestimated results. Moreover, these studies fail to present an economic analysis of the project or a life cycle assessment of its components. The main factors explaining the so far limited utilization of PCM based technology are as follows:

- Elevated price of the material and its implementation in the building
- Difficulties concerning the proper containment
- Physical phenomena that deteriorate the initial PCM performance
- Flammability risks and odor risks
- Absence of legislation concerning their implementation in the building

2.4 HVAC integrated PCM applications

In this section studies performed by various laboratories and associated with active LHS applications integrated into HVAC systems are presented. In these types of systems, the needed heat or cold is stored in specific apparatus (heat exchangers), thermally contained from the rest of the building and used only on demand and not automatically (i.e. active LHS applications).

Firstly, a detailed description of each case study is performed focusing on the experimental apparatus description, on the main results and the development of a numerical model (if any). Secondly, useful conclusions drawn from this study are presented in order to summarize the main elements, the operation principles, the design methods and the philosophy of active LHS ventilation systems.

2.4.1 Demonstration examples

2.4.1.1 Borderon et al. system

Borderon et al. (2012) proposed an LHS system aiming to cool a house by using the freshness of the cold night air. It is composed of horizontal PCM plates placed in a heat exchanger and coupled with a ventilation system. A fan forces the air through the exchanger so that the PCM absorbs or releases heat.

Indoor air is cooled by passing through the exchanger during the day and outside air is used to solidify the PCM during the night. A diffuser is used to equally distribute the air between each plate. The PCM used is the Energain® compound, a mixture of 60% microencapsulated paraffin in an ethylene based polymer, with a melting point around 21°C and a latent heat of 72 kJ/kg for 5 to 30 °C. It is used in the form of plates with dimensions of (1,20x1,20x0,05) m, each face of the plates being covered with an aluminum foil preventing leakage and fire risks.

The exact composition of the proposed heat exchanger (as seen in figure 2.10) is a first insulation layer, a combination of several Energain plates piled up one another, an air layer, a second PCM layer which doubles the thickness of the first one, a second air layer, a third and last PCM layer identical to the first one and finally a second insulation layer.

Figure 2.10: Borderon et al. heat exchanger unit

The two air layers are instrumented: the upper surface of the lower air layer and the lower surface of the upper air layer are equipped with flow meters and thermocouples (Type K, Chromel/Alumel). An omnidirectional (TSI™, 0-10 V) hot-wire anemometer (TSI™, 0-10 V) is placed in each air layer near the outlet. Two relative humidity sensors are placed on both sides of the prototype; they consist of 4-20 mA sensors associated with a 500 Ohm resistance and an output signal of 0-10 V.

In order to measure the heat flux between PCM and air, four flux meters were installed, two for each of the instrumented sides. The less than 1 mm thin sensors send an electrical signal that is proportional to the heat flow. For each of the flow meters, an air and a surface temperature measurement is made. Other air and surfaces temperature measuring thermocouples are spread over the plates. Air temperature is measured at the inlet and outlet of the exchanger and a differential thermocouple is used to directly measure inlet and outlet difference temperature. Data acquisition is performed with a National Instruments device and Labview software.

The experiments conducted with the developed heat exchanger allowed to issue temperature, relative humidity and airflow profiles.

Parallel to the experimental study, a bidimensional Matlab model was created based on the finite difference method and the equivalent heat capacity for the PCM. Experimental data are used to validate the numerical model, concerning convective coefficients and the hysteresis phenomenon.

Figure 2.11 illustrates the confrontation between experimental and simulated results for the outlet air temperature.

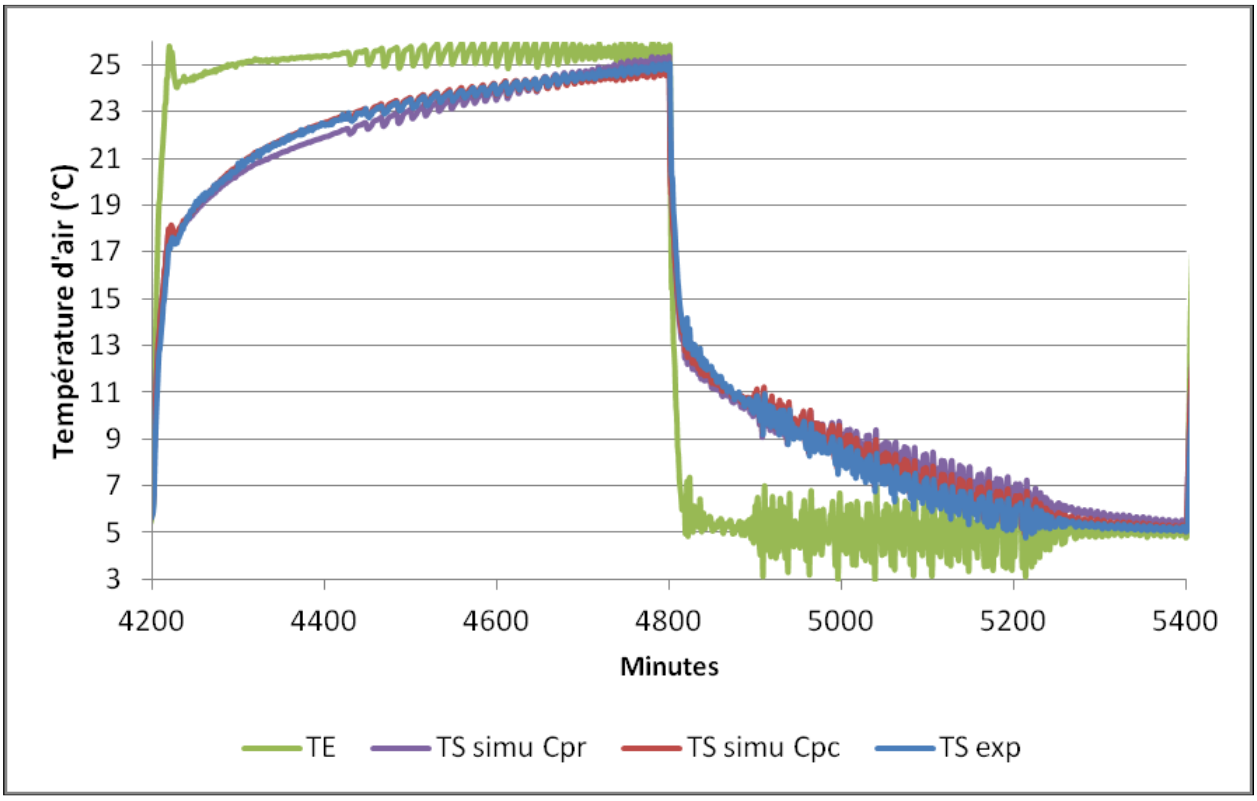

Figure 2.11: Outlet air temperature experimental and simulation results (Borderon et al.)

The validated model is then coupled to a TRNSYS model of house in order to evaluate the proposed system's behavior for different configurations and climates.

2.4.1.2 Zalba et al. system

Zalba et al. (2004) developed a system in order to test the performance of PCM in a cooling system that allows storage of outdoor coolness during the night, to supply it to the indoor environment during the day.

The proposed unit (figure 2.12) is a closed air circuit consisting of a fan for circulating the air, a device for heating and cooling the air at the desired temperature, a flow meter and the thermal energy storage system. The last one consists of flat plate rectangular encapsulation vesicles made with methacrylate to allow visualization of the phase change.

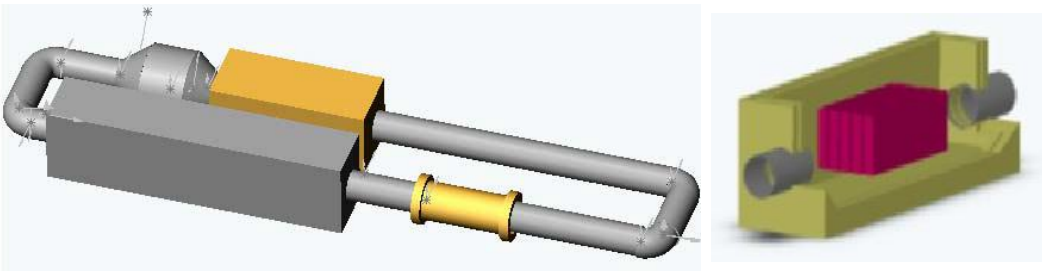

Figure 2.12: Zalba's et al. experimental set up (left) and heat exchanger unit (right)

Two PCMs were selected:

- A molecular alloy consisting of 34% C_{16} and 66% C_{18}, with a latent heat of 152 kJ / kg and a melting range between 19.5 °C and 22.2 °C.

- The RT25 Rubitherm paraffin, with a latent heat of 164 kJ/kg and a melting range between 18,8°C and 24,1 °C.

Inlet and outlet air temperatures were measured using five calibrated Pt100 sensors at the entrance and exit of the unit. Air flow was measured using a calibrated flow meter and customized software was used for data acquisition and evaluation.

The two following figures (2.13 and 2.14) show the experimental results for Zalba's et al. proposed unit. Figure 2.13 illustrates the exchanged heat and figure 2.14 the exchanged energy, both for the melting and solidification processes.

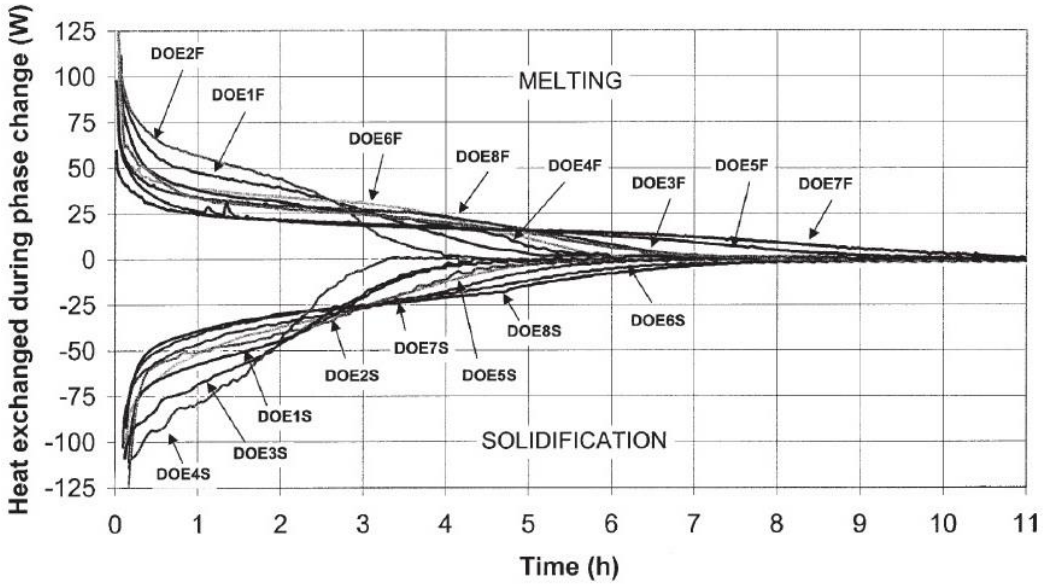

Figure 2.13: Zalba's et al. unit's heat transfer during phase change for different configurations

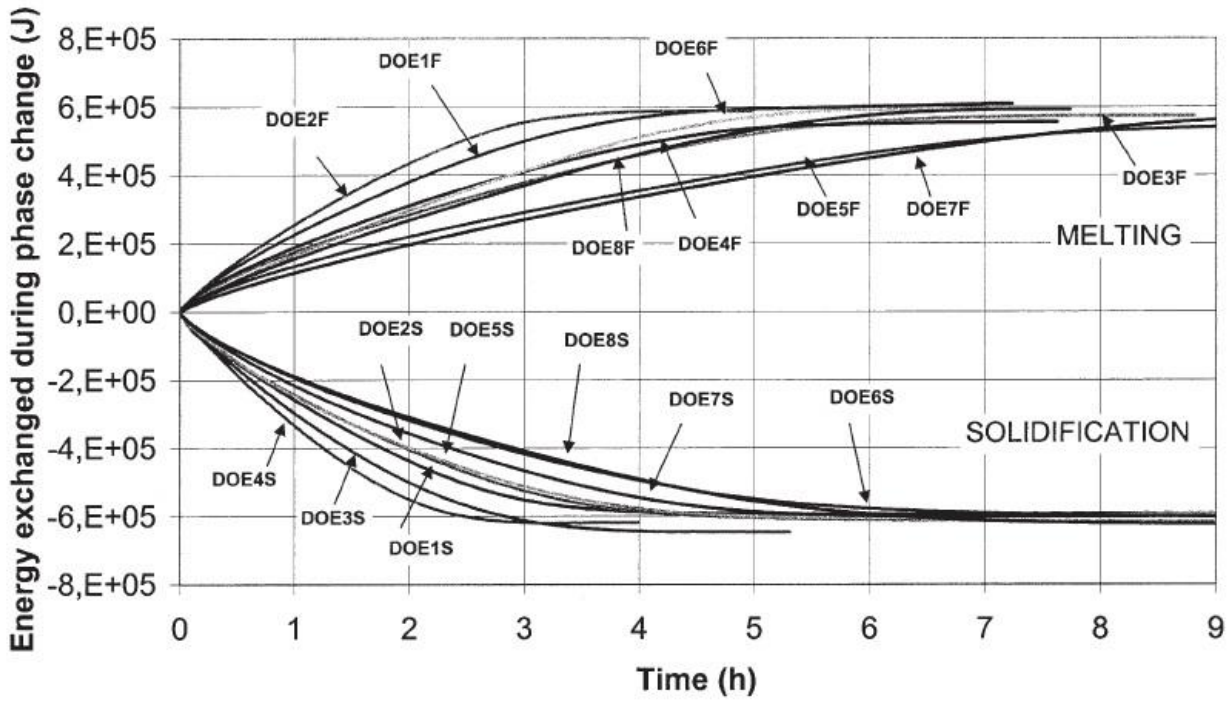

Figure 2.14: Zalba's et al. unit's heat exchange during phase change for different configurations

Studies performed on the designed system showed that for the solidification and the melting processes the most influential factors are the thickness of the encapsulate container, the inlet temperature of the air, the air flow, and the interaction thickness / temperature. The researchers also performed a viability analysis that showed that this kind of system can be developed in a real installation, regarding technical feasibility as well as economic advantages (when compared to existing cooling systems).

2.4.1.3 Arkar et al. system

Arkat et al. (2006) developed a latent heat thermal energy storage device in order to improve the cooling potential of a mechanical ventilation system. The device has a cylindrical form and is filled with PCM encapsulated spheres; the PCM used is the RT20 paraffin from Rubitherm GmbH.

For the optimization of the LHS device several parameters were taken into account: PCM characteristics, the ratio between PCM mass and airflow, and the ratio between the length and the diameter of the exchanger.

The developed heat exchanger prototype (figure 2.15) consists of a cylinder with a diameter of 0,34m and a height of 1,52m, filled with polyethylene spheres with a diameter of 50mm containing PCM. Arkar et al. investigated a system with two heat exchangers integrated in the mechanical ventilation system of a low energy building. The first heat exchanger was used for cooling the ambient air when it was hotter than indoor air temperature. The second one was used when additional cooling was needed, using re-circulated air when indoor air temperature was higher than a set point value.

Three operation modes were considered: a simple ventilation mode (constant airflow through the day), night cooling mode (increased airflow during the night) and free cooling mode (using the two heat exchangers).

Figure 2.15: Heat exchanger developed by Arkar et al.

Experiments were conducted in order to study the phase change process of the PCM and verify an adapted numerical model. Figure 2.16 shows the comparison between experimental and simulation results during charging and discharging phase.

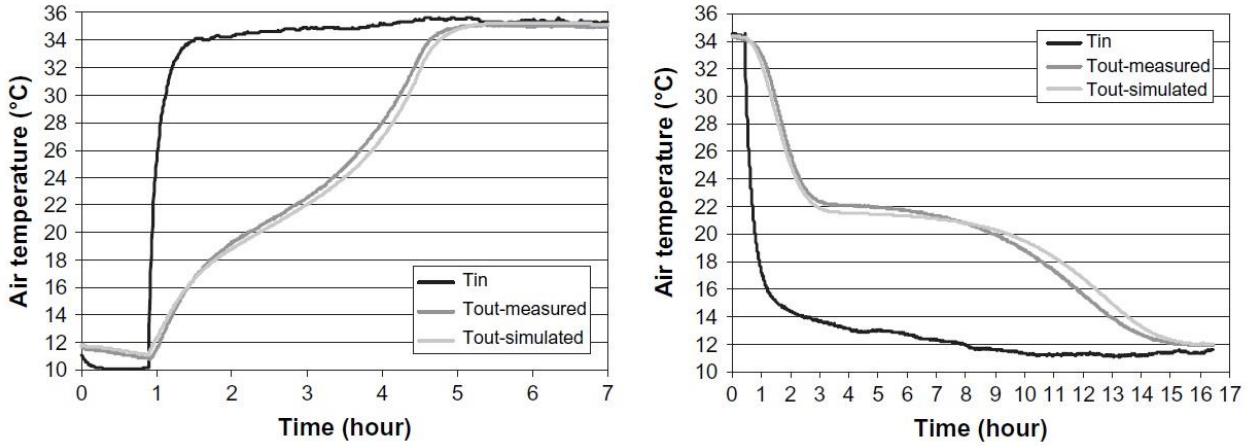

Figure 2.16: Experimental and simulation confrontation for the outlet air temperature of Arkar's et al. unit during the melting stage (left) and the solidification stage (right)

The model was then used to form a multi-parametric thermal response function that calculates the heat exchanger outlet temperature. Finally, a TRNSYS simulation program was developed, using the exchanger outlet temperatures as input and being able to predict the fresh or re-circulated air supply temperature.

With the numerical tool in hand, several simulations were performed altering the ventilation strategies, the air flow rates and the size of the heat exchanger. The investigation demonstrated the advantages of the proposed system in terms of reduction of the mechanical ventilation size, thermal comfort and fresh air supply.

As a perspective of their work, Arkar et al. mention the usage of the developed system during the heating season with the installation of a roof solar collector.

2.4.1.4 Nagano et al. system

Nagano et al. (2004) proposed a latent heat storage system, in which PCM granules consisting of porous media and paraffin wax are applied. In particular, the GR25 PCM made by Rubitherm GmbH was used to create granules in which paraffinic hydrocarbon was absorbed into granulated porous ceramics. The particle had a diameter from 1 to 3 mm and its composition was 65% ceramics and 35% paraffin wax by weight. The melting and the solidification points are 23.2 and 24.1 °C, respectively and latent heat is 45.3 kJ/kg.

The experimental setup (figure 2.17) consists of a cylindrical column made of chloroethene, with an internal diameter of 50 mm and a wall thickness of 5mm. The PCM granules were introduced in the column from 120 to 350 mm from the bottom. A constant air chamber supplied air to the bottom of the column with the use of an air pump. Passing through the PCM packed bed, the air was exhausted from the top of the column. A chloroethene plate with air holes was used to rectify it, placed at a height of 60 mm.

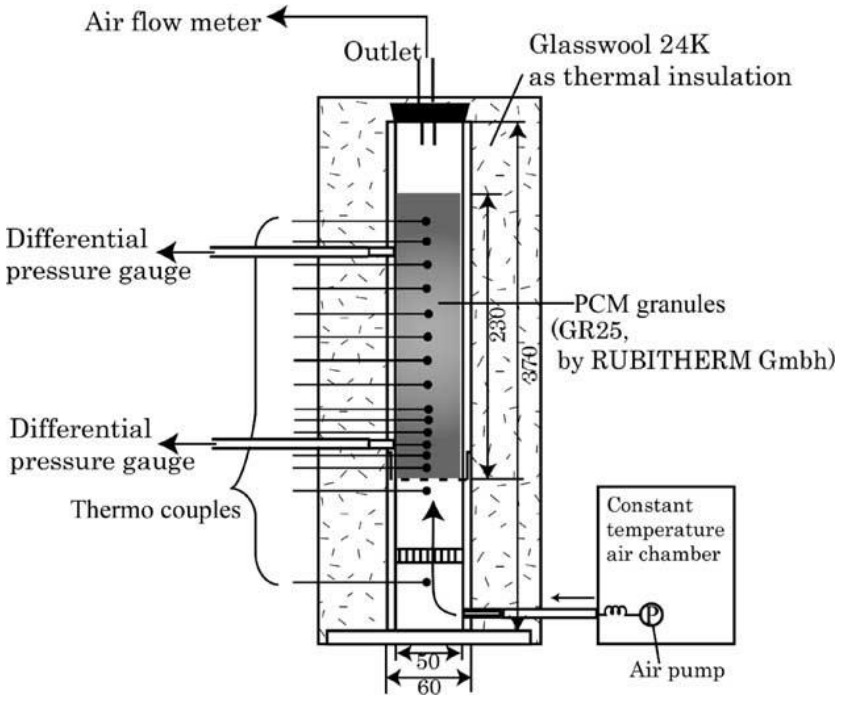

Figure 2.17: Nagano et al. experimental unit

PCM temperature measurement were performed using T-type thermocouples at 11 points and a propeller vane anemometer was used for air velocity measurements which led to air flow rate calculation.

Figures 2.18 illustrates temperature variations at different points of the PCM packed bed (1 cm interval) for various face velocities and supply temperatures.

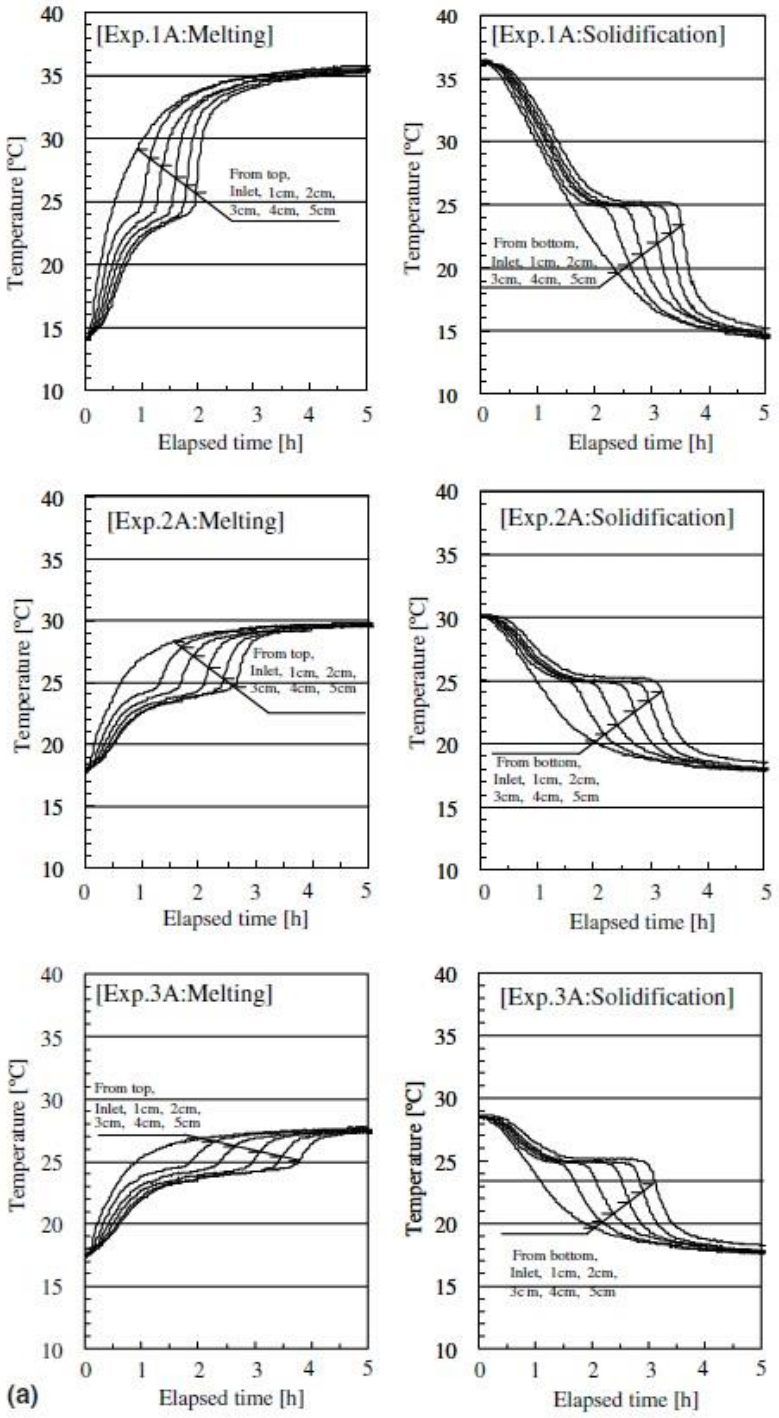

Figure 2.18: Temperature variation for different experimental configurations, Nagano's et al. unit

The experimental unit was used to observe the melting and the solidification process of the PCM and to verify DSC measurements. Further remarks were made considering the exchanged heat flux between the PCM granules and air. A numerical model was developed and validated with the use of experimental results.

2.4.1.5 Lazaro - et al. system

Lazaro et al. (2009) designed an experimental setup for free cooling purposes. Studies were made for different air to PCM heat exchangers, using a closed air loop setup to simulate indoor conditions. The developed system (figure 2.19, left) consisted of two different heat exchanger prototypes, an inlet air conditioner for various operating modes of simulation, air ducts and gates as well as numerous sensors to measure air/PCM temperatures and air flow.

The first prototype used aluminum pouches filled with an inorganic PCM (figure 2.19, right). A metallic grid was used to assure the vertical position of the apparatus. The air flowed parallel to the pouches from bottom to top. Tests with constant inlet air temperatures showed that the cooling rates were very low and that the total melting times were double the melting designed time. It was discovered that this was due to PCM leakage from torn pouches.

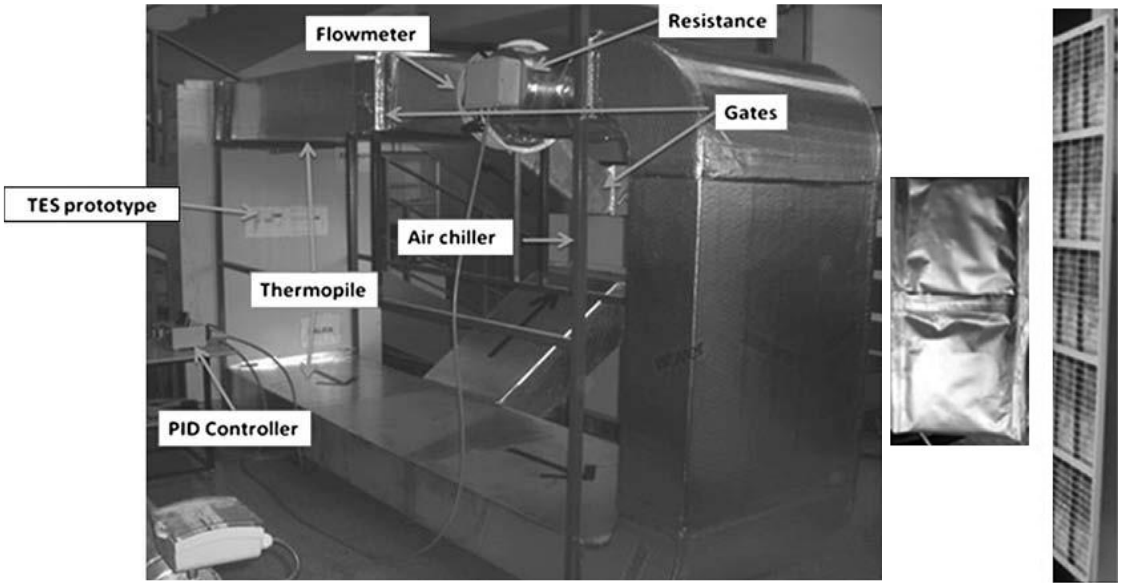

Figure 2.19: Lazaro et. al LHS system and first encapsulation method: aluminum pouches

In view of these events, a second prototype was developed using aluminum panels (as shown in figure 2.20) with organic PCM. As with the first prototype, the configuration was also vertical but this time air flowed from top to bottom. The PCM used for this configuration presented lower thermal conductivity than the first prototype and the total stored energy was also lower.

Concerning instrumentation, the inlet and outlet air temperature differences were measured with a six junction thermopile and air flow was calculated using fan velocity measurements. Inlet and outlet air humidity was also measured, showing a maximum variation of 0,006 kg/kg_{da}.

Figure 2.20: Lazaro et. al LHS second encapsulation method (aluminum panels)

The two following graphs (figure 2.21) show experimental results concerning the cooling rate for a constant rise of inlet air temperature and constant heating power. The second prototype resulted in a cooling capacity over 3KW for approximately 1,5 hour or approximately 1KW for more than 3h. This information can be useful when designing the optimal operation mode for different applications.

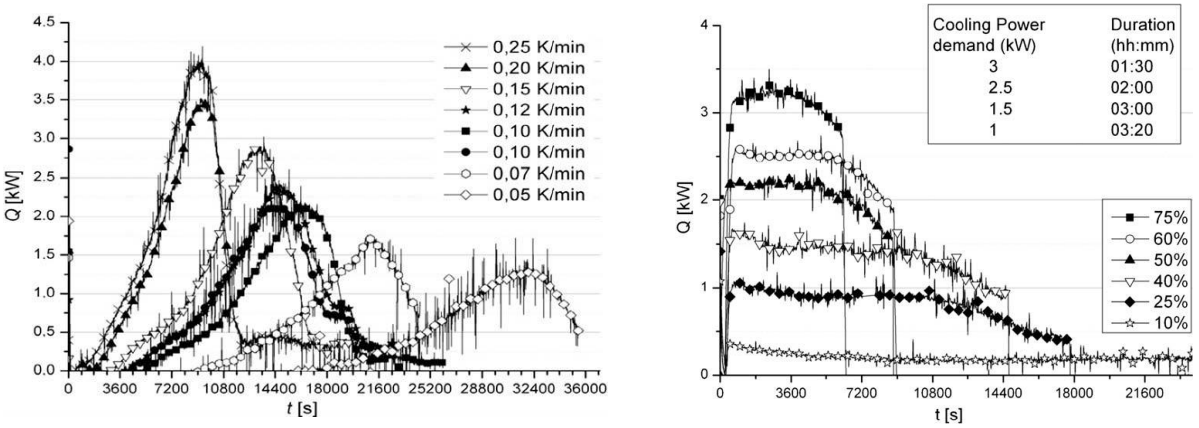

Figure 2.21: Cooling rate evolution with constant rise of inlet air temperature (left) and constant heating power for Lazato's et al. prototype 2

Lazaro et al. investigated two cases of LHS units. The second unit's optimized design led to higher cooling power and shorter melting rates. The researchers conclude that enhancement in the design of the heat exchanger can be more effective than the use of a higher conductivity PCM.

2.4.1.6 Dolado et al. system

Dolado et al. (2011) investigated the performance and thermal cycling of a real-scale PCM-Air heat exchanger. The unit in question was a modified version of Lazaro's et al. (2009, figure 2.19) experimental set up. Modifications included the creation of a single branch closed loop, the relocation of the chiller

and the removal of the second branch of the duct system and allowed the realization of thermal cycles (figure 2.22).

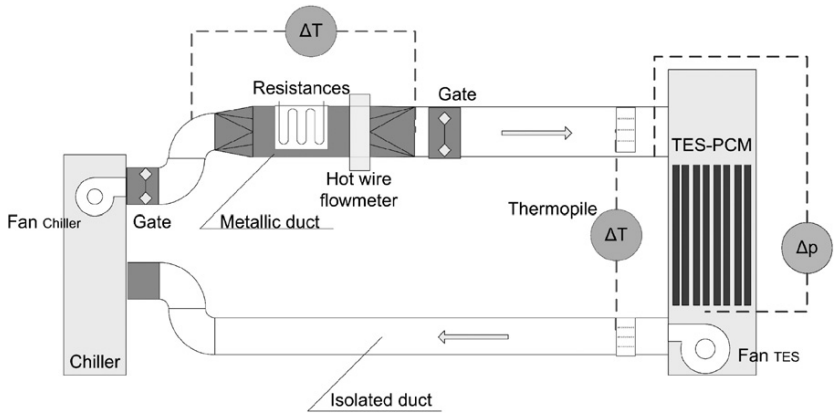

Figure 2.22: Dolado et al. modifications in Lazaro et al. system

Approximately 135 kg of the organic RT27 PCM were used in the LHS unit, macroencapsulated in 216 aluminum rigid slabs. These slabs were then assembled in a way to form parallels walls, separated by a 1 cm thick air layer. The LHS unit fan can be operated for three different speeds, varying from 675m^3/h to 1550 m^3/h, whereas the fun chiller was single speed.

Dolado et al.'s investigations led to the full thermal characterization of the LHS unit and the development of empirical designing tools. They observed the capacity of the proposed system to assure PCM solidification for specific time periods as well as the repetitive thermal cycling performance of the unit.

Figure 2.23 shows the evolution of the plate's surface temperature for a melting-solidification cycle. These temperatures were used as an indicator of the phase change advancement. A full melting process occurred in less than two hours with a 9.2°C temperature difference between inlet air temperature and average phase change of the PCM ($\Delta T_{air\text{-}PCM}$).

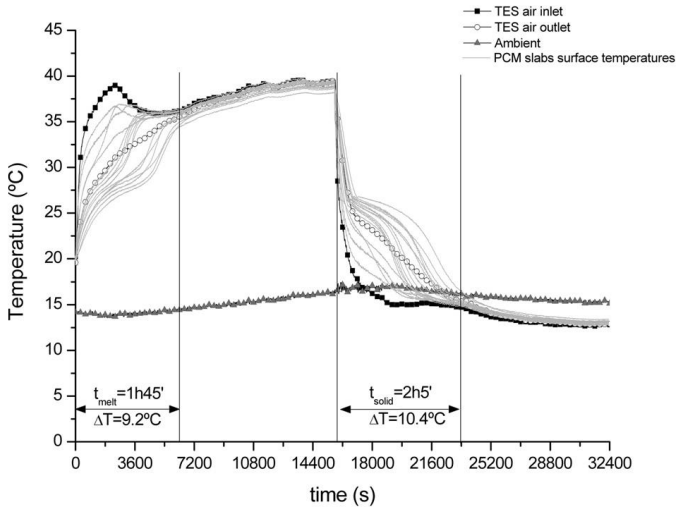

Figure 2.23: Inlet and outlet air temperature, ambient air, and surface temperature distribution for a full cycle of Dolado et al. proposed unit

Investigations were also performed for the evolution of the temperature of the PCM and encapsulation material for a single slab, with measurements occurring at three different points. The points are denoted as PCM Up, Middle and Down and Plate, Up, Middle and Down in figure 2.24. A 3°C temperature difference can be observed between PCM and surface temperature during the phase transition. It is noted that both melting and solidification processes start in the upper part and move towards the lower part of the plate.

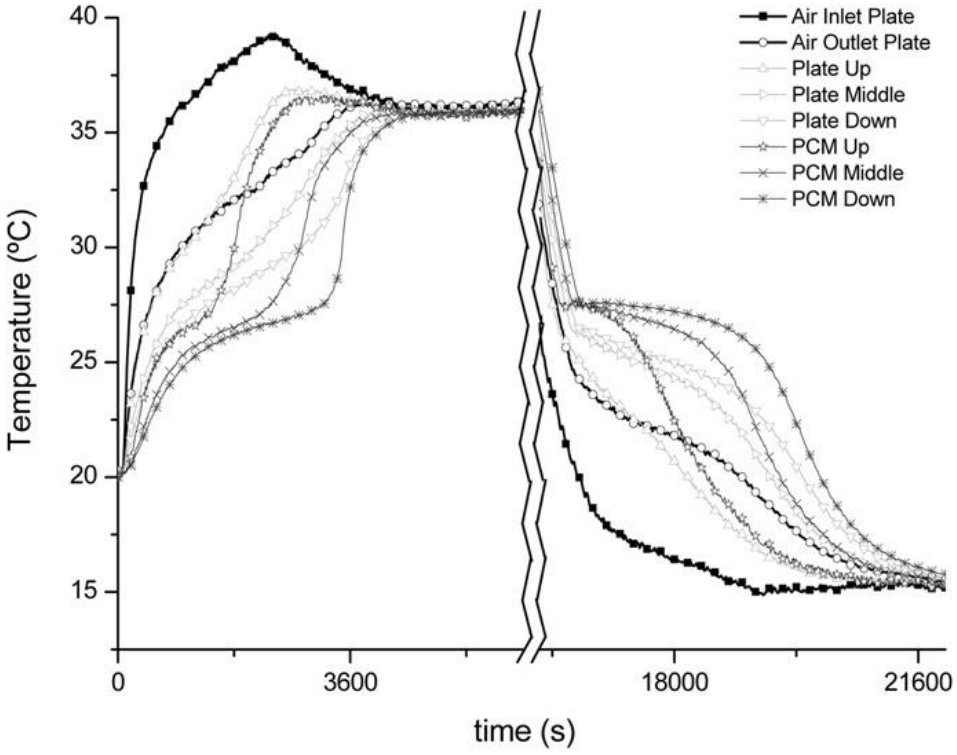

Figure 2.24: Air, plate and PCM temperatures of a single plate for a full cycle, Dolado et al. proposed unit

Characterization results were used to develop rules of thumb and an empirical model that can be used for LHS designing purposes.

Parallel to that, the experimentally obtained results also served for the validation of a numerical model aiming to be used as a designing tool for different applications of LHS systems.

2.4.1.7 Lin et al. system

Lin et al. (2007) developed a PCM based floor heating system with fan assistance for heating and peak power reduction purposes. Their aim was to surpass the limitations of a passive under-floor heating system by adding thermal storage to it.

The system was integrated in an experimental house and consists of an insulation layer (polystyrene120mm), electric heaters, PCM (15mm), an air layer (50mm), floor cover material (40 mm), cylindrical supports, air inlets and air outlets with fans (figure 2.25).

Figure 2.25: Lin et al. experimental house and enhanced floor heating system.

The PCM used consisted of 75% paraffin and 25% polyethylene; the fusion point of paraffin is 52°C and its heat of fusion is approximately 200 kJ/kg.

Concerning instrumentation, 18 thermocouples were used in order to measure air temperature at different heights and places of the house and a data logger was used for their recording. The tracer gas technique was used to calculate the air exchanges per hour and solar radiation was measured with a thermal radiometer.

The thermal behavior of the heating system and the instantaneous indoor temperature of the room were investigated. The operating principle was as follows: for a period of five days the electrical heating system was turned on and for the next five days they were turned off. For the first five days the electrical heaters worked from 23:00 to 07:00 and were shut down for temperatures higher than 65°C and for the period 07:00 to 23:00. Measurements were made for the indoor and outdoor temperature, solar radiation and electricity consumption every 5 minutes. Air outlets and inlets were opened and the air supply fans were operated from 09:00 to 16:00.

Results demonstrated that indoor temperature can be effectively increased with the use of the enhanced air supply during the working hour period. Total electrical energy consumption was shifted from peak to off-peak period, resulting in important economic benefits due to lower night electricity cost.

A previous numerical model was modified for this case study. With the use of experimental data investigations were made concerning the influence of various factors such as air supply velocity, thickness and fusion temperature of the PCM, thermal conductivity coefficient, heat of fusion as well as floor and air layer thickness. Indoor air temperature was calculated while changing one of these factors at a time, the final goal being to optimize the system's design for different conditions.

Figure 2.26 illustrates the comparison between experimental and simulation results of the indoor air temperature with (b) and without (a) air supply, and of the PCM surface temperature with (d) and without (c) air supply.

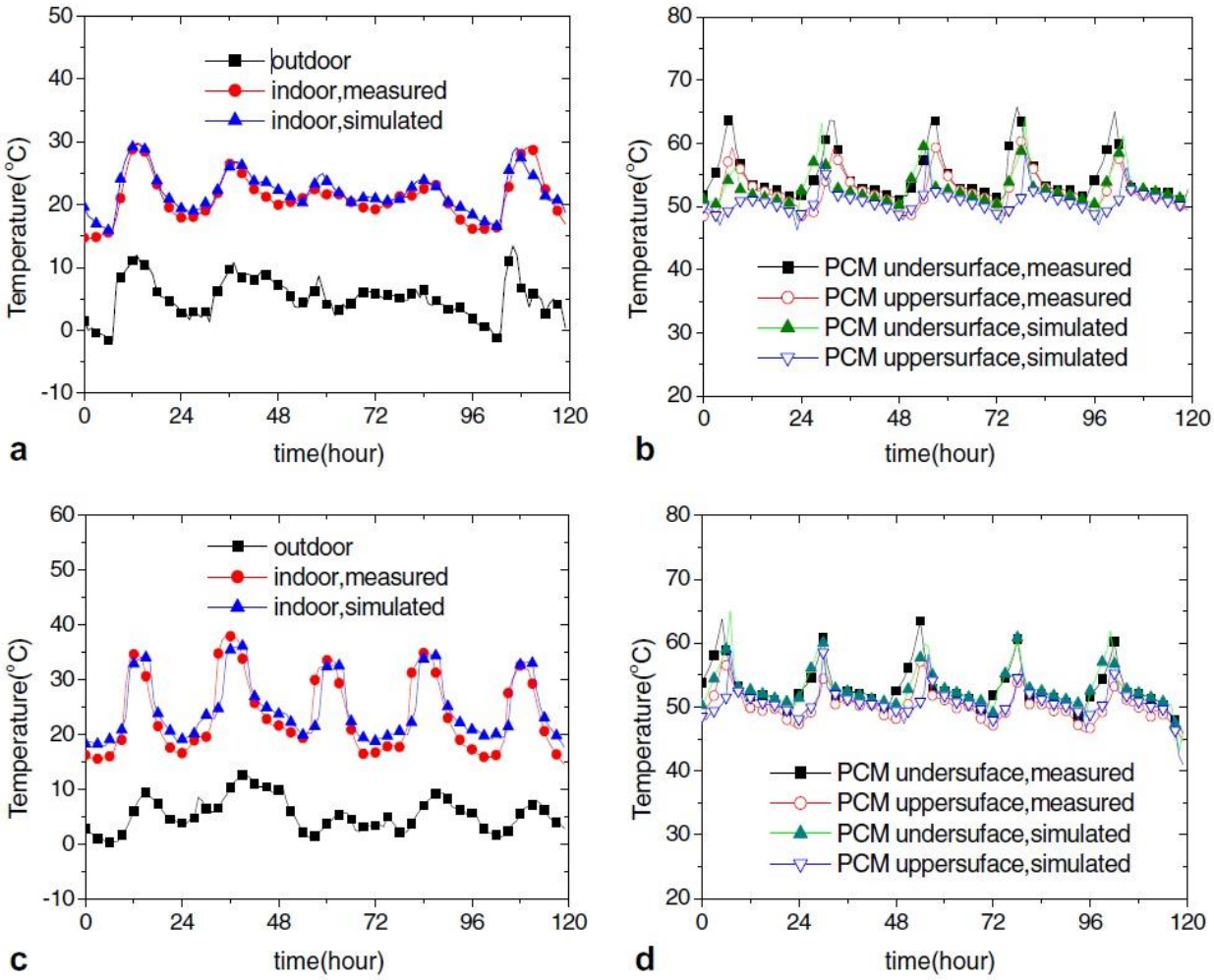

Figure 2.26: Lin et al. experimental vs simulation results for different configurations (a) indoor temperature without air supply, (b) indoor temperature with air supply, (c) PCM surface temperature without air supply and (d) PCM surface temperature with air supply

In the end, Lin et al. stated that their study showed the promising perspectives of the proposed system for different climate regions while providing simple and effective design and control methods.

2.4.1.8 Turnpenny et al. system

Turnpenny et al. (2001) proposed a cooling ventilation system aiming to reduce energy and economiccosts. The prototype consists of a number of PCM embedded heat pipes, circularly installed and mounted on a support; a fan is also installed in the center of the circle, just above the heat pipes (figure 2.27).

Figure 2.27: Turnpenny et al. LHS unit, overall view (left) and heat exchange pipes (right)

The PCM used is the Na2SO4.10H2O salt with a melting temperature of 21°C and a latent heat fusion of 198KJ/kg.

The operating principle is as follows: during the night cool air was directed towards the upper part of the unit with the use of a movable board. The ceiling fan blew this air downwards so as to pass over the heat PCM pipes and cool them. During the day, the ceiling fan was also used to blow air downwards, cooling it while it passed through the exchanger unit and absorbing internal and external heat gains.

Two PRT sensors on each side (unit and control) were used for temperature measurement and another one was placed outside of the vent. Three stainless steel thermistors were placed in the heat pipe-PCM unit in order to supply spot PCM temperatures at three different distances from the container wall. In this way, it was possible to estimate the phase change process. Air speed was measured by a movable hot-wire anemometer.

Figure 2.28 illustrates the results obtained over a 32 hour period for average PCM temperature, average room temperature and external temperature. Figure 2.29 shows upstream-downstream and upstream-PCM temperature difference. In both cases, the first cycle was performed with a 1 kW heat input and the second with a 2 kW one. Complete melting is assumed to occur when the mean PCM temperature rises above 23°C; with a 2°C difference between inlet and PCM temperature complete melting occurs after an 8 hour period whereas with a 3.5°C difference the time needed is 3 hours.

Studies were made to assess the overall cooling performance of the unit during the summer, including temperature monitoring, melting behavior of the PCM, cooling potential, tilting and covering of the heat pipes, different air passage configurations and heat transfer rates measurements.

Results showed that the system managed to ensure an adequate rate of heat storage and prevented overheating phenomena for a typical UK summer climate.

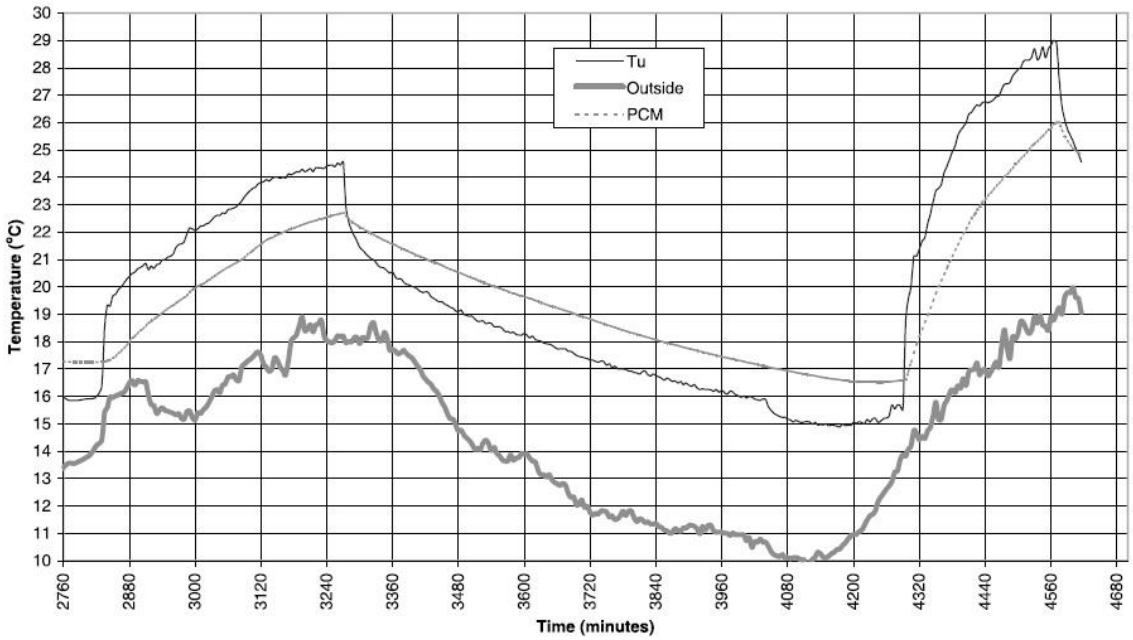

Figure 2.28: Air, PCM and external temperature for 1 and 2 kW heat input, Turnpenny et al. LHS unit

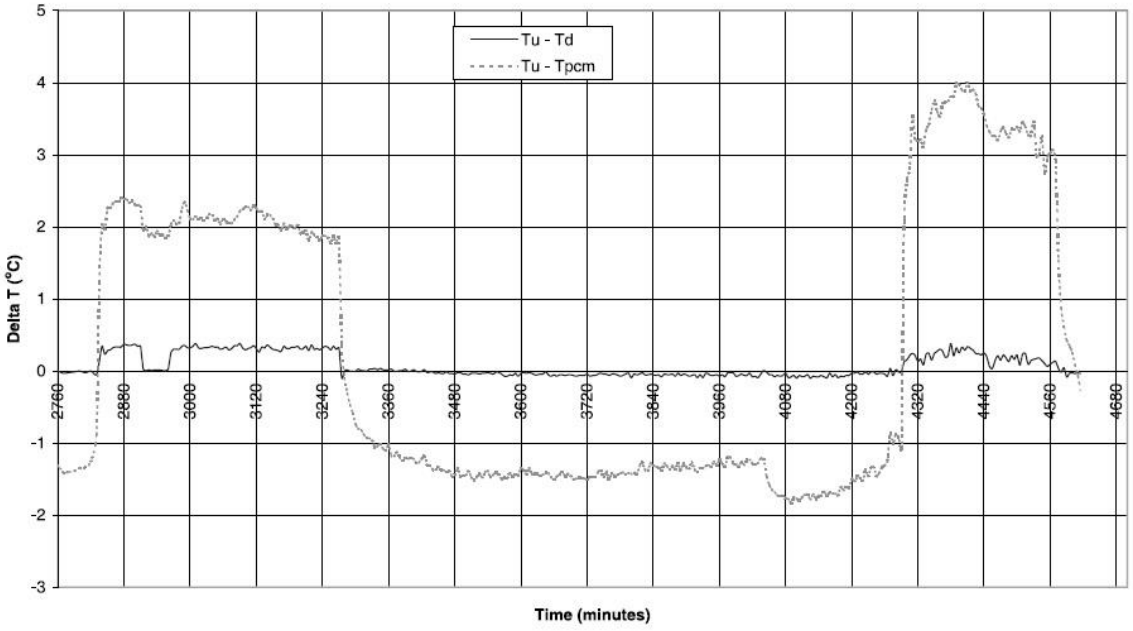

Figure 2.29: Upstream-downstream and upstream-PCM temperature difference for 1 and 2 kW heat input, Turnpenny et al. LHS unit

2.4.2 Comparative table of existing studies

Heat exchanger system	Compared Parameters			
	Objective	**PCM (Choice and encapsulation)**	**System integration in the building**	**Model**
Borderon et al.	Free cooling	Energain®, (60% microencapsulated paraffin in an ethylene based polymer) / Macro	False ceiling	Implicit finite difference method
Zalba et al.	Free cooling	Molecular alloy (C_{16} and 66% C_{18}) and RT25 Rubitherm paraffin / Macro encapsulation	-	Empirical
Arkar et al.	Free cooling	RT20 paraffin Rubitherm	Mechanical ventilation system	Finite difference method
Nagano et al.	PCM performance and numerical model validation	Paraffin GR25 Rubitherm and porous media / Macro encapsulation	-	Enthalpy method
Lazaro et al.	Free cooling	Inorganic PCM / Macro encapsulation	-	-
Dolado et al.	Characterization of the unit and empirical designing tools elaboration	Organic RT27 Rubitherm / Macro encapsulation	-	Empirical
Lin et al.	PCM enhanced floor heating system	75% paraffin and 25% polyethylene	Floor	Enthalpy method
Turnpenny et al.	Free cooling	Na2SO4.10H2O salt	Ceiling	One-dimensional mathematical model

Table 2.4: Comparative table of the different LHS units

2.5 Design and operation of active LHS ventilation systems

The presentation of eight active LHS examples was performed in order to study existing experimental and numerical studies and draw interesting remarks and conclusions, useful for the elaboration of this thesis. In this section we try to summarize all the necessary information concerning the design and operation of such systems.

2.5.1 Main elements of an active latent heat storage system

LHS systems are usually composed of four basic elements:

- The heat exchanger that contains the macroencapsulated or microencapsulated PCM; it is the main component of the system and the place where heat/cold is stored in latent (and sensible) form.
- A circuit that allows the flow of the heat transferring fluid (mostly air, sometimes water).
- An electrical or solar heat source that is used to heat the circulating fluid.
- A fan or a pump that regulates the flow of the circulating fluid in the system.

In addition to these elements, various sensors are usually installed in different part of the system in order to investigate the inlet/outlet air temperature, PCM temperature, airflow etc.

2.5.2 Operation principles

LHS applications are usually used to enhance the cooling or heating performance of mechanical ventilation systems and for peak power reduction needs.

Cooling of the building

During daytime, hot air flows through the heat exchanger at a higher temperature than the PCM's melting point. The PCM, initially in its solid form, absorbs heat from the air while obtaining its liquid form. The cooled air is then reintroduced into the building. In order to solidify the PCM, during the night exterior air is circulated at a temperature lower than the PCM's melting point.

Heating of the building

The principle is the same but the process is reversed. During daytime, hot air originating from the interior of the building or produced from a solar or electrical power system, flows through the heat exchanger of the LHS system and provides heat by melting the PCM. When heat is needed, cold or interior air is forced through the exchanger, capturing heat from the PCM, while solidifying it. The heated air is then reinjected into the building.

Peak power reduction

For both cooling and heating applications, the active thermal energy storage systems can be operated in view of reducing peak power consumption. Heat or cold is stored in the developed system during an off-peak period, preferably during the night (for lower electrical cost) or during the time when the COP of a heat pump is optimum (for example, when indoor and outdoor temperature difference is minimal).

Control strategies can be developed in order to predict the cooling/heating needs of the building and adjust the usage of the system accordingly.

To sum up, the latent heat storage systems can be integrated into any mechanical ventilation system. The benefits of such technology can be summarized as follows:

- ✓ Storing larger amount of energy per unit mass which allows a smaller temperature swing (better thermal comfort)
- ✓ Utilizing storage energy produced from passive or active solar heating/cooling and waste heat which comes from exothermic processes;
- ✓ Enabling the use of energy at lower cost during off-peak periods for storage and discharge at times when full rate would otherwise be charged.
- ✓ Allowing the use of a smaller HVAC system size and more efficient operation
- ✓ Reducing furnace/heater cycling

2.5.3 Design philosophy of a LHS system

This section tries to summarize the various parameters that influence the design philosophy of a TES active system.

One of the most important factors when designing such a unit is that the developed system must ensure a maximal heat exchange rate between the heat transfer fluid (air) and the latent heat storage medium (PCM). In general, one must bear in mind that the available periods of time for the solidification/fusion of the PCM can be limited. The geometry of the heat exchanger as well as the choice for the PCM storage (microencapsulation or macroencapsulation) play a significant role in this matter. Materials with high conductivity are preferred, as long as their price is not too high. In some of the macroencapsulated cases, fins have been used to enhance heat exchange between the air and the PCM container. The geometry of the heat exchanger also affects the pressure drop of the LHS system and as a result, the air pumping requirements and the electrical energy consumption.

The design of a LHS system also highly depends on the heat storage needs of the place where it is installed. Different PCMs with higher or lower latent heat values can offer solutions in this matter.

PCM thickness and airflow rates are also important aspects to take into account. Researchers often realize experimental and numerical studies to determine the optimized values for these parameters.

Another important factor is the size of the designed unit; smaller units are preferred as they can be implemented more easily in the building (in ventilation shafts, false ceilings, etc). A compromise must be found between heat storage capacity and the size of the proposed unit.

Attention must be given to the viability of the system, knowing that some PCMs present corrosive properties. In addition to that, the proper containment of the PCM can be a difficult task as dilatation is observed between phase changes. In some case studies PCM leakage has been observed due to this phenomenon (Lazaro et al., 2009).

When storing heat in the unit, it is important to consider the outlet air temperature due to risks of overheating the coupled building. A solution to overcome this issue can be the use of a closed loop air circuit or specially conceived control strategies.

The implementation of an LHS system in an inhabited building raises some more aspects to consider: fan noise, PCM odors or fire hazards will not be accepted by the occupants.

LHS system design is an elaborate task with various and controversial factors to consider. Experimental and empirical/numerical studies are useful tools for the development and further improvement of such units.

2.5.4 Design Methods

In the introduction to this chapter, the benefits and the increasing need of LHS systems were discussed, either as passive components of the building or active ones. In both cases, the development of advanced design methods and tools is needed, with the perspective of a better coordination between building and LHS design. This will lead to a more efficient integration (hence a better exploitation) of advanced LHS systems and can contribute towards the overall goal of net zero energy buildings.

The study of several LHS units integrated into HVAC systems which is performed in the latter part of this chapter, shows a lack of knowledge and design tools for a global and/or mutual concept of building and LHS system. Researchers have proposed experimental units together with empirical or numerical models. The models are then used for further amelioration of the unit and the investigation of different configurations. In some cases the models are coupled with building simulation programs (TRNSYS, EnergyPlus,…) for a more global approach . However, in most case studies, the outcome of the research focuses on the specific unit and cannot be expanded to a generalized context of integration of LHS systems in the building. This is due to the dependence of the proposed models on the characteristics of each study, in terms of the LHS unit (dimension, building integration, PCM properties: non-linear behavior, moving liquid-solid fraction, ...), as well as the experimental site (heating/cooling demands, dimension, insulation, usage, occupancy, …).

Further research could be made in this area, taking into consideration the large number of parameters covering the integration of LHS units into the buildings. The ultimate goal is to develop new and validated design tools that can cover the whole system Building + LHS system.

2.6 Conclusion

PCM technology has been studied and used in researches for over three decades in the built environment for heat storage purposes. The benefits of tis implementation in the building in terms of thermal comfort conditions, energy consumption and peak shifting have been demonstrated through a number of publications.

This chapter, presented various substances used as PCMs , along with information concerning their containment, enhancement techniques, limitations and implementation in the building. The interest of

this study lies lied in HVAC integrated heat storage systems and in that perspective several case studies were presented. The remarks that were noted were used as a guide for the development of an experimental PCM-Air heat exchanger and are presented in the following chapter.

Chapter 3

Development of an experimental PCM-Air heat exchanger

Chapter 3 : Development of an experimental PCM-Air heat exchanger

3.1 Introduction

The study presented in this thesis aims to provide solutions to the problem of increasing peak power demand in France. As discussed in the previous chapter, one of the possible solutions lies in the storage of heat into an exchanger unit and then using it to shift the consumption linked to electrical heating to an off-peak period.

This chapter describes in detail the development of such a system: TES technology choice, design considerations, components, instrumentation, data acquisition and assembly of the unit. In a second phase, a series of characterization tests is illustrated in order to obtain an overview of the system's behavior through different conditions. Finally, the coupling of the developed system to an experimental room is presented along with a preliminary control strategy.

The development of the experimental system is necessary for the validation of the numerical model (described in chapter 4) and in a later phase for the implementation of control strategies in realistic scenarios.

3.2 Experimental set up description

3.2.1 Thermal energy storage as a solution

In association with the Stock Air project a specific need was identified: developing an experimental unit that can store a sufficient amount of heat in order to substitute the elevated electrical heating consumption.

More specifically, the application was conceived for a low energy dwelling, in a way that it could be easily integrated into a HVAC system and be able to provide a power supply of 2KW over a period of 2 hours, which corresponds to the late afternoon (18:00-20:00) peak power demand.

These objectives resulted in a number of design considerations, sometimes conflicting with each other. They can be depicted as follows:

- ✓ Small volume (for HVAC integration)
- ✓ Sufficient energy storage to satisfy the 4KWh need
- ✓ Specific operation temperature range
- ✓ Elevated heat transfer for a rapid stocking/destocking process
- ✓ Rigid structure that will not affect or degrade the occupants' comfort/health

Among the available energy storage technologies presented in chapter 2, thermal storage was chosen as the one that best fits these considerations. Furthermore, PCM technology was decided to constitute the storage medium as it offers an increased heat storage to volume ratio.

3.2.2 Elaboration of a PCM-Air heat exchanger

The above considerations led to the need for the development of a PCM – Air heat exchanger that will constitute the central element of the experimental setup and the place where the heat storage will occur.

An analysis was performed by EDF laboratory Matériaux et Mécanique des Composants (partner of Stock Air project), comparing the properties of various materials that could be suitable for the proposed unit. The paraffin Microtek 37D was selected due to its advantageous properties (table 3.1). In particular it presents a melting/solidification temperature range around 37°C, a dilatation of 10% between phases and a latent heat of fusion of 230 KJ/kg. In its solid form it is a white powder (figure 3.1) whereas when melted it becomes a colorless liquid. It presents a mild wax odor. It is fabricated by Microtek Laboratories, Inc. based in Ohio, USA.

State	Density ($kg.m^{-3}$)	Thermal conductivity ($W.m^{-1}K^{-1}$)	Heat capacity ($kJ.kg^{-1}K^{-1}$)	Melting heat of fusion / crystallization ($kJ.kg^{-1}$)	Melting/ crystallization temperature range (°C)
Solid	870	0.24	2.36	230	33 - 39,6
Liquid	779	0.18	2.45	226.8	35,5 - 30,3

Table 3.1: Properties of the Microtek 37D paraffin

Figure 3.1: Microtek 37D in solid form

The heat exchanger was designed so that it could be integrated into a HVAC system, for example in a ventilation plenum, a false ceiling or the ceiling over a corridor. In regard to this, its size had to be modest and was established as follows: 1,05m in length, 0,80m in width and 0,25m in height.

The paraffin is macro-encapsulated in 34 aluminum plates, typical screed boards used in construction and masonry, with a (1x0,10x0,018)m dimension and openings at the two extremities (figure 3.2). They were selected because of the high conductivity value of aluminum on one hand and its relatively low price and ease of access on the other hand. The paraffin was inserted in liquid form and the plates were sealed using wooden caps and an elastic glue. The plates were assembled by two and then placed parallel one to another (figures 3.4 and 3.5).

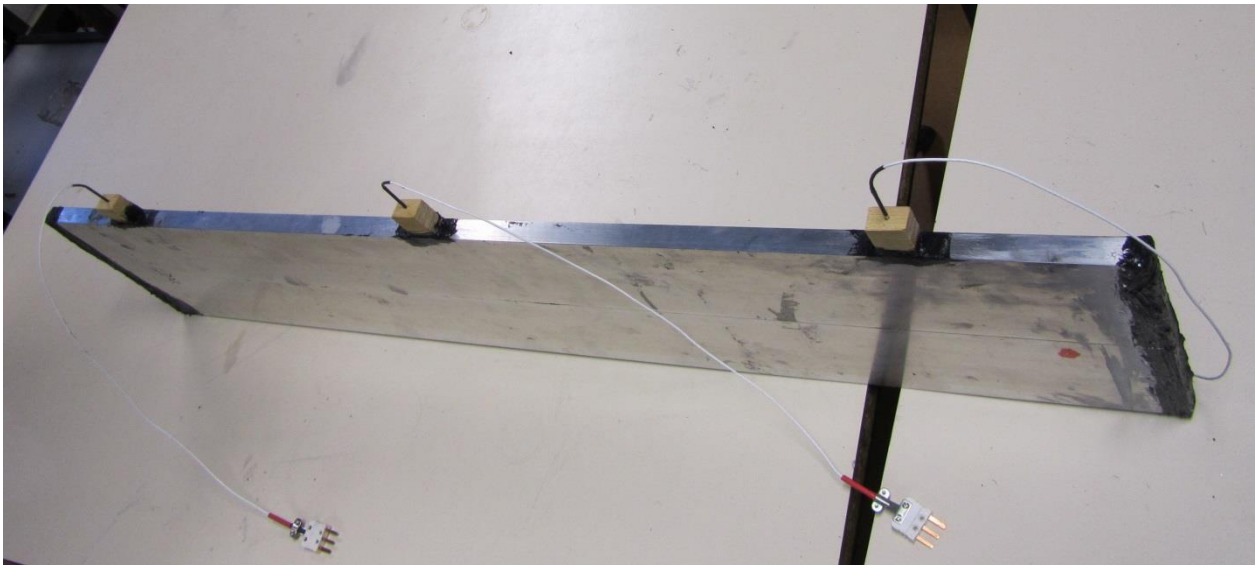

Figure 3.2: Aluminum plates used for PCM containment

Weight measurements were made before and after the encapsulation of the paraffin, in order to obtain the exact PCM mass. The result was a total of 31,44 kg of PCM (table 3.2).

Plate N°	Tare weight (g)	Laden weight (g)	PCM weight (g)
1	1572,5	3402	1829,5
2	1452,5	3282	1829,5
3	1452,5	3316	1863,5
4	1452,5	3284	1831,5
5	1452,5	3248	1795,5
6	1452,5	3377	1924,5
7	1452,5	3300	1847,5
8	1452,5	3322	1869,5
9	1642,5	3437	1794,5

10	1452,5	3325	1872,5
11	1452,5	3329	1876,5
12	1452,5	3377	1924,5
13	1452,5	3306	1853,5
14	1452,5	3295	1842,5
15	1452,5	3271	1818,5
16	1452,5	3322	1869,5
17	1572,5	3373	1800,5
		Total PCM mass:	31443,5 g

Table 3.2: PCM mass calculation

Aluminum fins, 0,019m thick, were introduced between the plates to increase the heat exchange (figures 3.3, 3.4 and 3.5). Three of the plates were equipped with additional pierced components that were used to introduce temperature sensors at variable depths inside the PCM, in three different parts of the plates: inlet, middle and outlet areas (figures 3.2 and 3.5). Polystyrene panels enclosed the PCM containers in order to thermally insulate it from the surrounding environment. Finally, wooden boards were used to assemble and ensure the stability of the structure (figures 3.5 and 3.6).

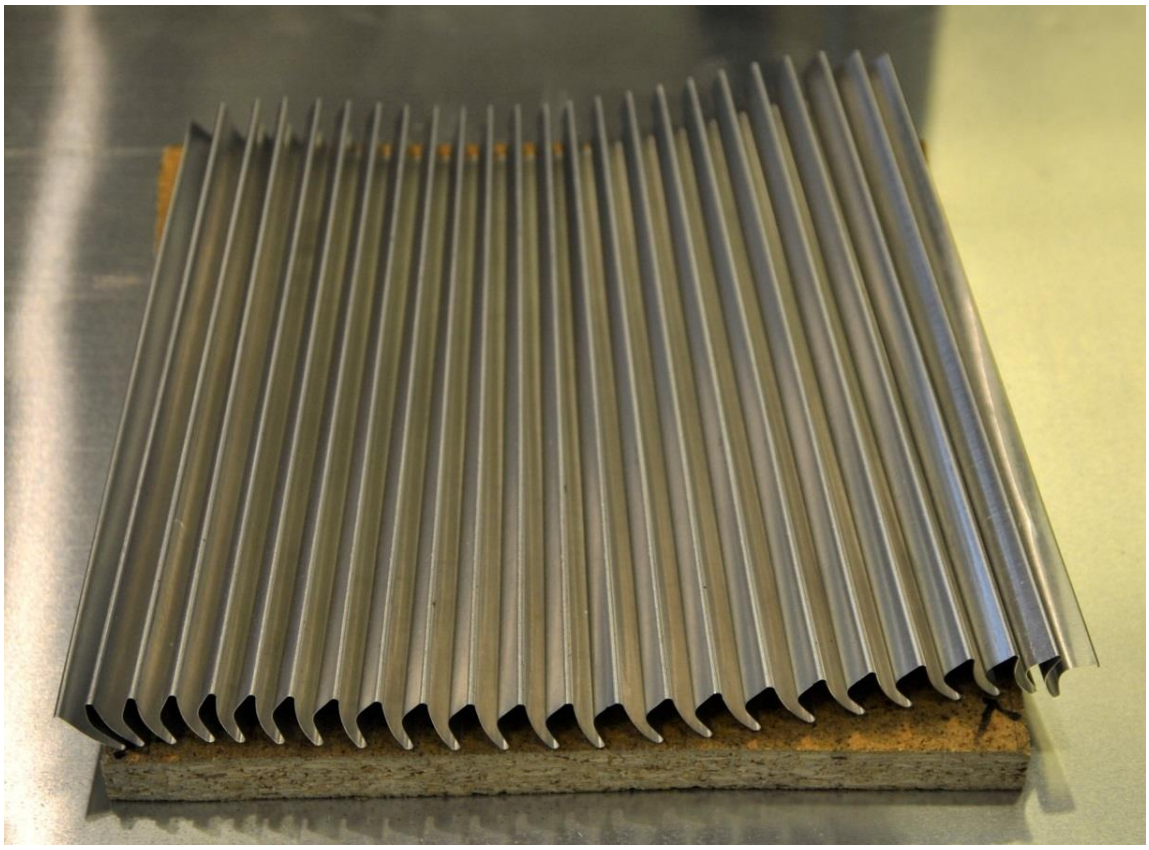

Figure 3.3: Aluminum fin

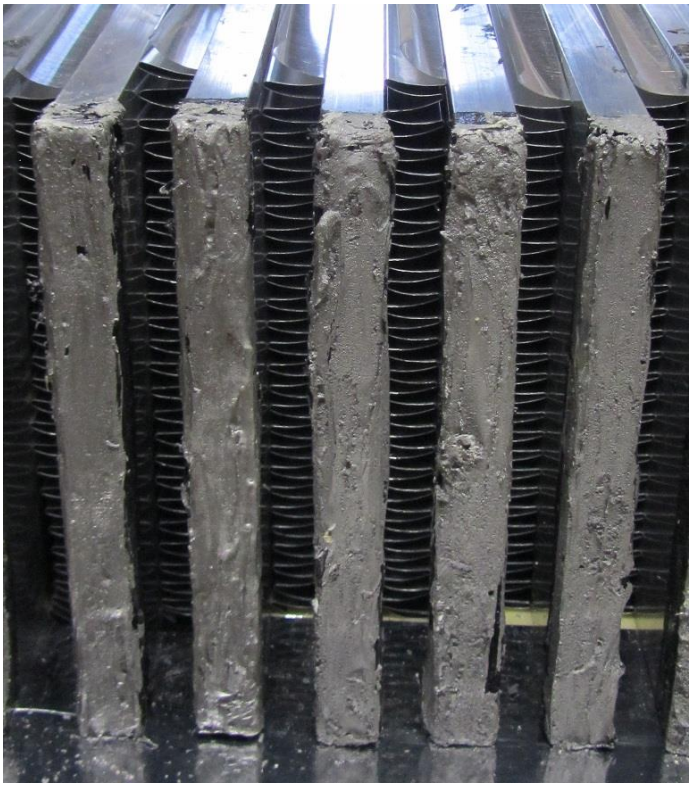

Figure 3.4: Fins between the PCM plates

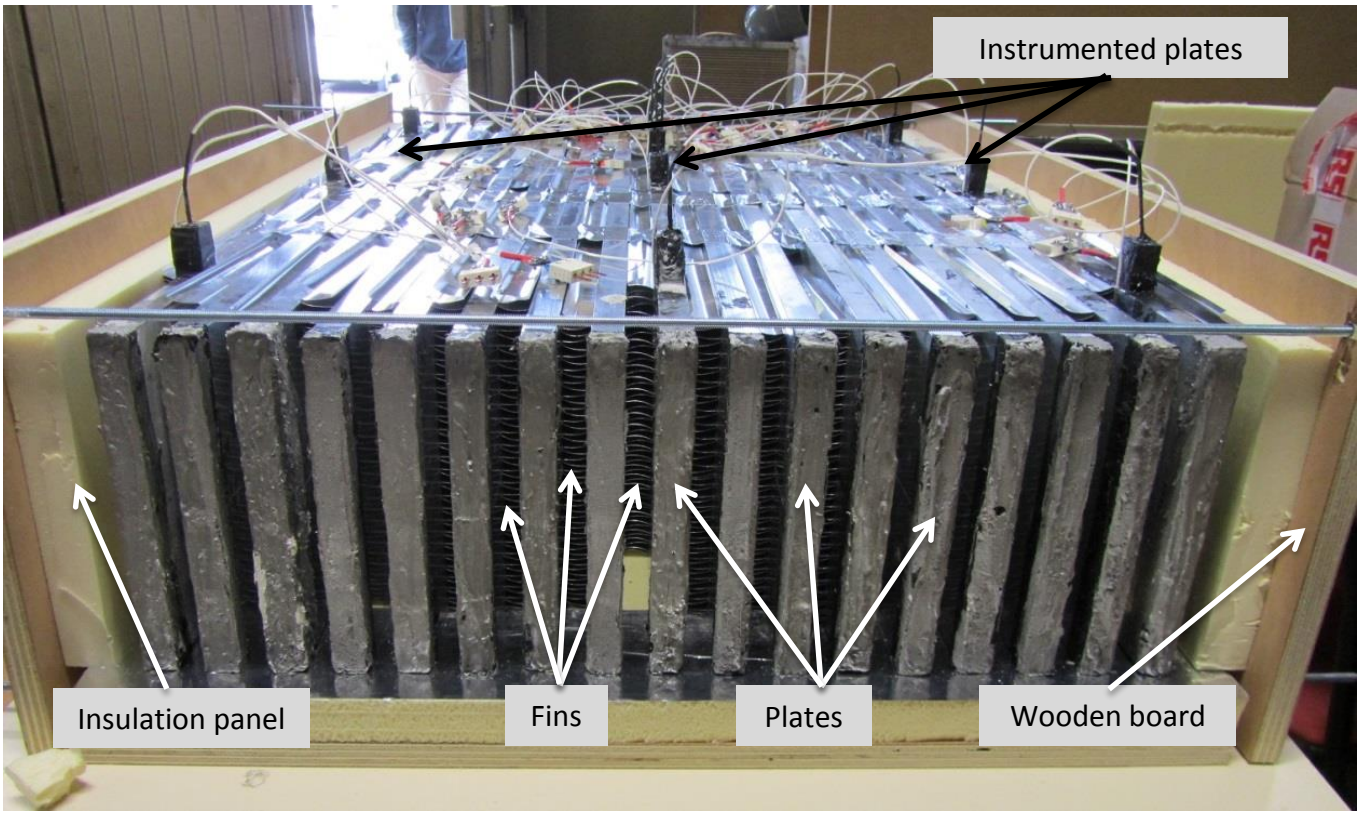

Figure 3.5: The heat exchanger during construction phase

Figure 3.6: The heat exchanger through the assembly process

3.2.3 Experimental platform

Furthermore, the utilization of the heat exchanger necessitated the construction of an experimental platform (figure 3.8), composed of the following components:

- Two centrifugal fans (controllable 0-10 Volts, maximum consumed power 121 W)
- Two electrical duct heaters (1KW each) with thermal protection (figure 3.9)
- An air diffuser and an air collector (fabricated out of wood) (figure 3.9)
- Several ventilation hoses and fittings to interconnect the previous elements
- An additional fan heater (2 KW) (occasional use for supplementary power)

The developed experimental platform ensures the circulation and heating of the air through the heat exchanger under specific conditions (temperature and airflow rate) and is used to couple the exchanger with a room or a building.

Figure 3.7: Electrical duct heater (left) and air diffuser (right)

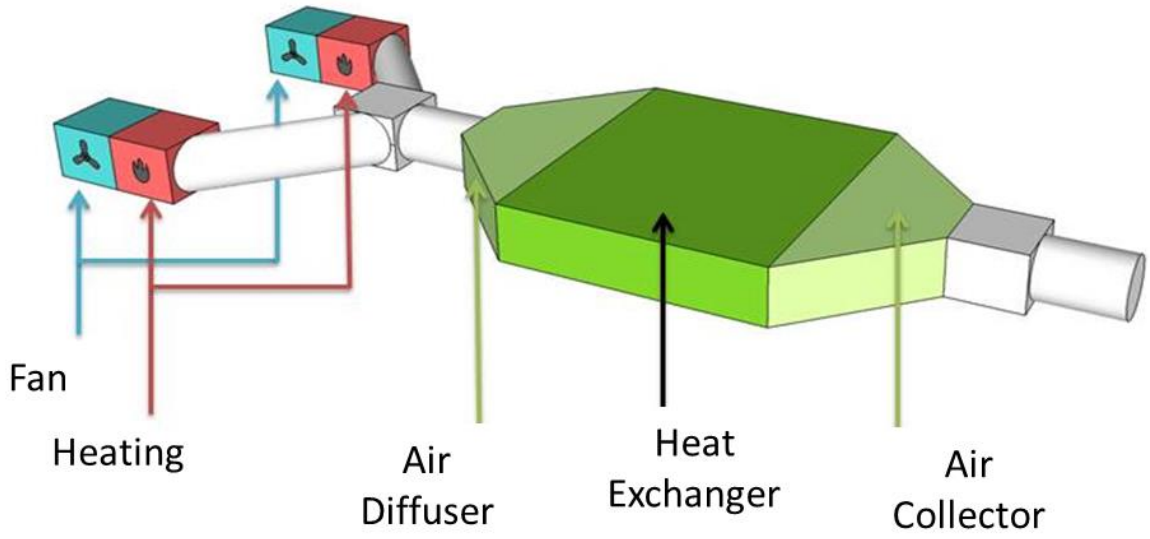

Figure 3.8: Experimental platform

3.2.4 Instrumentation, data acquisition and control-command interface

The use of the experimental platform necessitated the elaboration of a monitoring-control system. This system is composed of a chain of components that are used for the observation of thermal properties, data acquisition and control-command.

3.2.4.1 Instrumentation

Several sensors were installed in different parts of the platform and the heat exchanger, allowing to monitor the condition of the heat transferring fluid (air) and the heat storage material (PCM-paraffin).

Concerning the experimental platform, temperature and relative humidity sensors were installed before and after the heat exchanger in order to measure the inlet and outlet properties of the air. For the temperature measurement, platinum resistance temperature PT100 class A sensors were used (figure 3.9). They were selected due to their small cylindrical shape (1,6mm) and their precision (±0,15°C at 0°C, ±0,35 °C at 100°C). Relative humidity sensors offer a precision of ±2%.

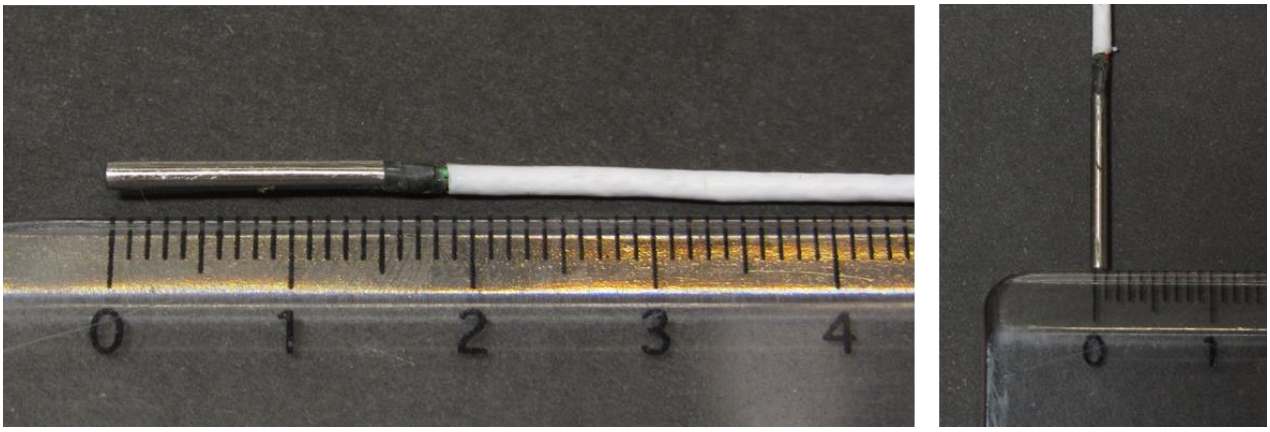

Figure 3.9: PT100 temperature sensor

The airflow rate measurement was performed at the outlet part of the exchanger using a Nozzle Pitot Flow Sensor, with a ±0,5% reading accuracy (figure 3.10). A Pitot Tube measures the fluid flow velocity based on the Bernoulli Equation, considering that no change in hydrostatic pressure (i.e. no elevation) occurs. The instrument performs pressure measurements at two points: one pointing at the moving fluid (static pressure, p_s) and one pointing at a position where the fluid is resting (stagnation pressure, p_t). Bernoulli's equation states that stagnation pressure is equal to the sum of the static pressure and the dynamic pressure (linked to the kinetic energy of the moving fluid) (3.1):

$$p_t = p_s + \left(\frac{\rho V^2}{2}\right) \qquad \text{equation 3.1}$$

Where V is the fluid velocity, p_t is the stagnation pressure, p_s is the static pressure ρ is the fluid density. The fluid flow velocity can then be calculated with the following equation :

$$V = \sqrt{\frac{2\cdot(p_t - p_s)}{\rho}} \qquad \text{equation 3.2}$$

Figure 3.10: Nozzle Pitot Flow Sensor

Concerning the heat exchanger, 3 plates were instrumented with temperature sensors at three specific points: inlet, middle and outlet part of the plate. Two sensors were installed for each point: one inside the PCM, allowing a direct measurement of the PCM temperature and one on the exterior plate surface. Regarding the PCM inserted sensors, small stainless steel tubes were used to avoid damaging risks and ensure proper and lasting positioning (figures 3.11). The three instrumented plates were placed on the middle and the two extremities of the heat exchanger (figure 3.5). Finally, temperature sensors were also installed on the exterior surface of each plate. These sensors were used to verify airflow uniformity and as a charging discharging indicator. The above mentioned temperature sensors are identical to the ones used for the air temperature measurement (PT100 class A).

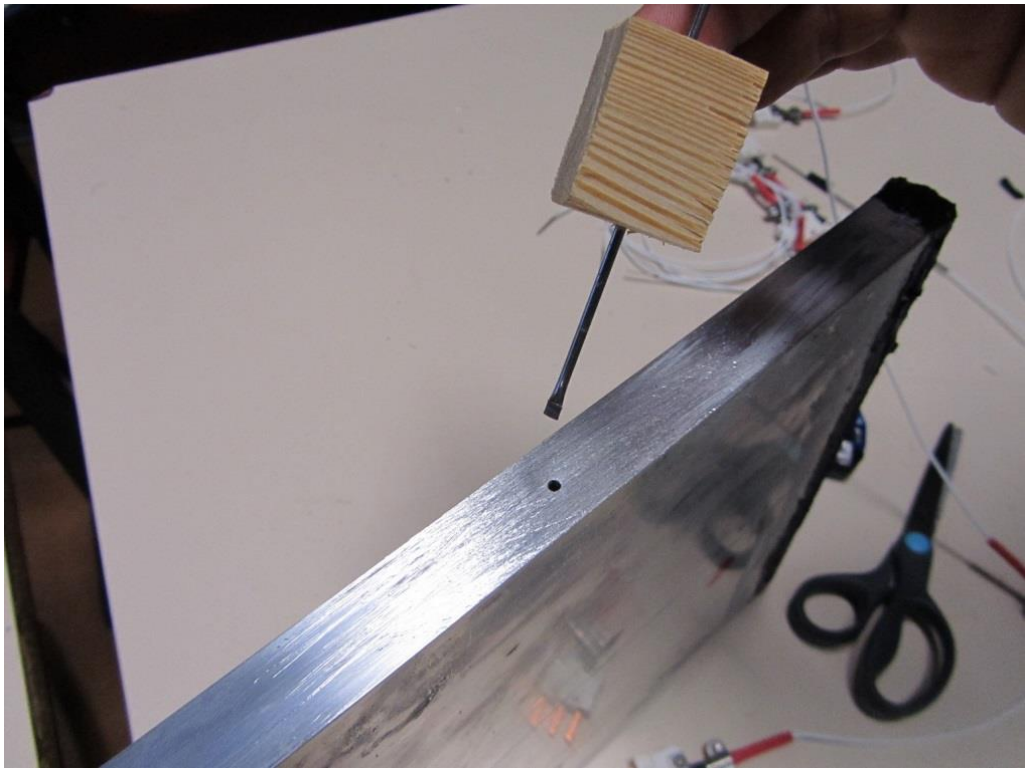

Figure 3.11: Insertion of temperature sensors inside the PCM

In conclusion, the instrumentation work was performed in order to provide all the necessary information concerning the fusion and the solidification of the PCM, the charge / discharge phases of the heat exchanger and the available stored heat.

Position	Physical parameter	Number of sensors	Accuracy
Heat exchanger	Temperature PCM Plate surface	 9 9+17	±0,15°C at 0°C ±0,35 °C at 100°C
Rest of the experimental platform	Air velocity Outlet part	1	±0,5% reading accuracy
	Relative humidity	2	±2%.
	Temperature Inlet and outlet part	2	±0,15°C at 0°C ±0,35 °C at 100°C

Table 3.3: Description of the instrumentation

3.2.4.2 Data acquisition and command interface

LabVIEW programming language and environment was used for data acquisition and control of the components of the experimental platform. The developed interface allows direct monitoring of air and PCM properties (figures 3.12 and 3.13), automation of characterization tests and elaboration of control strategies (figure 3.14).

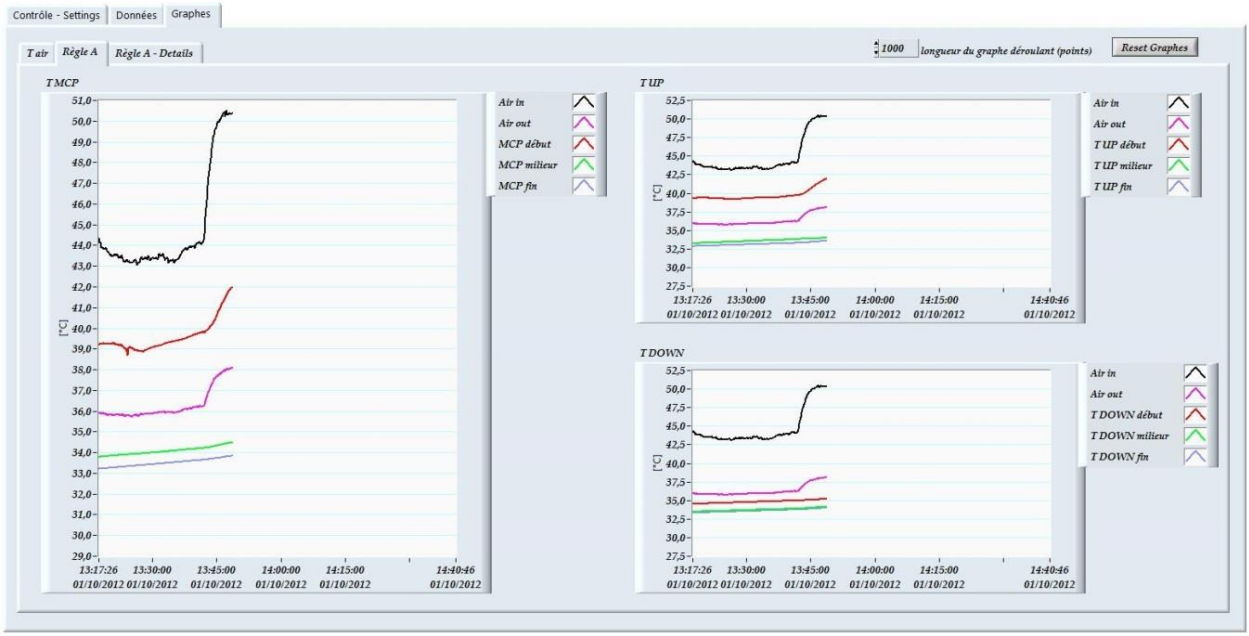

Figure 3.12: Air and PCM properties monitoring interface

The data logger is composed of 5 National Instruments Cards that are inserted in a Compact Daq modular system and connected to a PC through a USB port. The developed Labview interface performs data acquisition every 15 seconds. Several tabs were created, visualizing in real time the PCM properties at different parts of the heat exchanger (figure 3.13), as well as air properties (inlet-outlet air temperature, relative humidity and airflow rate) (figure 3.12). Furthermore, one tab presents the real time energy consumption in France as obtained by the RTE site (RTE) and another tab illustrates the characteristics of the PCM.

Power and energy consumption are also directly calculated from the acquired data and displayed on the interface. More specifically, the enthalpy of the air is calculated at the inlet and outlet parts of the exchanger with equation (3.3) (Albright, 1990):

$$H = 1{,}006 \cdot T + w \cdot (2501 + 1{,}805 \cdot T) \qquad \text{equation 3.3}$$

where H is enthalpy, T is temperature and w is the mixture ratio of water vapor mass and dry air mass, calculated with equation (3.4):

$$w = 0{,}6219 \cdot \frac{\varphi \cdot P_{sat}}{P_{atm} - (\varphi \cdot P_{sat})} \qquad \text{equation 3.4}$$

where ϕ is relative humidity, P_{sat} is saturation pressure and P_{atm} is standard atmospheric pressure (101,325 Pa).

The power of the heat exchanger is then calculated with equation 3.5:

$$P = \dot{m} \cdot \Delta H \qquad \text{equation 3.5}$$

where $\dot{m}$ is the air mass flow rate and ΔH is the enthalpy difference of the air between the inlet and outlet part of the exchanger.

Data are saved in a txt file; an Excel worksheet template was prepared, in which the data were copied and graphs were created concerning all the acquired information.

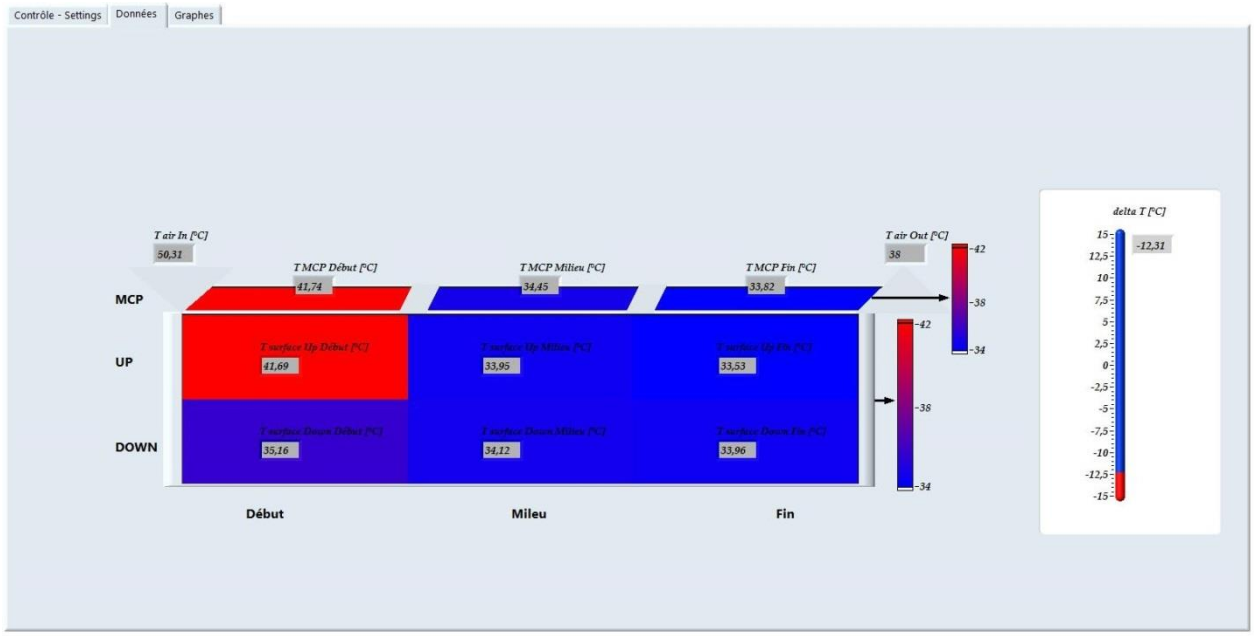

Figure 3.13: PCM and surface temperature monitoring interface

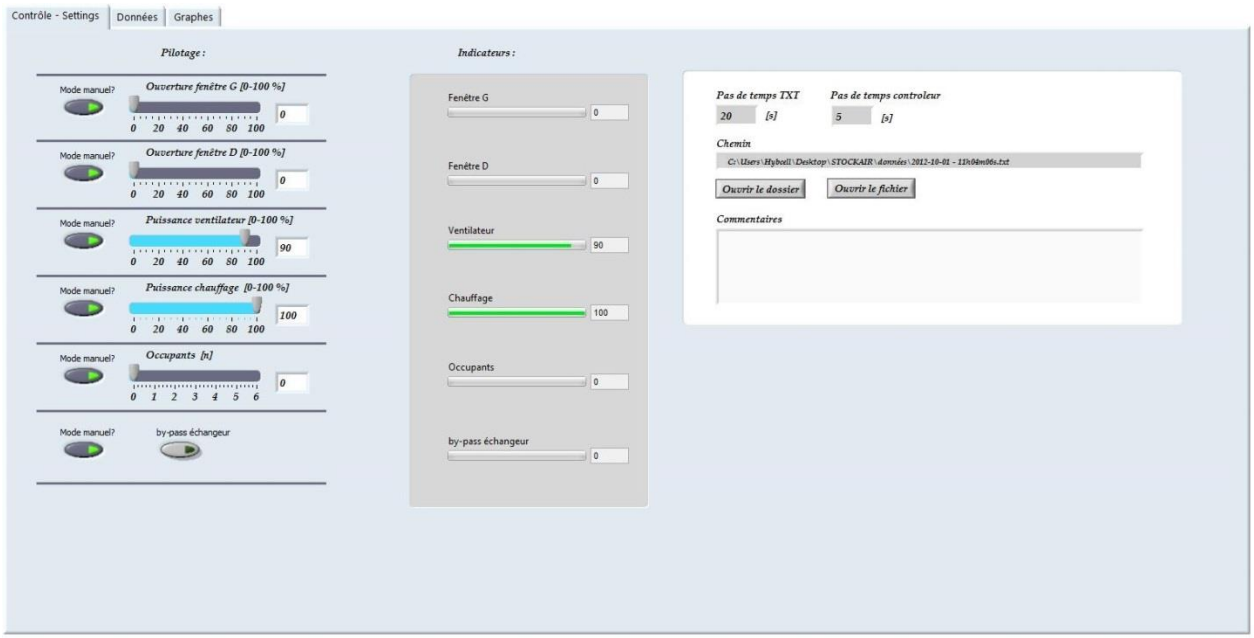

Figure 3.14: Data acquisition and command implementation interface

3.2.5 Operation principle and associated physical phenomena

The designed system can be used to enhance the heating performance of the mechanical ventilation system and to perform electrical load shifting.

According to the orders given by the command interface the two fans create an airflow, ranging from 0 to 550 m^3/h approximately. Hence, air constitutes the heat transferring medium of the unit. The air diffuser ensures a uniform distribution between the plates and the air collector re-concentrates the airflow to achieve the connection with a desired room.

When heat storage is required, the electrical duct heating is activated, hot air circulates between the plates and heats their surface by convection. The encapsulated PCM absorbs heat by conduction, at first in sensible form and when its melting temperature range is surpassed in latent form (charging process). As the PCM melts progressively along the plate, convection phenomena start to appear inside the plate as well. When all the PCM is melted, heat is absorbed once again in sensible form; PCM and outlet air tend to acquire inlet air temperature value. At that point, the stocking process is completed and the heat exchanger is considered to be fully charged. According to the desired control strategy the unit can be preserved in that state for a certain period (i.e. stocking period).

The opposite procedure is followed during the discharging phase: cold or interior air is forced through the plates, the PCM is cooled and starts to solidify, releasing the previously stored heat. The heated air is then reintroduced into the building. When the solidification process is completed, the discharging of the unit is achieved.

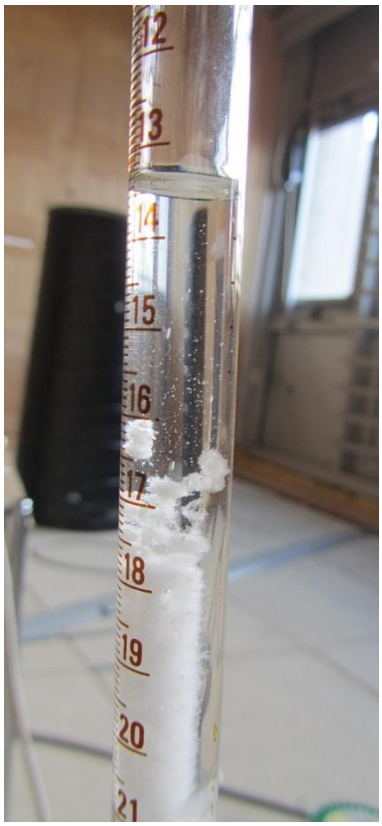

Figure 3.15: PCM during liquefaction

The recovered heat can be used for load shifting purposes. In order to do that, heat is stored during an off-peak period, for example throughout the night when consumption is minimal (figure 1.7) or during the time when the COP of a heat pump is optimum (for example, when indoor and outdoor temperature difference is minimal). The stored heat is then used during the peak period in order to replace the electrical heating and reduce the consumption. Predictive tools linked to weather forecasting and the behavior of the occupants can be developed and integrated in the control strategies elaboration process for optimal exploitation of the system.

Limitations appeared concerning the inlet air temperature range values. During the charging process the maximum acquired value was 50°C, as a thermal protection of the duct heating is activated above this value. Concerning the discharging procedure, inlet air temperature strongly depends on the air source. If the platform is installed in an interior space, inlet minimum air temperature value will not be inferior to 19°C.

The developed unit could be used for cooling purposes during the summer period (night cooling). This would require the replacement of the selected PCM (Mikrotek37 paraffin) with one that has different properties (for example lower melting point temperature). In such a

case, during daytime, hot air flows through the heat exchanger at a higher temperature than the PCM's melting point. The PCM, initially in its solid form, absorbs heat from the air while obtaining its liquid form. The cooled air is then injected into the building. In order to solidify the PCM, during the night exterior air is circulated at a temperature lower than the PCM's melting point.

3.2.6 Main components of the developed experimental system

The main components of the developed experimental system can be summarized as follows:

- The heat exchanger that contains the macroencapsulated paraffin and where the heat storage occurs
- The circuit that allows the air flow (as heat transferring fluid), consisting of the air collector, air diffuser and several ventilation ducts and fittings.
- The electrical heat source that is used to heat the air, consisting of two electrical resistances (total power of 2KW)
- Two fans that create and regulate the flow of the air in the system
- Various sensors installed in different parts of the system in order to monitor the inlet/outlet air temperature, the PCM temperature, the airflow etc.

3.2.7 Coupling with an experimental test cell

The experimental platform was coupled with an experimental test cell called Hybcell situated in the ENTPE facilities in Lyon, France (El Mankibi, 2003). Hybcell is 5.1 m long, 3.5 m wide, 2.9 m high and represents an office or small meeting room (figure 3.16). It is located within a large hall whose temperature can be controlled in order to create artificial environment conditions. The north-east side of the cell is in contact with the outdoor climate and possesses six automatized window openings for hybrid ventilation studies.

The cell is equipped with two electric heaters, a mechanical ventilation system and CO2 generation and sensible heat supply devices (for occupancy simulation). Various sensors (temperature, pressure, relative humidity, CO2 concentration, COV) are installed in the middle of the test cell (at one meter from the floor), as well as in the surrounding hall and outdoors. In addition, accurate measurement of the outdoor climatic conditions can be performed using the IDMP meteorological station which is located at the ENTPE facilities (Dumortier, 2003). The various components and sensors are linked to an existing software that manages data acquisition and command/control orders.

The heat exchanger was placed outside the Hybcell and was coupled to its mechanical ventilation system with the use of two fans and two electrical heating resistances. The developed software for the heat exchanger management was merged with the existing Hybcell software for a global and simultaneous operation of the system.

The coupling was performed in order to evaluate the performance of the heat exchanger in real life conditions and to elaborate control strategies.

Figure 3.16: The experimental test cell Hybcell

3.3 Characterization study

Several verification and characterization tests were realized for different airflow rates, aiming to:

- Confirm the correct operation of the various components of the experimental platform
- Confirm the correct operation of the data acquisition and control command interface
- Obtain an operation profile of the heat exchanger's behavior for various airflow rates
- Verify the airflow uniformity between the plates
- Verify the repeatability of the charging/discharging phases
- Acquire reliable experimental data for the validation of the numerical model

3.3.1 PCM temperature evolution curves

The developed system allows the monitoring of the temperature evolution in various parts of the exchanger. The following three figures illustrate the evolution of the PCM temperature (figure 3.17), plate surface temperature (figure 3.18) and inlet/outlet air temperature (figure 3.19) during a full thermal cycle for an airflow rate of 500 m^3/h, at three parts of the middle plate of the heat exchanger: inlet + 10cm, middle and outlet - 10cm part. During the charging phase, the inlet air temperature was set to 44°C and during the discharging one at 24°C, as these two temperature values are sufficiently distant from the melting/solidifying temperature range of the PCM.

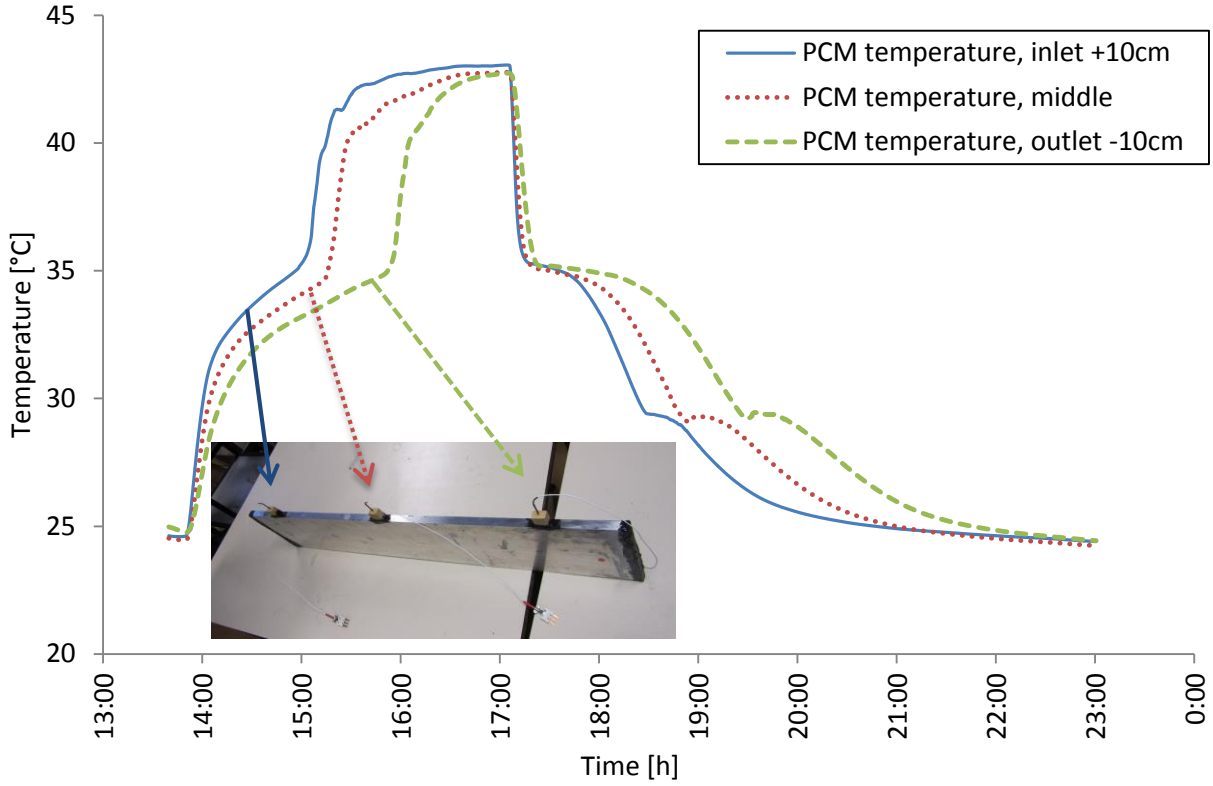

Figure 3.17: Downstream PCM temperature evolution

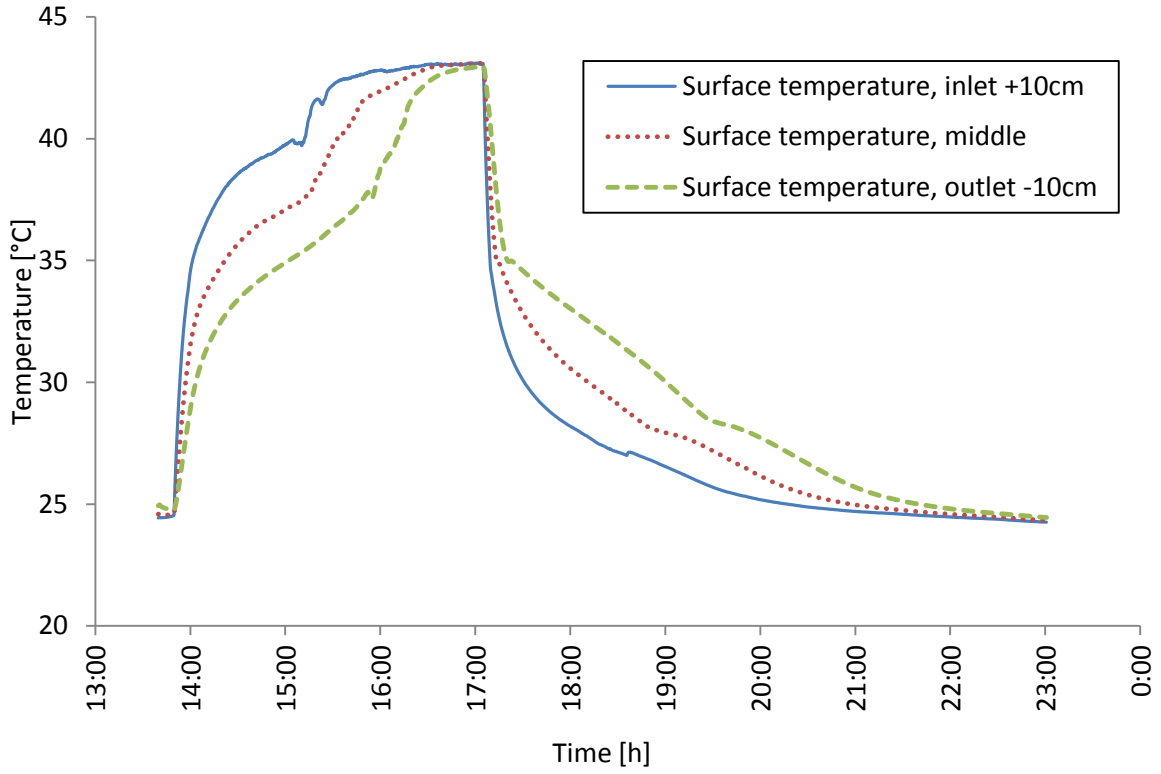

Figure 3.18: Downstream surface temperature evolution

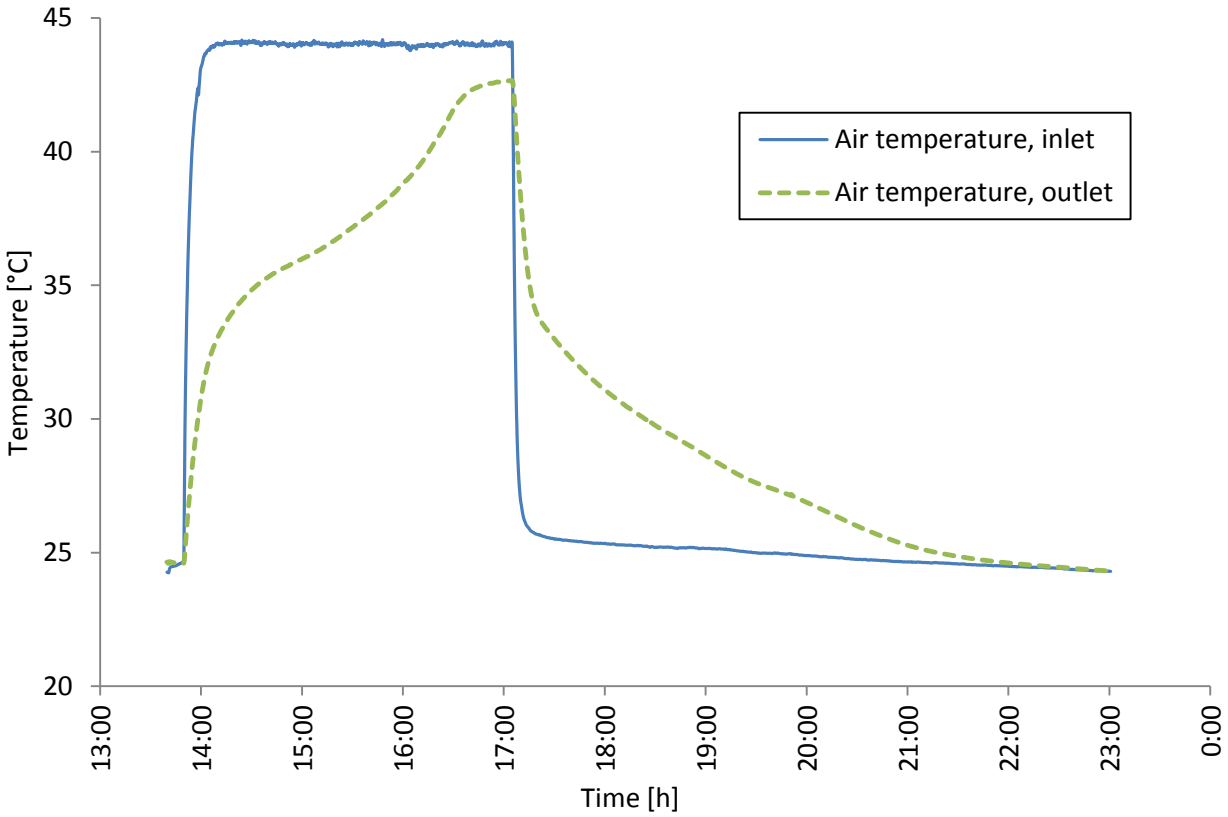

Figure 3.19: Inlet and outlet air temperature evolution

Two expected behaviors were verified:

- The non-linearity evolution of the temperature, due to the latent heat absorbed/released during the phase change process.

- The temperature evolution delay along the plate, as the inlet part is heated/cooled faster than the outlet part.

These two observations indicate that the heat stored in the PCM is not immediately available totally and depends on air flow rate as well as convective and conductive exchanges within the exchanger. Control strategies and improvements on the exchanger should provide solutions to this phenomenon.

3.3.4 Characterization results

As discussed earlier, the characterization study was performed in order to obtain a full operational profile of the heat exchanger and to obtain necessary experimental data that would validate the numerical model.

A characterization protocol was established and can be described as follows:

- Testing of two different configurations: with and without fins
- Realization of a full thermal cycle (charge, discharge) with an inlet air temperature of 44°C during stocking and 24°C during destocking phase
- Testing for five different airflow rates, from 100 to 500 m^3/h, with an increase step of 100m^3/h.

The obtained results are presented in figures 3.20 and 3.21, for the charging and discharging processes.

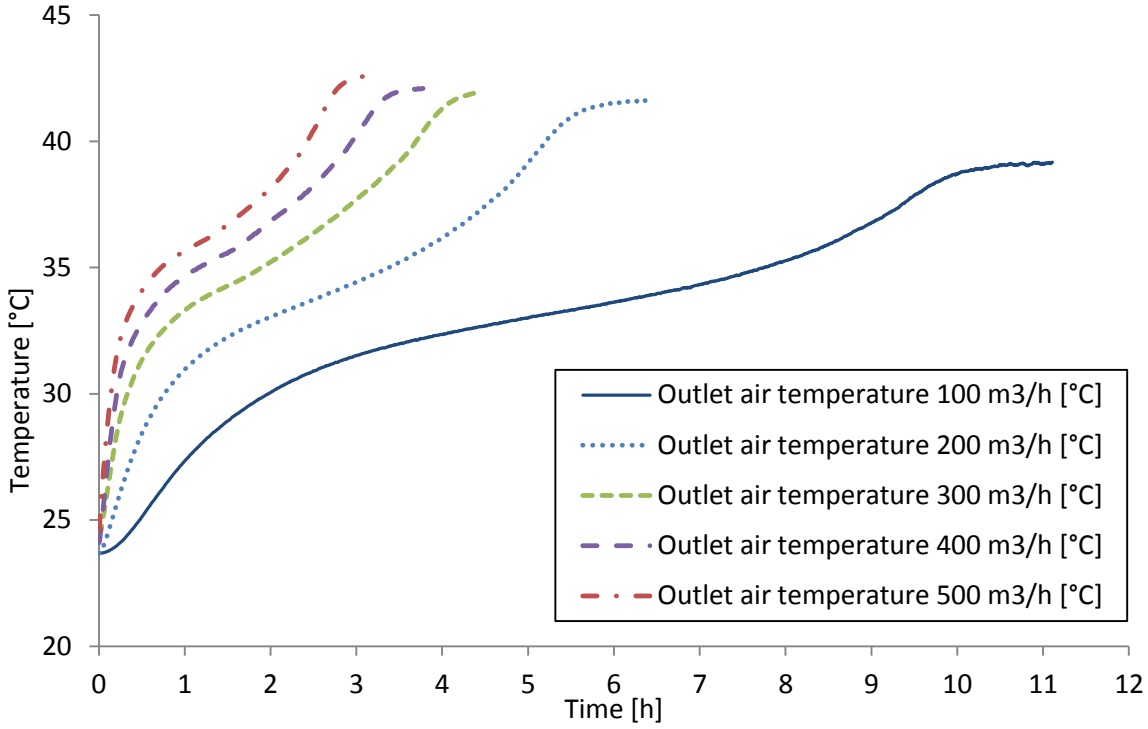

Figure 3.20: Characterization results: outlet air temperature for varying airflow rates, charging phase

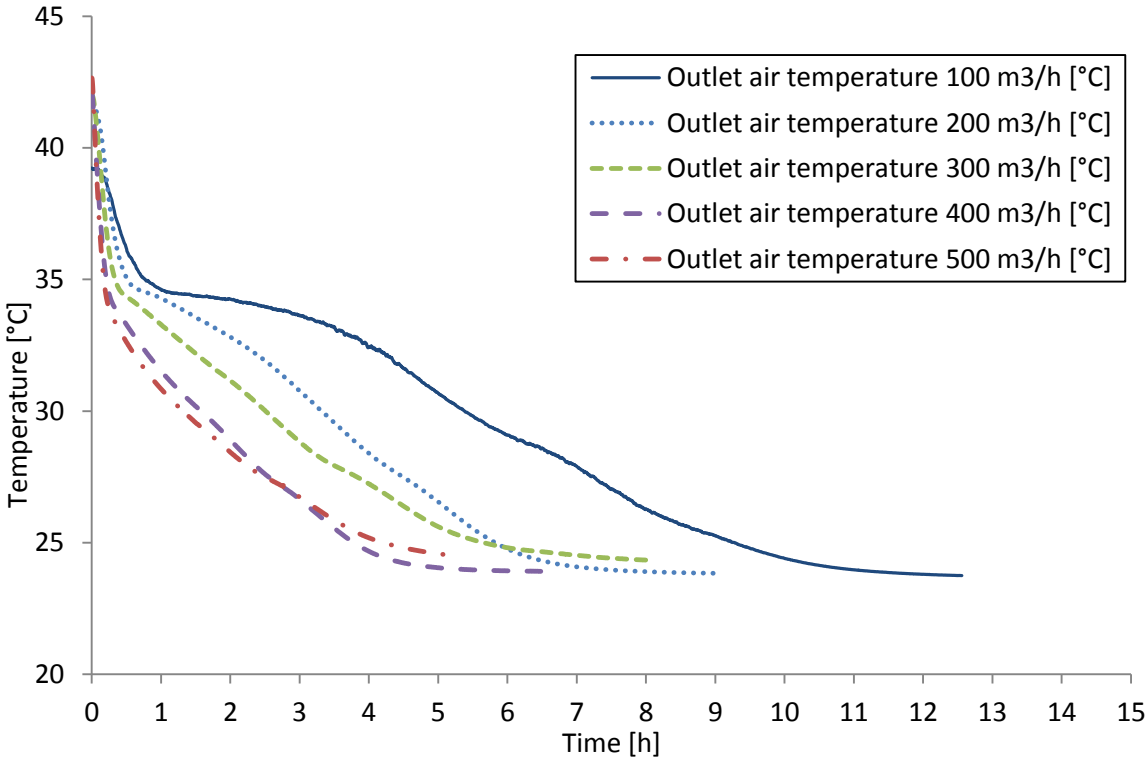

Figure 3.21: Characterization results: outlet air temperature for varying airflow rates, discharging phase

3.3.2 PCM leakage

Data analysis rapidly demonstrated an atypical behavior, as the outlet air temperature decreased at a faster rate for an airflow rate of 400 m^3/h than the one of an airflow rate of 500m^3/h. This means that an error occurred either in the fabrication process, or the instrumentation of the unit or the data acquisition. The experimental platform was dismantled in order to locate the source of the problem.

Despite the efforts for airtight containment of the PCM, some leakage was observed over the wooden caps. The leakage was probably provoked by the pressure that was created during the phase change and the dilatation of the PCM. Liquid paraffin had penetrated the wooden caps and the glue layer (figure 3.22). The amount of the leaked PCM was not important but the issue had to be resolved as it could lead to further deterioration of the heat exchanger and lack of knowledge of the real PCM quantity in the plates.

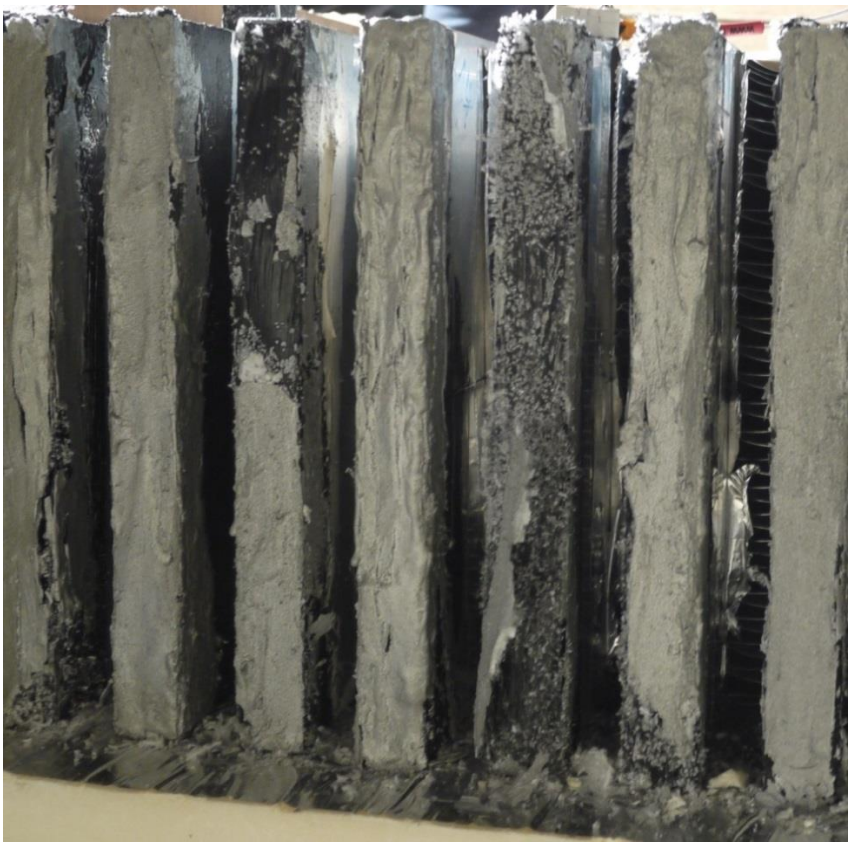

Figure 3.22: PCM leakage

3.3.3 Ameliorated plates

In view of these facts, the elaboration of new improved plates was decided. The new plates were manufactured on demand by a metallurgical factory using the extrusion process. The material used was once again aluminum. The plates had two openings for the pouring of the PCM and the evacuation of the pressure caused by dilation between solid and liquid phase (figures 3.23 and 3.24). Their dimensions were intended to be the same: (1x0,10x0,018)m. Nonetheless, minor dissimilarities occurred during the fabrication process as some small protrusions were created in some parts of the plates (figure 3.25).

When proceeding with the assembly of the heat exchanger and the parallel emplacement of the plates, the accumulated protrusions led to an increased thickness of each plate. This resulted in the removal of one plate in order to reach the former heat exchanger thickness. However, the new design of the plates permitted a higher filling and as a result the final PCM quantity was bigger than the initial one (table 3.4).

As before, three of the plates have additional pierced components that are used to introduce temperature sensors at variable depths inside the PCM, in three different parts of the plates: inlet, middle and outlet areas (figure 3.15).

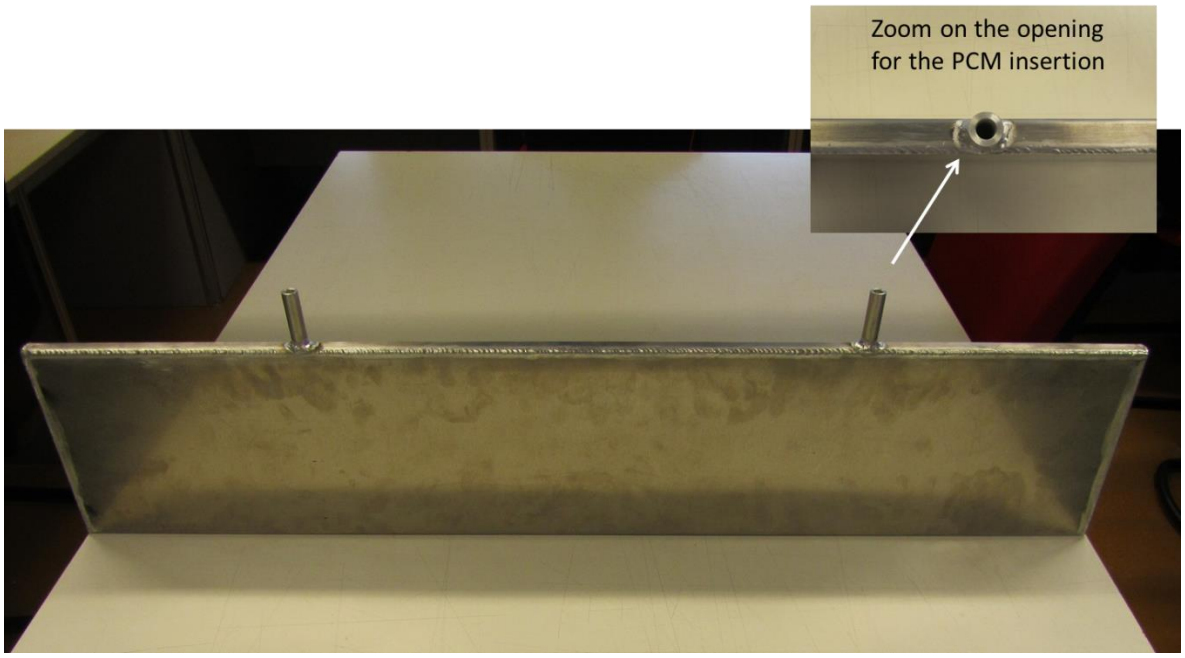

Figure 3.23: The improved aluminum plates used as PCM containers

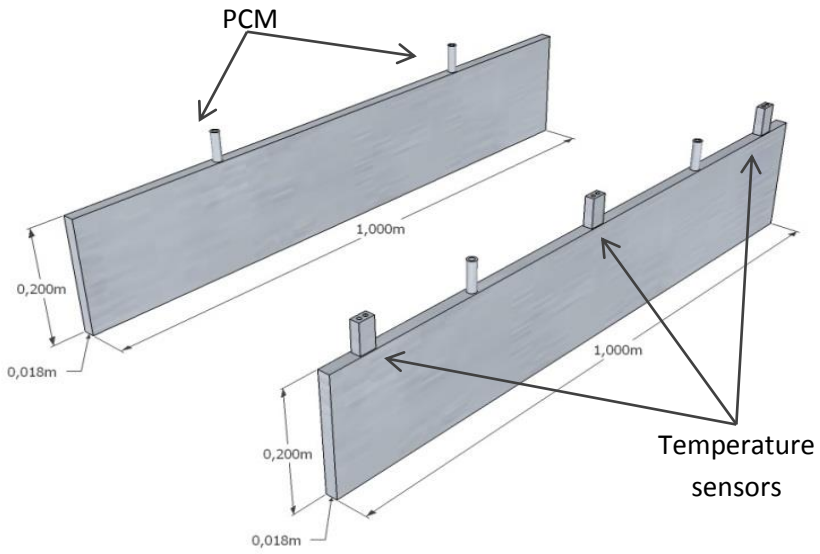

Figure 3.24: The improved aluminum plates used as PCM containers, sketch

PCM was recovered from the old plates and inserted into the new ones. The plates were once again weighed before and afteer the insertion of the PCM (table 3.4). The rest of the heat exchanger's structure and design was kept intact: polystyrene panels for thermal insulation and wooden boards for the assembly. The heat exchanger was reconstructed and coupled to the experimetnal platform and Hybcell.

Plate N°	Tare weight (g)	Laden weight (g)	PCM weight (g)
1	1806	3781	1975
2	1815	3811	1996
3	1820	3835	2015
4	1843	3884	2041
5	1793	3808	2015
6	1813	3820	2007
7	1818	3787	1969
8	1962	3987	2025
9	1811	3807	1996
10	1818	3776	1958
11	1820	3816	1996
12	1823	3791	1968
13	1835	3788	1953
14	1844	3800	1956
15	1951	3910	1959
16	1955	3920	1965
		Total PCM mass:	**31794 g**

Table 3.4: PCM mass calculation for the new heat exchanger

3.3.3 Verification tests

The verification tests were repeated and a full series of characterization tests was launched, providing the operation profile of the heat exchanger for various airflow rates. The tests verified the correct functioning of the heat exchanger, as well as the uniform distribution of the airflow between the plates..

Airflow uniformity

The outlet surface temperatures at the end of each plate were used at first to verify the uniformity of the airflow distribution between the plates. Figure 3.26 illustrates the average, maximum and minimum outlet surface temperature of 14 plates. The two plates at the extremity of the exchanger are not considered here, as they neighbor with the insulation panels and are submitted to different conditions. Results showed little variations between the different plates, which is regarded as acceptable, considering the small but existing dissimilarities in the shape of the containers that occurred during manufacturing (figure 3.25).

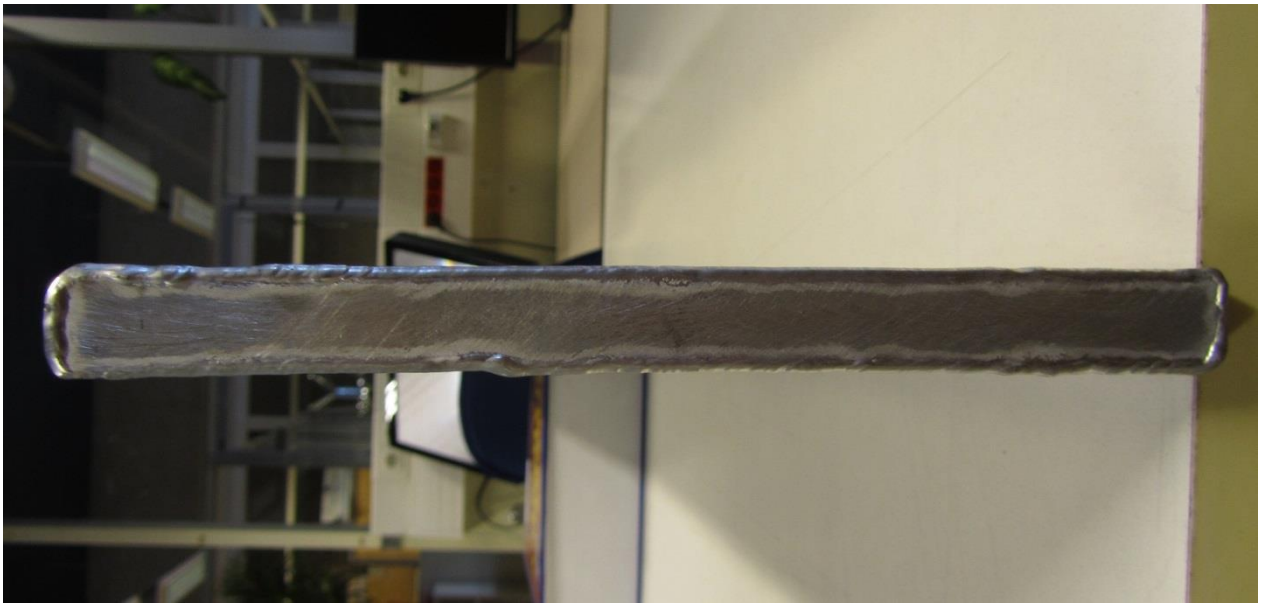

Figure 3.25: Deformation on containers linked to the extrusion process

Furthermore, these tests were performed during a no fins configuration. The emplacement of the fins would further ameliorate the air distribution, by adding to the existing pressure drop. In a second phase, these measurements were used as a global indicator of the charging/discharging state of the exchanger.

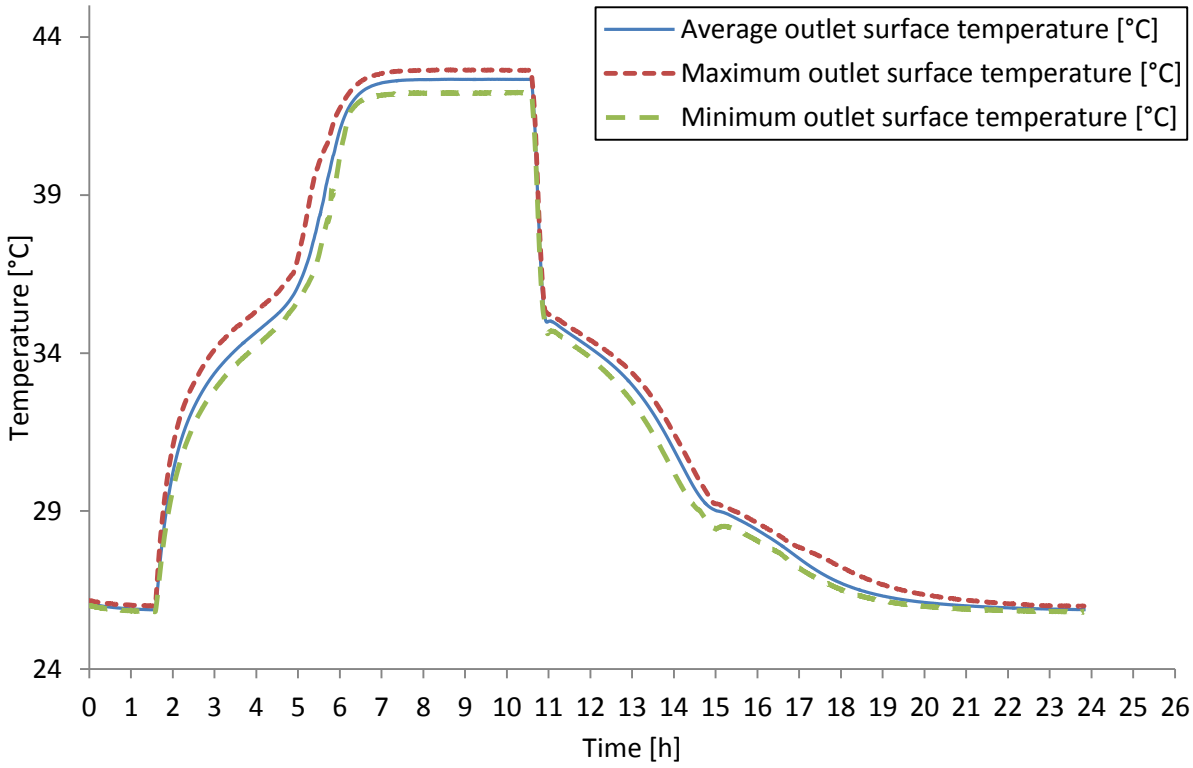

Figure 3.26: Average, maximum and minimum outlet surface temperatures for 14 plates (airflow rate of 300 m^3/h)

3.3.4 Characterization results

As discussed earlier, the characterization study was performed in order to obtain a full operational profile of the heat exchanger and to obtain the necessary experimental data that would validate the numerical model.

A characterization protocol was established and can be described as follows:

- Testing of two different configurations: with and without fins
- Realization of a full thermal cycle with an inlet air temperature of 44°C during stocking and 26°C during destocking phase
- Varying airflow rate values ranging from 100 to 500 m^3/h
- Airflow rate increase step of 100 m^3/h

3.3.4.1 Configuration without fins

The characterization results of the no fins configuration are presented in this section by illustrating the evolution of the outlet air temperature of the heat exchanger for the five different airflow rates, during the charging and discharging processes (figures 3.27 and 3.28).

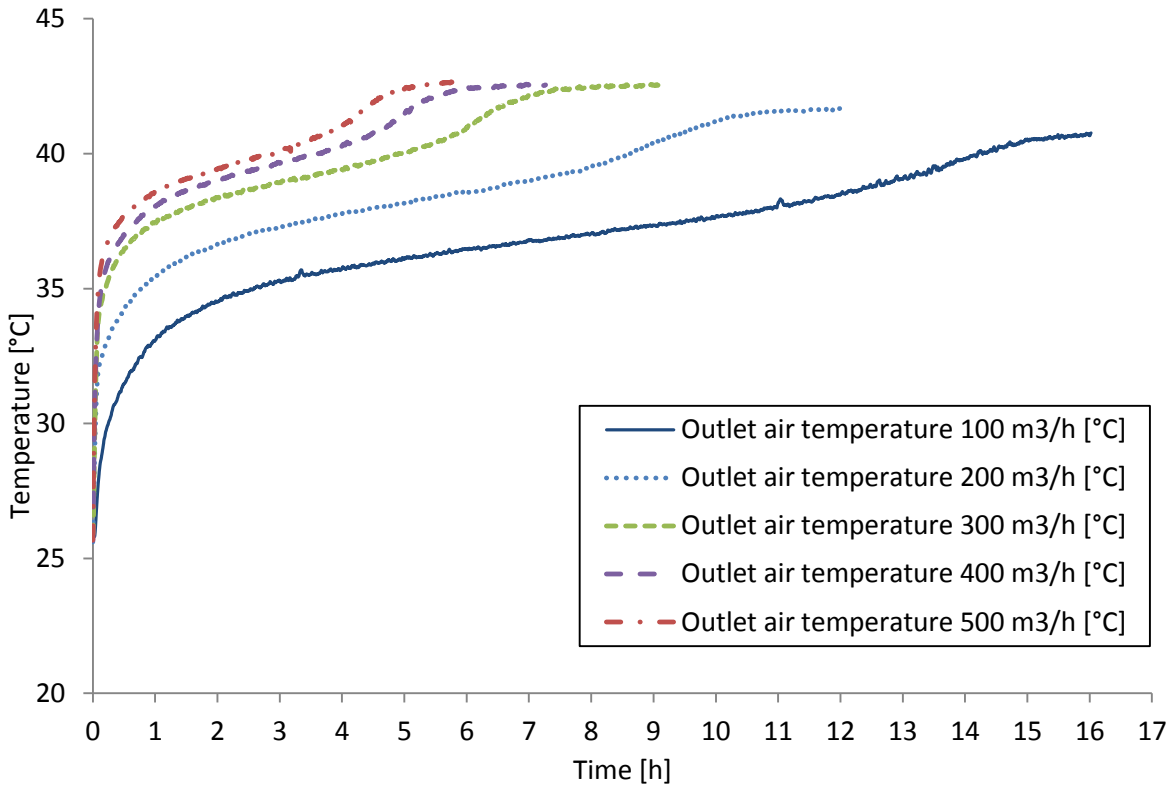

Figure 3.27: Characterization results without fins: outlet air temperature for varying airflow rates, charging phase

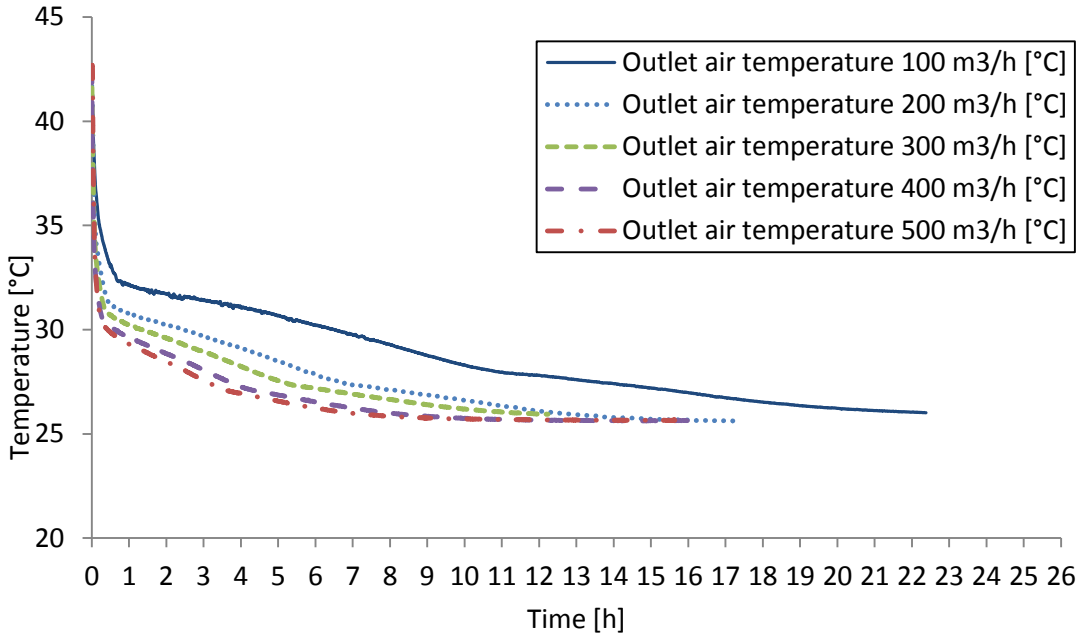

Figure 3.28: Characterization results without fins: outlet air temperature for varying airflow, discharging phase

3.3.4.2 Configuration with fins

In the second phase of the characterization results, fins were placed between the plates for augmented heat exchange performance. Results are presented in figures 3.29 and 3.30, for the five different airflow rates, during the charging and discharging processes.

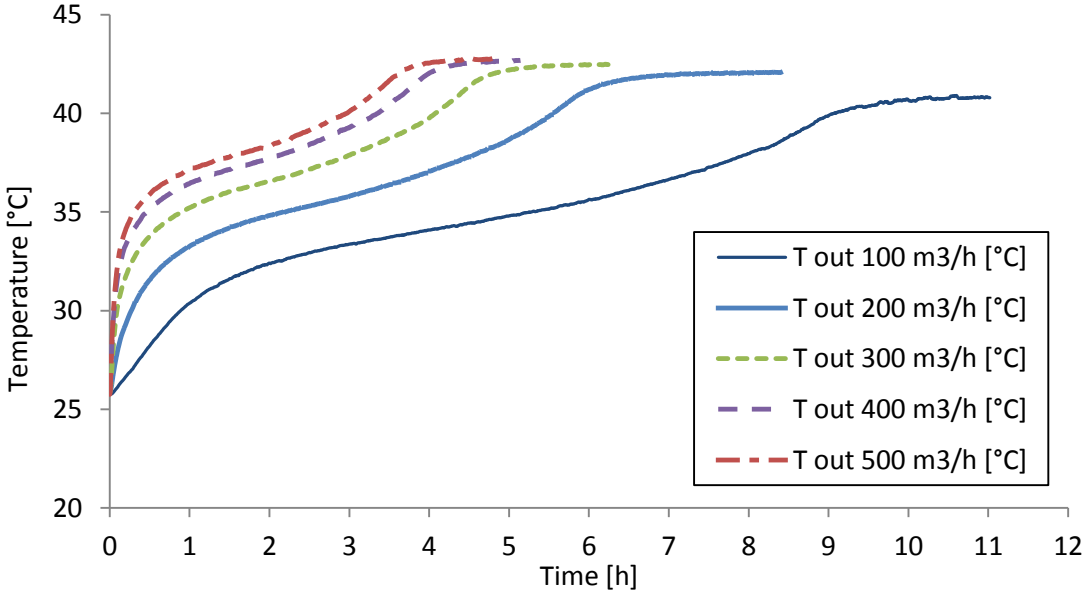

Figure 3.29: Characterization results with fins: outlet air temperature for varying airflow, charging phase

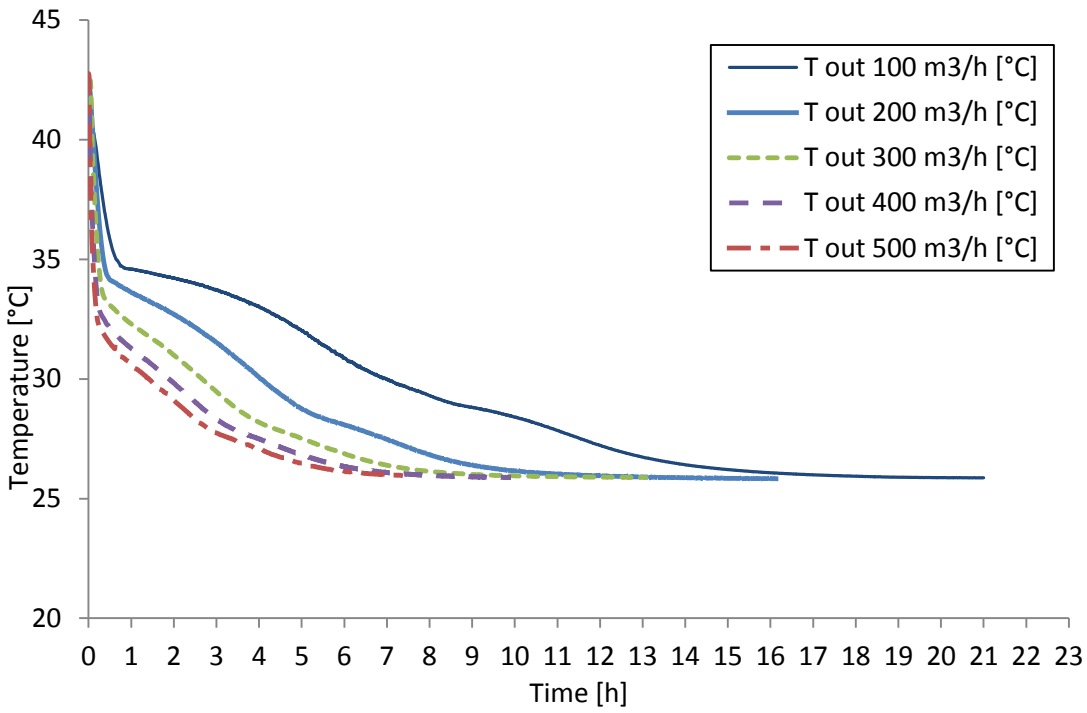

Figure 3.30: Characterization results with fins: outlet air temperature for varying airflow, discharging phase

3.3.4.3 Discussion of the characterization results

Figures 3.26 to 3.30 display the results of the characterization tests performed on the heat exchanger, under two different configurations, with and without fins. More specifically the evolution of the outlet air temperature is presented during the charging and the discharging processes for five different airflow rates.

Outlet air temperature evolution is presented as it constitutes the connecting element between the heat exchanger and the room in which the control strategies are applied. The two different configurations (with and without fins) were investigated in order to experimentally demonstrate the impact of the fins in the heat exchange process.

As expected, the configuration with fins presents a better performance in terms of needed time for stocking and destocking. During the stocking procedure an important additional period is observed for the full melting of the PCM, varying from approximately 1,5 hours with an airflow rate of 500 m^3/h to almost 5 hours for an airflow rate of 100 m^3/h. During the destocking process the extra time required for the full solidification of the PCM varied from 2,5 hours for an airflow rate of 500 m^3/h to approximately 6 hours for an airflow rate of 100 m^3/h.

As the configuration with fins presented a better performance, we will focus on it. Even though the heat transfer is accelerated with the presence of fins, a significant amount of time is still needed for fully charging or discharging the heat exchanger. For lower air flow rates the necessary interval was recorded to be 11 hours for the stocking and 18 hours for the destocking process. This can be disturbing mostly when destocking is needed, as the two hour barrier (during which the peak power demand occurs) is

largely exceeded. On the other hand a high air flow rate might deteriorate the occupants' comfort as non-negligible drafts may occur in the dwelling. High airflow rates can also provoke overheating of the residence during the storage phase.

Small thermal losses are also observed, as the outlet air temperature never reaches the inlet 44°C temperature. The difference between inlet and outlet temperature increases as the airflow rate decreases.

Characterization results gave us an overview of the LHS unit behavior for two different configurations and for varying airflow rates, focusing on the needed time for the charging and discharging phase. Furthermore, reliable and adequate experimental data were obtained which were used for the validation and calibration process of the numerical model.

3.4 Coupling with an experimental room and discussion

As presented earlier, the heat exchanger was coupled with the experimental test cell (Hybcell). It was implemented during a consecutive four day period, with similar climatic winter conditions (outdoor temperature is illustrated in figure 3.31). The aim of the developed strategy was to maintain a comfortable thermal environment inside the test cell throughout the testing period, using the exchanger experimental platform as a heat source. During the peak power hours (18:00-20:00) the electrical resistances were turned off and the heat absorbed by the exchanger was released into the cell.

The evolution of Hybcell's air temperature is illustrated in figure 3.31, along with the consumption of the electrical resistances (100% refers to 2000W), the airflow rate and the outdoor temperature.

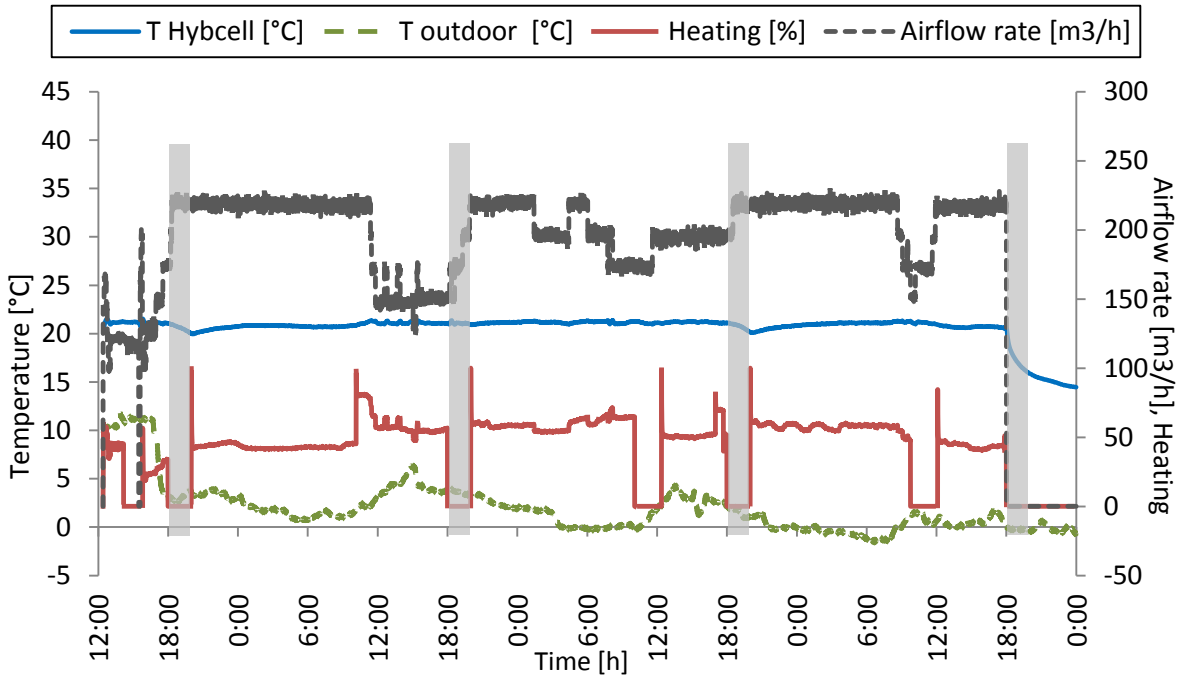

Figure 3.31: Integration of AIR-PCM exchanger and HVAC system of Hybcell

During the off-peak hours, part of the heat is absorbed by the heat exchanger and the rest is directed towards the test cell. A set point value of 21°C was established for Hybcell's temperature and the controller responded towards that goal by altering the airflow rate and the percentage of electrical heating used. The highlighted gray areas correspond to the 18:00-20:00 period (peak power period) when the electrical resistances were off. In this case, the control was operated only on the airflow rate. During this period, the indoor thermal comfort was maintained, using only the heat stored in the PCM; the indoor air temperature was kept constant at 21°C, with small discrepancies being observed. This means that the stored energy in the AIR-PCM exchanger is enough to provide the required thermal comfort while being able to reduce peak demand.

During the fourth day, starting from 18:00, the heating system and the ventilation system were turned off (i.e. no heating and no heat exchanger), resulting in a significant temperature drop down to 14°C. This day was taken as a reference day in order to assess the potential of the heat exchanger.

This example of preliminary control strategy demonstrates the applicability of the developed system in a realistic scenario during a consecutive 4 day winter period. Electricity heating usage is shifted to an off-peak power period while the thermal comfort inside the text cell is not degraded, during the charging or the discharging phase.

3.5 Conclusion

A PCM-Air heat exchanger was designed and fabricated, using paraffin as the heat storage medium. The unit was coupled to an experimental platform and then characterized for various airflow rates. A drawback was observed as PCM leakage occurred at the sealing points of the encapsulating plates. As a consequence, a second exchanger was fabricated, ensuring proper containment and no leakage.

The developed system was coupled to an experimental room and a preliminary control strategy was implemented. Results showed that the proposed system managed to perform peak load shifting while maintaining comfortable indoor conditions.

Nevertheless, the needed charging/discharging time was superior to the peak period, this observation leading to the need for an optimization study for the heat exchanger. For financial and time constraints, this study was performed using a numerical model.

The experimental data obtained through the characterization tests were used to validate the model. The development and the validation of the model are presented in the following chapter.

Chapter 4

Numerical model development

Chapter 4 : Numerical model development

4.1 Introduction

Even though an experimental unit was assembled and characterized, the development of a numerical model was found necessary. The advantages of the numerical model lie in its ability to reproduce the thermal performance of various configurations of the heat exchanger in a very short time period and with little financial investment.

This chapter presents the procedure followed for the model development step by step: the heat transferring phenomena considered, layer selection, nodal discretization, heat balance equation formulation, matrix writing and solution. The calibration study is also detailed, focusing on the creation of fictive heat capacity curves.

The model is validated using experimental data and the four day testing presented in the previous chapter is numerically recreated and compared to experimental results.

4.2 State of the art of existing models

Modelling and simulations have been used in several studies with multiple objectives, including analysis and understanding of PCM behavior and its applications, as well as optimization and design aspects. PCM studies comprise the difficulty of nonlinear behavior and the variation of thermo-physical properties of the studied medium during the phase change process. In order to overcome these obstacles, various methods and techniques have been developed. Fundamentally, the developed models are based on the formulation of a series of energy related equations and their solution using analytical and numerical methods.

Analytical methods are utilized in one-dimensional problems with mostly simple initial and boundary conditions and constant thermal properties. Examples of such techniques are the Neumann method (Lamberg et al., 2003) and the Heat balance integral method (Mitchell et al., 2012).

Numerical methods are more frequently used for phase change problems, as they offer the advantage of being able to change thermal properties values and to calculate the moving boundary of phases. Their main disadvantages are less (but sufficient) precision and possible discontinuities linked to the phase transition. Several reviews exist, describing the existing numerical methods for phase change modeling (Hu et al., 1996, Voller et al., 2006, Verma et al., 2008, Dutil et al., 2011, Idelsohn et all., 1994).

This category can be generally subdivided into three main methods:

- The fixed grid method

In this method, apart from the use of temperature as a dependent variable, enthalpy is introduced as well. As enthalpy is continuous only in time (and temperature only in space), the governing equation is the same for the two phases and can be solved over the whole space as a fixed domain. An example of this method can be found in Nedjar, 2002.

- The moving grid method

In this method, the exact location of the moving boundary is evaluated on a grid at each step, allowing to avoid the constraints of the fixed grid formulation. Two possibilities are offered for the grid definition: the interface-fitting grids (or variable time step method) that uses a uniform spatial grid but a non-uniform time step and the dynamic methods (or variable space grids) where the moving boundary lies on a particular grid point while the number of spatial intervals remains constant. An example of this method can be found in Mackenzie et al., 2002.

- Hybrid method

Finally, hybrid methods exist, using elements from the two previous methods. Example: Voller et al., 2006.

Some authors (Hu et al., 1996) distinguish another category, the latent heat evolution method. They subdivide it into the apparent heat capacity method (Arkar et al., 2005), the effective capacity method (Heim et al., 2004), the heat integration method (Rolph et al., 1982) and the source based method (Voller et al., 1991).

4.3 Numerical model development: Heat balance approach and apparent heat capacity method

Numerical models are powerful tools that can help overcome the limitations of experimental studies regarding time and financial issues. In this aspect, the development of a model that would simulate the behavior of the LHS unit was necessary. The model needs to be both fast and accurate to reproduce the use of the heat exchanger and be coupled with an existing building model for optimization and control strategies development.

Thus, a two dimensional numerical model was created in a Matlab/Simulink environment, using the heat balance approach and the apparent heat capacity method.

4.3.1 Matlab/Simulink and S-function choice

The Matlab/Simulink environment was chosen for a number of reasons:

- The existing building model (Hybcell 1.2) that would later be used for the control strategies development was also developed under the same environment; thus, the coupling between the two models was facilitated.

- Simulink offers a variety of controller toolboxes, such as On-Off, PID and Fuzzy.

- Simulink's graphical language is similar to LabVIEW's, which is the interface used for controlling the HYBCELL cell and other experimental devices. This similarity allows the transition from the numerical to the experimental in an easier way.

- Simulink also provides a flexible and user friendly environment, compared to a procedural programming language.

- It also offers a powerful optimization toolbox.
- Nevertheless, Matlab and Simulink are compatible with other programming languages.

In fact, the developed model was programmed in MATLAB® language and was integrated into Simulink using an S-function block (figure 4.1). S-functions (system functions) can extend the capabilities of the Simulink environment by automatically loading and computing a subroutine written in various programming languages (MATLAB®, C, C++, or Fortran). The S-function block interacts with the Simulink environment by requesting input variables and supplying output results.

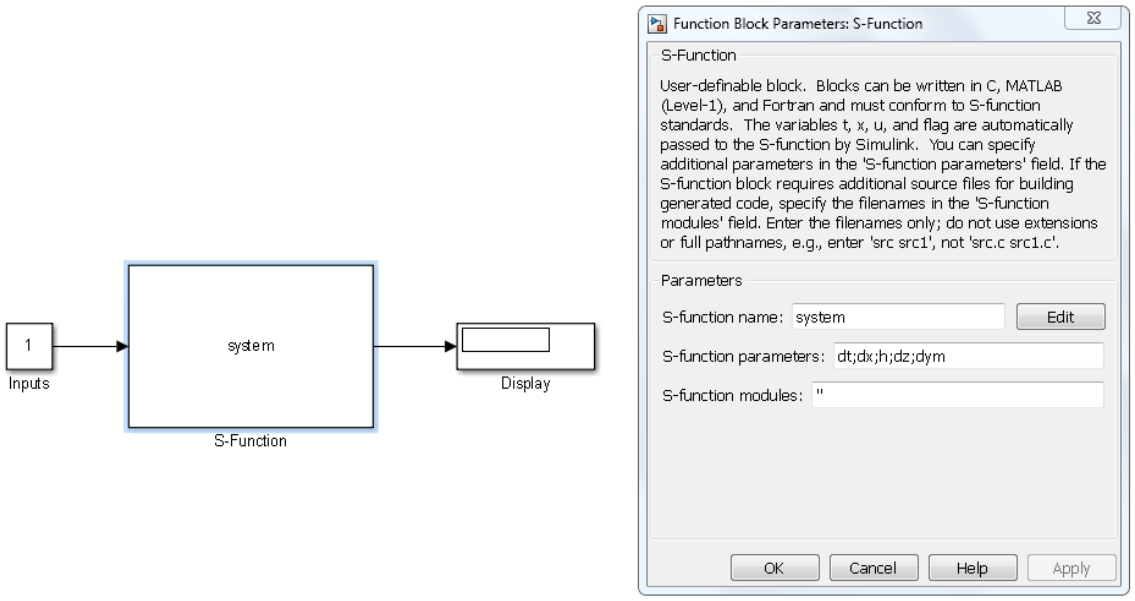

Figure 4.1: S-function block under Simulink environment (left) and parameters definition block (right)

4.3.2 Heat balance approach

The energy balance equation states that at any given location (or control volume or node) in a system, the heat entering into that location is equal to the heat exiting the location, plus any heat that is stored (heat storage is reflected in the increase of heat capacity values).

The heat balance approach is based on the division of the considered medium into a sufficient number of volume elements and the application of the energy balance equation on each element. This is performed by achieved through the formulation of a nodal discretization and the assumption that the temperature value is the same for the volume that corresponds at each node. If several components or mediums are investigated (solid, liquid, PCM), different layers can be considered in order to represent the varying properties of each layer. All relevant energy flows can be taken into account, including conduction, convection, advection and radiation. The heat balance equation is formed for every node and solved at each time step to calculate the temperature evolution at the considered nodes. The finite difference method is employed where needed to approximate the partial differential equations.

This approach offers the possibility to vary the materials' properties with temperature and time and provides flexibility in the choice of simulation time step.

Summarizing the heat balance approach, three main steps can be identified:

- Nodal discretization of the considered layer(s).
- Heat balance formulation for each node considering all the relevant energy flows.
- Transformation of the obtained equations to matrix equations and solution for each time step.

A detailed description of the followed procedure of this study is presented in subsection 4.3.4.

4.3.3 Apparent heat capacity method

This method consists in representing the phase change of the heat storage medium (paraffin here) through an apparent increase of the storage medium's heat capacity values for a certain temperature range, corresponding to the latent heat absorption/release. If the process is performed uniformly, the apparent heat capacity can be defined as:

$$C_{p,app} = \begin{cases} C_{p,s}\,, T < T_s \ \ (solid\ phase) \\ C_p(T),\ T_s < T < T_l\ (phase\ change) \\ C_{p,l}\,,\ \ T > T_l\ (liquid\ phase) \end{cases}, \text{[J/(kg·K)]} \qquad \text{equation 4.1}$$

Where $C_p(T)$ represents the specific heat capacity between phase changes; it is dependent on the temperature value and is represented by a curve.

4.3.4 Nodal discretization and application of the heat balance approach

The main component of this study is the PCM-Air heat exchanger. For the numerical representation of this unit, there are three principle mediums were heat transfer occurs: air, container (aluminum) and PCM. Consequently, three layers were considered for nodal discretization: air, aluminum and PCM.

Half the thickness of the experimental air layer and the PCM layer thickness is considered in the numerical study, considering that by symmetry the results can be extended to the other half (where similar conditions apply).

Each layer was then discretized into n equal regions (nodes) of length dx=L/n, where L is the total length of the heat exchanger (figure 4.2).

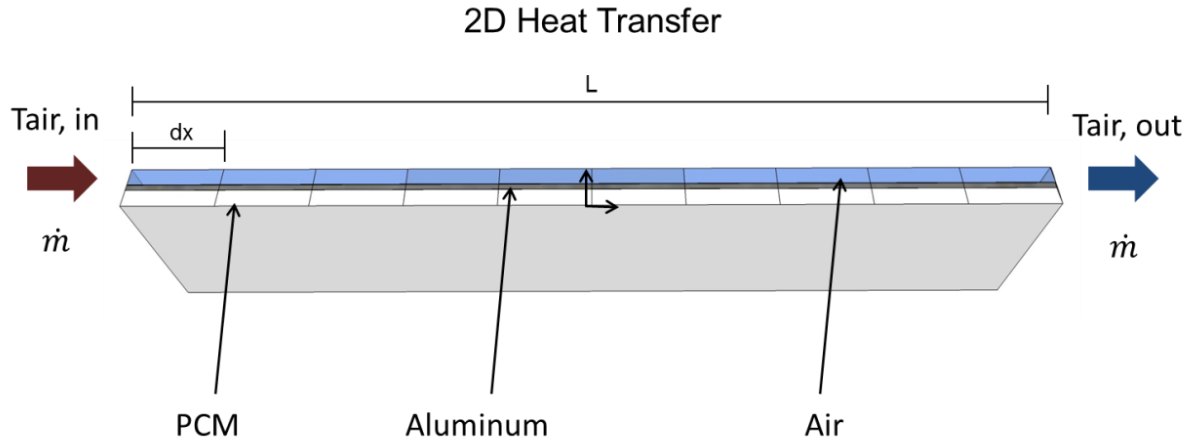

Figure 4.2: Schematic representation of the considered layers for temperature evolution calculation

The PCM layer was further discretized crosswise in m nodes. The discretization into multiple nodes offers the possibility of a more thorough treatment of the medium where the phase change occurs. Figure 4.4 illustrates in a more detailed form the nodal discretization of the three layers: one crosswise node for the air and aluminum layer (denoted as T_a and T_p respectively) and m nodes for the PCM layer (denoted as T_m). Lengthwise n nodes are considered for each layer. Subscript letter i signifies the nodal lengthwise position for each layer (i=1 to n) and the subscript j signifies the nodal crosswise position in the PCM layer (j=1 to m).

The thermal resistances are formulated between nodes (figure 4.4), with different coefficients being used for inlet and outlet nodes, where necessary (see next section). Inlet air temperature and airflow rate are introduced for every time step (denoted as T_{in} and $\dot{m}$ respectively).

4.3.5 Energy balance equation leading to matrix formulation

At a random node i and depending on the considered layer, several heat transfers occur, as described in subsection '3.2.5 Operation principle and associated physical phenomena'. Considering that all possible transfer phenomena take place at that node (apart from those stated in later subsection 4.3.6 'Model assumptions') the energy balance equation can be written as follows:

$$\begin{Bmatrix} Temperature \\ change\ rate \\ in\ node \end{Bmatrix} = \begin{Bmatrix} Conduction \\ transfers \\ in\ node \end{Bmatrix} + \begin{Bmatrix} Convective \\ transfers \\ in\ node \end{Bmatrix} + \begin{Bmatrix} Advection \\ transfers \\ in\ node \end{Bmatrix} \qquad \text{equation 4.2}$$

The temperature change rate (or storage of heat in the node) can be expressed as follows:

$$\begin{Bmatrix} Temperature \\ change\ rate \\ in\ node \end{Bmatrix} = \rho C_p V \frac{dT}{dt} \qquad \text{equation 4.3}$$

Where

ρ :	Density of the node's medium	[kg/m^3]
C_p :	Specific heat capacity of the node's medium	[J/(kg·K)]
For the PCM layer $C_p = C_{app}$ as described in equation 4.1		
$V_a = dy \cdot dx \cdot dz$:	Volume of the node	[m^3]
dy	Width of air node	[m]
dx	Length of node	[m]
dz	Height of node	[m]
T :	Temperature of the node	[°C]
t :	Time	[s]

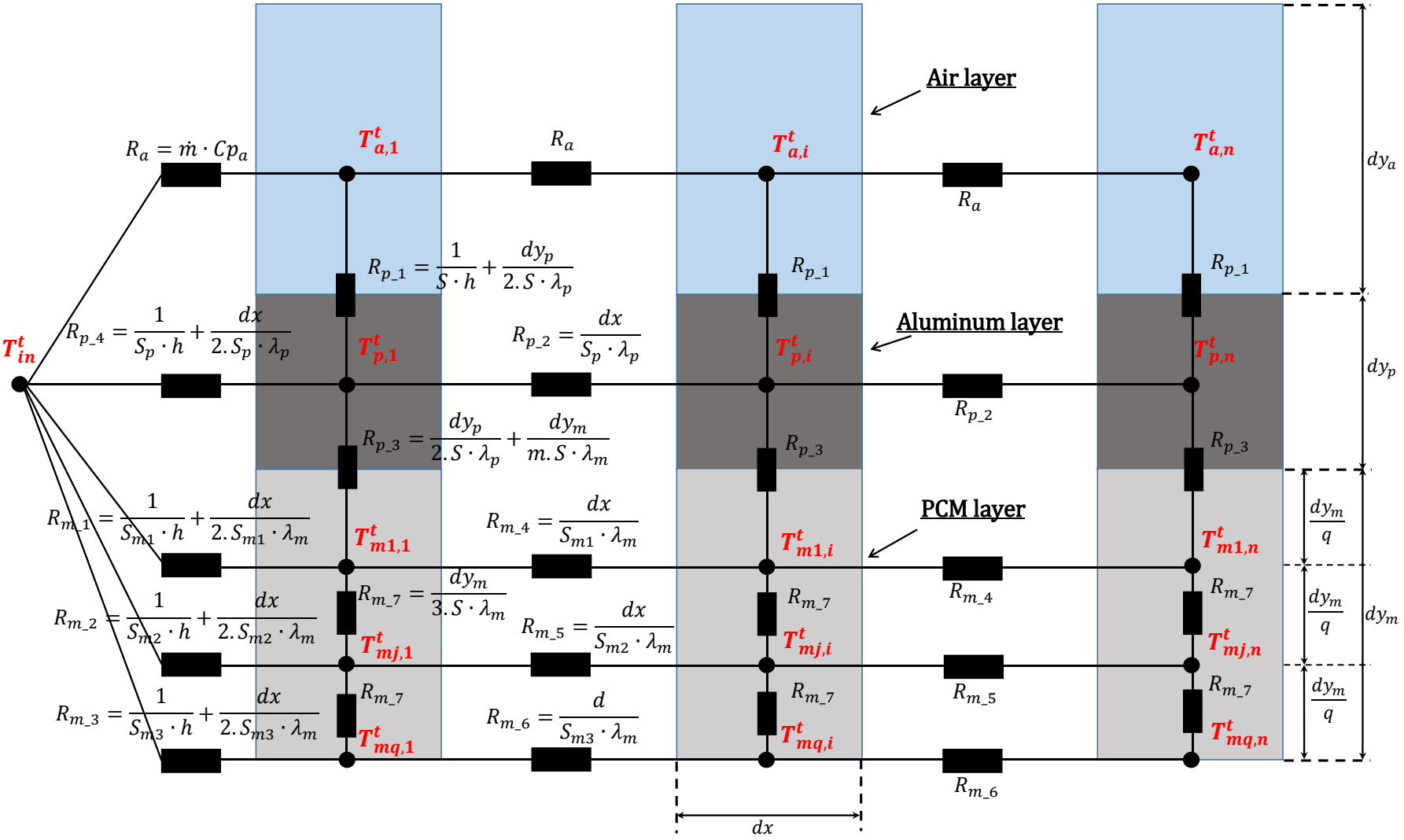

Figure 4.3: Upper view of the nodal representation of the layers: air (a), aluminum (p) and PCM (m)

The conduction term concerns the aluminum and PCM. It is given by the following equation:

$$\begin{Bmatrix} Conduction \\ transfers \\ in\ node \end{Bmatrix} = \frac{T_{i-1} - 2.T_i + T_{i+1}}{R} \qquad \text{equation 4.4}$$

Where

T_i :	Node temperature at node i	[°C]
T_{i-1} :	Node temperature at node i-1	[°C]
T_{i+1} :	Node temperature at node i+1	[°C]
$R = \frac{dx}{S \cdot \lambda}$:	Thermal resistance between neighboring nodes	[W/K]
dx:	Length of node	[m]
S:	Contact surface between neighboring aluminum nodes	[m^2]
λ	Conductivity of the node's material	[W/(m·K)]

The advection term concerns the air layer and represents the heat transported into an air node i from a neighboring air node i-1. In its explicit form, the advection term is given by the following equation:

$$\begin{Bmatrix} Advection \\ transfers \\ in\ node \end{Bmatrix} = \dot{m} Cp_a (T_{a,i-1} - T_{a,i}) \qquad \text{equation 4.5}$$

Where

Cp_a :	Specific heat capacity of the air	[J/(kg·K)]
$\dot{m}$:	Airflow rate	[kg/s]
$T_{a,i}$:	Air temperature at node i	[°C]
$T_{a,i-1}$:	Air temperature at node i-1	[°C]

The energy balance equation is written for each node, taking into account that the heat entering into that node is equal to the heat exiting that position.

The average temperature $\overline{T} = \frac{T^t + T^{t-dt}}{2}$ is introduced as the temperature variation is considered to be linear and the heat balance equation is formulated for each layer. The finite difference method is used to approximate the temperature derivative terms and the final form of the equations leads to a matrix formulation for each layer. The following section presents this analysis for the air, aluminum and PCM layers. Regarding the PCM layer, m was considered equal to three, meaning that a three node discretization was performed for this layer crosswise.

4.3.5.1 Air layer

The application of the heat balance equation for the i[th] air node results in the following equation:

$$\rho_a Cp_a V_a \frac{dT_{a,i}}{dt} = \dot{m} Cp_a \left(T_{a,i-1} - T_{a,i}\right) + hS\left(T_{p,i} - T_{a,i}\right) \qquad \text{equation 4.6}$$

Where

ρ_a :	Air density	[kg/m^3]
Cp_a :	Specific heat capacity of the air	[J/(kg·K)]
$V_a = dy_a \cdot dx \cdot dz$:	Volume of the air node	[m^3]
dy_a	Width of air node	[m]
dx	Length of node	[m]
dz	Height of node	[m]
$T_{a,i}$:	Air temperature at node i	[°C]
$\dot{m}$:	Airflow rate	[kg/s]
$T_{a,i-1}$:	Air temperature at node i-1	[°C]
h :	Convection coefficient	[W/m^2·K]
$S = dx.dz$:	Contact surface between air and plate surface	[m^2]
$T_{p,i}$	Surface temperature at node i	[°C]

By introducing the average temperature term, equation 4.6 becomes:

$$\frac{2.\rho_a.Cp_a.V_a}{dt}.\left(\overline{T_{a,i}} - T_{a,i}^{t-dt}\right) = \dot{m}.Cp_a.\left(\overline{T_{a,i-1}} - \overline{T_{a,i}}\right) + h.S.\left(\overline{T_{p,i}} - \overline{T_{a,i}}\right)$$

Out of which $T_{a,i}^{t-dt}$ can be expressed as a function of $\overline{T_{a,i}}$, $\overline{T_{a,i-1}}$ and $\overline{T_{p,i}}$:

$$\overline{T_{a,i}} - T_{a,i}^{t-dt} = \frac{\dot{m}.dt}{2.\rho_a.V_a}.\left(\overline{T_{a,i-1}} - \overline{T_{a,i}}\right) + \frac{h.S.dt}{2.\rho_a.Cp_a.V_a}.\left(\overline{T_{p,i}} - \overline{T_{a,i}}\right)$$

$$T_{a,i}^{t-dt} = \left(1 + \frac{\dot{m}.dt}{2.\rho_a.V_a} + \frac{h.S.dt}{2.\rho_a.Cp_a.V_a}\right).\overline{T_{a,i}} - \frac{\dot{m}.dt}{2.\rho_a.V_a}.\overline{T_{a,i-1}} - \frac{h.S.dt}{2.\rho_a.Cp_a.V_a}.\overline{T_{p,i}},$$

Setting

$a_a = 1 + b_a + c_a$,

$b_a = \frac{\dot{m}.dt}{2.\rho_a.V_a}$ and

$c_a = \frac{h.S.dt}{2.\rho_a.Cp_a.V_a}$

The final equation 4.7 is obtained

$$T_{a,i}^{t-dt} = a_a.\overline{T_{a,i}} - b_a.\overline{T_{a,i-1}} - c_a.\overline{T_{p,i}}$$ equation 4.7

For node i=1:

$$T_{a,1}^{t-dt} = a_a.\overline{T_{a,1}} - b_a.\overline{T_{in}} - c_a.\overline{T_{p,1}}$$ equation 4.8

Equation 4.7 and 4.8 can then be written in a matrix equation, representing nodes 1 to n:

$$\begin{bmatrix} T_{a,1}^{t-dt} \\ \vdots \\ T_{a,i}^{t-dt} \\ \vdots \\ T_{a,n}^{t-dt} \end{bmatrix} = \begin{bmatrix} a_a & 0 & \cdots & \cdots & 0 \\ -b_a & \ddots & \ddots & & \vdots \\ 0 & \ddots & a_a & \ddots & \vdots \\ \vdots & & \ddots & \ddots & 0 \\ 0 & \cdots & 0 & -b_a & a_a \end{bmatrix} \times \begin{bmatrix} \overline{T_{a,1}} \\ \vdots \\ \overline{T_{a,i}} \\ \vdots \\ \overline{T_{a,n}} \end{bmatrix} + \begin{bmatrix} -c_a & 0 & \cdots & \cdots & 0 \\ 0 & \ddots & \ddots & & \vdots \\ \vdots & \ddots & -c_a & \ddots & \vdots \\ \vdots & & \ddots & \ddots & 0 \\ 0 & \cdots & \cdots & 0 & -c_a \end{bmatrix} \times \begin{bmatrix} \overline{T_{p,1}} \\ \vdots \\ \overline{T_{p,i}} \\ \vdots \\ \overline{T_{p,n}} \end{bmatrix} + \begin{bmatrix} -b_a.\overline{T_{in}} \\ 0 \\ \vdots \\ \vdots \\ 0 \end{bmatrix}$$

4.3.5.2 Aluminum layer

The application of the heat balance equation for the i[th] aluminum node results to the following equation:

$$\rho_p.Cp_p.V_p.\frac{dT_{p,i}}{dt} = \frac{T_{a,i}-T_{p,i}}{R_{p\_1}} + \frac{T_{p,i-1}-2.T_{p,i}+T_{p,i+1}}{R_{p\_2}} + \frac{T_{m1,i}-T_{p,i}}{R_{p\_3}}$$ equation 4.9

Where

ρ_p :	Aluminum density	[kg/m^3]
Cp_p :	Specific heat capacity of aluminum	[J/(kg·K)]
$V_p = dy_p \cdot dx \cdot dz$:	Volume of the aluminum node	[m^3]
dy_p	Width of aluminum node	[m]
$T_{a,i}$:	Air temperature at node i	[°C]
$T_{p,i}$:	Aluminum temperature at node i	[°C]
$T_{p,i-1}$:	Aluminum temperature at node i-1	[°C]
$T_{p,i+1}$:	Aluminum temperature at node i+1	[°C]
$T_{m1,i}$:	First PCM temperature at node i	[°C]
$R_{p\_1} = \frac{1}{S \cdot h} + \frac{dy_p}{2.S \cdot \lambda_p}$:	Thermal resistance between air and aluminum nodes	[W/K]
$R_{p\_2} = \frac{dx}{S_p \cdot \lambda_p}$:	Thermal resistance between neighboring aluminum nodes	[W/K]
$S_p = dy_p \cdot dz$:	Contact surface between neighboring aluminum nodes	[m^2]
$R_{p\_3} = \frac{dy_p}{2.S \cdot \lambda_p} + \frac{dy_m}{3.S \cdot \lambda_m}$:	Thermal resistance between aluminum and PCM nodes	[W/K]

λ_p:	Aluminum conductivity	[W/(m·K)]
λ_m :	PCM conductivity	[W/(m·K)]
dy_m:	Width of PCM node	[m]

By introducing the average temperature term, equation 4.9 becomes:

$$\frac{2.\rho_p.Cp_p.V_p}{dt}.\left(\overline{T_{p,\iota}} - T_{p,i}^{t-dt}\right) = \frac{\overline{T_{a,\iota}} - \overline{T_{p,\iota}}}{R_{p\_1}} + \frac{\overline{T_{p,\iota-1}} - 2.\overline{T_{p,\iota}} + \overline{T_{p,\iota+1}}}{R_{p\_2}} + \frac{\overline{T_{m1,\iota}} - \overline{T_{p,\iota}}}{R_{p\_3}}$$

Out of which, $T_{p,i}^{t-dt}$ can be expressed as a function of $\overline{T_{a,\iota}}, \overline{T_{p,\iota}}$, $\overline{T_{p,\iota-1}}, \overline{T_{p,\iota+1}}$ and $\overline{T_{m,\iota}}$:

$$T_{p,i}^{t-dt} = \left[1 + \left(\frac{dt}{2.\rho_p.Cp_p.V_p}\right).\left(\frac{1}{R_{p\_1}} + \frac{2}{R_{p\_2}} + \frac{1}{R_{p\_3}}\right)\right].\overline{T_{p,\iota}} - \frac{dt}{2.\rho_p.Cp_p.V_p.R_{p\_2}}.\left(\overline{T_{p,\iota-1}} + \overline{T_{p,\iota+1}}\right) - \frac{dt}{2.\rho_p.Cp_p.V_p.R_{p\_1}}.\overline{T_{a,\iota}} - \frac{dt}{2.\rho_p.Cp_p.V_p.R_{p\_3}}.\overline{T_{m1,\iota}},$$

Setting

$$a_p = 1 + 2.b_p + c_p + d_p,\ b_p = \frac{dt}{2.\rho_p.Cp_p.V_p.R_{p\_2}},\ c_p = \frac{dt}{2.\rho_p.Cp_p.V_p.R_{p\_1}}\ and\ d_p = \frac{dt}{2.\rho_p.Cp_p.V_p.R_{p\_3}}$$

The final equation 4.10 is obtained

$$T_{p,i}^{t-dt} = a_p.\overline{T_{p,\iota}} - b_p.\left(\overline{T_{p,\iota-1}} + \overline{T_{p,\iota+1}}\right) - c_p.\overline{T_{a,\iota}} - d_p.\overline{T_{m1,\iota}} \qquad \text{equation 4.10}$$

For node i=1:

$$a_{p\_1} = 1 + b_p + c_p + d_p + e_p\ \ and\ \ e_p = \frac{dt}{2.\rho_p.Cp_p.V_p.R_{p\_4}}$$

Obtaining:

$$T_{p,1}^{t-dt} = a_{p\_1}.\overline{T_{p,1}} - b_p.\overline{T_{p,2}} - c_p.\overline{T_{a,1}} - d_p.\overline{T_{m1,1}} - e_p.\overline{T_{in}} \qquad \text{equation 4.11}$$

For node i=n

$$a_{p\_n} = 1 + b_p + c_p + d_p$$

Obtaining:

$$T_{p,n}^{t-dt} = a_{p\_n}.\overline{T_{p,n}} - b_p.\overline{T_{p,n-1}} - c_p.\overline{T_{a,n}} - d_p.\overline{T_{m1,n}} \qquad \text{equation 4.12}$$

Equation 4.10, 4.11 and 4.12 can then be written in a matrix equation, representing nodes 1 to n:

$$\begin{bmatrix} T_{p,1}^{t-dt} \\ \vdots \\ T_{p,i}^{t-dt} \\ \vdots \\ T_{p,n}^{t-dt} \end{bmatrix} = \begin{bmatrix} a_{p\_1} & -b_p & \cdots & \cdots & 0 \\ -b_p & a_p & \ddots & & \vdots \\ 0 & \ddots & a_p & \ddots & \vdots \\ \vdots & & \ddots & a_p & -b_p \\ 0 & \cdots & 0 & -b_p & a_{p\_n} \end{bmatrix} \times \begin{bmatrix} \overline{T_{p,1}} \\ \vdots \\ \overline{T_{p,i}} \\ \vdots \\ \overline{T_{p,n}} \end{bmatrix} + \begin{bmatrix} -c_p & 0 & \cdots & \cdots & 0 \\ 0 & \ddots & \ddots & & \vdots \\ \vdots & \ddots & -c_p & \ddots & \vdots \\ \vdots & & \ddots & \ddots & 0 \\ 0 & \cdots & \cdots & 0 & -c_p \end{bmatrix} \times \begin{bmatrix} \overline{T_{a,1}} \\ \vdots \\ \overline{T_{a,i}} \\ \vdots \\ \overline{T_{a,n}} \end{bmatrix}$$
$$+ \begin{bmatrix} -d_p & 0 & \cdots & \cdots & 0 \\ 0 & \ddots & \ddots & & \vdots \\ \vdots & \ddots & -d_p & \ddots & \vdots \\ \vdots & & \ddots & \ddots & 0 \\ 0 & \cdots & \cdots & 0 & -d_p \end{bmatrix} \times \begin{bmatrix} \overline{T_{m1,1}} \\ \vdots \\ \overline{T_{m1,i}} \\ \vdots \\ \overline{T_{m1,n}} \end{bmatrix} + \begin{bmatrix} -e_p . \overline{T_{in}} \\ 0 \\ \vdots \\ \vdots \\ 0 \end{bmatrix}$$

4.3.5.3 PCM layers

As discussed previously, the PCM layer was further discretized in m nodes crosswise. In this section (for illustration purposes), m was considered equal to 3, meaning that a three node discretization was performed for this layer.

4.3.5.3.1 First PCM node (PCM volume in contact with aluminum)

The application of the heat balance equation for the i[th] and first crosswise (j=1) PCM node results in the following equation:

$$\rho_m . Cp_m . V_{m1} . \frac{dT_{m1,i}}{dt} = \frac{T_{p,i} - T_{m1,i}}{R_{p\_3}} + \frac{T_{m1,i-1} - 2.T_{m1,i} + T_{m1,i+1}}{R_{m\_4}} + \frac{T_{m2,i} - T_{m1,i}}{R_{m\_7}} \qquad \text{equation 4.13}$$

Where

ρ_m :	PCM density	[kg/m^3]
Cp_m :	Specific heat capacity of the PCM	[J/(kg·K)]
$V_{m1} = S_{m1} \cdot dx$:	Volume of the first PCM node	[m^3]
$S_{m1} = \left(\frac{dy_m}{3} + \frac{dy_m}{6}\right) \cdot dz$:	Contact surface between neighboring PCM nodes	[m^2]
$T_{m2,i}$:	Second PCM temperature at node i	[°C]
$T_{m1,i-1}$:	First PCM temperature at node i-1	[°C]
$T_{m1,i+1}$:	First PCM temperature at node i+1	[°C]
$R_{m\_4} = \frac{dx}{S_{m1} \cdot \lambda_m}$:	Thermal resistance between neighboring PCM nodes	[W/K]
$R_{m\_7} = \frac{dy_m}{3.S \cdot \lambda_m}$:	Thermal resistance between first and second PCM nodes	[W/K]

By introducing the average temperature term, equation 4.13 becomes:

$$\frac{2.\rho_m.Cp_m.V_{m1}}{dt}.\left(\overline{T_{m1,\iota}}-T_{m1,i}^{t-dt}\right)=\frac{\overline{T_{p,\iota}}-\overline{T_{m1,\iota}}}{R_{p\_3}}+\frac{\overline{T_{m1,\iota-1}}-2.\overline{T_{m1,\iota}}+\overline{T_{m1,\iota+1}}}{R_{m\_4}}+\frac{\overline{T_{m2,\iota}}-\overline{T_{m1,\iota}}}{R_{m\_7}}$$

Out of which, $T_{m1,i}^{t-dt}$ can be expressed as a function of $\overline{T_{p,\iota}}, \overline{T_{m1,\iota}}$, $\overline{T_{m1,\iota-1}}, \overline{T_{m1,\iota+1}}$ and $\overline{T_{m2,\iota}}$:

$$T_{m1,i}^{t-dt}=\left[1+\left(\frac{dt}{2.\rho_m.Cp_m.V_{m1}}\right).\left(\frac{1}{R_{p\_3}}+\frac{2}{R_{m\_4}}+\frac{1}{R_{m\_7}}\right)\right].\overline{T_{m1,\iota}}-\frac{dt}{2.\rho_m.Cp_m.V_{m1}.R_{m\_4}}.\left(\overline{T_{m1,\iota-1}}+\overline{T_{m1,\iota+1}}\right)-\frac{dt}{2.\rho_m.Cp_m.V_{m1}.R_{p\_3}}.\overline{T_{p,\iota}}-\frac{dt}{2.\rho_m.Cp_m.V_{m1}.R_{m\_7}}.\overline{T_{m2,\iota}},$$

Setting:

$$a_{m1}=1+2.b_{m1}+c_{m1}+d_{m1}, b_{m1}=\frac{dt}{2.\rho_m.Cp_m.V_{m1}.R_{m\_4}}, c_{m1}=\frac{dt}{2.\rho_m.Cp_m.V_{m1}.R_{p\_3}} \quad and \quad d_{m1}=\frac{dt}{2.\rho_m.Cp_m.V_{m1}.R_{m\_7}}$$

The final equation 4.14 is obtained

$$T_{m1,i}^{t-dt}=a_{m1}.\overline{T_{m1,\iota}}-b_{m1}.\left(\overline{T_{m1,\iota-1}}+\overline{T_{m1,\iota+1}}\right)-c_{m1}.\overline{T_{p,\iota}}-d_{m1}.\overline{T_{m2,\iota}} \qquad \text{equation 4.14}$$

For node i=1:

$$\frac{2.\rho_m.Cp_m.V_{m1}}{dt}.\left(\overline{T_{m1,1}}-T_{m1,1}^{t-dt}\right)=\frac{\overline{T_{p,1}}-\overline{T_{m1,1}}}{R_{p\_3}}+\frac{\overline{T_{m1,0}}-\overline{T_{m1,1}}}{R_{m\_1}}+\frac{\overline{T_{m1,2}}-\overline{T_{m1,1}}}{R_{m\_4}}+\frac{\overline{T_{m2,1}}-\overline{T_{m1,1}}}{R_{m\_7}}$$

$$T_{m1,1}^{t-dt}=\left[1+\left(\frac{dt}{2.\rho_m.Cp_m.V_{m1}}\right).\left(\frac{1}{R_{p\_3}}+\frac{1}{R_{m\_1}}+\frac{1}{R_{m\_4}}+\frac{1}{R_{m\_7}}\right)\right].\overline{T_{m1,1}}-\frac{dt}{2.\rho_m.Cp_m.V_{m1}.R_{m\_1}}.\left(\overline{T_{m1,0}}\right)-\frac{dt}{2.\rho_m.Cp_m.V_{m1}.R_{m\_4}}.\left(\overline{T_{m1,2}}\right)-\frac{dt}{2.\rho_m.Cp_m.V_{m1}.R_{p\_3}}.\overline{T_{p,1}}-\frac{dt}{2.\rho_m.Cp_m.V_{m1}.R_{m\_7}}.\overline{T_{m2,1}},$$

Setting:

$$a_{m1\_1}=1+b_{m1}+c_{m1}+d_{m1}+e_{m1} \quad with\ e_{m1}=\frac{1}{2.\rho_m.Cp_m.V_{m1}.R_{m\_1}}$$

$$T_{m1,1}^{t-dt}=a_{m1\_1}.\overline{T_{m1,1}}-b_{m1}.\overline{T_{m1,2}}-c_{m1}.\overline{T_{p,1}}-d_{m1}.\overline{T_{m2,1}}-e_{m1}.\overline{T_{\iota n}} \qquad \text{equation 4.15}$$

For node i=n:

$$\frac{2.\rho_m.Cp_m.V_{m1}}{dt}.\left(\overline{T_{m1,n}}-T_{m1,n}^{t-dt}\right)=\frac{\overline{T_{p,n}}-\overline{T_{m1,n}}}{R_{p\_3}}+\frac{\overline{T_{m1,n-1}}-\overline{T_{m1,n}}}{R_{m\_4}}+\frac{\overline{T_{m2,n}}-\overline{T_{m1,n}}}{R_{m\_7}}$$

$$T_{m1,n}^{t-dt}=\left[1+\left(\frac{dt}{2.\rho_m.Cp_m.V_{m1}}\right).\left(\frac{1}{R_{p\_3}}+\frac{1}{R_{m\_4}}+\frac{1}{R_{m\_7}}\right)\right].\overline{T_{m1,n}}-\frac{dt}{2.\rho_m.Cp_m.V_{m1}.R_{m\_4}}.\left(\overline{T_{m1,n-1}}\right)-\frac{dt}{2.\rho_m.Cp_m.V_{m1}.R_{p\_3}}.\overline{T_{p,n}}-\frac{dt}{2.\rho_m.Cp_m.V_{m1}.R_{m\_7}}.\overline{T_{m2,n}}$$

Setting:

$$a_{m1\_n} = 1 + b_{m1} + c_{m1} + d_{m1}$$

$$T_{m1,n}^{t-dt} = a_{m1\_n}.\overline{T_{m1,n}} - b_{m1}.\overline{T_{m1,n-1}} - c_{m1}.\overline{T_{p1,n} - d_{m1}.T_{m2,n}} \qquad \text{equation 4.16}$$

Equation 4.14, 4.15 and 4.16 can then be written in a matrix equation, representing nodes 1 to n:

$$\begin{bmatrix} T_{m1,1}^{t-dt} \\ \vdots \\ T_{m1,i}^{t-dt} \\ \vdots \\ T_{m1,n}^{t-dt} \end{bmatrix} = \begin{bmatrix} a_{m1\_1} & -b_{m1} & \cdots & \cdots & 0 \\ -b_{m1} & a_{m1} & \ddots & & \vdots \\ 0 & \ddots & a_{m1} & \ddots & \vdots \\ \vdots & & \ddots & a_{m1} & -b_{m1} \\ 0 & \cdots & 0 & -b_{m1} & a_{m1\_n} \end{bmatrix} \times \begin{bmatrix} \overline{T_{m1,1}} \\ \vdots \\ \overline{T_{m1,\iota}} \\ \vdots \\ \overline{T_{m1,n}} \end{bmatrix} + \begin{bmatrix} -c_{m1} & 0 & \cdots & \cdots & 0 \\ 0 & \ddots & \ddots & & \vdots \\ \vdots & \ddots & -c_{m1} & \ddots & \vdots \\ \vdots & & \ddots & \ddots & 0 \\ 0 & \cdots & \cdots & 0 & -c_{m1} \end{bmatrix} \times \begin{bmatrix} \overline{T_{p,1}} \\ \vdots \\ \overline{T_{p,\iota}} \\ \vdots \\ \overline{T_{p,n}} \end{bmatrix}$$

$$+ \begin{bmatrix} -d_{m1} & 0 & \cdots & \cdots & 0 \\ 0 & \ddots & \ddots & & \vdots \\ \vdots & \ddots & -d_{m1} & \ddots & \vdots \\ \vdots & & \ddots & \ddots & 0 \\ 0 & \cdots & \cdots & 0 & -d_{m1} \end{bmatrix} \times \begin{bmatrix} \overline{T_{m2,1}} \\ \vdots \\ \overline{T_{m2,\iota}} \\ \vdots \\ \overline{T_{m2,n}} \end{bmatrix} + \begin{bmatrix} -e_{m1}.\overline{T_{in}} \\ 0 \\ \vdots \\ \vdots \\ 0 \end{bmatrix}$$

4.3.5.3.2 Second PCM node (internal PCM volume)

The application of the heat balance equation for the i[th] and first crosswise (j=2) PCM node results in the following equation:

$$\rho_m.Cp_m.V_{m2}.\frac{dT_{m2,i}}{dt} = \frac{T_{m1,i} - 2.T_{m2,i} + T_{m3,i}}{R_{m\_7}} + \frac{T_{m2,i-1} - 2.T_{m2,i} + T_{m2,i+1}}{R_{m\_5}} \qquad \text{equation 4.17}$$

Where

$V_{m2} = S_{m2} \cdot dx$:	Volume of the second PCM node	[m^3]
$S_{m2} = \frac{dy_m}{2} \cdot dz$:	Contact surface between neighboring PCM nodes	[m^2]
$T_{m3,i}$:	Third PCM temperature at node i	[°C]
$T_{m2,i-1}$:	First PCM temperature at node i-1	[°C]
$T_{m2,i+1}$:	First PCM temperature at node i+1	[°C]
$R_{m\_5} = \frac{dx}{S_{m2}.\lambda_m}$: :	Thermal resistance between neighboring PCM nodes	[W/K]

By introducing the average temperature term, equation 4.17 becomes:

$$\frac{2.\rho_m.Cp_m.V_{m2}}{dt}.\left(\overline{T_{m2,\iota}} - T_{m2,i}^{t-dt}\right) = \frac{\overline{T_{m1,\iota}} - \overline{2.T_{m2,\iota}} + \overline{T_{m3,\iota}}}{R_{m\_7}} + \frac{\overline{T_{m2,\iota-1}} - 2.\overline{T_{m2,\iota}} + \overline{T_{m2,\iota+1}}}{R_{m\_5}}$$

Out of which, $T_{m2,i}^{t-dt}$ can be expressed as a function of $\overline{T_{m1,\iota}}$, $\overline{T_{m2,\iota-1}}$, $\overline{T_{m2,\iota+1}}$ and $\overline{T_{m3,\iota}}$:

$$T_{m2,i}^{t-dt} = \left[1 + \left(\frac{dt}{2.\rho_m.Cp_m.V_{m2}}\right).\left(\frac{2}{R_{m\_4}} + \frac{2}{R_{m\_7}}\right)\right].\overline{T_{m1,\iota}} - \frac{dt}{2.\rho_m.Cp_m.V_{m2}.R_{m\_5}}.\left(\overline{T_{m2,\iota-1}} + \overline{T_{m2,\iota+1}}\right) - \frac{dt}{2.\rho_m.Cp_m.V_{m2}.R_{m\_7}}.\left(\overline{T_{m1,\iota}} + \overline{T_{m3,\iota}}\right)$$

Setting:

$$a_{m2} = 1 + 2.b_{m2} + 2.d_{m2},\ b_{m2} = \frac{dt}{2.\rho_m.Cp_m.V_{m2}.R_{m\_5}}\ and\ d_{m2} = \frac{dt}{2.\rho_m.Cp_m.V_{m2}.R_{m\_7}}$$

The final equation 4.18 is obtained:

$$T_{m2,i}^{t-dt} = a_{m2}.\overline{T_{m2,\iota}} - b_{m2}.\left(\overline{T_{m2,\iota-1}} + \overline{T_{m2,\iota+1}}\right) - d_{m2}.\overline{T_{m1,\iota}} - d_{m2}.\overline{T_{m3,\iota}} \qquad \text{equation 4.18}$$

For node i=1

$$a_{m2\_1} = 1 + b_{m2} + 2.d_{m2} + e_{m2}\ \ with\ e_{m2} = \frac{1}{2.\rho_m.Cp_m.V_{m2}.R_{m\_2}}$$

Obtaining:

$$T_{m2,1}^{t-dt} = a_{m2\_1}.\overline{T_{m2,1}} - b_{m2}.\overline{T_{m2,2}} - d_{m2}.\overline{T_{m1,1}} - d_{m2}.\overline{T_{m3,1}} - e_{m2}.\overline{T_{in}} \qquad \text{equation 4.19}$$

For node i=n:

$$a_{m2\_n} = 1 + b_{m2} + 2.d_{m2}$$

Obtaining:

$$T_{m2,n}^{t-dt} = a_{m2\_n}.\overline{T_{m2,n}} - b_{m2}.\overline{T_{m2,n-1}} - d_{m2}.\overline{T_{m1,n}} - d_{m2}.\overline{T_{m3,n}} \qquad \text{equation 4.20}$$

Equation 4.18, 4.19 and 4.20 can then be written in a matrix equation, representing nodes 1 to n:

$$\begin{bmatrix} T_{m2,1}^{t-dt} \\ \vdots \\ T_{m2,i}^{t-dt} \\ \vdots \\ T_{m2,n}^{t-dt} \end{bmatrix} = \begin{bmatrix} a_{m2\_1} & -b_{m2} & \cdots & \cdots & 0 \\ -b_{m2} & a_{m2} & \ddots & & \vdots \\ 0 & \ddots & a_{m2} & \ddots & \vdots \\ \vdots & & \ddots & a_{m2} & -b_{m2} \\ 0 & \cdots & 0 & -b_{m2} & a_{m2\_n} \end{bmatrix} \times \begin{bmatrix} \overline{T_{m2,1}} \\ \vdots \\ \overline{T_{m2,\iota}} \\ \vdots \\ \overline{T_{m2,n}} \end{bmatrix} + \begin{bmatrix} -d_{m2} & 0 & \cdots & \cdots & 0 \\ 0 & \ddots & \ddots & & \vdots \\ \vdots & \ddots & -d_{m2} & \ddots & \vdots \\ \vdots & & \ddots & \ddots & 0 \\ 0 & \cdots & \cdots & 0 & -d_{m2} \end{bmatrix} \times \begin{bmatrix} \overline{T_{m1,1}} \\ \vdots \\ \overline{T_{m1,\iota}} \\ \vdots \\ \overline{T_{m1,n}} \end{bmatrix} + \begin{bmatrix} -d_{m2} & 0 & \cdots & \cdots & 0 \\ 0 & \ddots & \ddots & & \vdots \\ \vdots & \ddots & -d_{m2} & \ddots & \vdots \\ \vdots & & \ddots & \ddots & 0 \\ 0 & \cdots & \cdots & 0 & -d_{m2} \end{bmatrix} \times \begin{bmatrix} \overline{T_{m3,1}} \\ \vdots \\ \overline{T_{m3,\iota}} \\ \vdots \\ \overline{T_{m3,n}} \end{bmatrix} + \begin{bmatrix} -e_{m2}.\overline{T_{in}} \\ 0 \\ \vdots \\ \vdots \\ 0 \end{bmatrix}$$

4.3.5.3.3 Third PCM node (final PCM volume located at the middle of the PCM layer)

The application of the heat balance equation for the i[th] and first crosswise (j=3) PCM node results in the following equation:

$$\rho_m . Cp_m . V_{m3} . \frac{dT_{m3,i}}{dt} = \frac{T_{m2,i} - T_{m3,i}}{R_{m\_7}} + \frac{T_{m3,i-1} - 2.T_{m3,i} + T_{m3,i+1}}{R_{m\_6}} \qquad \text{equation 4.21}$$

Where

$V_{m3} = S_{m3} \cdot dx$:	Volume of the third PCM node	[m^3]
$S_{m2} = \frac{dy_m}{6} \cdot dz$:	Contact surface between neighboring PCM nodes	[m^2]
$T_{m3,i-1}$:	Third PCM temperature at node i-1	[°C]
$T_{m3,i+1}$:	Third PCM temperature at node i+1	[°C]

By introducing the average temperature term, equation 4.21 becomes:

$$\frac{2.\rho_m . Cp_m . V_{m3}}{dt} . \left(\overline{T_{m3,i}} - T_{m3,i}^{t-dt}\right) = \frac{\overline{T_{m2,i}} - \overline{T_{m3,i}}}{R_{m,7}} + \frac{\overline{T_{m3,i-1}} - 2.\overline{T_{m3,i}} + \overline{T_{m3,i+1}}}{R_{m\_6}}$$

Setting:

$$a_{m3} = 1 + 2.b_{m3} + d_{m3},\ b_{m3} = \frac{dt}{2.\rho_m . Cp_m . V_{m3} . R_{m\_6}}\ \ and\ \ d_{m3} = \frac{dt}{2.\rho_m . Cp_m . V_{m3} . R_{m,7}}$$

The final equation 4.22 is obtained:

$$T_{m3,i}^{t-dt} = a_{m3} . \overline{T_{m3,i}} - b_{m3} . \left(\overline{T_{m3,i-1}} + \overline{T_{m3,i+1}}\right) - d_{m3} . \overline{T_{m2,i}} \qquad \text{equation 4.22}$$

For nodes i=1 and i=n

$$a_{m3\_1} = 1 + b_{m3} + d_{m3} + e_{m3},\ a_{m3\_n} = 1 + b_{m3} + d_{m3}\ \ with\ \ e_{m3} = \frac{1}{2.\rho_m . Cp_m . V_{m3} . R_{m\_3}}$$

Obtaining:

$$T_{m3,1}^{t-dt} = a_{m3_1} . \overline{T_{m3,1}} - b_{m3} . \overline{T_{m3,2}} - d_{m3} . \overline{T_{m2,1}} - e_{m3} . \overline{T_{in}} \qquad \text{equation 4.23}$$

and

$$T_{m3,n}^{t-dt} = a_{m3\_n} . \overline{T_{m3,n}} - b_{m3} . \overline{T_{m3,n-1}} - d_{m3} . \overline{T_{m2,n}} \qquad \text{equation 4.24}$$

Equations 4.22, 4.23 and 4.24 can then be written in a matrix equation, representing nodes 1 to n:

$$\begin{bmatrix} T_{m3,1}^{t-dt} \\ \vdots \\ T_{m3,i}^{t-dt} \\ \vdots \\ T_{m3,n}^{t-dt} \end{bmatrix} = \begin{bmatrix} a_{m3\_1} & -b_{m3} & \cdots & \cdots & 0 \\ -b_{m3} & a_{m3} & \ddots & & \vdots \\ 0 & \ddots & a_{m3} & \ddots & \vdots \\ \vdots & & \ddots & a_{m3} & -b_{m3} \\ 0 & \cdots & 0 & -b_{m3} & a_{m3\_n} \end{bmatrix} \times \begin{bmatrix} \overline{T_{m3,1}} \\ \vdots \\ \overline{T_{m3,i}} \\ \vdots \\ \overline{T_{m3,n}} \end{bmatrix} + \begin{bmatrix} -d_{m3} & 0 & \cdots & \cdots & 0 \\ 0 & \ddots & \ddots & & \vdots \\ \vdots & \ddots & -d_{m3} & \ddots & \vdots \\ \vdots & & \ddots & \ddots & 0 \\ 0 & \cdots & \cdots & 0 & -d_{m3} \end{bmatrix} \times \begin{bmatrix} \overline{T_{m2,1}} \\ \vdots \\ \overline{T_{m2,i}} \\ \vdots \\ \overline{T_{m2,n}} \end{bmatrix} + \begin{bmatrix} -e_{m3}.\overline{T_{in}} \\ 0 \\ \vdots \\ \vdots \\ 0 \end{bmatrix}$$

4.3.5.3.4 Centralized matrix and solution

In the end, the matrix equations obtained from each layer are assembled into the following centralized matrix equation:

$$\bar{T} = A^{-1}.\left(T^{t-dt} - B\right) \qquad \text{equation 4.25}$$

Where

$\bar{T}$ is a n*(m+2) column matrix containing average temperature values for the air, aluminum and PCM layers,

A is a n*(m+2) x n*(m+2) matrix containing thermal resistance coefficients,

T^{t-dt} is a n*(m+2) column matrix containing temperature values for the three layers at the previous time step and

B is a n*(m+2) containing initial temperature values for the three layers.

Finally, air, aluminum and PCM temperatures at each node and at each time step are calculated using inlet air temperature, neighboring nodes temperature and temperatures calculated at the previous time step with the final equation:

$$T^{t} = 2.\bar{T} - T^{t-dt} \qquad \text{equation 4.26}$$

In the end, the use of the heat balance approach and the finite difference method as presented in the previous subsections was reduced to the solution of the matrix equation shown in figure 4.4.

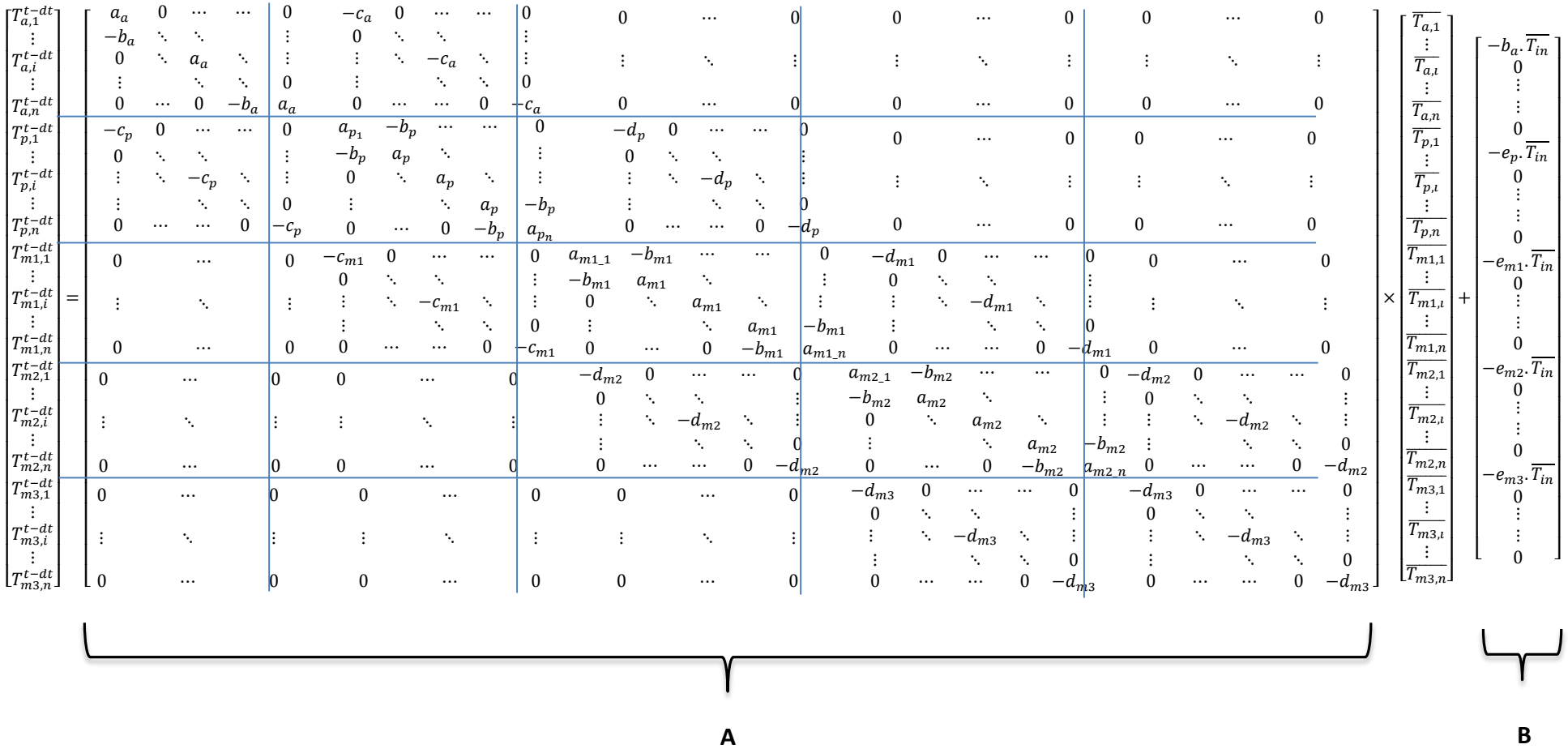

Figure 4.4 Centralized matrix equation

4.3.6 Model assumptions

The main objective of the numerical study is to develop a model that uses as entries the air temperature and airflow rate and calculates the outlet air temperature, emphasizing on the calculation speed and not necessarily on the complexity of the phenomena taking place inside the PCM. In view of this fact, several assumptions and simplifications were made. First of all, the plates are considered to be fully filled with PCM, whereas in reality a small percentage was left vacant to avoid leakage risks. Airflow is considered equal for all air layers; this is performed by simply dividing the initial total airflow by the number of air layers. In reality and as presented in the previous chapter small variations may exist.

As seen in figure 4.2, the model calculates heat transfers in two dimensions (lengthwise and crosswise), considering that same conditions are met height wise. The model calculates the temperature evolution for half of the air and PCM layers, assuming that by symmetry the results can be extended to the other half (where similar conditions apply). The model considers convection transfers between the air and the aluminum layers and conduction transfers for aluminum and PCM layers. However, it does not take into account convection inside the PCM during the melting and the liquid phases, as well as radiative emissions between plates.

Concerning the volume change between phases, the model integrates a change of the PCM density value but does not consider the increase of the PCM level inside the container.

Finally, the convective heat transfer coefficient was treated as a calibration factor and was empirically determined at 50 W/m^2K for an airflow rate of $100m^3/h^1$, with a corresponding increase of 5 W/m^2K for every $100m^3/h$ augmentation of the airflow rate.

4.4 Numerical model calibration, specific heat capacity importance

As previously mentioned, a partner of the Stock-Air project (EDF R&D Matériaux et Mécanique des Composants) was assigned to determine the properties of the Microtek 37D properties, including thermal conductivity, density, heat capacity and phase change temperature range. Table 3.1 presents these values for the solid and liquid phases of the paraffin. The value of each property was altered at each node, according to the PCM temperature using a Matlab interpolation function (interp1).

These values were used in the developed numerical model, providing promising but not satisfying results, when compared to experimental ones. After various factors were investigated, the importance of the PCM heat capacity (C_p) values was made clear.

4.4.1 DSC Method

The heat capacity values of the PCM were obtained by EDF R&D Matériaux et Mécanique des Composants using the Differential Scanning Calorimetry (DSC) method. DSC is a measuring technique where a sample material (in this case paraffin) is compared to a reference material (with known properties) while undergoing a heating or cooling process. More specifically, known masses of the sample and of the reference material are placed on two symmetrically mounted sample holders (or pans). Two heating elements are used to heat the materials at a constant rate. A temperature control

system measures the temperature difference between the two pans and adjusts this difference to zero by controlling a differential component of the total heating power. The measurement of this differential power and the knowledge of the heat capacity value of the reference material allow the calculation of the heat capacity of the sample material.

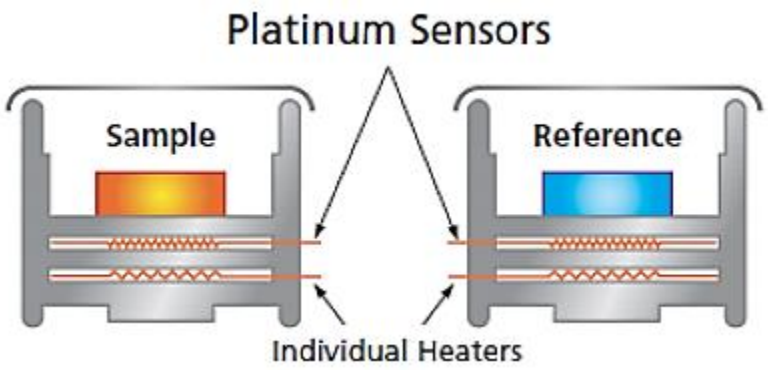

Figure 4.5: Representation of the DSC method (Borderon, 2012)

For the Microtek 37D paraffin, measurements were made on a 0.22623 g sample, for three different heating/cooling rates of 0.15 °C/min, 0.5 °C/min and 1 °C/min. Results are illustrated in figure 4.6. During the heating process, the phase change occurs between 30°C and 42 °C, shifting towards higher temperatures as the heating rate increases. During the cooling process, the phase change occurs between 25 and 35°C, shifting towards lower temperatures as the cooling rate increases.

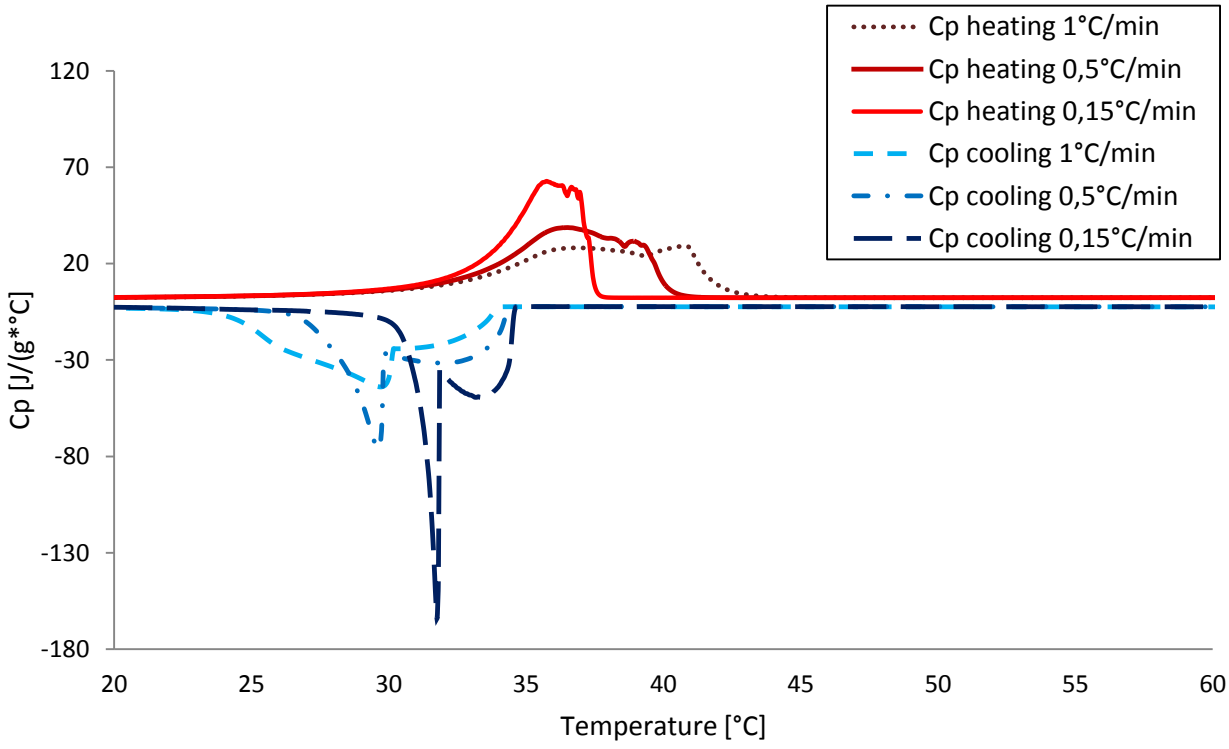

Figure 4.6: DSC obtained heat capacity curves for three different heating/cooling rates

The integration of the heat capacity values over temperature equals the enthalpy change for a determined increase/decrease of temperature, for example from T_1 to T_2, as shown in equation 4.27:

$$\Delta H = \int_{T_1}^{T_2} C_p dT \qquad \text{equation 4.27}$$

The enthalpy change for the six heat capacity curves obtained through the DSC method was calculated in Matlab using the trapezoidal numerical integration function (trapz). This function integrates the heat capacity values with temperature spacing increment by breaking the area down into trapezoids with more easily computable areas. Results are presented in table 4.1.

	Heating / Cooling rate		
	0,15 °C/min	0,5 °C/min	1 °C/min
Enthalpy change during the heating process (J/g)	364,23	361,53	356,35
Enthalpy change during the cooling process (J/g)	-362,38	-362,65	-360,59

Table 4.1: Enthalpy change during heating/cooling of the PCM based on DSC results

Even though six different curves were integrated, the obtained enthalpy change values are similar for the different heating/cooling rates. Three options were then offered as heat capacity values for the numerical model. The ones corresponding to the 0,5°C/min heating/cooling rates were initially selected and a full thermal cycle of charging and discharging was numerically reproduced in order to compare the results with the experimental ones. The model uses as inputs the experimental inlet air temperature and airflow rate values to calculate the downstream temperature evolution of the air, aluminum and PCM layer for every time step dt=10s. An interpolation Matlab function was used to associate heat capacity values to temperature values. Furthermore, the model switches between the heating curve and the cooling one by comparing the PCM temperature value during two consecutive time steps.

Discussion of simulation results using DSC heat capacity values

Simulations were carried out for five airflow rates, in accordance to the experimental characterization tests of the heat exchanger. Results for an airflow rate of 300m3/h are presented here as they are representative of the rest. Therefore, the two following figures illustrate the comparison between experimental and numerical results for the inlet and outlet air temperature values (figure 4.7) as well as the PCM temperature values at the middle of the PCM layer (node n=5 lengthwise, figure 4.8).

Results show that the numerical model underestimates the temperature values, this occurring with an increasing rate downstream. No distinct end of the phase change process is observed (end of the melting procedure), as the temperature values increase with an almost constant rate after the beginning of the melting phase. All this results in lower temperatures at the end of the charging phase and higher temperatures at the end of the discharging phase, compared to experimental data. Lastly, during the discharge phase, two peaks appear in the experimental data for the PCM temperature values, linked to

the intrinsic properties of the paraffin (figures 4.8 and 3.17). However, and even though the heat capacity values used during simulation present two peaks, numerical results do not reproduce the experimentally observed phenomenon (figure 4.8).

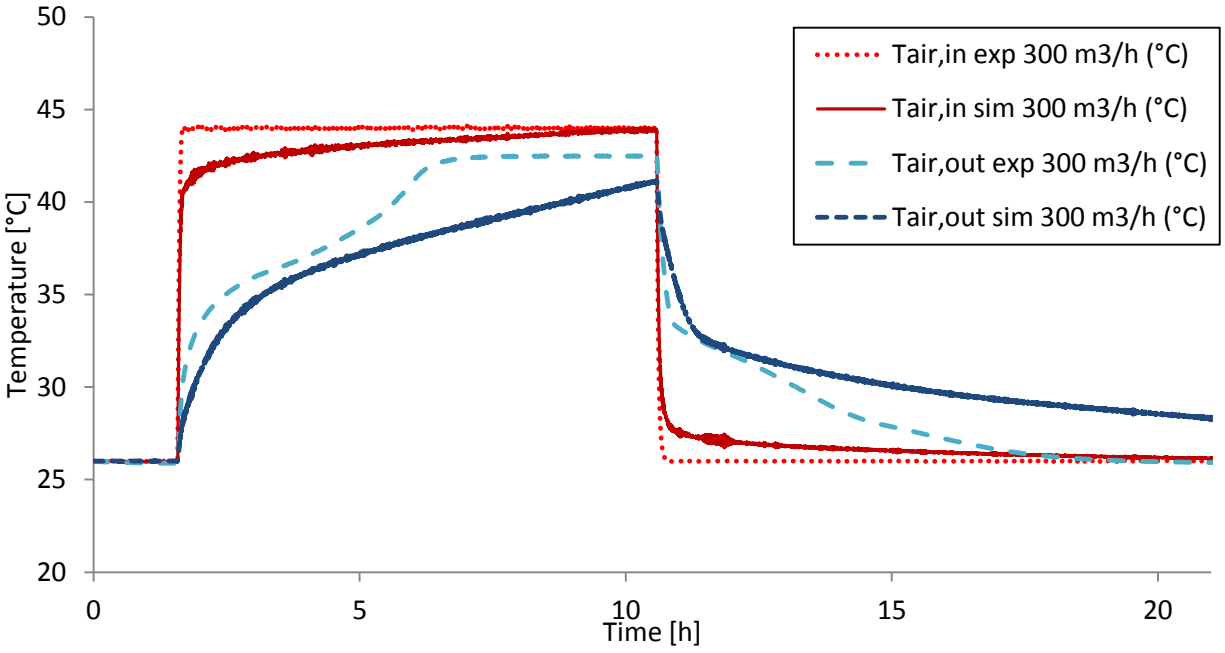

Figure 4.7: Simulation results for inlet and outlet air temperature using DSC obtained heat capacity curves and comparison with experimental data

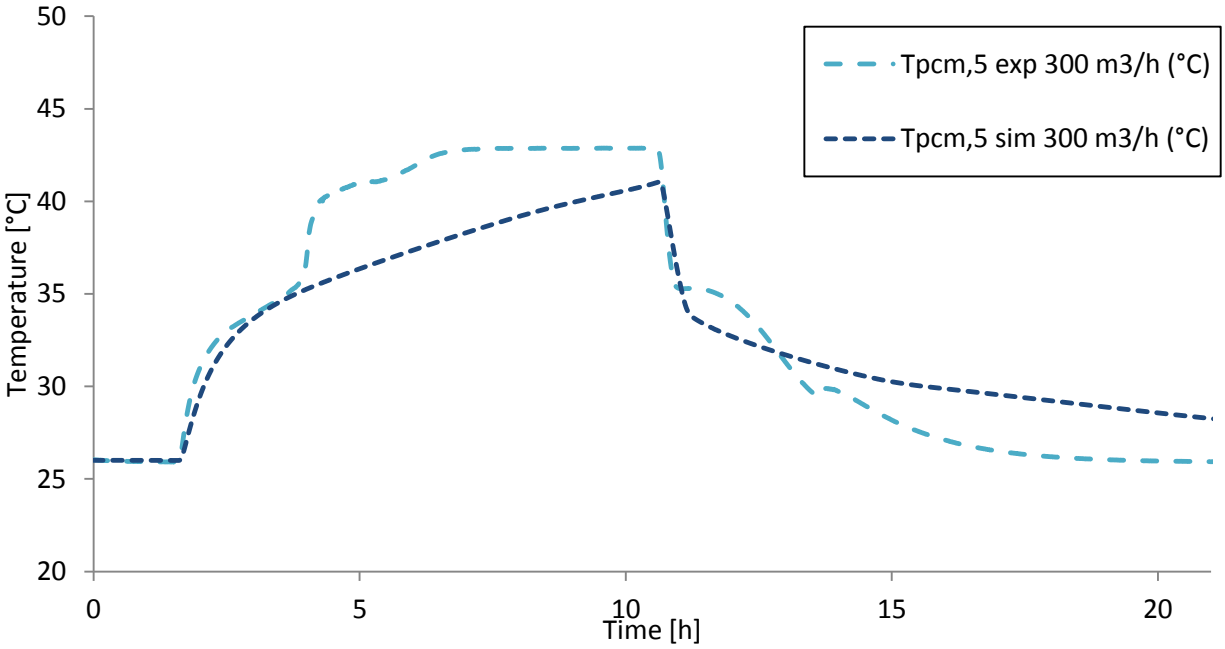

Figure 4.8:Simulation results for PCM temperature at node 5 using DSC obtained heat capacity curves and comparison with experimental data

Albright et al. conclude that the DSC process can provide inaccurate data due to undesired thermal gradients within the sample and that corrections should be made. In addition, as noted in the final report of IEA Annex 17, DSC results depend on the heating rate. This dependency was also observed for the PCM in question and the results obtained using the DSC method, where different curves are acquired for different heating/cooling rates (figure 4.6 again).

4.4.2 Creation of adequate heat capacity values

The aforementioned observations led to the investigation of the heat capacity values and the creation of adequate curves based on DSC results. This was performed through a several steps process, each time observing the impact of the created heat capacity curves on the simulation results and comparing them to experimental data. This process is presented in the following subsections.

4.4.3 First approach: isosceles triangle

The first approach consisted in representing the heat capacity values with a curve having the form of an isosceles triangle (figure 4.9). The same curve was used for the heating and cooling processes. The underestimation of numerical temperature values pointed to a decrease of the heat capacity values, as, physically speaking, this quantity represents the amount of heat needed to raise a material's temperature the temperature of a material by one degree. Indeed, the calculated enthalpy change (integration of heat capacity over temperature) for the created heat capacity curve was 220 J/g, significantly lower than the DSC values (around 360 J/g, table 4.1).

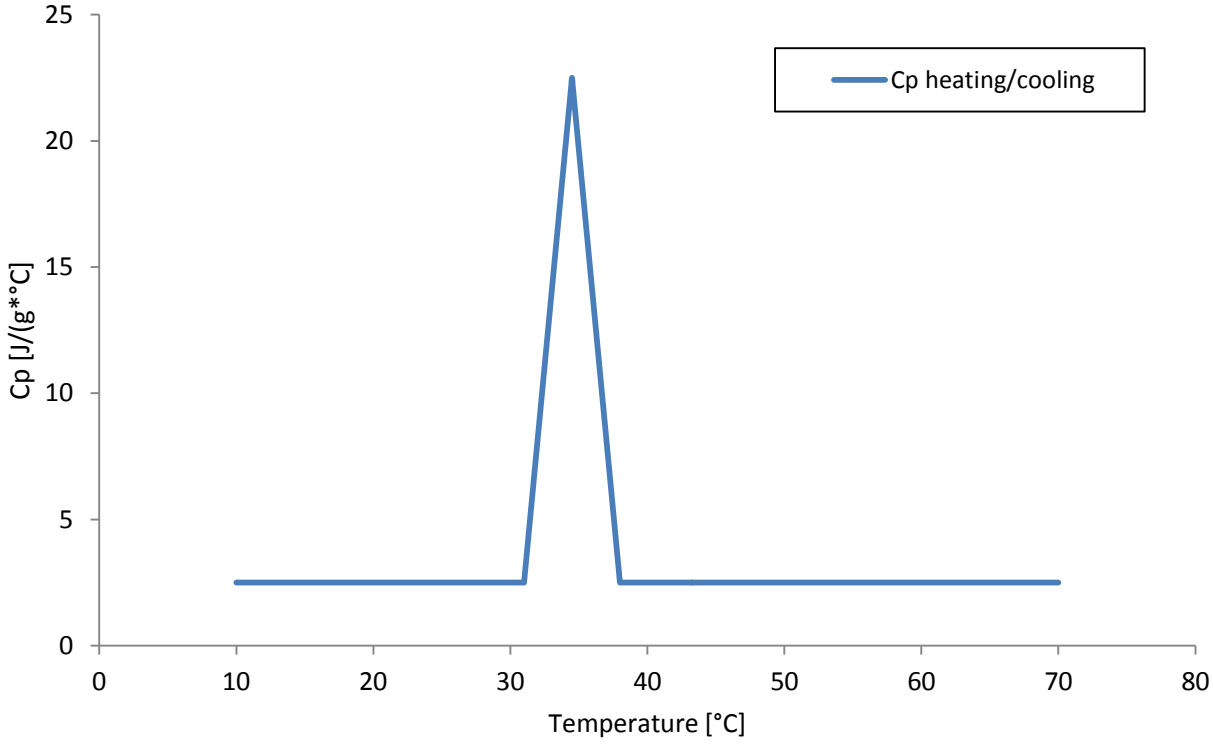

Figure 4.9: Fictive Heat capacity values, first approach

Discussion of simulation results using isosceles triangle shaped heat capacity values

The numerical reproduction of the characterization tests demonstrated that this modification was on the right path. Figures 4.10 and 4.11 illustrate, as before, the comparison between experimental and numerical results for the inlet and outlet air temperature values as well as the PCM temperature values at the middle of the PCM layer (node n=5 lengthwise). This time, the model managed to provide results closer to the experimental ones. Nevertheless, the two peaks observation during the experimental discharge phase was still not apparent in the numerical results.

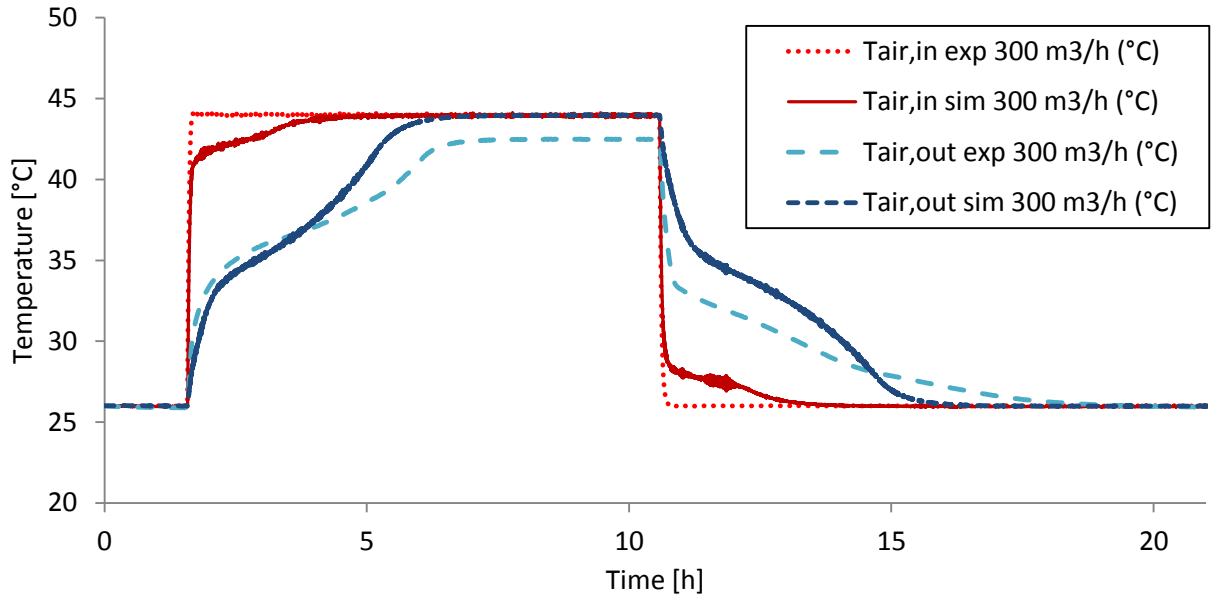

Figure 4.10: Simulation results for inlet and outlet air temperature using first approach's heat capacity curves and comparison with experimental data

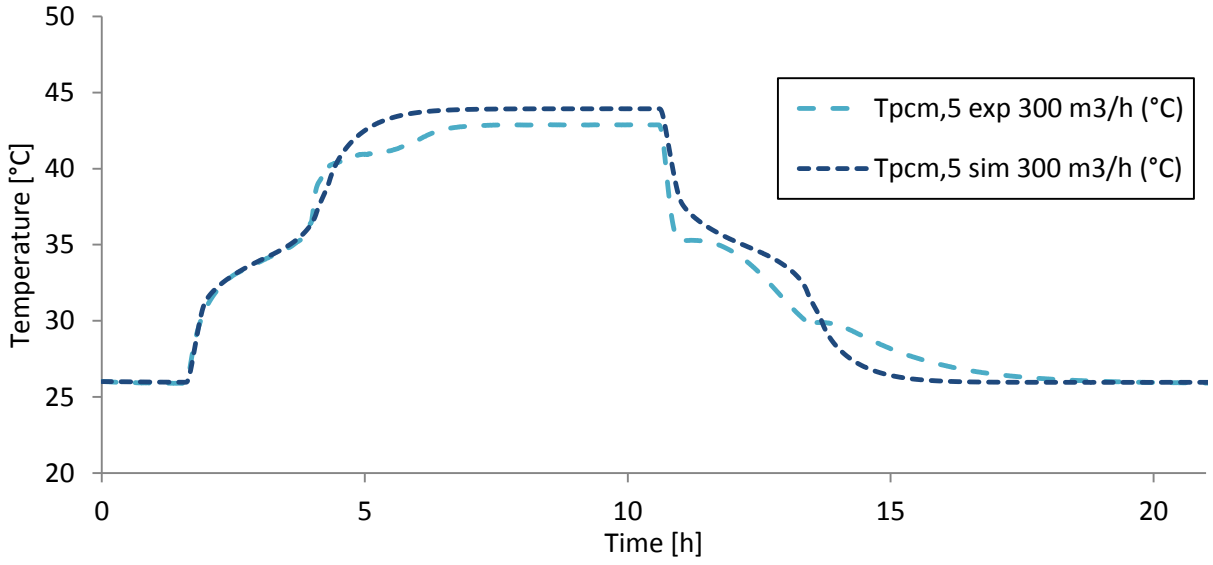

Figure 4.11: Simulation results for PCM temperature at node 5 using first approach's heat capacity curves and comparison with experimental data

4.4.4. Second approach: two peaks curve for the discharge phase

A second approach was considered, creating a right triangle for the charging phase and an irregular polyhedron for the discharging phase. Two peaks were created for the discharging phase. An effort was made to maintain the same enthalpy change value. After calculation ΔH,heating= 220,58 J/g and ΔH,cooling= -234,79 J/g.

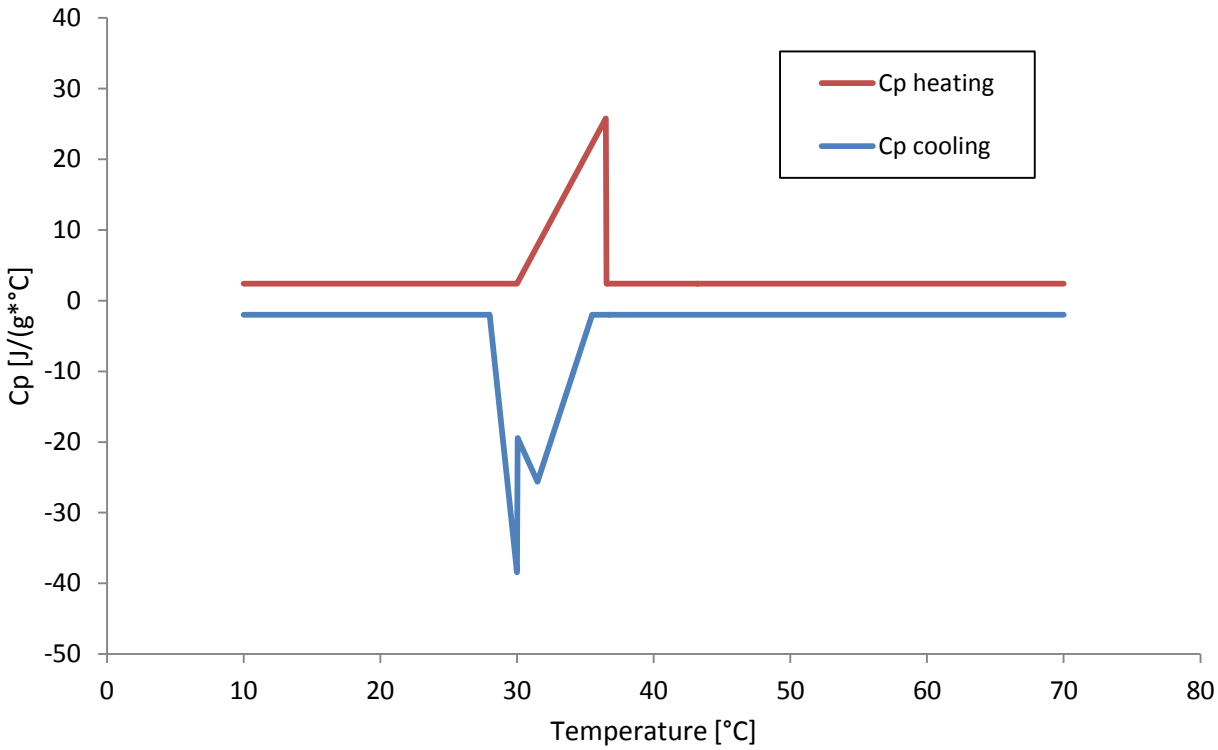

Figure 4.12: Fictive Heat capacity values, second approach

Discussion of simulation results using a two peaks curve for the discharge phase

Results of the second approach are presented in figure 7.13 and 7.14, illustrating the comparison between experimental and numerical results for the inlet and outlet air temperature values as well as the PCM temperature values at the middle of the PCM layer (node n=5 lengthwise). The introduction of two peaks in the heat capacity values resulted in the apparition of two peaks in the PCM temperature evolution curve (figure 7.14). However, these peaks were small and misplaced as they are on lower temperature values.

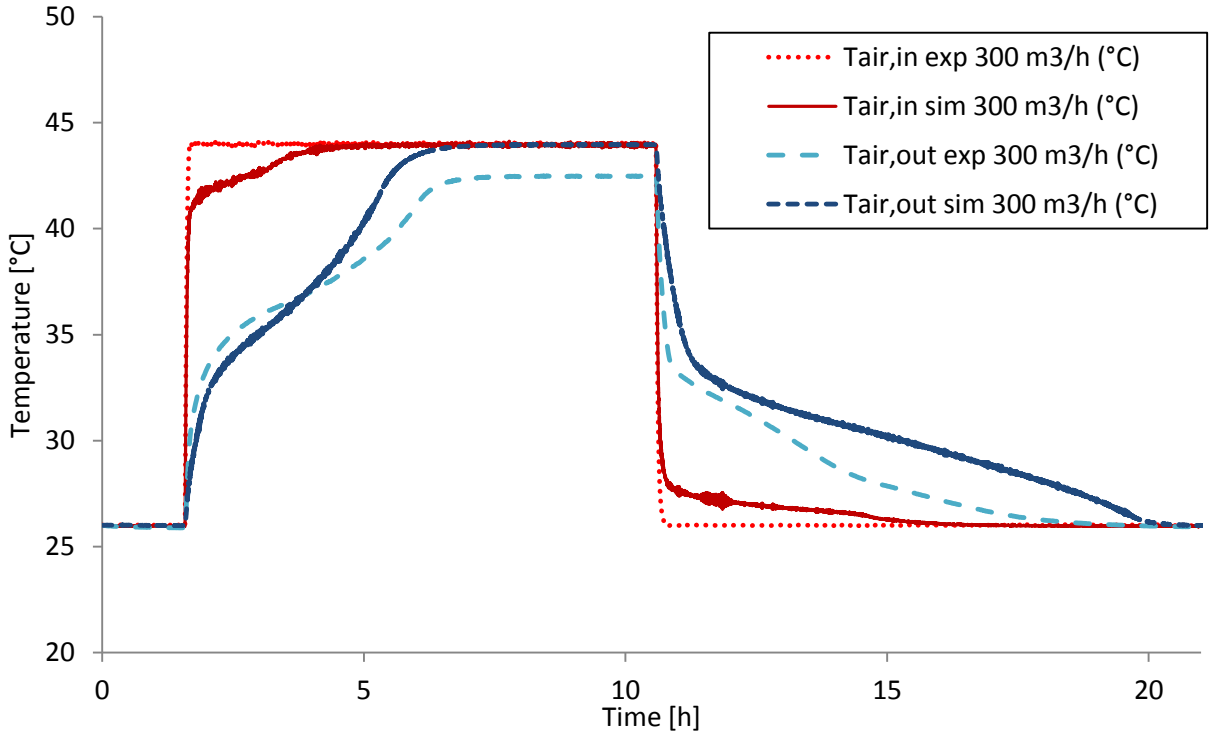

Figure 4.13: Simulation results for inlet and outlet air temperature using second approach's heat capacity curves and comparison with experimental data

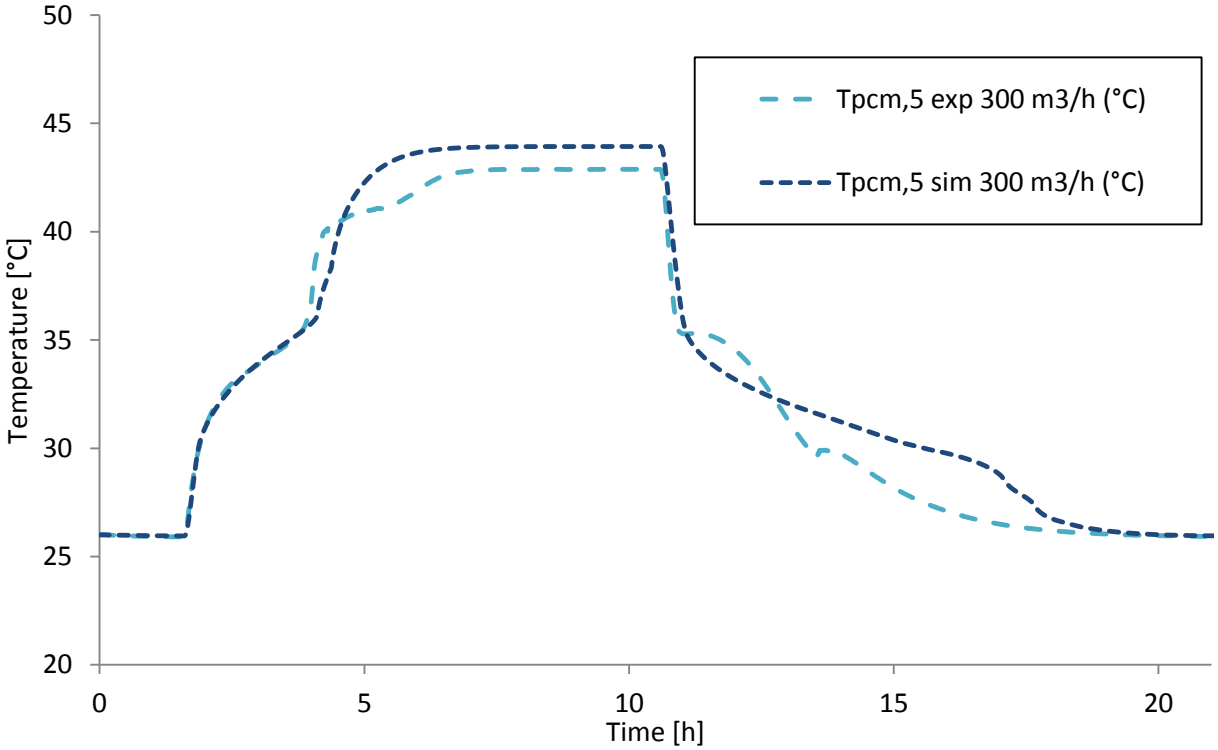

Figure 4.14: Simulation results for PCM temperature at node 5 using second approach's heat capacity curves and comparison with experimental data

4.4.5. Third approach: 2 separate triangles for the discharge phase

Following the remarks of the last approach, a third one was tested, introducing two separate peaks for the heat capacity values of the discharge phase. As before, the enthalpy change was calculated, obtaining ΔH,cooling= -221,37 J/g.

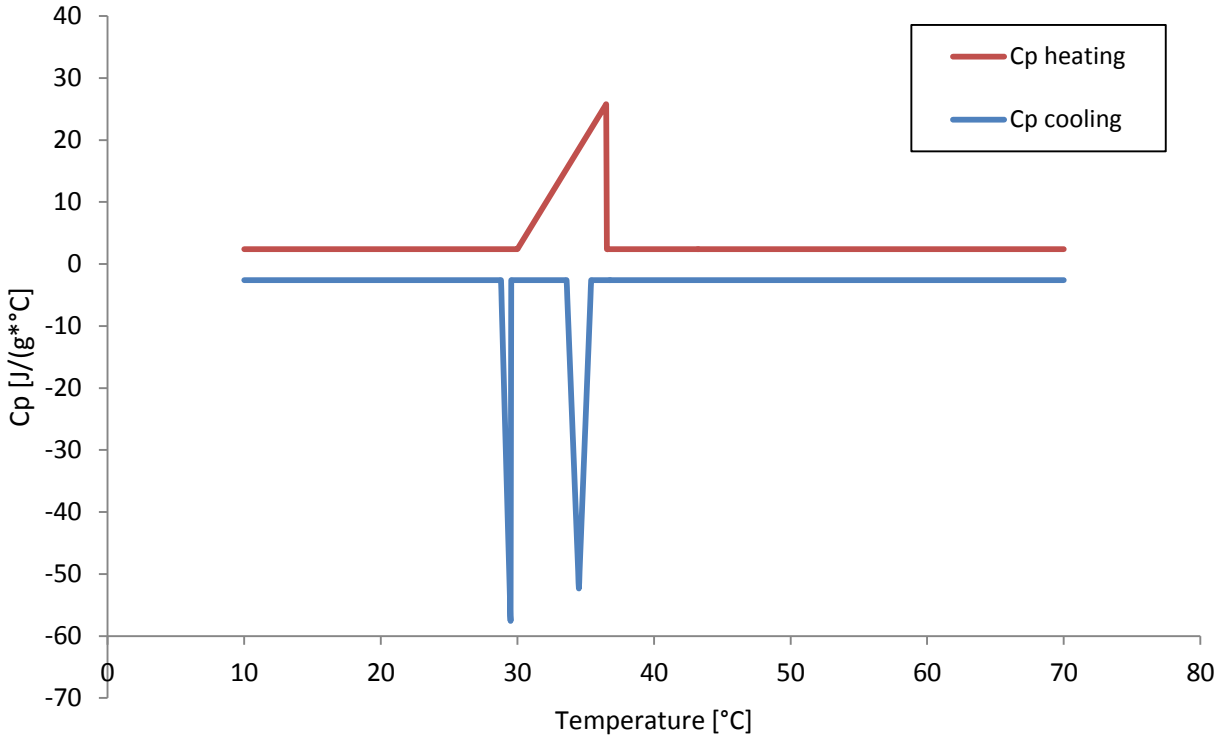

Figure 4.15: Fictive Heat capacity values, third approach

Discussion of simulation results using 2 separate triangles for the discharge phase

The results of the second approach are illustrated in figure 4.16 and 4.17. Two separate and distinctive peaks appear on the PCM temperature curve during the discharging phase, following the peaks observed on experimental data (figure 4.17). This approach provided satisfying results but an offset was still observed for the PCM temperature values along the plate (inlet, middle and outlet parts).

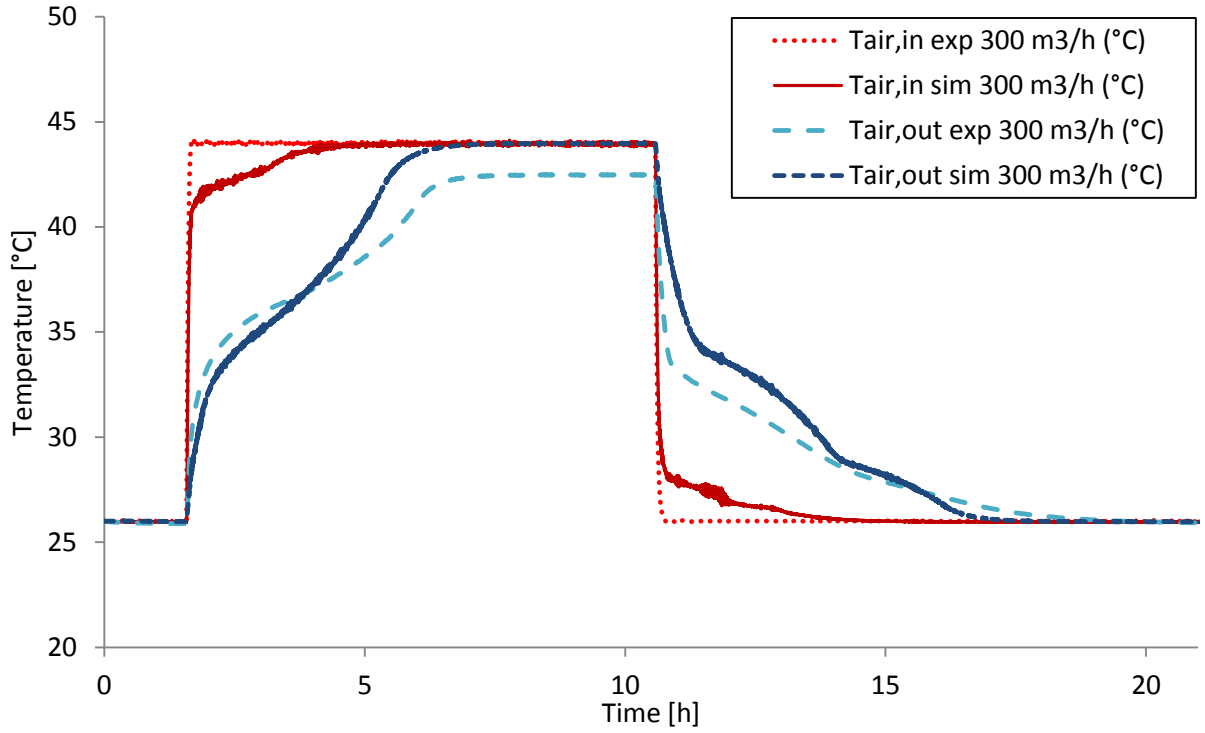

Figure 4.16: Simulation results for inlet and outlet air temperature using third approach's heat capacity curves and comparison with experimental data

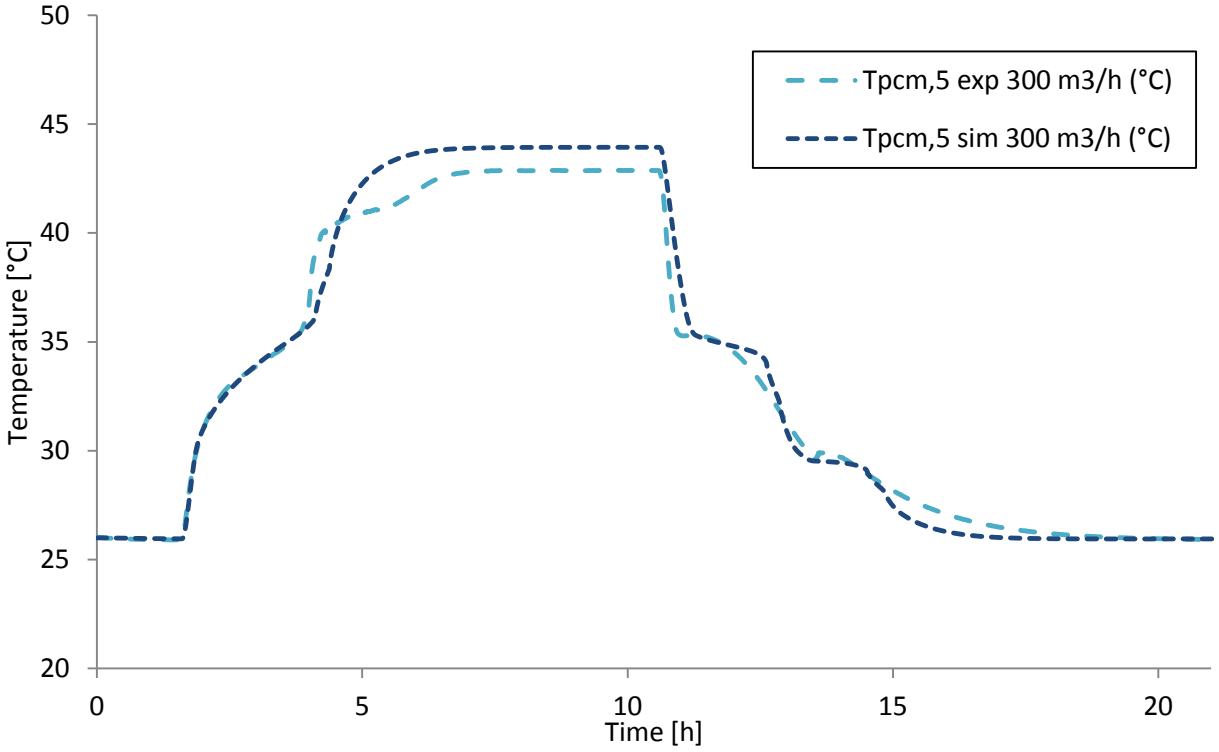

Figure 4.17: Simulation results for PCM temperature at node 5 using third approach's heat capacity curves and comparison with experimental data

4.4.6 Final approach: heat capacity values for different positions along the PCM layer

The observed offset and the remarks of Annex 17 report led to an investigation of experimental results by the downstream positioning of the heat exchanger. Detailed analysis of the experimental data resulted in two observations: heating/cooling rates of the PCM also depend on the stage of stocking/destocking process as well as the part of the plate that we are considering (inlet, middle, and outlet).

This can be observed on figure 4.18 where the surface temperature difference at specific points of the middle plate is illustrated within a one minute interval. More specifically, the temperature difference per minute is calculated at seven points, located at a 15 cm distance from each other. The data presented here correspond to a slightly different setup, as the fins (initially installed between the containers) were totally removed from the heat exchanger in order to install temperature sensors on the surface of the middle plate.

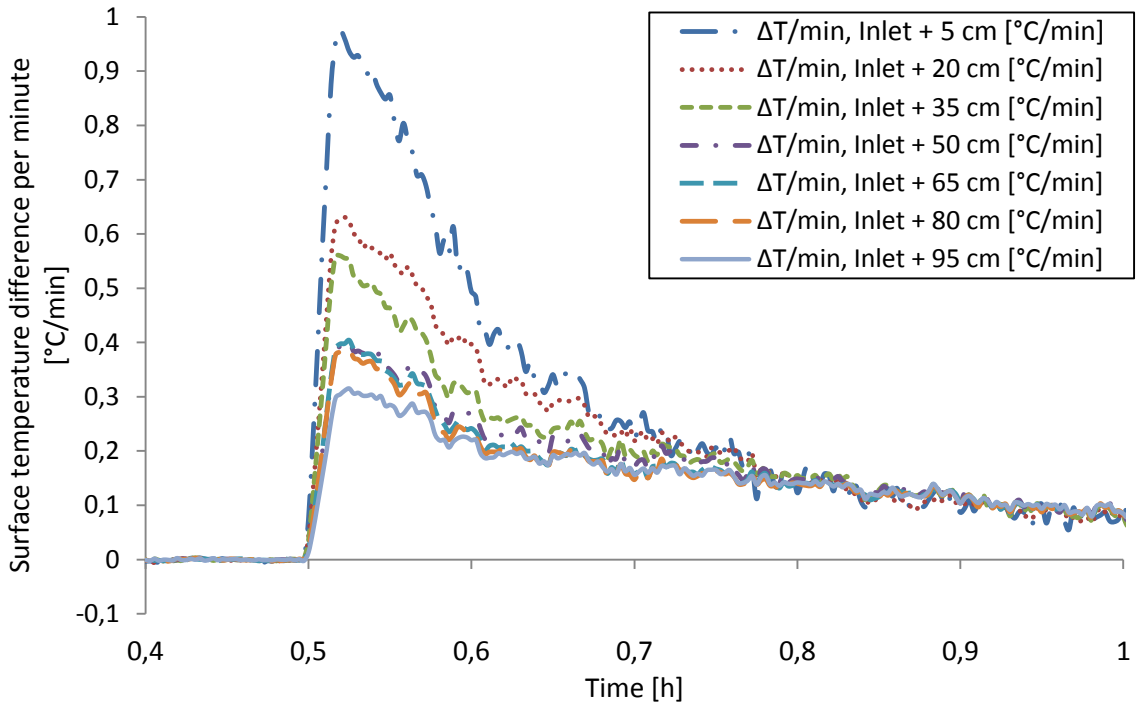

Figure 4.18: Surface temperature difference per minute at different parts of the plate

Data treatment confirms the intuitive observation that the temperature difference decreases as the distance from the inlet part increases. The temperature difference also varies with the stage of the melting/cooling process. These two observations demonstrate that the heating or cooling rates are not the same alongside the plates and that their exact determination can be quite complex to determine considering the various heat transfer processes, the phase change, the eventual changes of the airflow rate, etc. On the contrary, during the DSC measurement heating/cooling rates (ΔT/dt) are kept constant at all times.

This last observation led to the separation of the considered PCM section into three parts (inlet, middle and outlet) and the use of different heat capacity values for each part. For example, for a discretization of n=10 nodes, one curve is used for the four first nodes, a second curve for the next three ones and a final curve for the remaining three (figure 4.19).

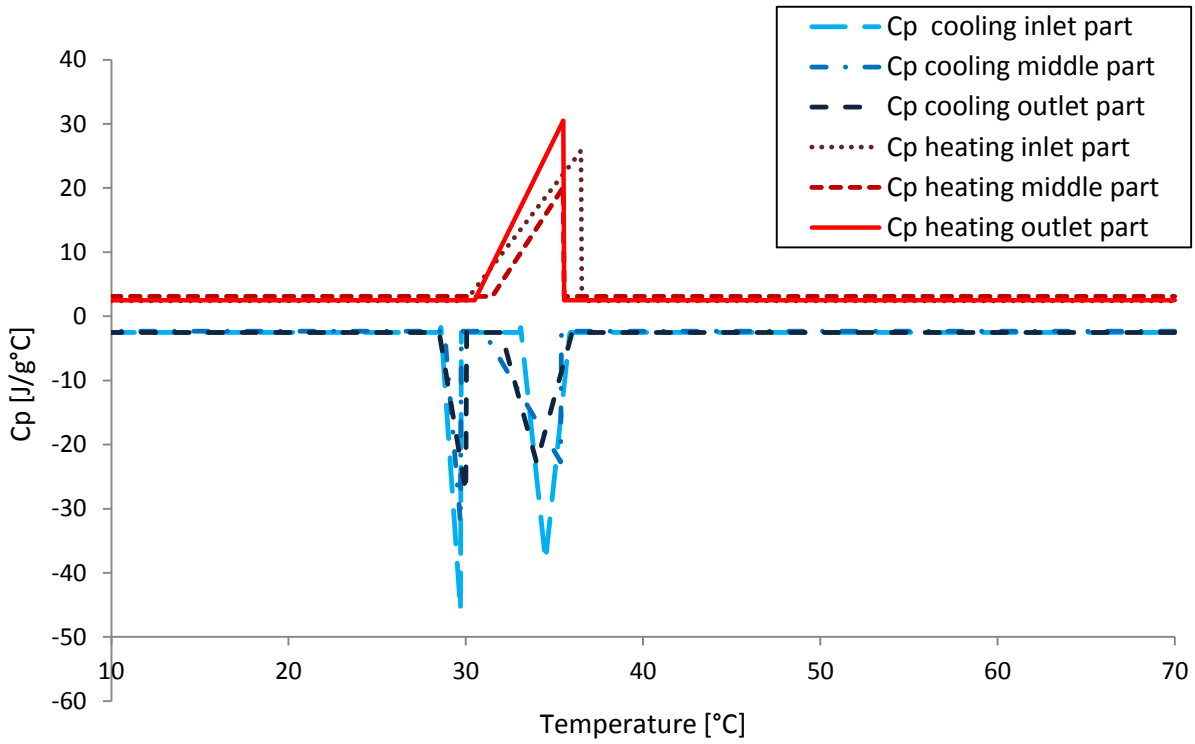

Figure 4.19: Calibrated cp values created for the numerical model

The curves were calibrated having experimental data as a reference and the enthalpy change was once again calculated. The best results were obtained for the values presented in table 4.2.

	Heating / Cooling rate		
	Node 1 to 4	Node 5 to 7	Node 8 to 10
Enthalpy change during the heating process (J/g)	220,58	220,43	220,70
Enthalpy change during the cooling process (J/g)	-223,23	-196,92	-209,96

Table 4.2: Enthalpy change for the three part discretization heat capacity curves (heating and cooling)

4.5 Numerical model validation

Results obtained using the last calibrated heat capacity values (figure 4.19) are demonstrated in this section. The model's ability to reproduce the heat exchanger's behavior is demonstrated with a vast comparison of numerical and experimental results.

More specifically, results are presented for three different airflow rates (100, 300 and 500 m^3/h) at various parts of the heat exchanger:

- Inlet and outlet air temperature (figures 4.20 and 4.21)
- Surface temperature at nodes 1, 5 and 10 length wise (figure 4.22, 4.23 and 4.24)
- PCM temperature at nodes 1, 5 and 10 length wise (figure 4.25, 4.26 and 4.27)

The non-linearity of the temperature evolution during the phase changes is reproduced, including the two peaks that occur during the solidification stage (linked to the intrinsic properties of the paraffin). The small deviations observed on the outlet air temperature are due to the difficulty of the model to integrate the thermal losses of the experimental unit.

Overall, the developed model manages to accurately simulate the heat exchanger's behavior as observed through the experimental platform and is considered validated.

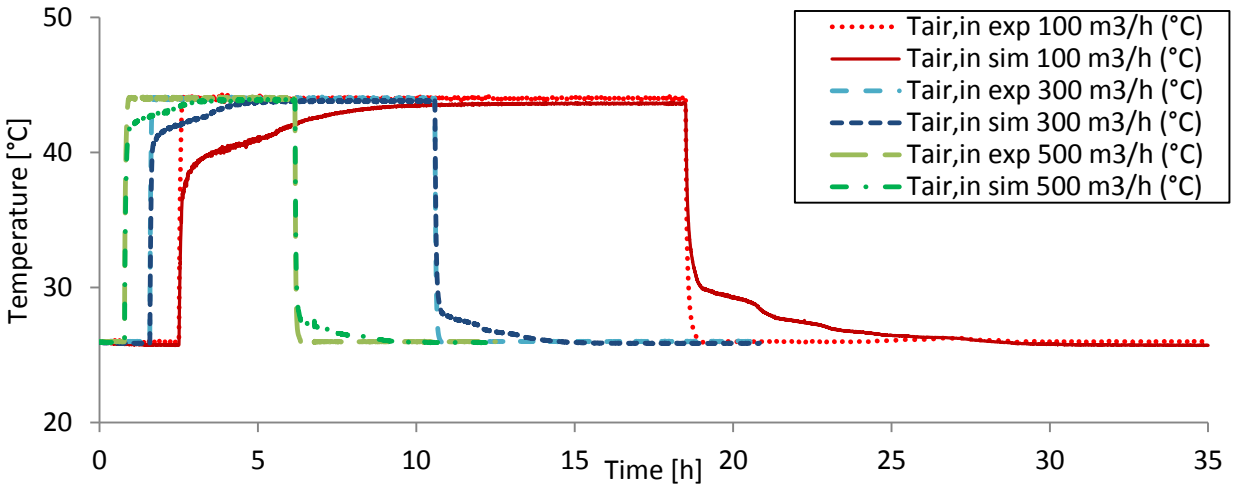

Figure 4.20: Numerical and experimental results for inlet air temperature, for 100, 300 and 500 m3/h

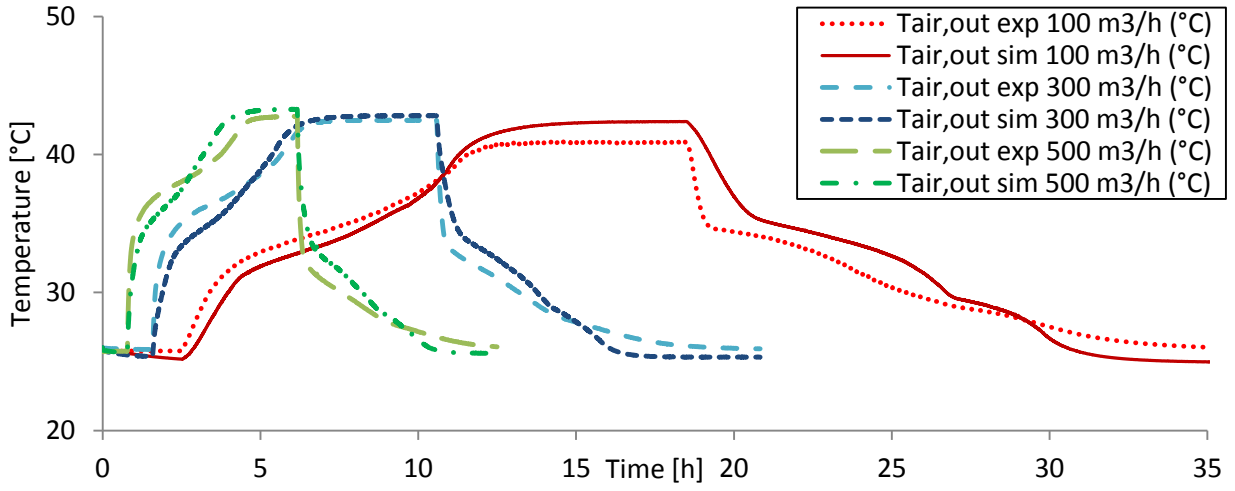

Figure 4.21: Numerical and experimental results for outlet air temperature, for 100, 300 and 500 m3/h

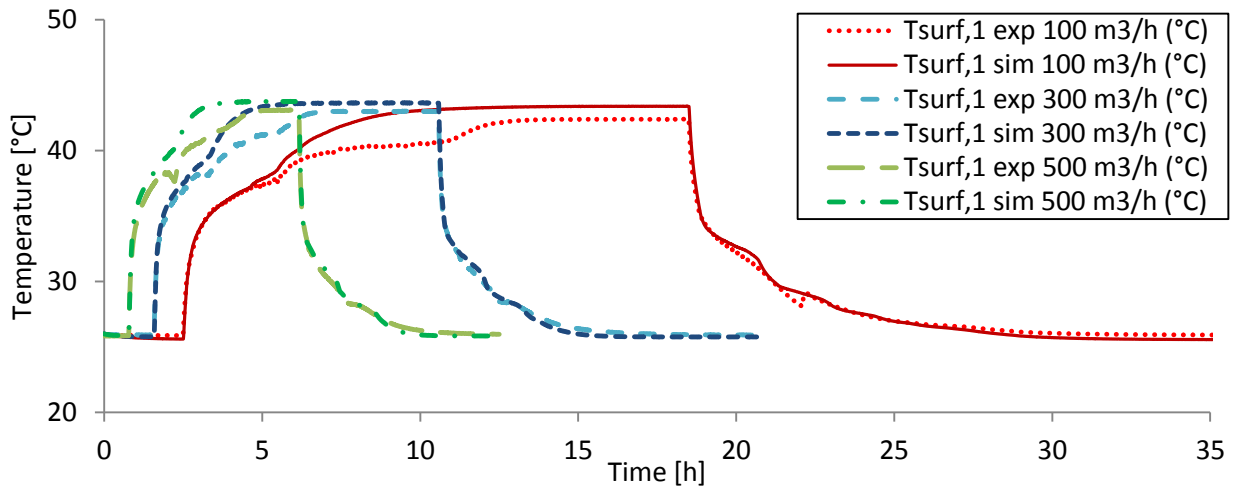

Figure 4.22: Numerical and experimental results for surface temperature at node 1, for 100, 300 and 500 m3/h

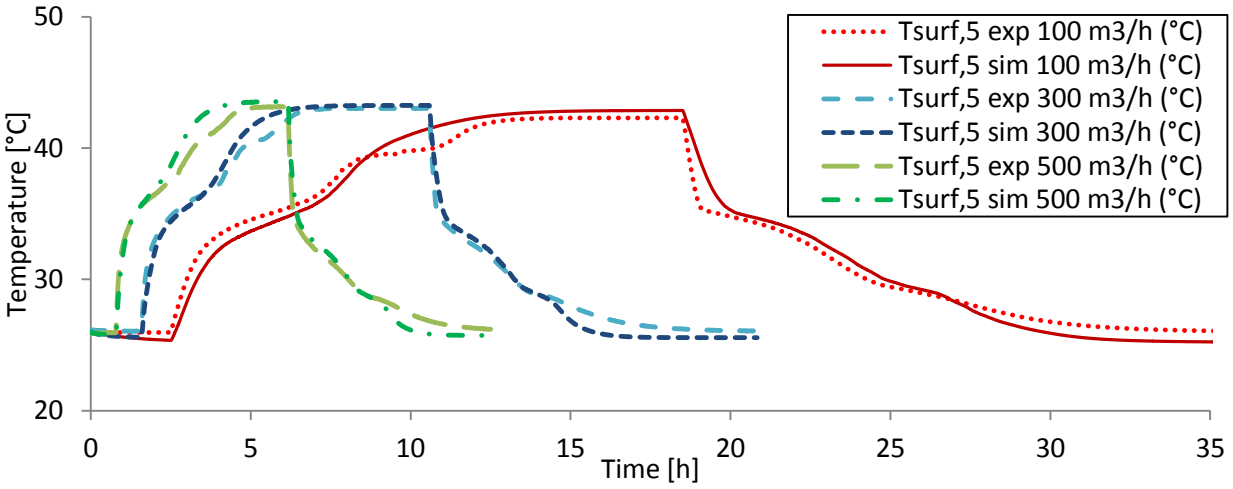

Figure 4.23: Numerical and experimental results for surface temperature at node 5, for 100, 300 and 500 m3/h

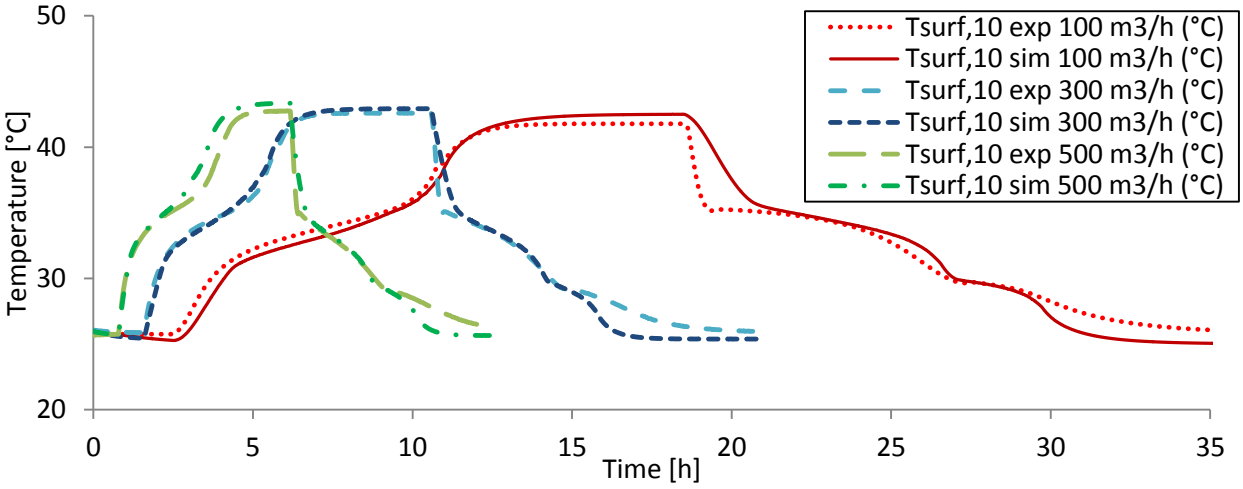

Figure 4.24: Numerical and experimental results for surface temperature at node 10, for 100, 300 and 500 m3/h

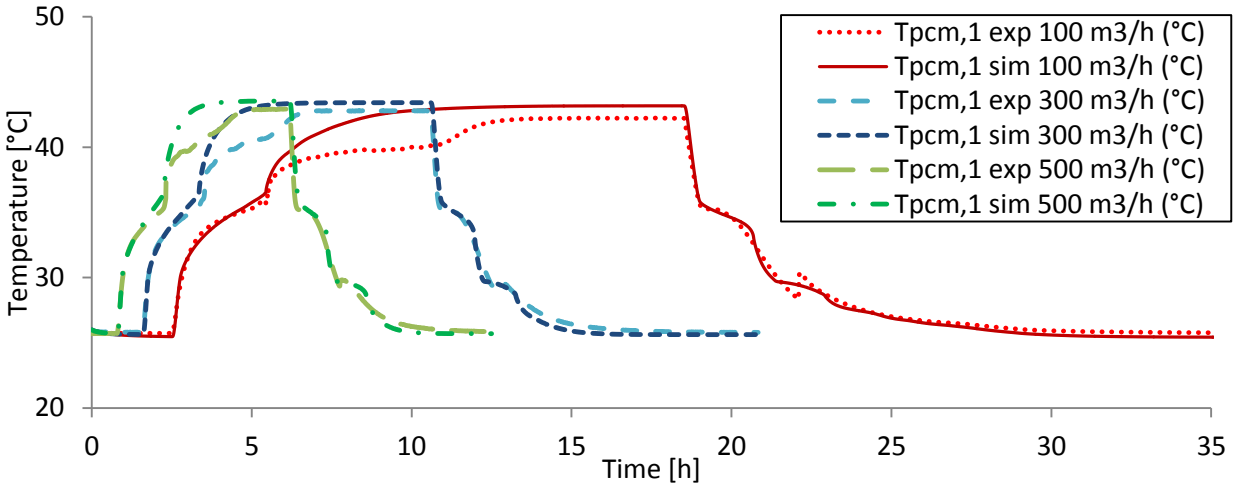

Figure 4.25: Numerical and experimental results for PCM temperature at node 1, for 100, 300 and 500 m3/h

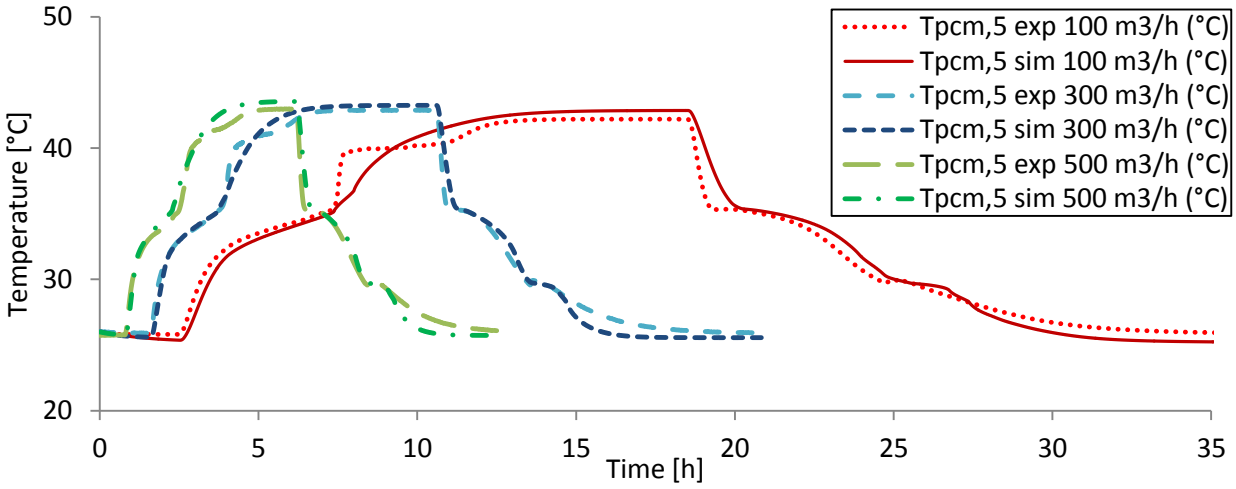

Figure 4.26: Numerical and experimental results for PCM temperature at node 5, for 100, 300 and 500 m3/h

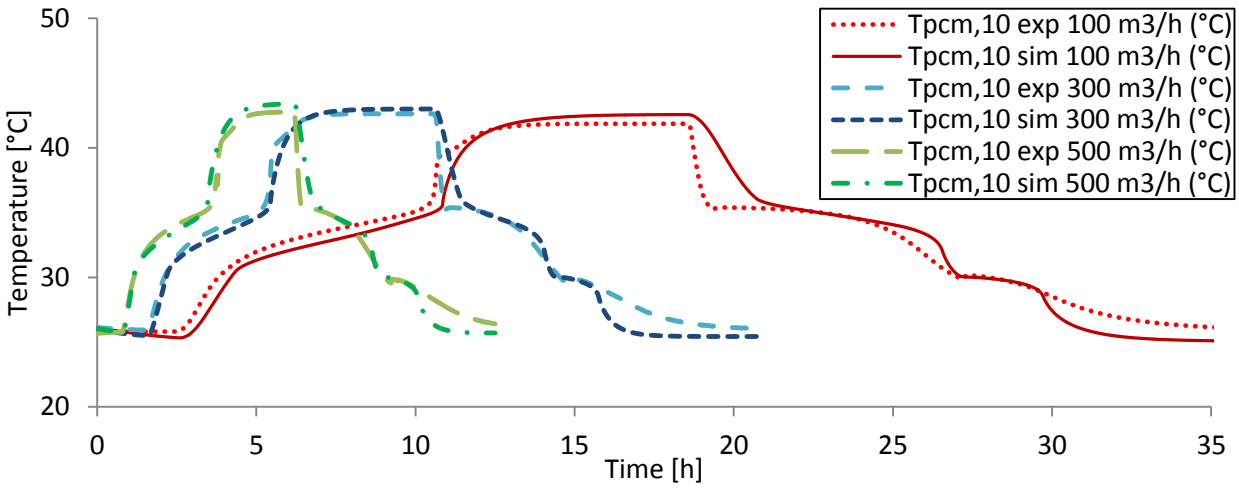

Figure 4.27: Numerical and experimental results for PCM temperature at node 10, for 100, 300 and 500 m3/h

4.6 Coupling with existing building model

4.6.1 Building's model: Hybcell 1.2

Once validated, the numerical model was coupled to an existing building model, the HYBCELL 1.2 (El Mankibi, 2003). HYBCELL 1.2 was developed at LGCB/ENTPE laboratory, under Matlab/Simulink environment by coupling a thermal model and a pressure air flow model.

The thermal model can be divided into three parts: the envelope model based on the finite differences method, the short wavelength radiation model based on an accurate description of the sunspot inside the simulated building and the long wavelength radiation model using the radiosity method. The air flow model is a pressure model that takes into account the effect of the wind and the thermal buoyancy of air to calculate the airflow through the openings of the building.

Indoor air temperature is calculated taking into account several thermal evolution phenomena, such as heat transfer through the walls, air infiltration and ventilation, internal heat gains and auxiliary heating or cooling. Schedule and occupation patterns can also be integrated in the model (figure 4.28).

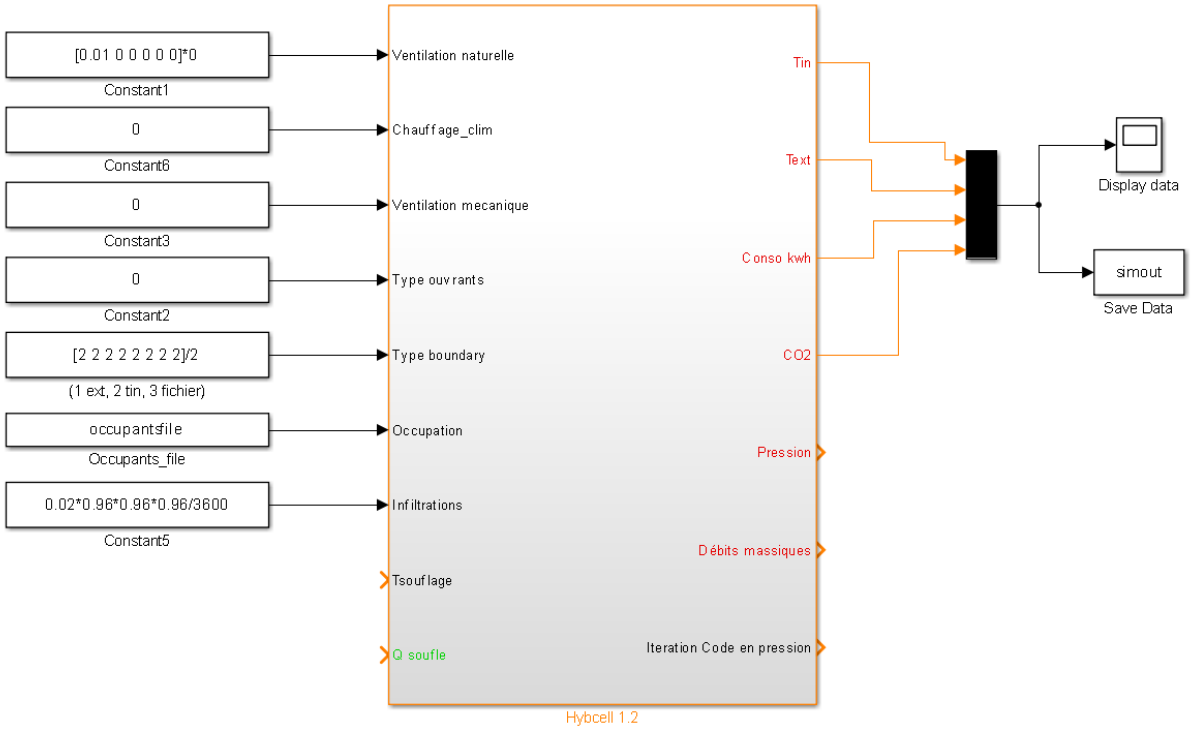

Figure 4.28: Hybcell 1.2 model for building simulation

4.6.2 Definition of the experimental test cell

The characteristics of the experimental test cell were introduced into Hybcell 1.2, including geometry, orientation, openings and composition of the envelope (figure 4.29). The four walls, floor and ceiling were introduced, defining their composition and properties, such as reflection, absorption and emissivity coefficients (figures 4.30 and 4.31, north-east wall). Likewise, the six window openings were introduced in the north-east wall, entering the exact position, materials, and properties of each one (figure 4.31).

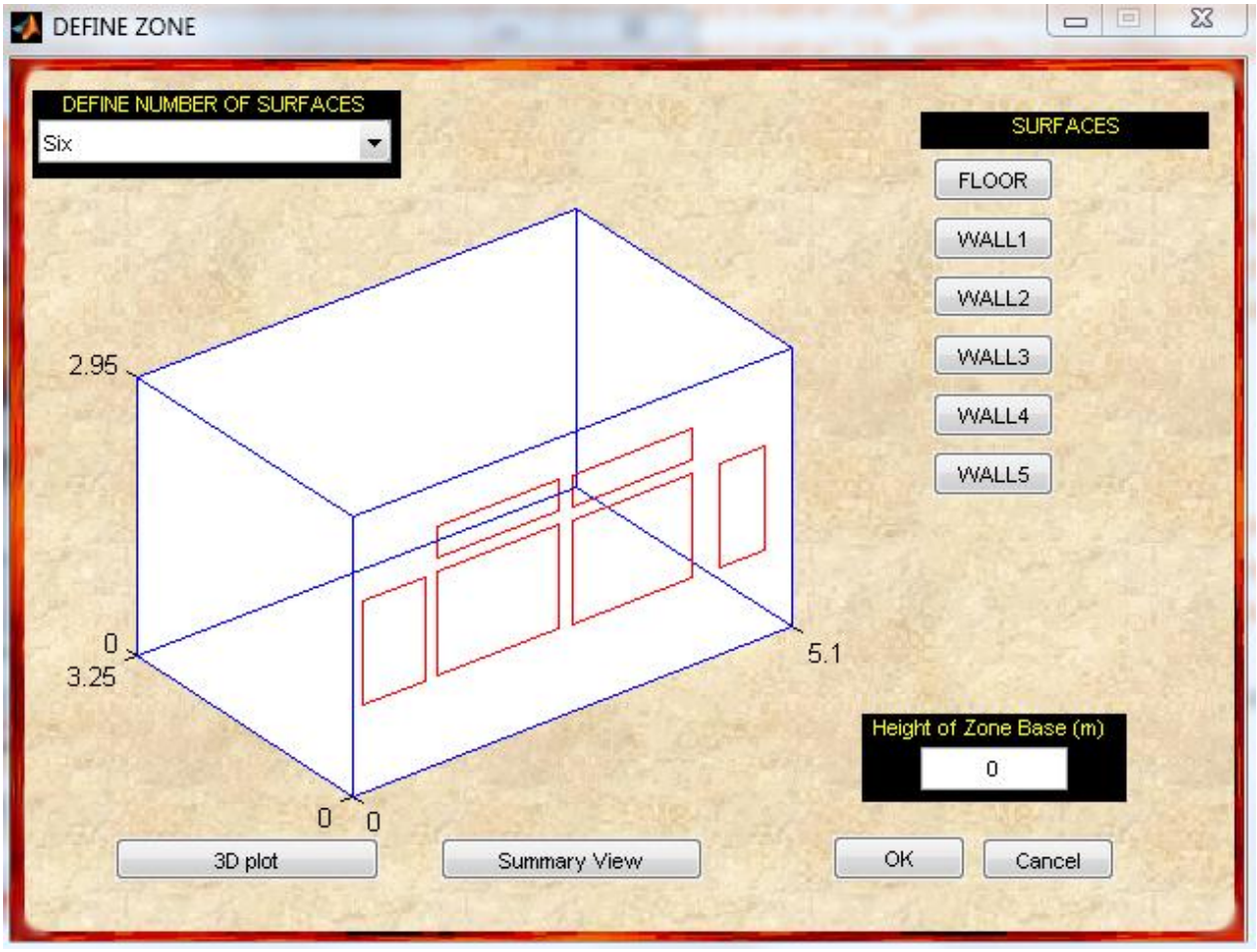

Figure 4.29: Visual representation of the modeled experimental cell

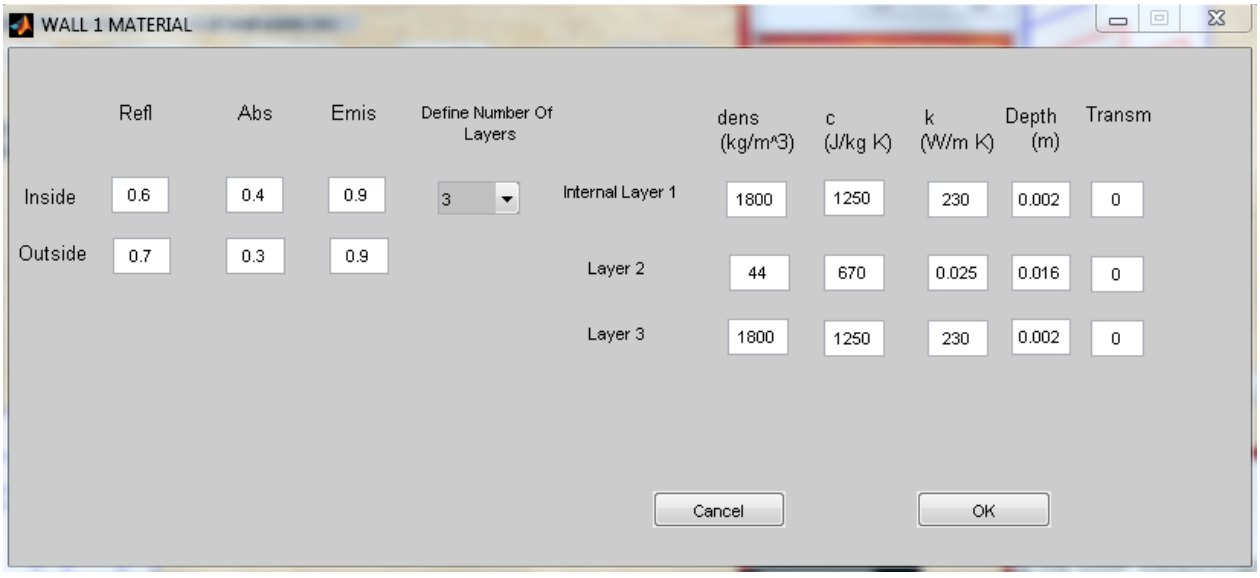

Figure 4.30: Composition and properties of Hybcell's north-east wall

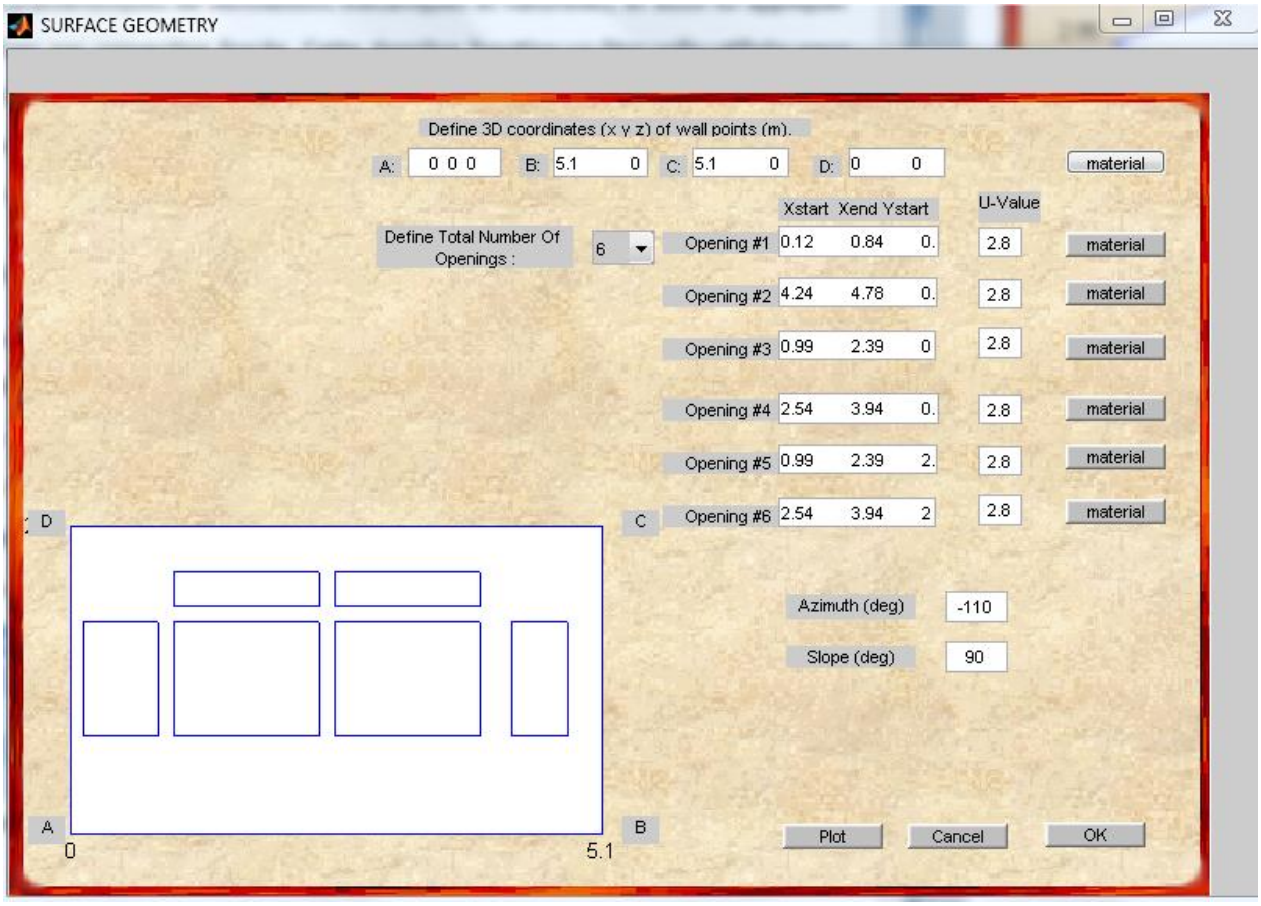

Figure 4.31: North-east wall definition, including openings

4.6.3 Reproduction of an experimentally tested scenario and comparison

The four day test realized at the Hybcell room (section 3.4) was reproduced with the use of the heat exchanger model coupled to the building model (figure 4.32). The test consisted in a four consecutive day scenario, during which load shifting was implemented for the three four days and the last day was taken as a reference (no heating at all).

As before, the heat exchanger model uses, the experimental inlet air temperature and the airflow rate as input; this time these values vary according to the implemented control strategy during the experimental test. The outlet air temperature (as calculated from the exchanger's model) and the airflow rate are then employed as ventilation inputs for the Hybcell 1.2 model.

Figures 4.33 and 4.34 illustrate the obtained numerical results and a comparison is performed with experimental ones. The heat exchanger model manages to reproduce the experimentally observed behavior even for varying inlet air temperature and airflow rate (figure 4.33). Likewise, the building model after calibration represents with precision the evolution of the indoor air temperature for the three days of peak load shifting and the fourth reference day (figure 4.34).

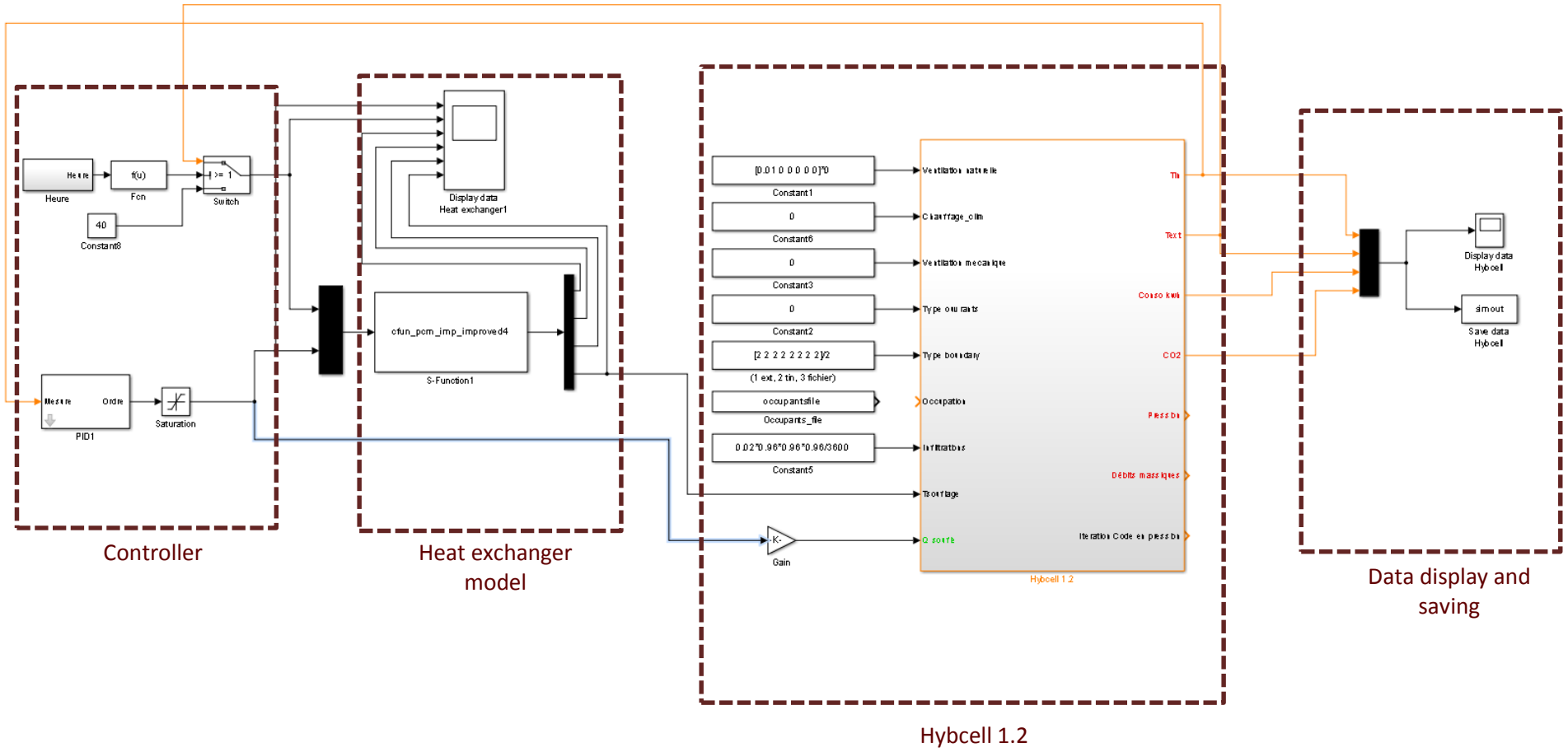

Figure 4.32: Coupling of the heat exchanger's model with the building's model Hybcell 1.2 under Simulink environment

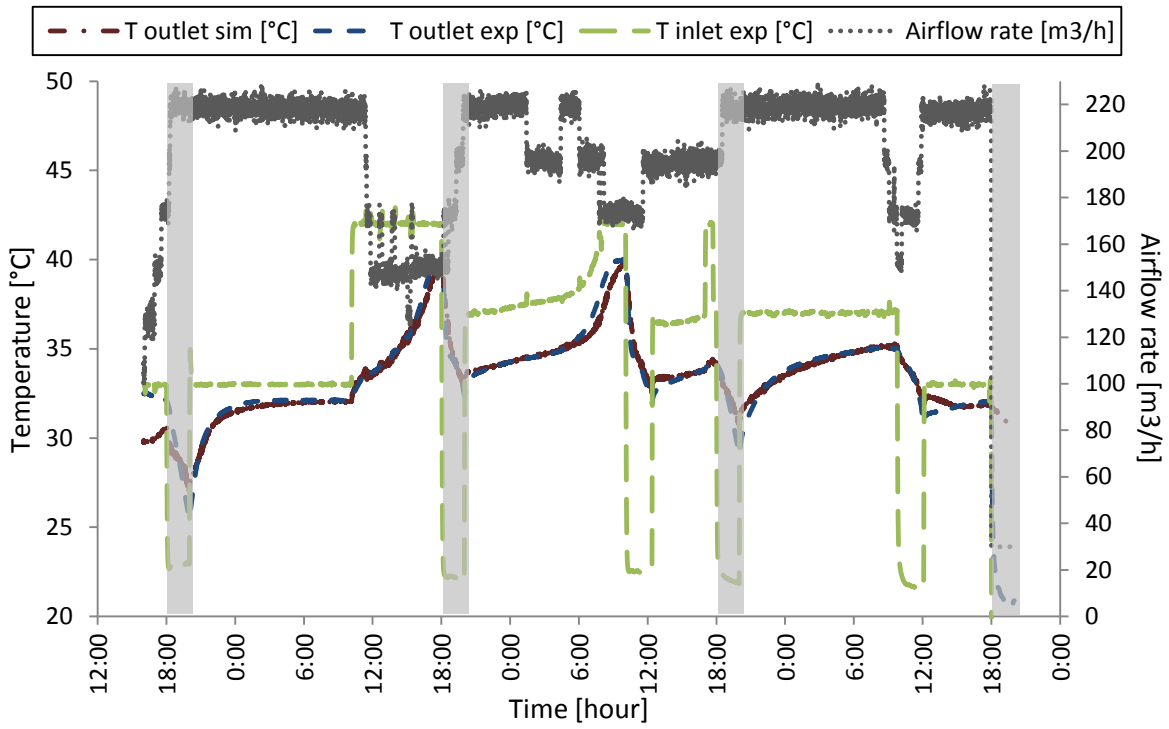

Figure 4.33: Numerical and experimental results for the heat exchanger unit and the Hybcell room coupling during a 4 days test

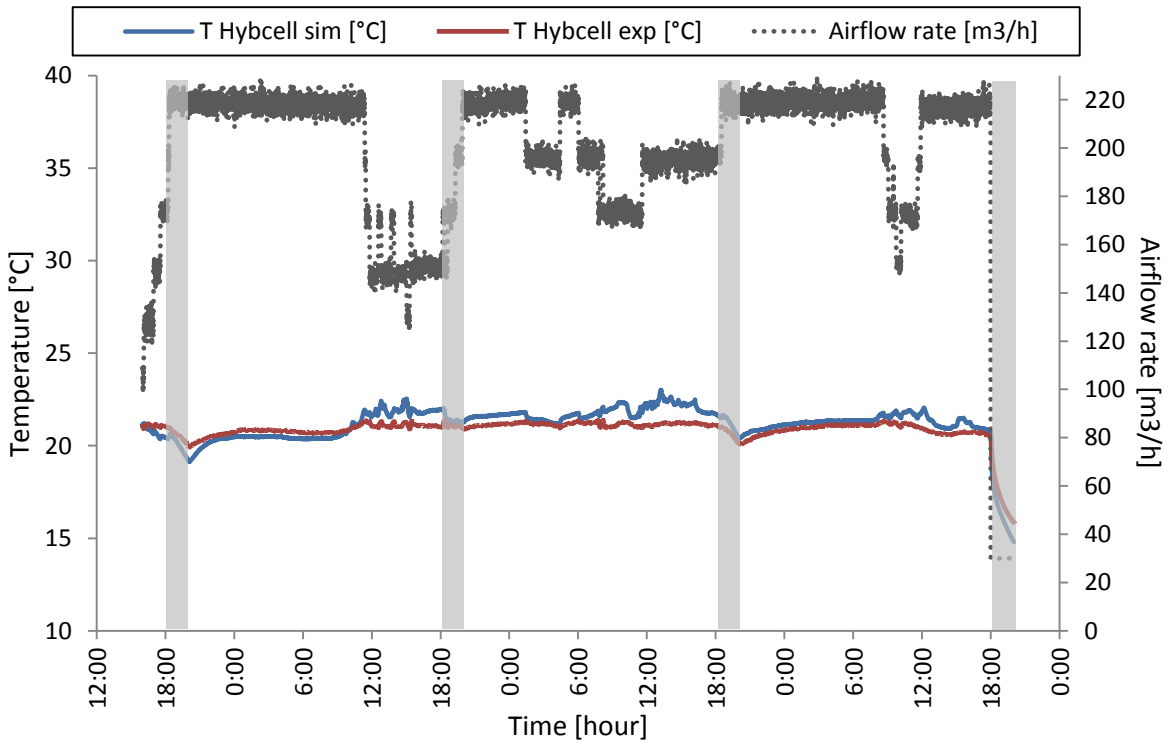

Figure 4.34: Numerical and experimental results for the heat exchanger unit and the Hybcell room coupling during a 4 days test

4.7 Conclusion

A numerical model was developed, based on the formulation of heat balance equations and the apparent heat capacity method. It considers three heat transferring mediums, air, aluminum surface and PCM, and is able to reproduce the downstream temperature evolution for each of them. A significant part of the study focused on the specific heat capacity values through the phase change and the creation of suitable fictive curves, based on DSC results.

It was validated using experimental data and used to reproduce a preliminary control strategy (presented in the previous chapter). The model manages to accurately and quickly reproduce the performance of the heat exchanger unit under different conditions, such as varying airflow rate and inlet air temperature.

The model will then be used for an optimization study of the heat exchanger and the development of control strategies when coupled to a building.

Chapter 5

Heat exchanger optimization and control strategies implementation

Chapter 5 : Heat exchanger optimization and control strategies implementation

5.1 Introduction

So far, we discussed the French peak power problem, along with its strong ties with electrical space heating. The advantages of latent heat storage technology were presented, along with the benefits of HVAC integrated PCM heat exchangers able to provide load shifting solutions. Following this, the development of a PCM-Air heat exchanger prototype and of a numerical model that simulates its behavior was described in detail. Nevertheless, the characterization results demonstrated that there were some limitations concerning the time needed to charge and discharge the proposed unit as well as the final amount of stored heat.

This chapter presents at first the verification of such reasoning as the exchanger is numerically coupled to an 80m^2 house and tested under different configurations (inlet exchanger air temperature and discharging period). As the necessity of an optimization study became clear, two approaches were considered. The first one focused on the modification of the heat exchanger's dimensions, by altering the height of the unit, the thickness of the PCM and the air layer, and investigating the impact on energy consumption and thermal comfort when the unit was coupled to a room. The second one concentrated on both the dimensions of the heat exchanger and the properties of the PCM and targeted the configurations with minimum time for stocking and maximum heat storage.

5.2 Conception of a low energy house

5.2.1 Materials and properties of the house

In order to evaluate the performance of the heat exchanger and test it under different operation scenarios, a building was designed numerically. The Hybcell 1.2 model was once again used for this purpose (see description in subsection 4.6.2).

The designed building is an 80m^2 single zone dwelling having a rectangular shape (10m long, 8m wide and 3m high). South, east and west walls have two window openings each with a 2.5mx1.5 dimension (figure 5.1).

The properties of the walls and of the windows were defined in a way that corresponds to a low energy house, as the heat exchanger is conceived for such a case. The properties of the used materials are presented in table 5.1.

	Density(kg/m^3)	Specific heat (J/kg.K)	Conductivity (W/m.k)
Concrete	2300	880	2.3
Rockwool	100	900	0,036
Plaster	680	960	0,25
Parquet flooring	500	1600	0,13

Table 5.1: Properties of the materials used for the definition of the building

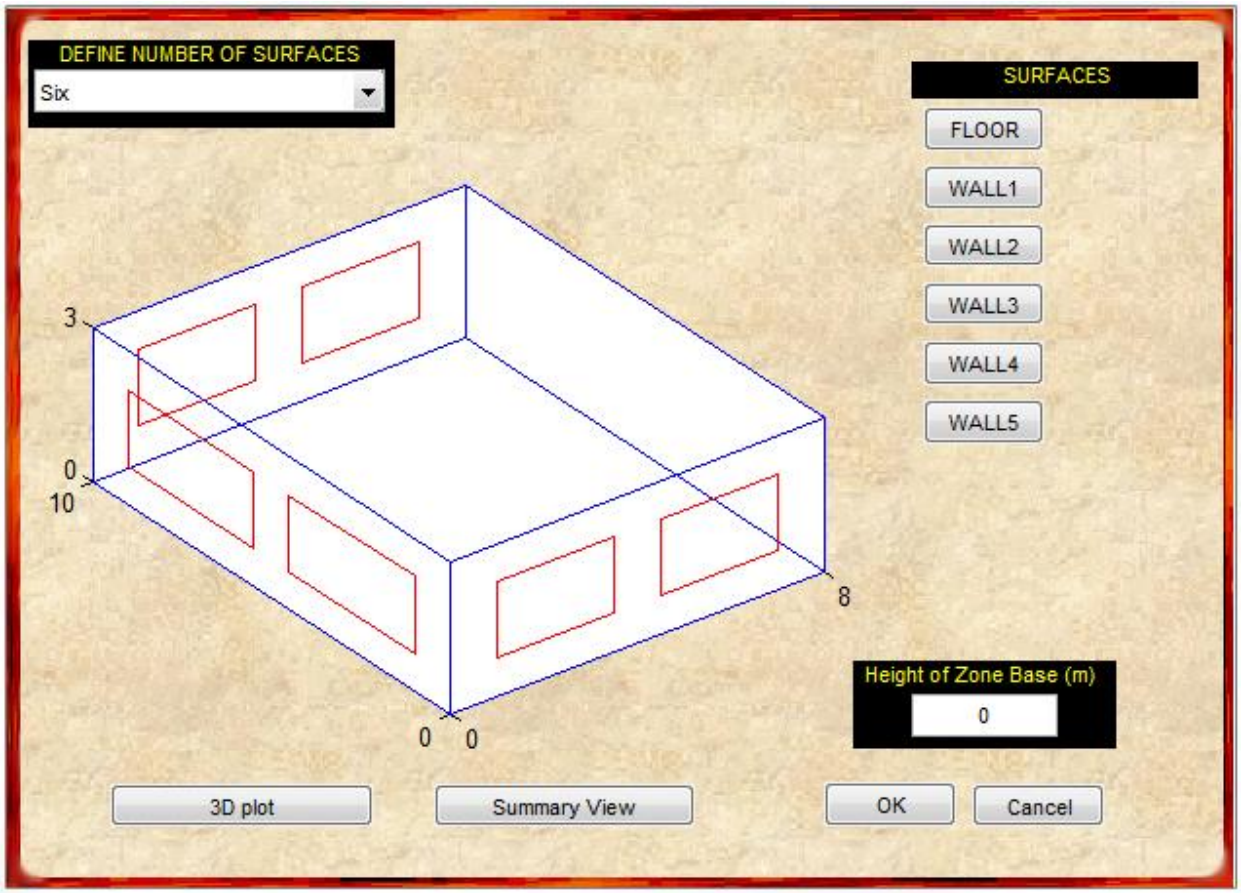

Figure 5.1: The conceived mono zone house, as presented in Hybcell 1.2 model

The composition and the thickness of the different surfaces are presented in table 5.2.

	Internal	Middle	External
Floor	Parquet flooring 0,01m	Rockwool 0,12m	Concrete 0,20m
Ceiling	Plaster 0,0125m	Rockwool 0,18m	Concrete 0,20m
Wall	Plaster 0,0125m	Concrete 0,20m	Rockwool 0,18m

Table 5.2: Composition of the building's surfaces

The U value obtained for each element is as follows: Uceiling=0,188W/m^2.K, Ufloor=0,187W/m^2.K and Uwall=0,188W/m^2.K, confirming efficient thermal insulation performance (IEA, 2008). Windows are double glazed, with a 1.2 U value that corresponds to a 4/16/4 type window with an argon blade and a low emissivity layer on the internal face of the glazing.

5.2.2 Climate definition

Meteorological data were acquired using the IDMP station located on the ENTPE campus (Dumortier, 2003) and correspond to the weather condition in Vaulx-en-Velin (Lyon, France) for the year 2013. Figure 5.2 illustrates the outdoor temperature for January 2013, as this month constitutes the selected testing period for most of the simulations.

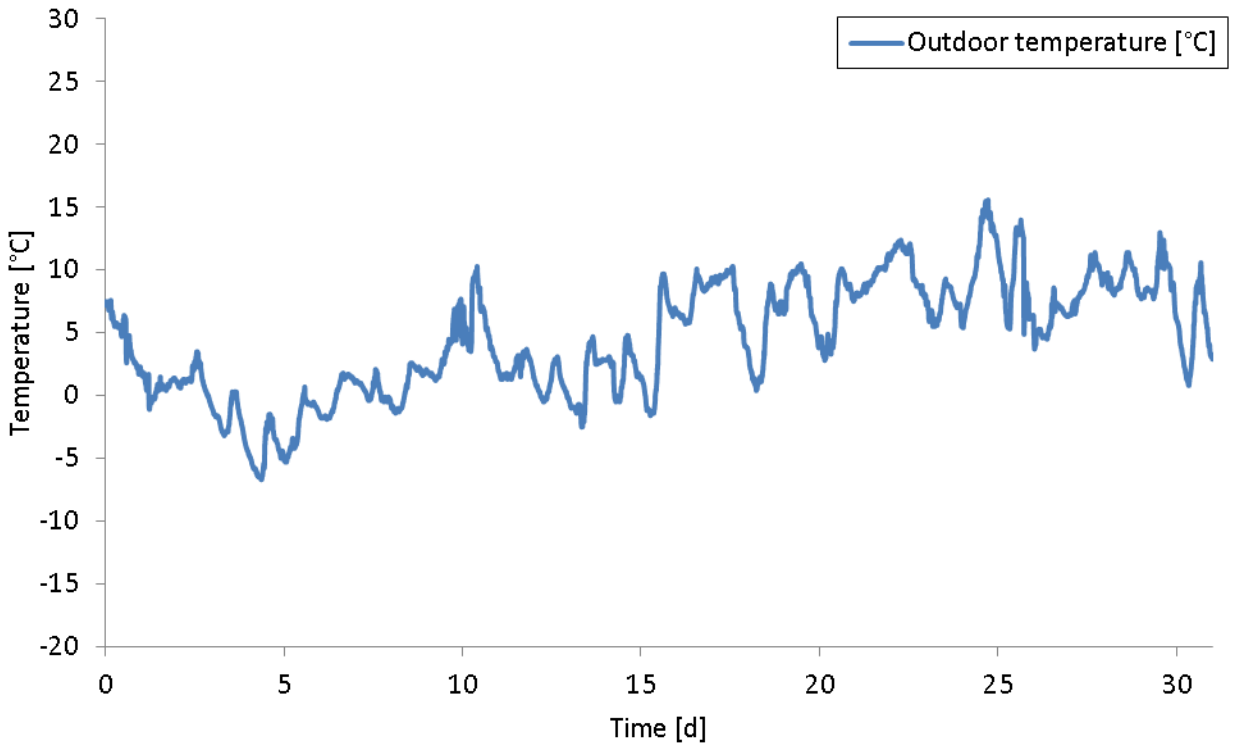

Figure 5.2: Outdoor temperature for the tested month (January 2013)

5.2.3 Heating needs of the house

In order to verify that the building satisfies the low energy consumption criteria (50 KWH/m^2/year), a simulation was performed for the month of January 2013, using a conventional heating mode (i.e. without heat exchanger). A PID controller was linked to the heating component of the model in order to maintain an indoor air temperature of 20°C (figure 5.3). After calibration of several factors, the monthly heating needs of the building were calculated at 652,23 KWh, or 48,9 KWH/m^2/year; a value lower than the initial target of 50 KWH/m^2/year.

However, the indoor temperature presents peaks for some of the tested days, during the afternoon hours, linked to horizontal radiation and the fact that the house is well insulated. Furthermore, indoor temperature reaches lower than the set point values, usually after the afternoon temperature peaks, as the PID controller encounters difficulties to deal with sharp changes. These peaks and troughs appear in the simulations performed with the heat exchanger as well.

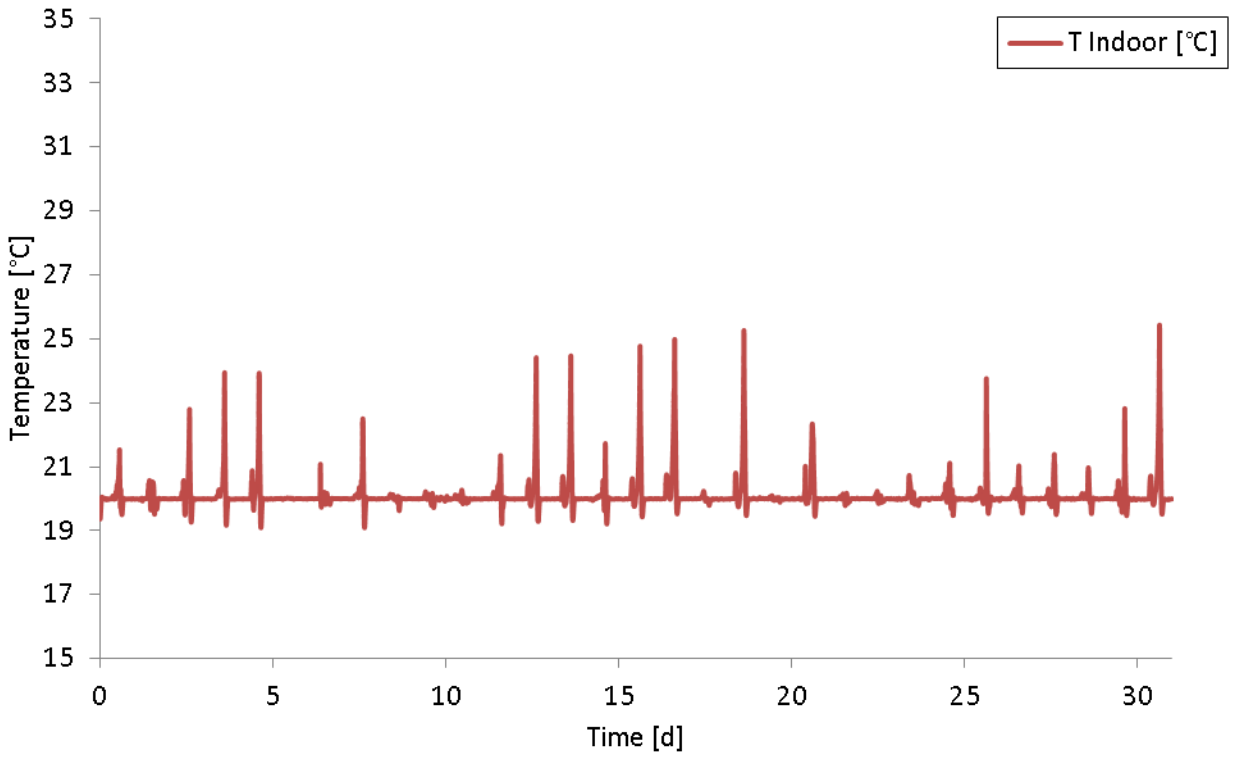

Figure 5.3: Indoor air temperature using conventional heating, setpoint of 20°C

The building model was then used to determine the heating needs of the house during the peak power hours (18:00-20:00) over the tested period, using a conventional heating mode. Results are presented in figure 5.4. Heating needs vary from 1.37 to 2.77 KWh for the period in question, depending on weather conditions.

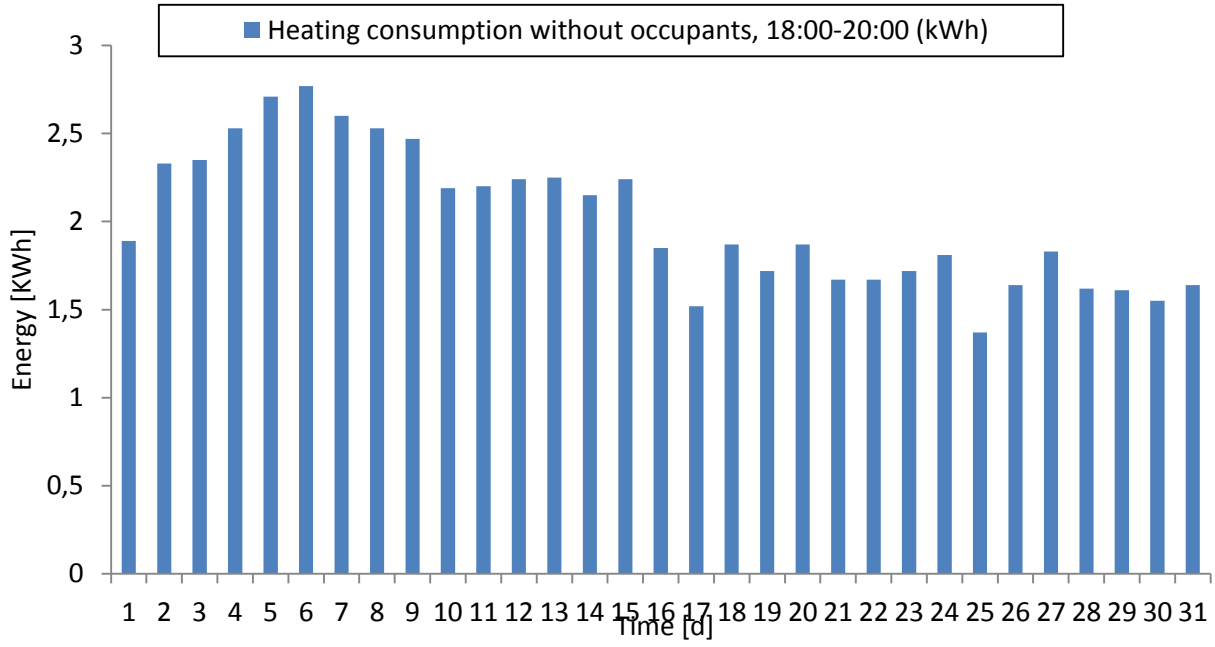

Figure 5.4: Heating needs during 18:00-20:00 for the conceived house

5.3 Testing of the initial exchanger

As presented in the previous subsection, a house was designed in order to test the performance of the heat exchanger for several scenarios over a one month period. The heat exchanger model was coupled to the building model Hybcell 1.2 in its initial form (dimension, PCM quantity and properties), as described in section 4.6. The conventional heating module was disconnected and the house was only heated using the heat exchanger.

A first control strategy was tested, aiming to investigate whether the exchanger would manage to shift the electrical heating consumption while maintaining thermal comfort. The heat exchanger was discharged during the peak power period (18:00-20:00) and charged during the off peak period. A PID controller regulated the airflow rate according to the thermal needs of the building; an upper limit of 720m^3/h was established (3 volumes per hour). The inlet air temperature of the exchanger was initially set at 38°C during the charging phase, as this value surpasses the PCM's melting temperature. During the peak power period, the inlet air temperature was taken equal to the indoor air temperature, meaning that no heating takes place before the heat exchanger.

For a better demonstration of the obtained results, figure 5.5 illustrates days 3 to 8, as a presentation of 31 days offers limited detail concerning the evolution of the represented parameters.

These five days presented increased heating needs (figure 5.4) and for that reason they will be used for demonstration purposes for each test from now on. During the charging phase the inlet exchanger air temperature is 38°C and the controller regulates the airflow rate in order to maintain the house's air temperature at 20°C. During the afternoon hours, some peaks are observed in the house's temperature, linked as already mentioned to solar radiation. During these peaks, no heating is required and the airflow rate diminishes or is set to zero. During the discharging phase, the inlet exchanger air temperature is equal to the house's air temperature and the controller significantly increases the airflow rate to provide more power to the house (while destocking the heat stored to the exchanger).

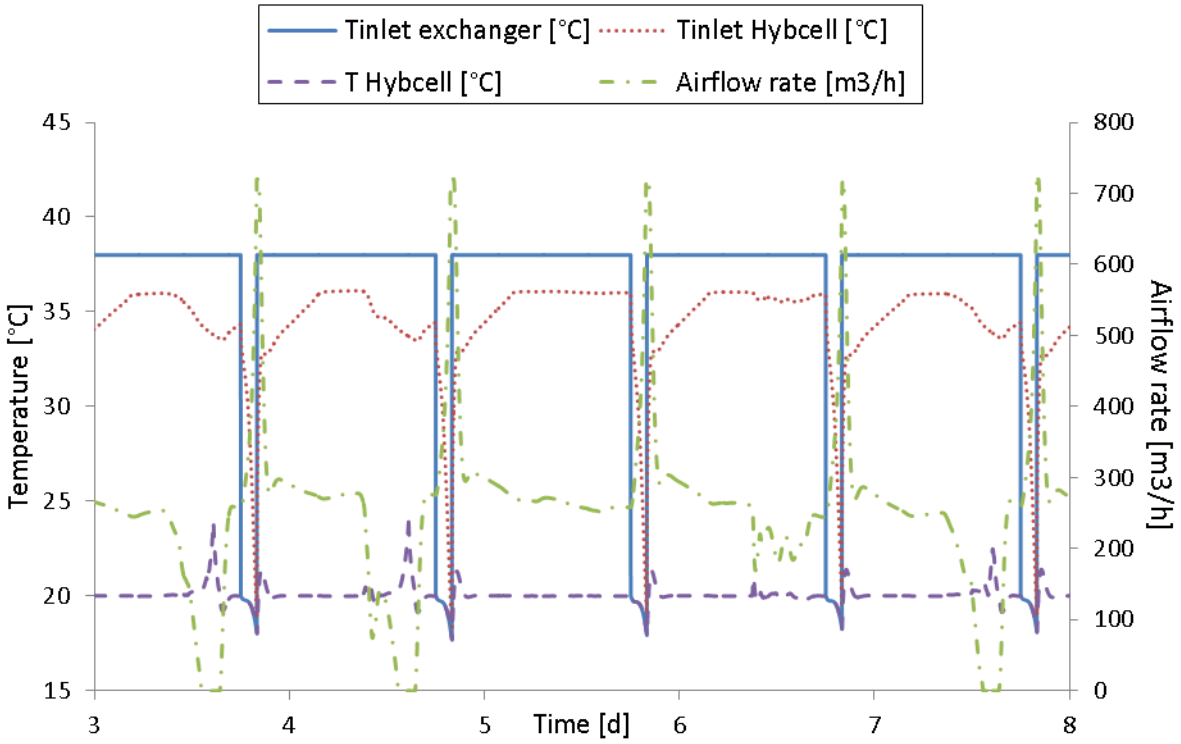

Figure 5.5: Performance of the initial exchanger, destocking 18:00-20:00, inlet exchanger temperature 38°C

Towards the end of the discharging phase the airflow rate reaches its maximum value, but even at this value the indoor air temperature presents a significant drop, almost reaching 18°C.

As the current configuration failed to produce the desired temperature conditions, the inlet exchanger air temperature was augmented, and tests were performed for 40, 42 and 44°C. Results are presented in figure 5.6.

Even when the inlet exchanger air temperature was augmented, the use of the heat exchanger failed to maintain comfortable conditions, the indoor temperature showing values near 18°C.

We were then interested to investigate the performance of the heat exchanger for a longer load shifting period, first with a two hour increase (17:00-21:00) and then with a four hour increase (16:00-22:00). Two inlet exchanger air temperature values were tested for each case: 38°C and 44°C. Results are presented in figure 5.7.

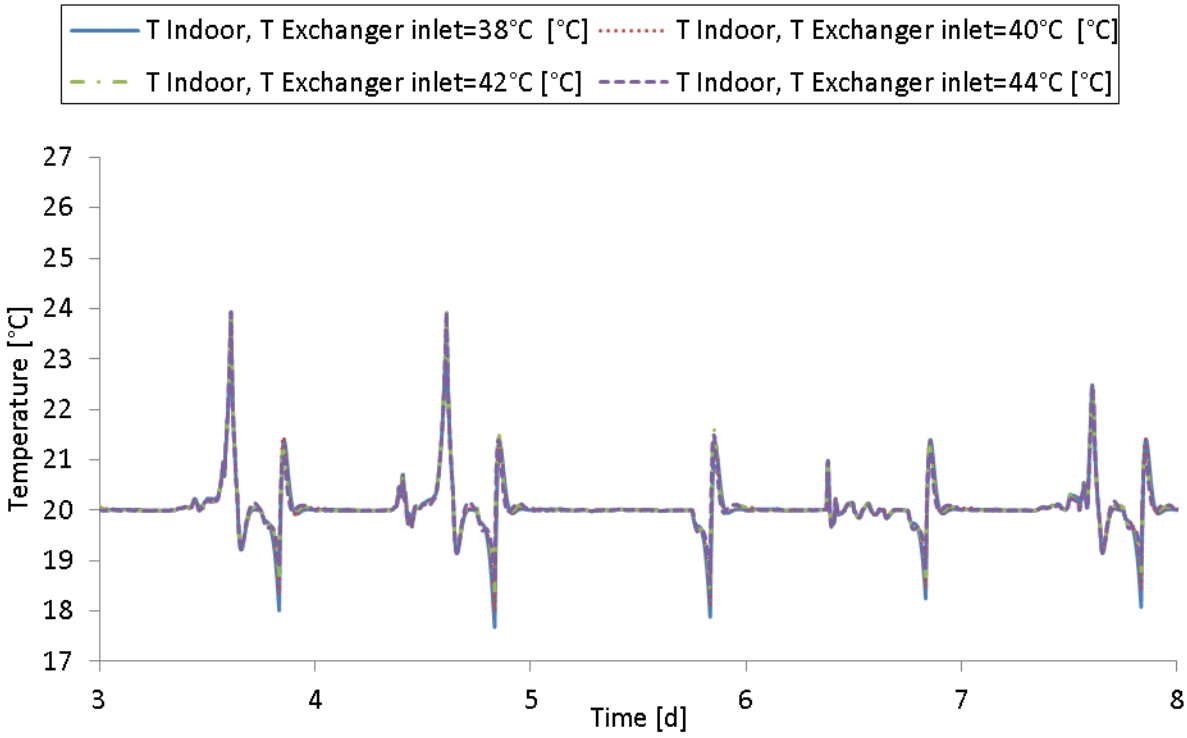

Figure 5.6: Indoor temperature for different inlet exchanger air temperatures

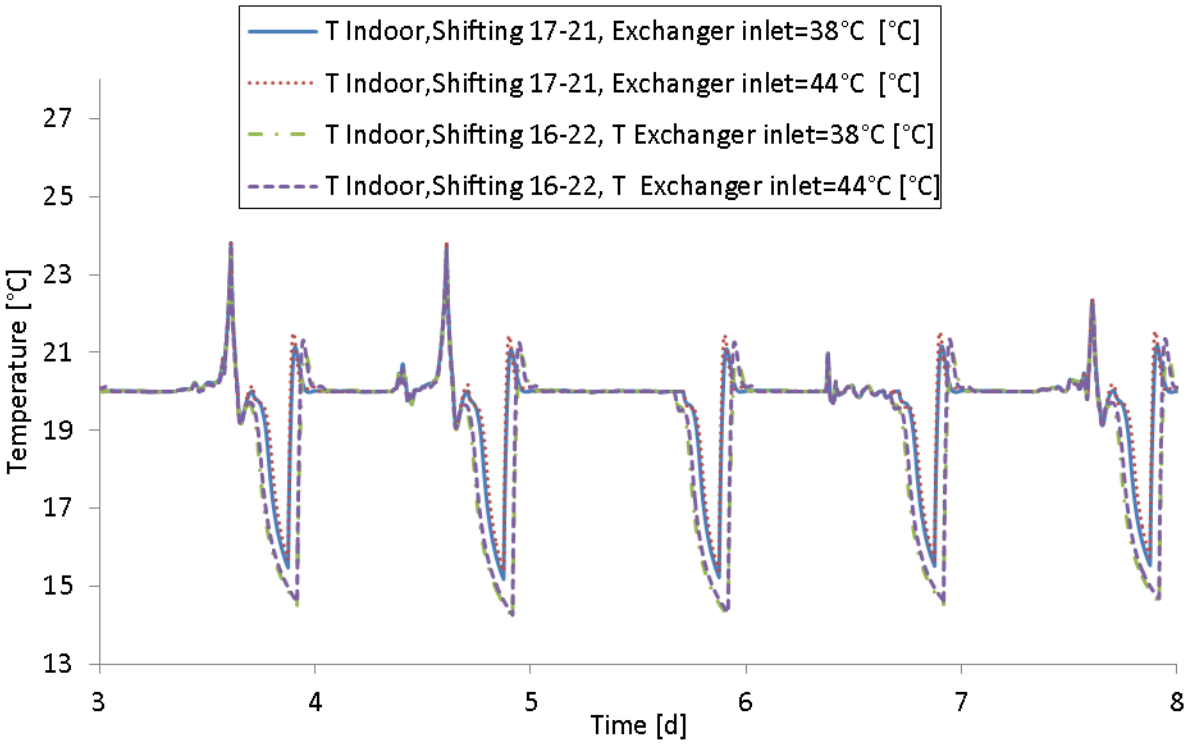

Figure 5.7: Indoor temperature for different load shifting periods, initial exchanger

In all four cases a serious degradation of thermal comfort was observed, as indoor temperatures decrease to values near 15°C.

As a final step of the testing of the initial exchanger performance, the price rate of each case was calculated, using the values proposed by the French Electricity power company (EDF). In fact, EDF has established a cheaper night tariff, starting from 22:00 and ending at 06:00, in an effort to motivate clients to use high energy consuming appliances at night (water heater, washing machine, etc). The night and day tariffs are presented in table 5.3.

	Electricity price rates (EDF, France)
Day rates 06:00-22:00	0,1510 €/KWh
Night rates 22:00-06:00	0,1044 €/KWh

Table 5.3: French electricity price rates during the day and during the night

These tariffs were used to calculate the monthly energy cost for space heating of the house for the cases presented so far. Results are presented in the following table.

Shifting period (h)	Inlet exchanger air temperature (C°)	Monthly energy consumption (KWh)	Monthly electricity bill (€)	Load shifting	Thermal comfort
Conventional heating	-	652,23	86,10	×	✓
18:00-20:00	38	768,26	100,36	✓	×
18:00-20:00	40	773,44	101,20	✓	×
18:00-20:00	42	777,448	101,91	✓	×
18:00-20:00	44	780,77	102,51	✓	×
17:00-21:00	38	758,77	97,83	✓	×
17:00-21:00	44	771,21	100,04	✓	×
16:00-20:00	38	740,85	90,08	✓	×
16:00-20:00	44	751,64	91,16	✓	×

Table 5.4: Monthly energy consumption and cost for different inlet air temperature values and load shifting periods for the initial exchanger

Several cases were investigated, altering the inlet exchanger air temperature and the load shifting period, leading to the conclusion that the initial configuration of the heat exchanger was not efficient

enough to guarantee acceptable indoor thermal conditions. Initial assumptions regarding the need for an optimization study were verified.

5.4 Optimization first approach

5.4.1 Definition of the optimization parameters

The numerical coupling and usage of the heat exchanger confirmed the experimental observations considering the limited energy storage and the important time needed for this storage to occur. The first optimization approach of the experimental unit consisted in the usage of the developed model to modify several parameters of the heat exchanger.

More specifically, the investigated parameters concerned the dimensions of the unit and were identified as follows:

- The height of the three considered layers, PCM, air and aluminum (dz)
- The thickness of the PCM layer (dym)
- The thickness of the air layer (dya)

The parameters are noted in the figure 5.8, representing the front view of the heat exchanger.

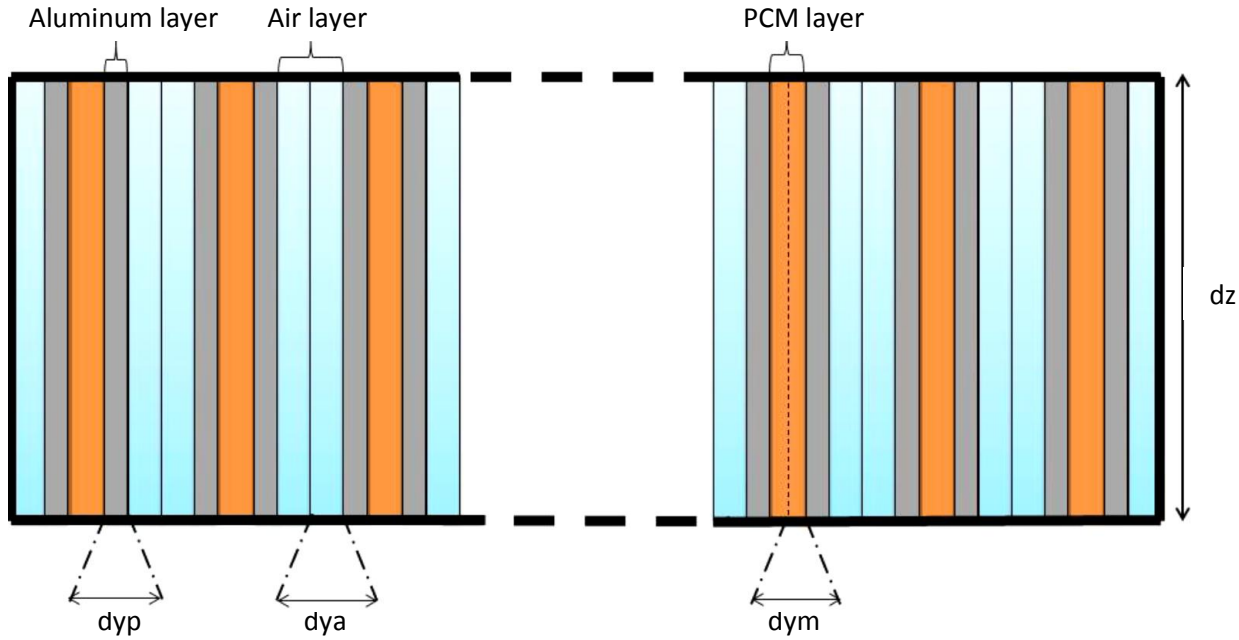

Figure 5.8: Representation of the modified parameters (PCM and air layers, height of the unit)

Three parameters were introduced in the numerical model as multiplying factors of the dimensions in question. The values of these parameters were defined as follows:

- The height was multiplied by 1, 1,5 and 2
- The PCM layer thickness was multiplied by 1, 2, 3 and 4

- The air layer thickness was multiplied by 1, 2, 3 and 4

5.4.2 Testing protocol

Considering the combination of all the possibilities, a total of 48 configurations occurred. In order to test these configurations, it was decided to perform the simulations for a 3,5 day period. This period corresponds to the test presented in subsection 3.4 (4 to 8 February 2013), only this time the building on which the simulation were tested was the 80m^2 low energy one. We decided to run the simulations at this period for rapidity reasons and because the meteorological data were already acquired and available in the building model.

For this series of tests we decided to increase the discharging period from two hours to six hours (16:00-22:00) and set the inlet exchanger air temperature during the charging phase to 38°C. During the discharging phase the inlet exchanger temperature was taken equal to the building's indoor temperature. The airflow rate was regulated using a PID controller, with a maximum value of 720 m^3/h. Three criteria were established: load shifting realization, minimum monthly consumption and no degradation of thermal comfort. A decrease of 0,5°C of the house's air temperature was tolerated.

5.4.3 Selection of three configurations

Results showed that the configuration presenting minimum consumption is the '1/4/1' (75,6 KWh), but with a significant impact on thermal comfort, as the indoor temperature reaches 18,5°C. After investigation of all the 48 configurations three of them were selected as they fulfilled the established criteria. They are presented in the following table:

Description	Configuration 1	Configuration 2	Configuration 3
Multiplying factors (dz/dym/dya)	1,5/4/1	1/3/2	1,5/2/2
Final exchanger dimensions (m)	1x1,04x0,27	1x1,56x0,18	1x0,85x0,27
PCM mass (kg)	132	99	66
3,5 days consumption (KWh)	76,05	77,68	81,79
Annual consumption (kWh/m^2)	48,89	49,94	53,3

Table 5.5: Characteristics of the three selected configurations

All three configurations manage to maintain acceptable indoor conditions (with a 0,5°C temperature decrease tolerance), as illustrated in figures 5.9, 5.10 and 5.11. The highlighted green areas correspond to the load shifting period (16:00-22:00). The first configuration uses more PCM, thus having a bigger volume, but consumes less energy. The second and third ones present decreasing PCM mass and volume but increasing energy consumption. All three, offer different points of interest and were chosen for the testing of the coupled system 'heat exchanger + building' through different scenarios.

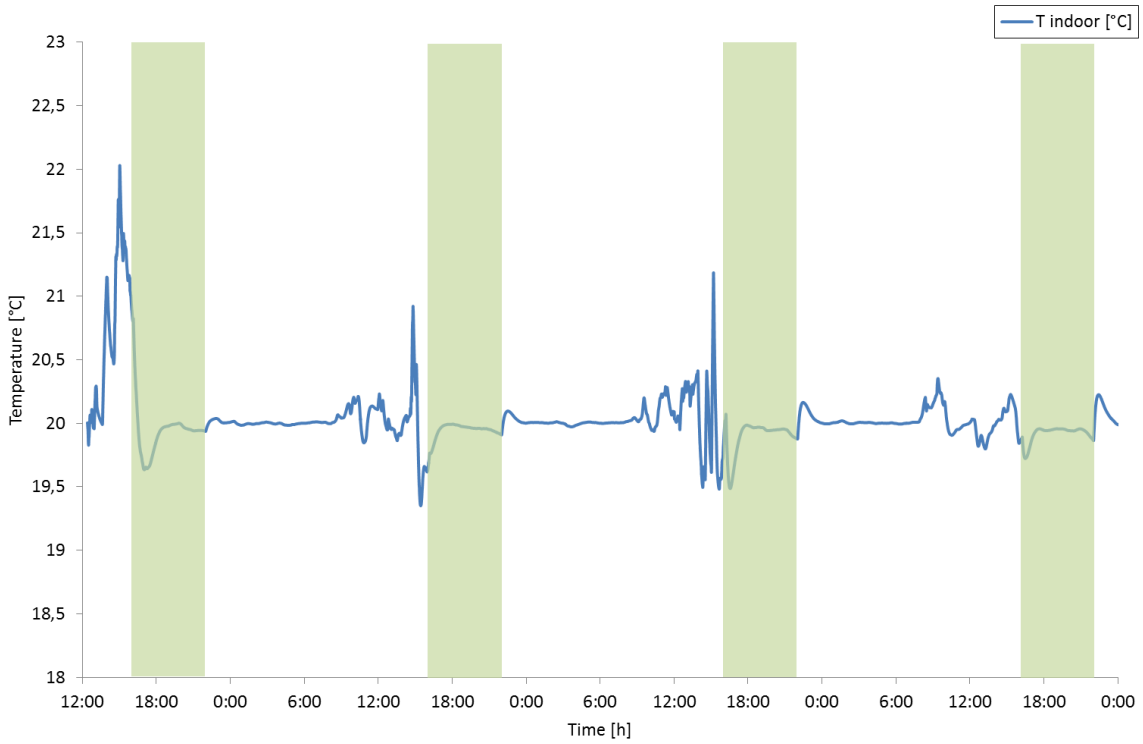

Figure 5.9: Indoor air temperature, 3,5 days testing, optimized exchanger 1

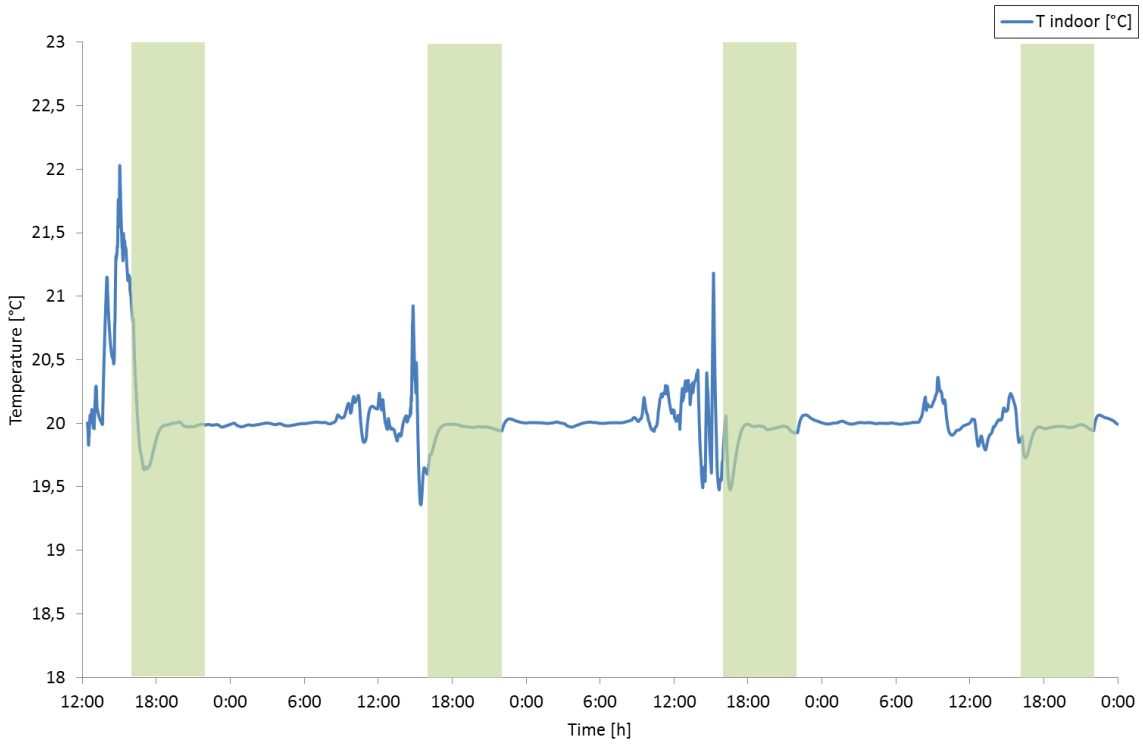

Figure 5.10: Indoor air temperature, 3,5 days testing, optimized exchanger 2

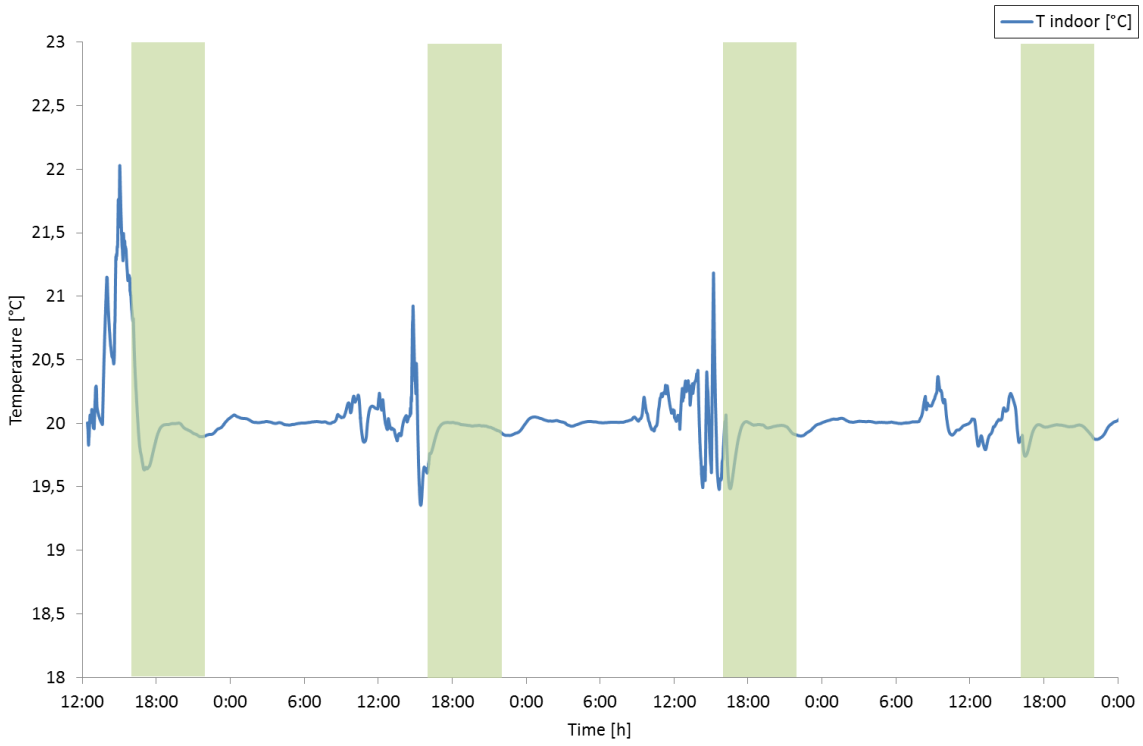

Figure 5.11: Indoor air temperature, 3,5 days testing, optimized exchanger 3

5.4.5 First scenario: simple load shifting

In order to evaluate the performance of the heat exchanger, the selected configurations were tested for a larger time scale. The month of January 2013 was once again selected for this purpose, as it represents a winter climate and offers a sufficient amount of time for thermal inertia phenomena to take place.

The first scenario was established as before: charging of the heat exchanger between 22:00 and 16:00 and discharging during a six hour period (16:00-22:00). The inlet exchanger air temperature was set at 38°C and the airflow was regulated from a PID controller. Table 5.6 summarizes the operation conditions of the first scenario.

The aim of this test was to verify the efficient performance of the heat exchanger (load shifting and thermal comfort) for a longer time period and to calculate the energy consumption and electricity bill at the end of the month. Figures 5.12, 5.13 and 5.14 present the results of the simulation for the three configurations. For a better demonstration of the obtained results, these figures zoom on days 3 to 8, as higher heating power is needed during these days.

For all three configurations, the heat exchanger managed to maintain the indoor air temperature at 20°C during the shifting and the non-shifting period. As before, the highlighted green areas represent the shifting period (16:00-22:00).

	Time		
	00:00-16:00	16:00-22:00	22:00-00:00
Inlet exchanger air temperature	38°C	Indoor air temperature	38°C
Airflow rate exchanger	PID on temperature	PID on temperature	PID on temperature
Inlet house air temperature	Exchanger outlet	Exchanger outlet	Exchanger outlet
Airflow rate house	Same as exchanger	Same as exchanger	Same as exchanger
Conventional heating	No	No	No

Table 5.6: Simple load shifting operation description, first optimization approach

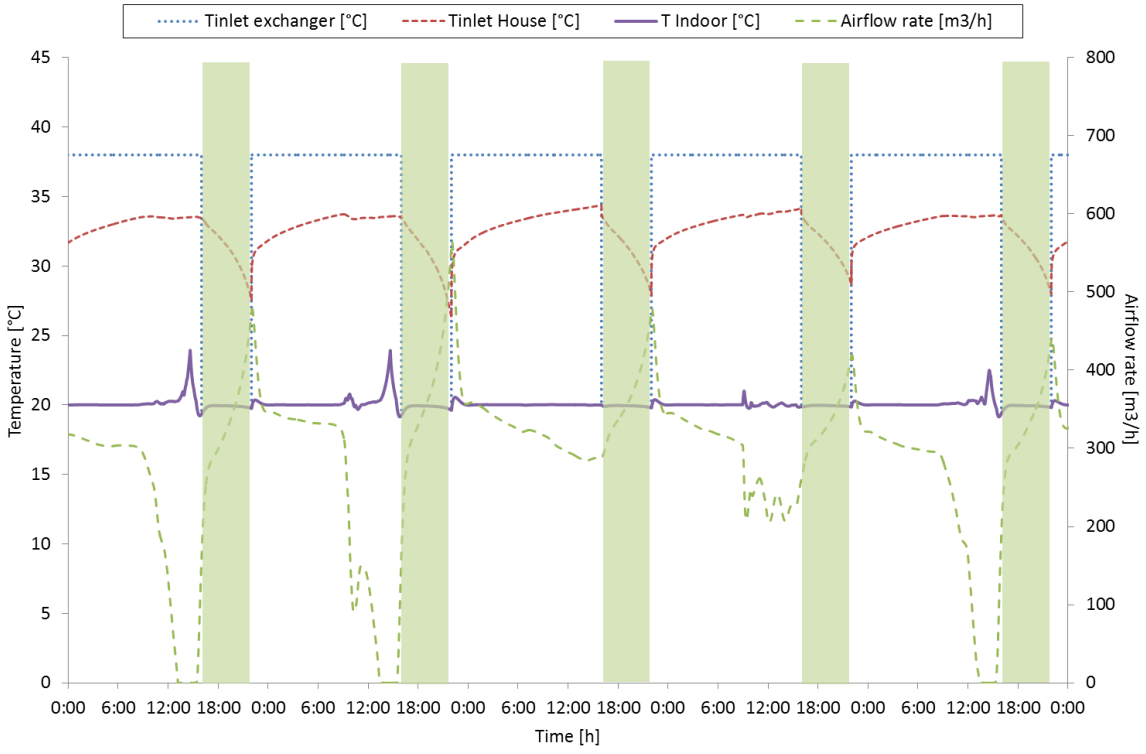

Figure 5.12: Performance of the heat exchanger, days 3-8, configuration 1, simple load shifting scenario, first optimization approach

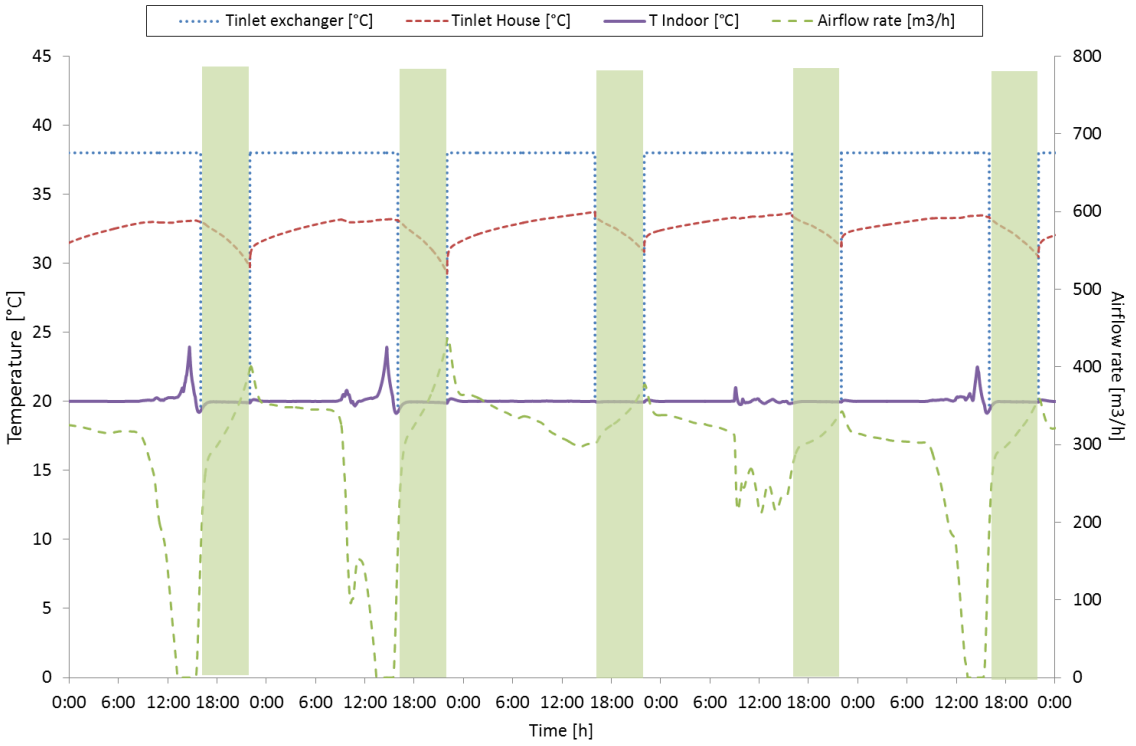

Figure 5.13 Performance of the heat exchanger, days 3-8, configuration 2, simple load shifting scenario, first optimization approach

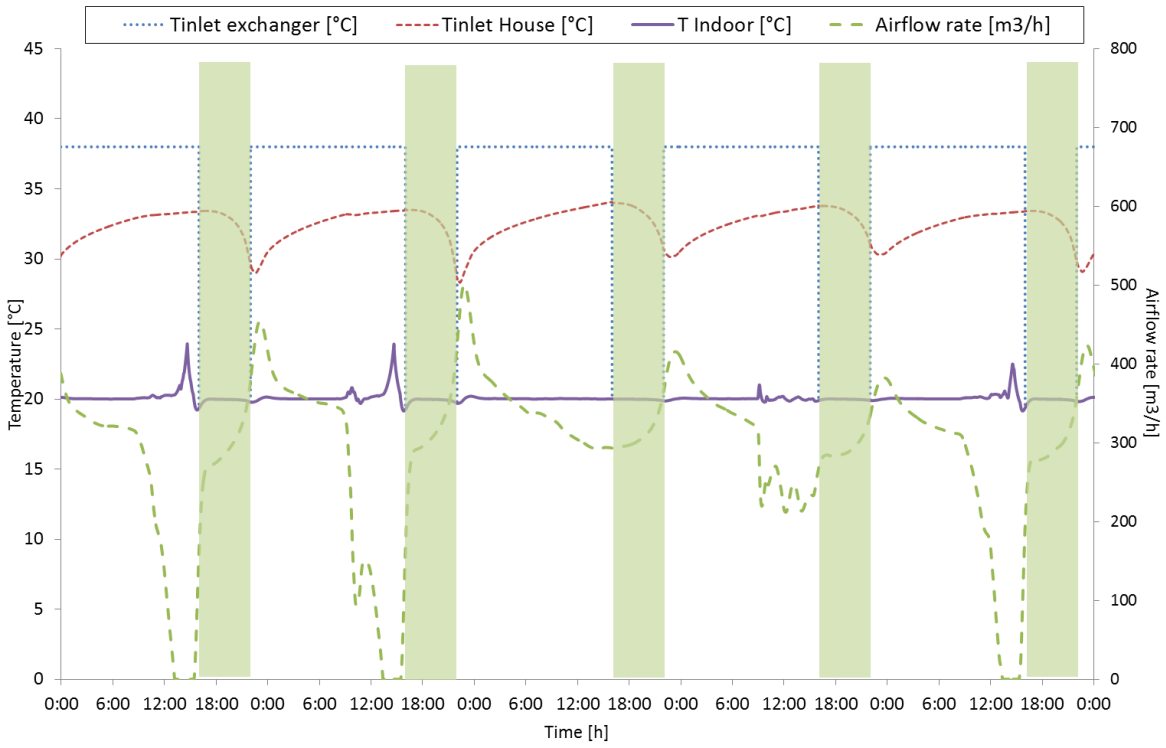

Figure 5.14: Performance of the heat exchanger, days 3-8, configuration3, simple load shifting scenario, first optimization approach

Energy consumption and the electricity bill corresponding to the three configurations are presented in table 5.7. The previous observation concerning a lower consumption when more PCM is used is confirmed. All three configurations consume more energy when compared to conventional heating appliance.

Configuration	Monthly energy consumption (KWh)	Monthly electricity bill (€)	Load shifting	Thermal comfort
Conventional heating	652,23	86,10	×	✓
1 (1,5/4/1)	669,43	82,83	✓	✓
2 (1/3/2)	687,30	85,20	✓	✓
3 (1,5/2/2)	720,28	88,79	✓	✓

Table 5.7: Monthly performance of the three tested configurations, simple load shifting scenario, first optimization approach

5.4.6 Second scenario: charging of the heat exchanger during the night

A detailed observation of the heating needs of the house indicates that in some cases no heating is required during the day. Figure 5.15 demonstrates the heating power provided to the house using a conventional heating system for 3 consecutive days, from January 11 to January 13. Depending on external weather conditions (mostly solar gains) the power needed decreases or even becomes zero from 10:00 to 16:00.

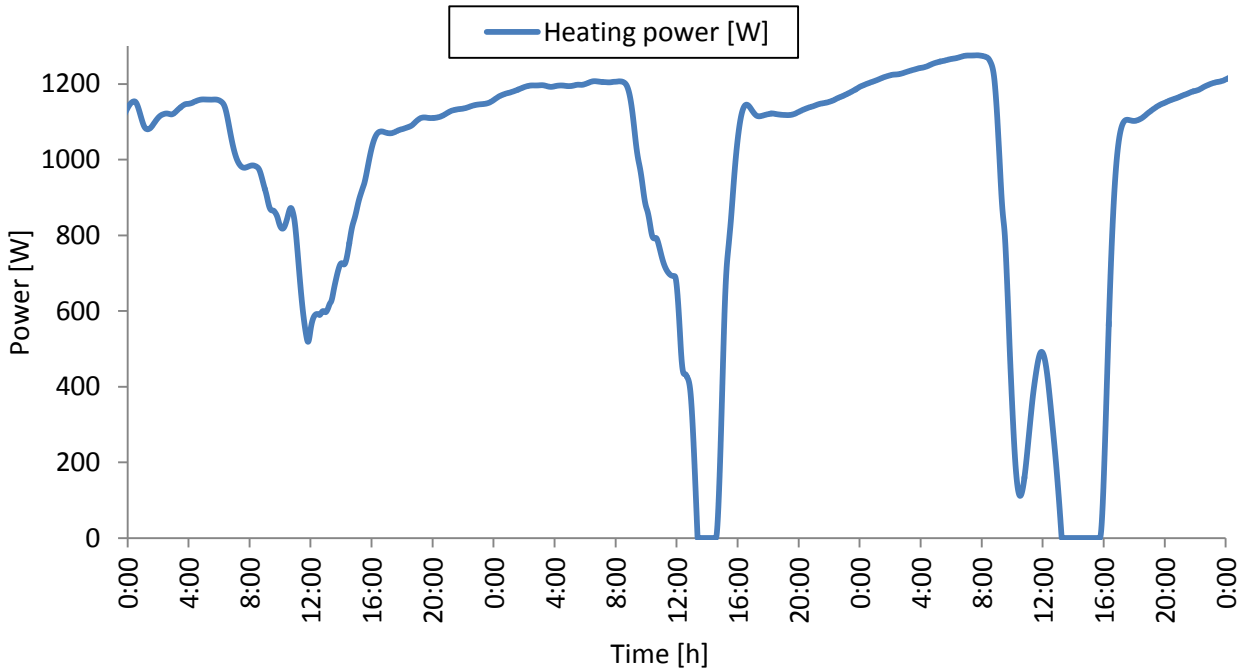

Figure 5.15: Heating needs from 11 to 13 January

This observation led us to the creation of a night charging scenario. In this case, the heat exchanger is charged during the night, starting at 22:00 and finishing at 06:00 in the morning. Until the start of the load shifting period (16:00) conventional heating is used, if necessary. This means that the heat exchanger is charged during an 8 hour period and is kept in that state during the day and until the initiation of the shifting process. Table 5.8 summarizes the operation of the system for the night charging scenario.

	Time			
	00:00-6:00	06:00-16:00	16:00-22:00	22:00-00:00
Inlet exchanger air temperature	38°C, 44°C	Indoor air temperature	Indoor air temperature	38°C
Airflow rate exchanger	PID on temperature	0	PID on temperature	PID on temperature
Inlet house air temperature	Exchanger outlet	Exchanger outlet	Exchanger outlet	Exchanger outlet
Airflow rate house	Same as exchanger	0	Same as exchanger	Same as exchanger
Conventional heating	No	Yes, PID	No	No

Table 5.8: Night charging scenario operation description, first optimization approach

Figure 5.16 presents the obtained results for configuration 1, with an inlet exchanger air temperature of 38°C. During the discharging phase, the indoor temperature decreases to 17.5 °C, meaning that thermal comfort is deteriorated and that the current configuration failed to provide efficient control of the house. Further tests were then performed, raising the inlet exchanger air temperature at 40, 42 and 44°C. Better results were acquired with the last temperature value and are presented in figure 5.17.

Configurations 2 and 3 were also tested for different inlet air exchanger temperatures. Comfortable indoor air conditions were obtained with 44°C and are presented in graphs 5.18 and 5.19.

The charging of the heat exchanger strictly during the night presents the advantage of moving the load shifting process to a period with lower energy consumption and a cheaper electricity price.

Monthly energy consumption and electricity bill are calculated for the four presented cases and are presented in table 5.9. Once again more PCM led to less energy consumption. All three configurations managed to provide good results, but with an increased inlet exchanger air temperature.

Even though the energy consumption was increased using the heat exchanger, a decrease of the final cost is observed as the exchanger is charged during the night, when lower tariffs apply. This observation is valid for the first two configurations as the last one led to an important increase of energy that was also reflected on the final electricity bill.

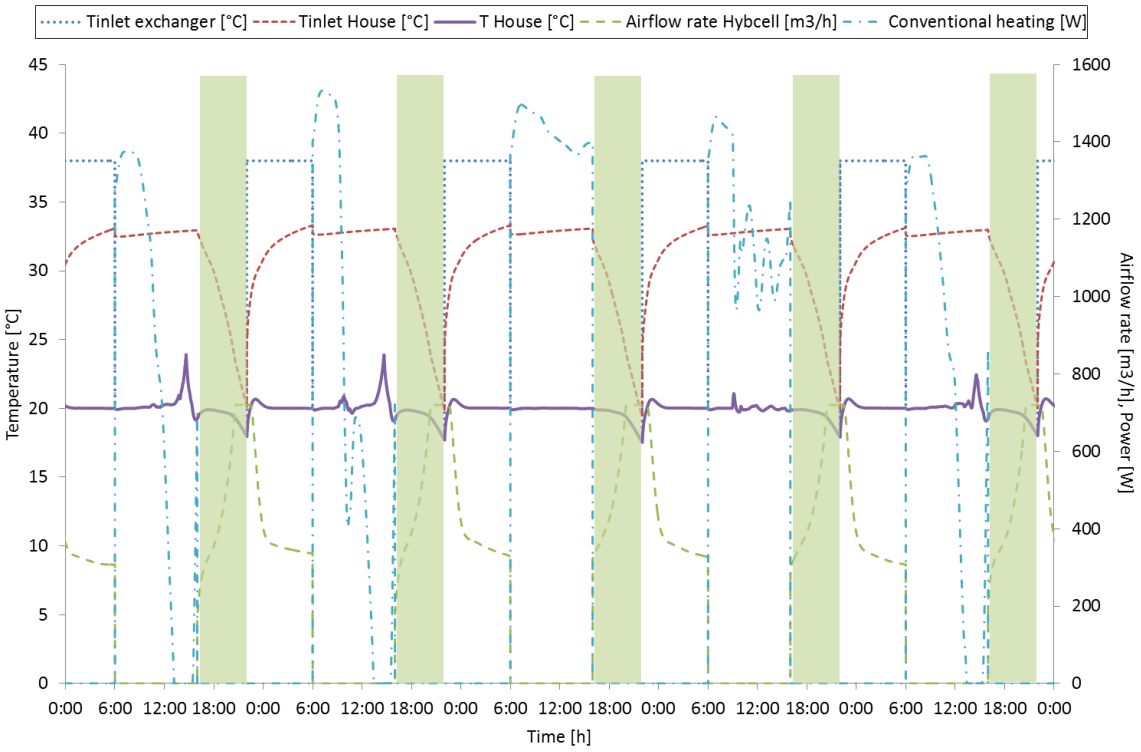

Figure 5.16: Performance of the heat exchanger, days 3-8, configuration 1, inlet exchanger air temperature=38°C, night charging scenario, first optimization approach

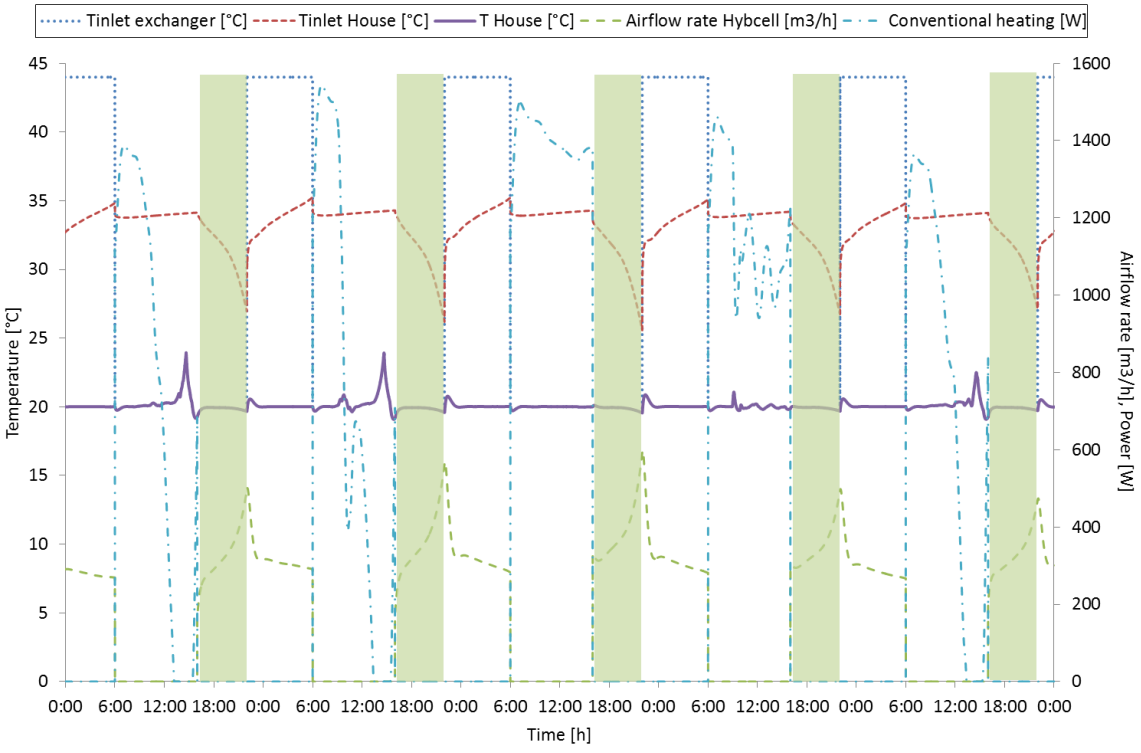

Figure 5.17: Performance of the heat exchanger, days 3-8, configuration 1, inlet exchanger air temperature=44°C, night charging scenario, first optimization approach

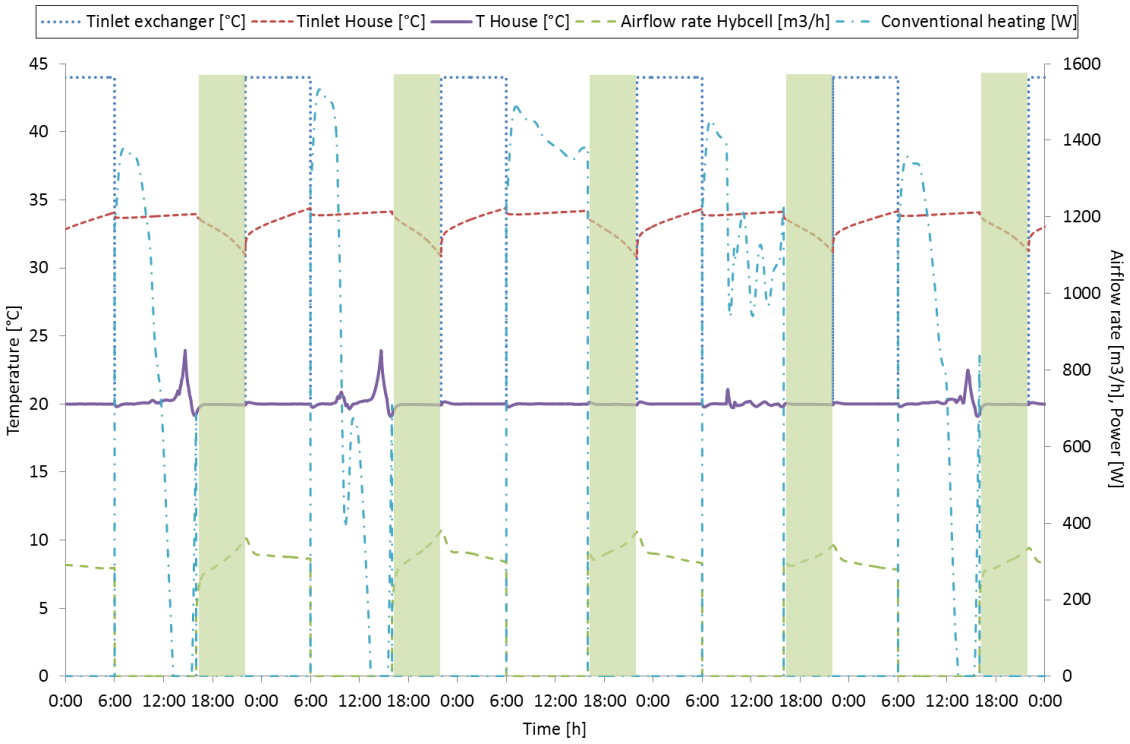

Figure 5.18: Performance of the heat exchanger, days 3-8, configuration 2, inlet exchanger air temperature=44°C, night charging scenario, first optimization approach

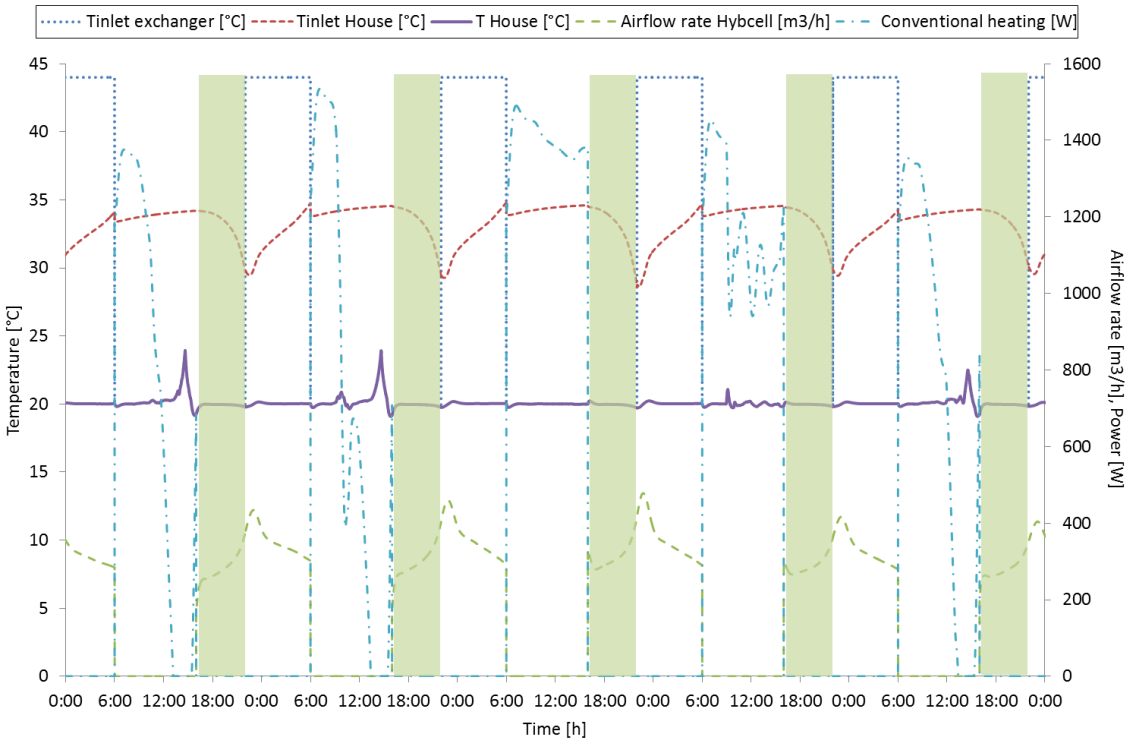

Figure 5.19: Performance of the heat exchanger, days 3-8, configuration 3, inlet exchanger air temperature=44°C, night charging scenario, first optimization approach

Configuration	Inlet exchanger air temperature (°C)	Monthly energy consumption (KWh)	Monthly electricity bill (€)	Load shifting	Thermal comfort
Conventional heating	-	652,23	86,10	×	✓
1 (1,5/4/1)	38	676,29	80,19	✓	×
1 (1,5/4/1)	44	686,40	81,15	✓	✓
2 (1/3/2)	44	686,49	81,17	✓	✓
3 (1,5/2/2)	44	747,34	87,53	✓	✓

Table 5.9: Monthly performance of the three tested configurations, night charging scenario, first optimization approach

5.4.7 Third scenario: occupancy and indoor air quality

5.4.7.1 Occupancy pattern definition

Lastly, a third and last scenario was tested, introducing the presence of a four person family to the building model. The occupancy simulation causes two significant changes compared to the two previous scenarios: carbon dioxide (CO_2) concentration increase and heat release from each occupant. The occupants are considered to exhale CO_2 when present in the building, augmenting the initial non polluted concentration of 400 parts per million (ppm). Augmented CO_2 concentration has been linked to health problems (drowsiness, headaches, lethargy) and lower productivity levels (Siskos et al., 2001). Extremely high CO_2 concentration during long exposure periods can be lethal. As humans are the main indoor source of CO_2, the concentration of this compound was used in this study as an indicator of the adequacy of the ventilation of the house.

For the integration of the four person family into the model a weekly occupancy program was established. The presence of the occupants varies according to the day and time; in general all four persons are present during the night and mostly absent during the day. The weekly occupancy program is illustrated in figure 5.20. According to ASHRAE (2013), an indoor CO_2 concentration not exceeding 1000 to 1200 ppm is an indicator of a good indoor air quality (IAQ). With respect to that, a value of 1000 ppm was set in this study, as the upper limit of CO_2 concentration.

Concerning the heat gains from the human presence, the model considers that each occupant constitutes a heat source equivalent to 100W.

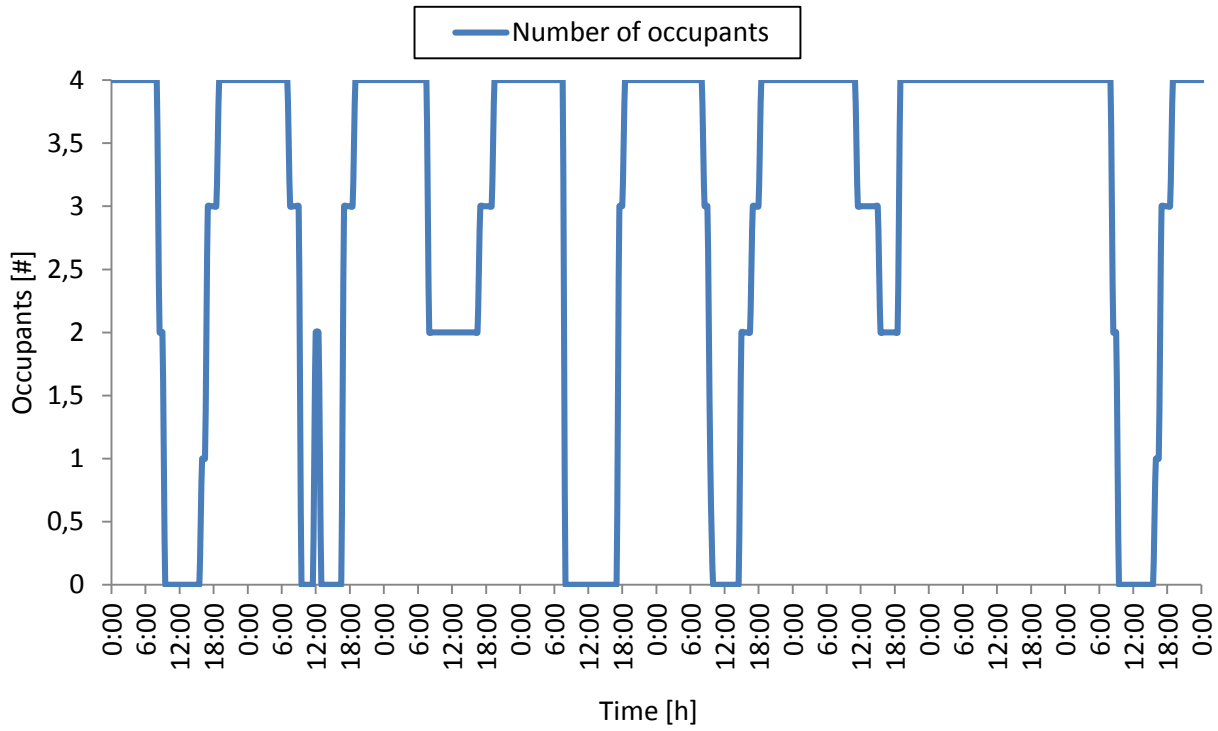

Figure 5.20: Weakly occupancy program

5.4.7.2 System operation description

The presence of the occupants introduces some changes in the operation of the system, compared to the first two scenarios. First of all, the indoor air temperature can no longer be taken equal to the house's air temperature, as this would mean that indoor polluted air would be recycled in the house. A more advanced ventilation system is conceived for this scenario. More specifically an energy recovery ventilation (or double flow ventilation) system is considered to use the heat from stale indoor air before expelling it from the house to heat the incoming fresh air. In that way, the air used to ventilate the house is warmer than the outside air and not CO2 polluted. A relationship was used to calculate the temperature of incoming air, considering a 90% efficient energy recovery ventilation system:

$$T_{air,incoming} = T_{air,exterior} + (T_{air,interior} - T_{air,exterior}) \cdot \varepsilon \qquad \text{equation 5.1}$$

Where ε the efficiency of the heat recovery system; here ε=90%.

Figure 5.21 illustrates the obtained incoming air temperature for an indoor air temperature of 20°C and 18°C and the outside temperature values for the month of January 2013.

Furthermore, a bypass system was also considered, meaning that the incoming air can circulate through the PCM-Air heat exchanger or be injected directly into the house. This allows the renewal of the indoor air without affecting the heat exchanger's state.

All the above considered, the operation of the system is as follows:

- From 00:00 to 06:00 the inlet air exchanger temperature is heated and used to charge the unit (night charging scenario still active).

- From 06:00 to 16:00 the heat exchanger is bypassed and the double flow ventilation system is used to ventilate the house. A PID controller ensures that the limit of 1000 ppm is not surpassed. Conventional heating is used to heat the house during this period, if needed.
- From 16:00 to 22:00 the PCM-Air heat exchanger is used to heat the house; its inlet air is the outlet double flow ventilation air. A second airflow rate PID controller is introduced for the IAQ management, along with the one that regulates the indoor air temperature. The maximum value of these two controllers is finally retained as the airflow rate used in the model.
- From 16:00 to 00:00 the same conditions apply as for the first period (00:00-06:00).

The operation of the system for the occupancy scenario is summarized in table 5.10.

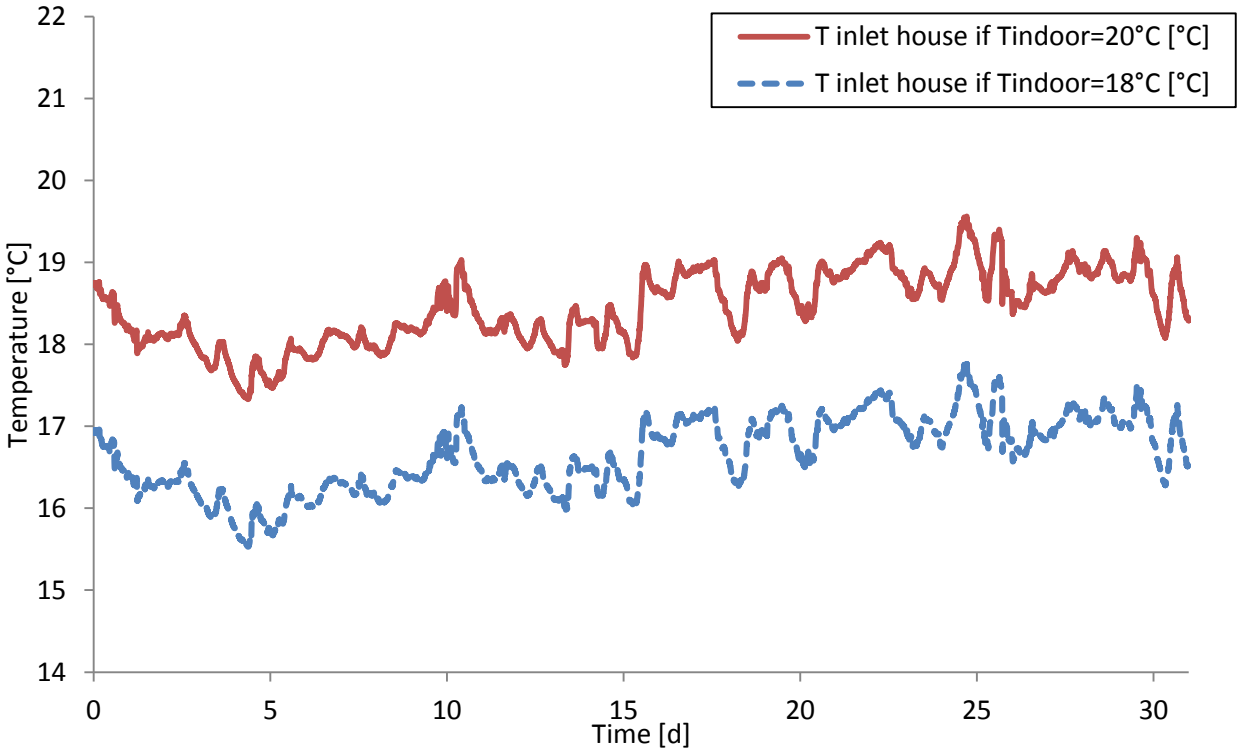

Figure 5.21: Incoming air temperature for an indoor temperature of 18 and 20 °C

	Time			
	00:00-6:00	06:00-16:00	16:00-22:00	22:00-00:00
Inlet exchanger air temperature	38°C	Indoor air temperature	Indoor air temperature	38°C
Airflow rate exchanger	PID on temperature and IAQ	0	PID on temperature and IAQ	PID on temperature
Inlet house air	Exchanger outlet	Indoor air	Exchanger outlet	Exchanger outlet

temperature		temperature		
Airflow rate house	Same as exchanger	PID on IAQ	Same as exchanger	Same as exchanger
Conventional heating	No	Yes, PID	No	No

Table 5.10: Occupancy scenario operation description, first optimization approach

5.4.7.3 Occupancy scenario results

As with the first two scenarios, the three selected configurations were tested for the occupancy scenario. This time configuration 3 was initially tested with an inlet exchanger temperature of 38°C (figure 5.22). The proposed control strategy managed to maintain CO_2 levels below the 1000 ppm limit but failed to provide acceptable thermal comfort conditions.

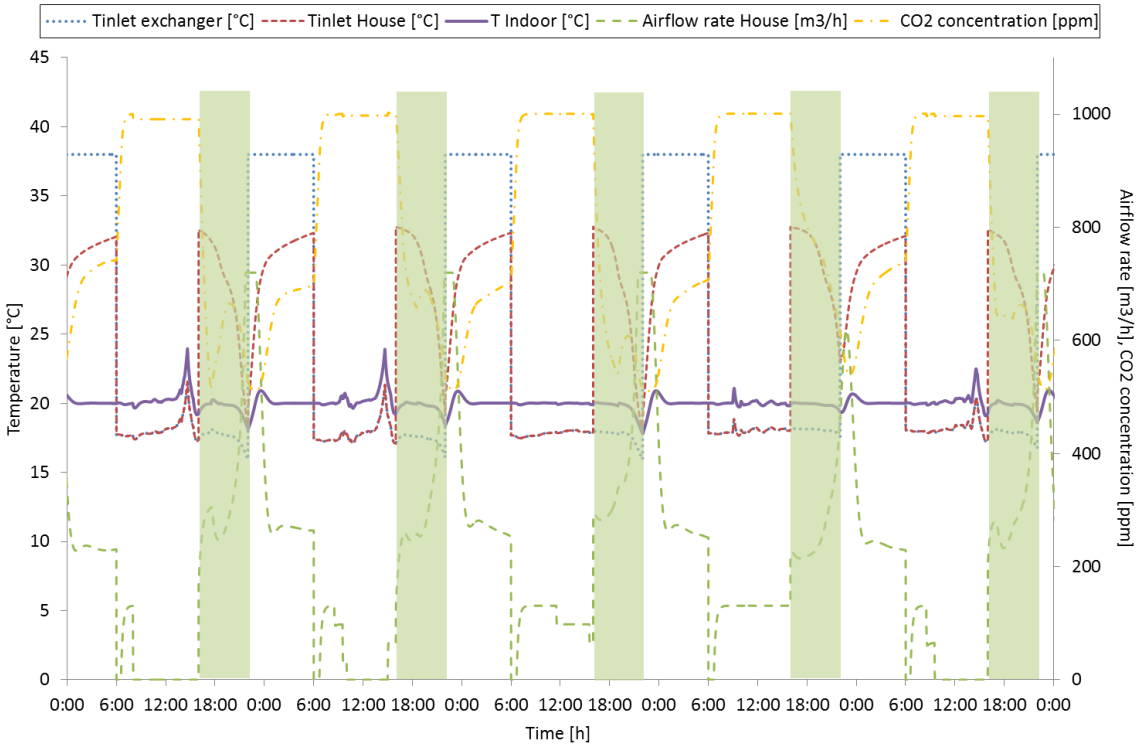

Figure 5.22: Performance of the heat exchanger, days 3-8, configuration 3, inlet exchanger air temperature=38°C, occupancy scenario, first optimization approach

A second test was then launched, increasing the inlet exchanger air temperature to 44°C (figure 5.23). This change issued better results as the indoor air temperature was stabilized at 20°C during the load shifting period. The test was reproduced for configurations 1 and 2; results are presented in figures 5.24 and 5.25.

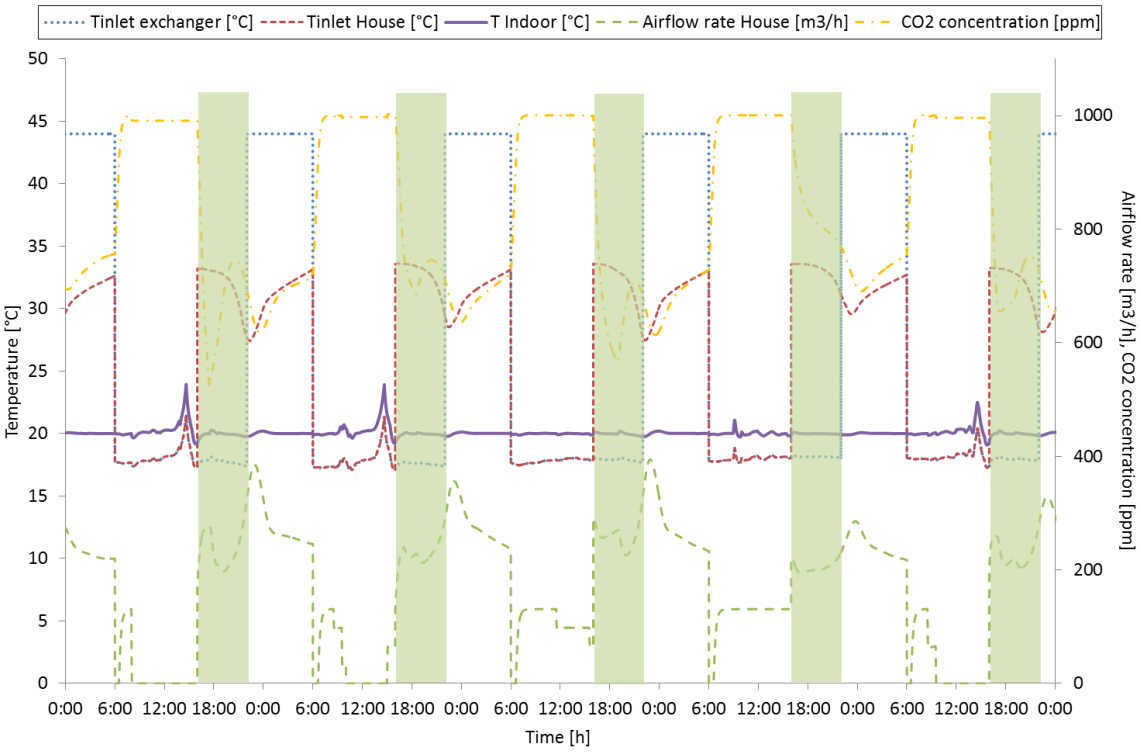

Figure 5.23: Performance of the heat exchanger, days 3-8, configuration 3, inlet exchanger air temperature=44°C, occupancy scenario, first optimization approach

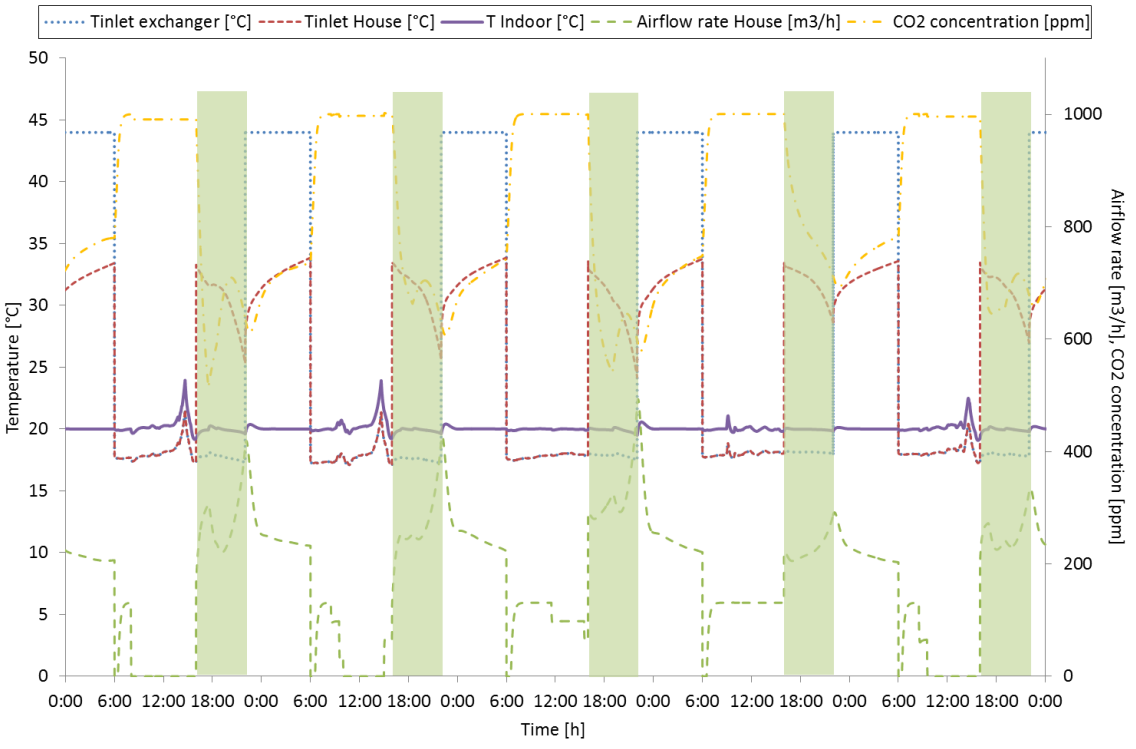

Figure 5.24: Performance of the heat exchanger, days 3-8, configuration 1, inlet exchanger air temperature=44°C, occupancy scenario, first optimization approach

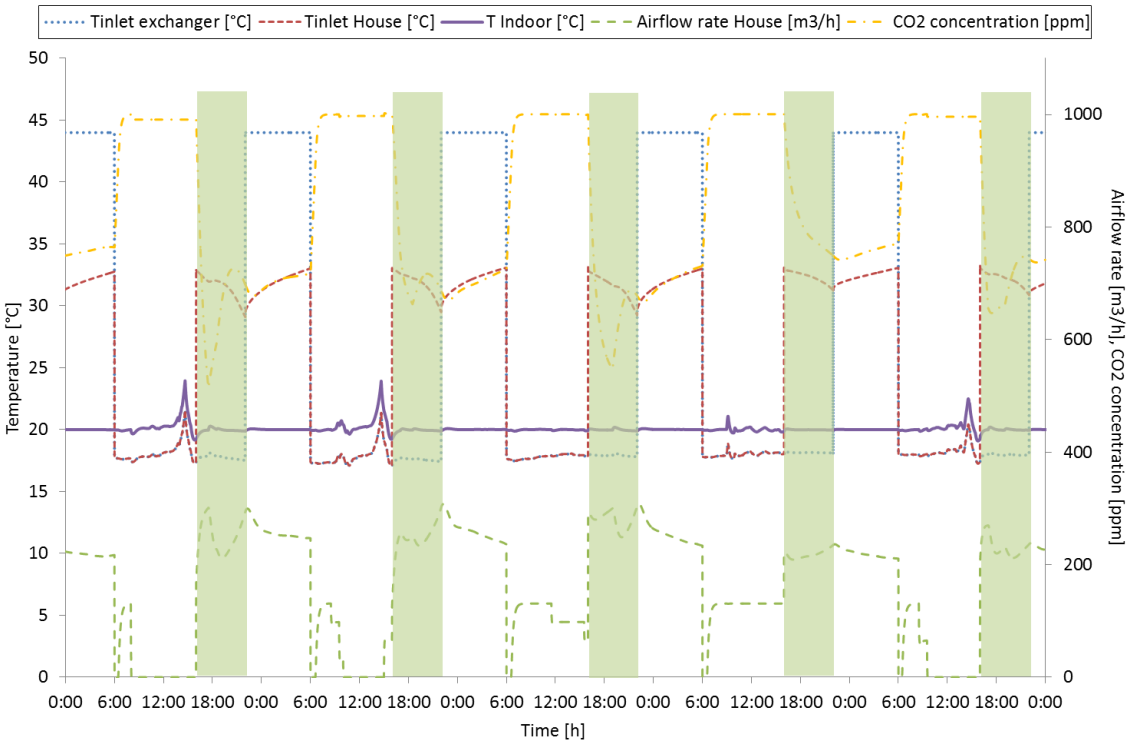

Figure 5.25: Performance of the heat exchanger, days 3-8, configuration 2, inlet exchanger air temperature=44°C, occupancy scenario, first optimization approach

The proposed optimized system managed to provide acceptable indoor conditions (thermal comfort and IAQ) for all three configurations.

The exchanger airflow rate was mostly defined by the IAQ controller but this did not interfere with the charging of the heat exchanger or the indoor air temperature. Had the need for fresh air supply been stronger, the predominance of the CO_2 controller might have deteriorated the performance of the system in terms of thermal comfort.

Heating needs were lowered when the occupants were present in the house. This was also confirmed with the testing of the house using a conventional heating mode (no heat exchanger) and a CO2 controller using the aforementioned double flow ventilation system (469,86 KWh instead of 652,23 KWh). Monthly energy consumption and electricity bill for this case are presented in table 5.11 along with the tested heat exchanger configurations results. Once again, energy consumption increases but the electricity bill decreases as the heat exchanger is charged during the night.

Configuration	Inlet air exchanger temperature (°C)	Monthly energy consumption (KWh)	Monthly electricity bill (€)	Load shifting	Thermal comfort	Indoor air quality
Conventional heating	-	469,86	62,44	×	✓	✓

1 (1,5/4/1)	44	490,07	58,14	✓	✓	✓
2 (1/3/2)	44	491,87	58,40	✓	✓	✓
3 (1,5/2/2), 38	38	509,93	60,45	✓	×	✓
3 (1,5/2/2), 38	44	529,30	62,37	✓	✓	✓

Table 5.11: Monthly performance of the three tested configurations, occupancy scenario, first optimization approach

5.4.8 Conclusions of the first approach

The first optimization approach was based on a study of different dimensions of the heat exchanger and the performance of the unit when coupled to a house, regarding load shifting, thermal comfort and acceptable IAQ.

We were able to demonstrate the benefits of the proposed optimized unit under different scenarios. However, the first optimization approach presented some limits:

- The PCM quantity and the volume of the heat exchanger were increased compared to the initial experimental unit. This increase leads to a higher manufacturing cost of the unit and complicates its integration into the ventilation system of the building.
- The increased PCM mass also resulted in a longer load shifting period (16:00-22:00 instead of 18:00-20:00).

As a result, a second optimization approach was found necessary in order to overcome these limitations.

5.5 Optimization second approach

5.5.1 Introduction

The limitations of the first optimization approach demonstrated the need for a second optimization study of the heat exchanger. The second approach was aimed to focus on the performance of the heat exchanger by itself (i.e. without investigation at a first stage of the impact on the building).

This time, apart from the modification of the dimensions of the unit, the PCM properties were also altered. Two assessment parameters were identified as optimization criteria:

- The time needed to fully charge the heat exchanger;
- The energy that is stocked to the unit during this period.

The aim was to find the configuration that would charge the sufficient quantity of energy during the smallest amount of time.

5.5.2 Definition of the modified parameters

The parameters of the heat exchanger that were investigated during the second optimization approach are those concerning the heat exchanger dimensions and those concerning the PCM properties.

The dimension parameters were modified in a way that does not change the total PCM quantity. For example, a decrease of the thickness of the PCM layer resulted in a proportionate increase of the height or the length of the same layer (and of the exchanger respectively).

Concerning the PCM properties, the modified parameters were conductivity, density and specific heat. Lastly, the container conductivity was also investigated. Different available PCMs were reviewed and a range of values was proposed for each property. The same process was performed for the container, as the investigation of the conductivity of different materials (copper, steel, etc) provided a range of conductivity values. As the PCM properties change values between solid and liquid phases, a coefficient was used to modify (multiply) the initial paraffin values. Three new values for each property were tested according to the desired range established.

Concerning the heat exchanger dimension treatment, the following modifications were tested:

- Modification of the PCM layer thickness (dym) while inversely modifying its height (dz)
- Modification of the PCM layer thickness (dym) while inversely modifying its length (dx)
- Modification of the PCM layer thickness (dym) while inversely modifying both its height (dz) and length (dx)

Table 5.12 summarizes the modified parameters, presenting the initial paraffin values, the range according to the properties of other PCMs, the three multiplying coefficients and the three new values, used for the second optimization study.

For each of the three different dimension configurations, the combination of all the possible PCM properties values led to a total of 243 cases.

Parameters	Initial values	Range	Modified parameters					
			Coef.	New values	Coef.	New values	Coef.	New values
PCM conductivity (W/(m.K))	0.24 / 0.18	0.18-0.7	2	0.48-0.36	3	0.72-0.54	4	0.96-0.72
PCM density (kg/m³)	870 / 780	700-1600	0.9	783-700	1.4	1220-1090	1.84	1600-1435
PCM specific heat (kJ/(kg.K))	2.4 / 2	1.4-3.6	0.7	1.7-1.4	1.25	3- 2.5	1.5	3.6-3
Container conductivity (W/(m.K))	250	20 -400	0.5	125	1.3	325	1.6	400

PCM layer thickness vs length (m)	0.09 0.10	0.006-0.015 0.06-0.15	0.66 0.66^{-1}	0.006 0.15	1.33 1.33^{-1}	0.012 0.075	1.66 1.66^{-1}	0.015 0.06
PCM layer thickness vs height (m)	0.09 0.18	0.006-0.015 0.108-0.272	0.66 0.66^{-1}	0.006 0.272	1.33 1.33^{-1}	0.012 0.135	1.66 1.66^{-1}	0.015 0.108
PCM layer thickness vs height and length (m)	0.09 0.10 0.18	0.006-0.015 0.077-0.123 0.139-0.221	0.66 $0.66^{-1/2}$ $0.66^{-1/2}$	0.006 0.123 0.221	1.33 $1.33^{-1/2}$ $1.33^{-1/2}$	0.012 0.086 0.156	1.66 $1.66^{-1/2}$ $1.66^{-1/2}$	0.015 0.077 0.139

Table 5.12: Modified parameters for the second optimization approach

5.5.3 Testing of the modified parameters

The optimization tests were performed in Matlab environment for a full charging and a full discharging process. For the charging cycle the inlet air temperature was set at 44°C and for the discharging one at 20°C. The PCM temperature before the starting of the test was set at 26°C for the first case and 44°C for the second one. A criterion had to be established in order to define the end of the charging/discharging phase. The difference of the outlet exchanger temperature of the heat exchanger was calculated for a two minute interval. The mean value of this calculation was determined taking into account the last six values. If this number was inferior to 0,005 °C then the charging or discharging of the unit was considered finished. The previous statement can be represented as follows in the following relation:

$$\sum_{t-n\cdot dt}^{t}\left(T_{out}^{t}-T_{out}^{t-2min}\right)<0{,}005 \Rightarrow end\ simulation \qquad \text{equation 5.2}$$

The stocked or destocked energy until the end of the simulation was calculated as follows:

$$E=\sum_{t=0}^{t=end}\left[\dot{m}\cdot Cp_a\cdot\left(T_{air,inlet}-T_{air,outlet}\right)\cdot dt/3600\right] \qquad \text{equation 5.3}$$

Where

E	Stocked or destocked energy	[KWh]
Cp_a :	Specific heat capacity of the air	[J/(kg·K)]
$\dot{m}$:	Airflow rate	[kg/s]
$T_{air,inlet}$:	Inlet exchanger air temperature	[°C]
$T_{air,outlet}$:	Outlet exchanger air temperature	[°C]
dt	Time step	[s]

Results were classified according to the minimum time for energy storage or release. Simulations were performed for the stocking process and the destocking one; they were repeated for three different airflow rates: 100, 300 and 500 m^3/h. Lastly, simulations were also carried out for the initial dimension of

the heat exchanger, while modifying the values of the PCM properties. All configurations combined a total of 4860 simulations was performed.

A drawback appeared in the 100 m^3/h tests, as the slow heat exchange rates led to the ending of the simulation before the full charge or discharge of the exchanger for some of the tests. Consequently, these tests were not considered reliable and were not taken into account.

A Matlab script was used to automatize this procedure and classify the configurations according to the selected criteria. Part of the results is demonstrated in table 5.13. These results correspond to the first seventy configurations for charging the unit with an airflow rate of 300m^3/h. Column 1 states the classification of the configurations according to the time needed for the charging to take place, columns 2 to 5 illustrate the multiplying coefficients for the PCM and container properties, columns 6 to 8 present the tested dimensions; the last two columns present the selected criteria for the second optimization approach: the time needed for charging and the stocked energy during that time. Some of these configurations were used for the coupling with the building and are investigated in the following parts of this chapter.

More results are presented in appendix A.

Classification	PCM Conductivity	PCM Density	PCM Specific heat	Container conductivity	Thickness (m)	Length (m)	Height (m)	Time (h)	Energy (KWh)
1	4	0,9	0,7	0,5	0,006	0,1231	0,2216	3,35	2721,2
2	3	0,9	0,7	0,5	0,006	0,1231	0,2216	3,37	2725,62
3	2	0,9	0,7	0,5	0,006	0,1231	0,2216	3,4	2729,83
4	4	0,9	0,7	1,3	0,006	0,1231	0,2216	3,5	2751,41
5	3	0,9	0,7	1,3	0,006	0,1231	0,2216	3,52	2753,57
6	4	0,9	0,7	1,6	0,006	0,1231	0,2216	3,54	2758,54
7	2	0,9	0,7	1,3	0,006	0,1231	0,2216	3,55	2756,05
8	3	0,9	0,7	1,6	0,006	0,1231	0,2216	3,56	2760,62
9	2	0,9	0,7	1,6	0,006	0,1231	0,2216	3,59	2762,72
10	4	0,9	0,7	0,5	0,012	0,0868	0,1561	3,94	2387,77
11	3	0,9	0,7	0,5	0,012	0,0868	0,1561	4,01	2394,55
12	4	0,9	0,7	1,3	0,012	0,0868	0,1561	4,03	2397
13	4	0,9	0,7	1,6	0,012	0,0868	0,1561	4,05	2398,52
14	3	0,9	0,7	1,3	0,012	0,0868	0,1561	4,09	2402,43
15	3	0,9	0,7	1,6	0,012	0,0868	0,1561	4,12	2404,6
16	2	0,9	0,7	0,5	0,012	0,0868	0,1561	4,14	2400,49
17	2	0,9	0,7	1,3	0,012	0,0868	0,1561	4,22	2406,53
18	2	0,9	0,7	1,6	0,012	0,0868	0,1561	4,24	2408,48
19	4	0,9	0,7	0,5	0,015	0,0777	0,1398	4,27	2311,24
20	4	0,9	0,7	1,3	0,015	0,0777	0,1398	4,34	2316,97
21	4	0,9	0,7	1,6	0,015	0,0777	0,1398	4,35	2317,88

22	3	0,9	0,7	0,5	0,015	0,0777	0,1398	4,37	2321,58
23	3	0,9	0,7	1,3	0,015	0,0777	0,1398	4,43	2325,74
24	3	0,9	0,7	1,6	0,015	0,0777	0,1398	4,45	2326,66
25	2	0,9	0,7	0,5	0,015	0,0777	0,1398	4,57	2329,98
26	2	0,9	0,7	1,3	0,015	0,0777	0,1398	4,62	2332,91
27	2	0,9	0,7	1,6	0,015	0,0777	0,1398	4,64	2333,55
28	4	1,4	0,7	0,5	0,006	0,1231	0,2216	4,86	4050,71
29	3	1,4	0,7	0,5	0,006	0,1231	0,2216	4,88	4056,92
30	2	1,4	0,7	0,5	0,006	0,1231	0,2216	4,94	4064,84
31	4	1,4	0,7	1,3	0,006	0,1231	0,2216	5,04	4087,51
32	3	1,4	0,7	1,3	0,006	0,1231	0,2216	5,06	4091,68
33	4	1,4	0,7	1,6	0,006	0,1231	0,2216	5,09	4096,06
34	2	1,4	0,7	1,3	0,006	0,1231	0,2216	5,11	4095
35	3	1,4	0,7	1,6	0,006	0,1231	0,2216	5,12	4100,17
36	2	1,4	0,7	1,6	0,006	0,1231	0,2216	5,16	4102,46
37	4	0,9	1,25	0,5	0,006	0,1231	0,2216	5,47	4598,93
38	3	0,9	1,25	0,5	0,006	0,1231	0,2216	5,5	4606,99
39	2	0,9	1,25	0,5	0,006	0,1231	0,2216	5,56	4615,19
40	4	0,9	1,25	1,3	0,006	0,1231	0,2216	5,66	4638,49
41	3	0,9	1,25	1,3	0,006	0,1231	0,2216	5,69	4642,1
42	4	0,9	1,25	1,6	0,006	0,1231	0,2216	5,72	4647,35
43	2	0,9	1,25	1,3	0,006	0,1231	0,2216	5,74	4645,71
44	3	0,9	1,25	1,6	0,006	0,1231	0,2216	5,74	4650,97
45	4	1,4	0,7	0,5	0,012	0,0868	0,1561	5,74	3607,86
46	2	0,9	1,25	1,6	0,006	0,1231	0,2216	5,8	4654,41
47	3	1,4	0,7	0,5	0,012	0,0868	0,1561	5,84	3617,59
48	4	1,4	0,7	1,3	0,012	0,0868	0,1561	5,85	3618,16
49	4	1,4	0,7	1,6	0,012	0,0868	0,1561	5,88	3620,31
50	3	1,4	0,7	1,3	0,012	0,0868	0,1561	5,94	3626,07
51	3	1,4	0,7	1,6	0,012	0,0868	0,1561	5,97	3627,56
52	2	1,4	0,7	0,5	0,012	0,0868	0,1561	6,04	3626,19
53	2	1,4	0,7	1,3	0,012	0,0868	0,1561	6,12	3631,33
54	4	1,84	0,7	0,5	0,006	0,1231	0,2216	6,15	5213,87
55	2	1,4	0,7	1,6	0,012	0,0868	0,1561	6,15	3632,9
56	3	1,84	0,7	0,5	0,006	0,1231	0,2216	6,19	5222,88
57	4	1,4	0,7	0,5	0,015	0,0777	0,1398	6,22	3502,55
58	2	1,84	0,7	0,5	0,006	0,1231	0,2216	6,25	5232,21
59	4	1,4	0,7	1,3	0,015	0,0777	0,1398	6,29	3508,13
60	4	1,4	0,7	1,6	0,015	0,0777	0,1398	6,31	3509,24
61	4	1,84	0,7	1,3	0,006	0,1231	0,2216	6,35	5254,49
62	3	1,4	0,7	0,5	0,015	0,0777	0,1398	6,36	3516,69

63	3	1,84	0,7	1,3	0,006	0,1231	0,2216	6,38	5259,19
64	4	0,9	1,5	0,5	0,006	0,1231	0,2216	6,4	5447
65	4	1,84	0,7	1,6	0,006	0,1231	0,2216	6,41	5264,21
66	3	1,4	0,7	1,3	0,015	0,0777	0,1398	6,43	3520,35
67	3	1,84	0,7	1,6	0,006	0,1231	0,2216	6,44	5268,14
68	2	1,84	0,7	1,3	0,006	0,1231	0,2216	6,44	5263,56
69	3	0,9	1,5	0,5	0,006	0,1231	0,2216	6,44	5456,69
70	3	1,4	0,7	1,6	0,015	0,0777	0,1398	6,45	3521,21

Table 5.13: Classification of the obtained results for the charging of the unit according to faster charging time, airflow rate of 300m3/h

5.5.4 Results of the second optimization approach

The great number of simulations and the observation of the classification of the configurations led to the verification of our initial thoughts concerning the impact of the investigated parameters and the formulation of a pattern concerning the configurations with the minimum time needed for charging/discharging.

These observations can be summarized as follows:

- A thinner PCM layer led to a faster charging of the unit.
- Smaller values of the PCM specific heat and density values led to faster charging but with less stored energy.
- Larger values of the PCM conductivity led to faster charging, even though the differences were not very important.
- Oddly, the opposite effect is observed for the container conductivity values, as the smaller the value of this property, the shorter the time needed to charge. Nevertheless, the impact of the change of this value is very small, linked probably to the limited thickness of the layer (2mm).
- Concerning the comparison between the configurations involving a thinner PCM layer with increased length versus increased height, no clear conclusions could be drawn. The impact of the modification of the height or the length of the exchanger was similar for the two cases.

These observations are reflected in the classification of the tested configurations (table 5.13). Configurations positioned at the first places were those with smaller specific heat and density values, thinner PCM layer and larger conductivity values. A similar pattern was detected for all different testing conditions (charging/discharging, different airflow rates), even though small variations existed.

The following table presents the time needed for a full charge of the initial version of the heat exchanger and compares this value with optimized versions of the unit for a similar amount of energy storage.

Configuration	Air flow rate (m^3/h)	Energy stored (KWh)	Time (h)
Initial	300	3,872	5,97
Case 28 (dymvs dx vs dz)	300	4,050	4,86
Case 28 (dymvs dz)	300	4,055	4,91
Case 28 (dymvs dx)	300	4,045	4,80
Initial	500	3,677	4,34
Case 27 (dymvs dx vs dz)	500	3,804	3,34
Case 25 (dymvs dz)	500	3,798	3,29
Case 22 (dymvs dx)	500	3,791	3,23

Table 5.14: Comparison between initial and optimized version of the heat exchanger

The comparison between the initial and the optimized versions of the heat exchanger shows a quicker charge of the unit for the same (or even slightly increased) amount of heat storage. The optimized versions present a one hour decrease for the required charging time.

Furthermore, the values presented in this table verify that the way that is used to compensate for the modifications of the PCM layer thickness is indifferent, as whether it concerns the height, the length or both, results are very similar.

The results of the second optimization study provided us with a large list of configurations, each presenting advantages and disadvantages for our case study. The scenarios that were tested with the results of the first optimization approach were then reproduced using the newly obtained configurations.

5.5.3 Simple scenario, second approach

The simple scenario of the first optimization approach involved the testing of three selected optimized versions of the heat exchanger, without occupants, in order to shift the electrical heating load during the period 16:00-22:00 for the month of January 2013.

One of the objectives of the second approach was to reduce the load shifting period in order to better comply with the peak power problem observed in France. The same scenario was therefore reproduced, modifying nevertheless the load shifting period to 18:00-20:00 and testing the configurations obtained with the second approach.

Observation of the second study results showed that the same or similar configurations were classified in the same order for the charging and discharging process and for different airflow rates. Following this,

configurations that correspond to the 300 m^3/h case (table 5.13) will be used for the assessment of testing of the previously established scenarios.

Table 5.15 is a reminder of the operation conditions of the simple load shifting scenario.

	Time				
	00:00-6:00	06:00-18:00	18:00-20:00	20:00-22:00	22:00-00:00
Inlet exchanger air temperature	38°C	38°C	Indoor air temperature	38°C	38°C
Airflow rate exchanger	PID on temperature	PID on temperature	PID on temperature	PID on temperature	PID on temperature
Inlet house air temperature	Exchanger outlet	Indoor air temperature	Exchanger outlet	Exchanger outlet	Exchanger outlet
Airflow rate house	Same as exchanger	PID on CO2	Same as exchanger	Same as exchanger	Same as exchanger
Conventional heating	No	No	No	No	No

Table 5.15: Simple load shifting operation description, second optimization approach

The first tested configuration was the one that presented the quickest charge (case 1, table 5.13). This configuration was tested for various values of the inlet exchanger air temperature. Figure 5.26 illustrates the performance of the heat exchanger for this configuration with the last tested inlet air value, 44°C. The highlighted green areas represent the shifting period (18:00-20:00).

The configuration failed to provide satisfying results, as the indoor air temperature decreased during the load shifting period. The airflow rate significantly increases in an effort to provide more power but the heat exchanger cannot provide the needed power.

A second test was performed, using the 28th configuration (table 5.13 again) as it is the configuration presenting a significant increase in the amount of energy stored in the heat exchanger (compared to the previous ones). This configuration was also tested for increasing inlet exchanger air temperature but none of them managed to maintain a stable indoor air temperature during the load shifting period. Figure 5.27 presents the results obtained for this case with an inlet air temperature of 44°C.

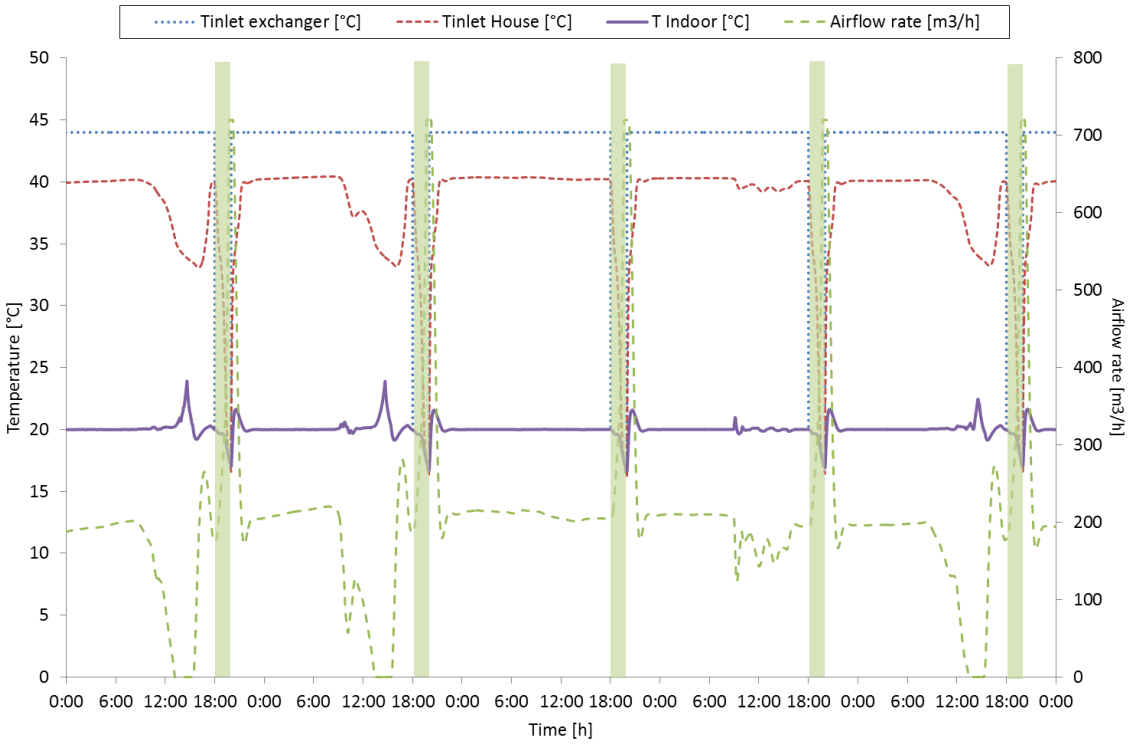

Figure 5.26: Performance of the heat exchanger, days 3-8, case 1, inlet exchanger air temperature=44°C, simple load shifting scenario, second optimization approach

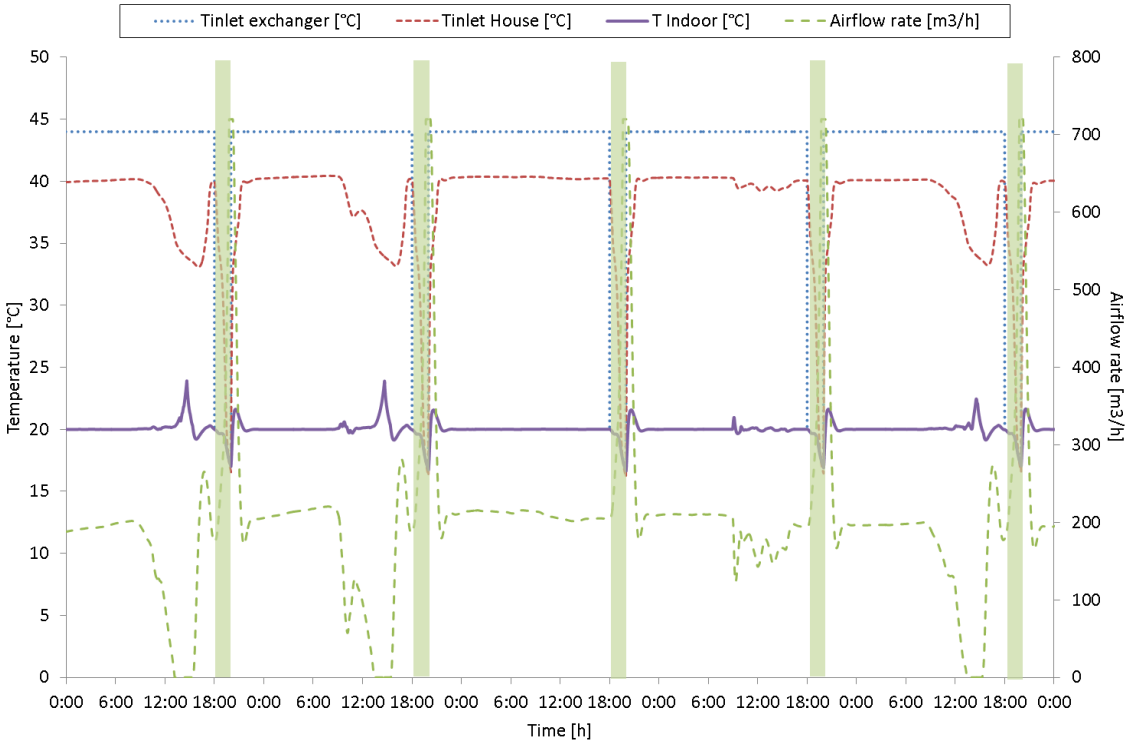

Figure 5.27: Performance of the heat exchanger, days 3-8, case 28, inlet exchanger air temperature=44°C, simple load shifting scenario, second optimization approach

After the inadequacy of the first two cases, a third configuration was tested. The configuration that was tested was the configuration 38 which corresponds to the configuration presenting the same time for a full charging as with the initial version of the exchanger for an airflow rate of 300m^3/h. The augmented stored energy of this configuration permitted an efficient performance of the system, as can be observed in figure 5.28.

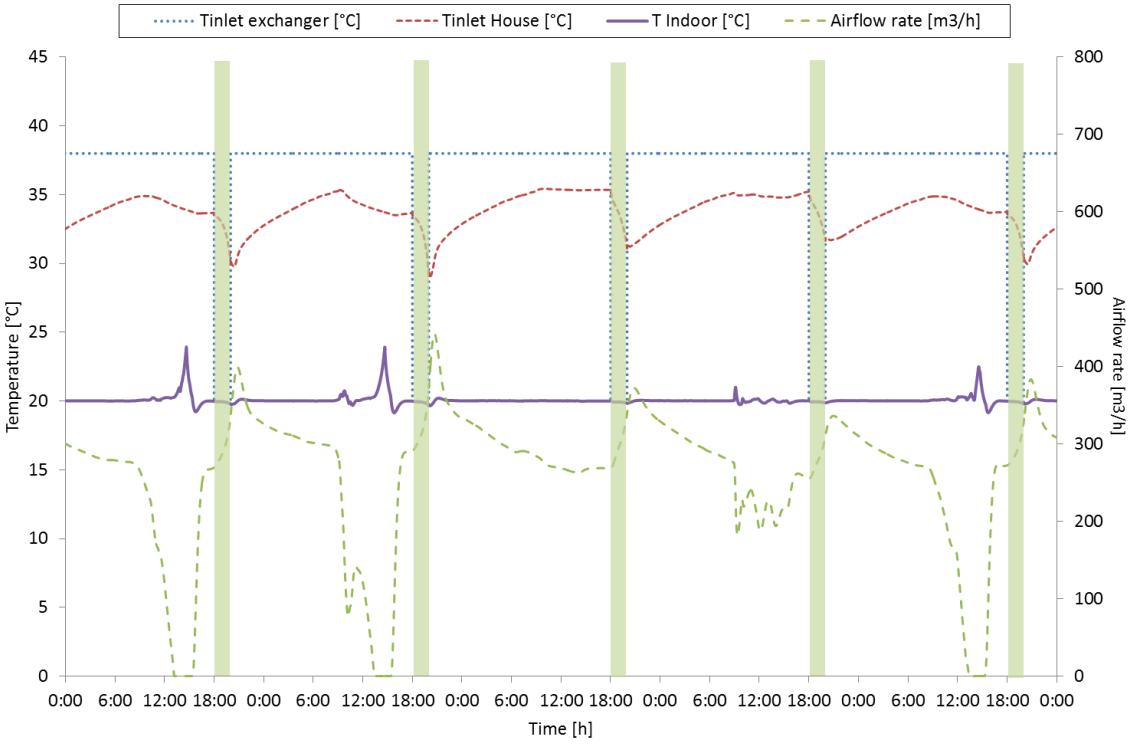

Figure 5.28: Performance of the heat exchanger, days 3-8, case 38, inlet exchanger air temperature=38°C, simple load shifting scenario, second optimization approach

We then wanted to test the performance of this configuration with a more difficult scenario. As described in the occupancy scenario of the first optimization study, in case of human presence indoor air can no longer be reinjected into the house, as it is considered to be polluted. In order to overcome this obstacle a heat recovery system was used, providing air at a lower temperature than the indoor one (equation 5.1, figure 5.21).

This time we tested this option but with a more challenging condition: the inlet exchanger air temperature was given the value of indoor air temperature minus 4°C, during the load shifting period, exceeding the lower values obtained by the heat recovery system.

The testing of the 38th configuration under such conditions showed that an increase of the inlet exchanger air temperature during the off peak period was needed in order to obtain stable thermal comfort conditions. Figure 5.29 presents the performance of the 38th configuration with a 44°C air temperature during the charging of the unit. A minor decrease of the indoor air temperature is observed during the load shifting period. Lastly, a configuration with even more increased energy storage was tested (case 64, table 5.13). This configuration managed to provide an efficient operation of the system

with a 38°C inlet exchanger air temperature during the charging process and an indoor minus 4°C during the discharging one (figure 5.30).

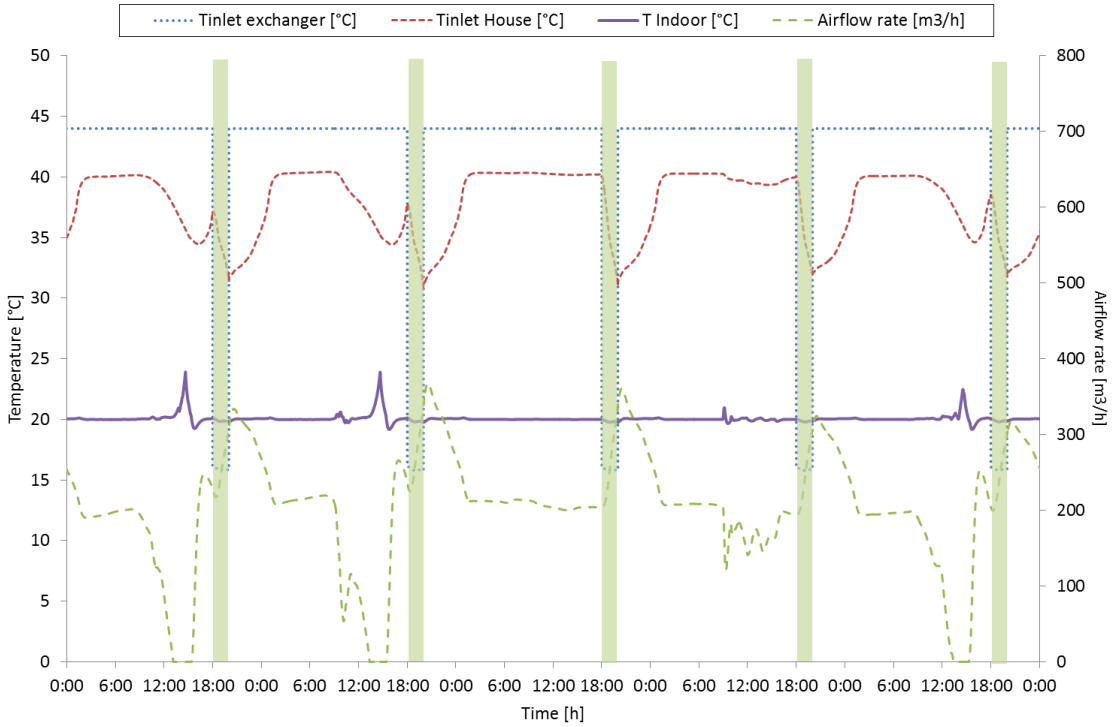

Figure 5.29: Performance of the heat exchanger, days 3-8, case 38, inlet exchanger air temperature=44°C, inlet house air temperature= outlet exchanger –4°C, simple load shifting scenario, second optimization approach

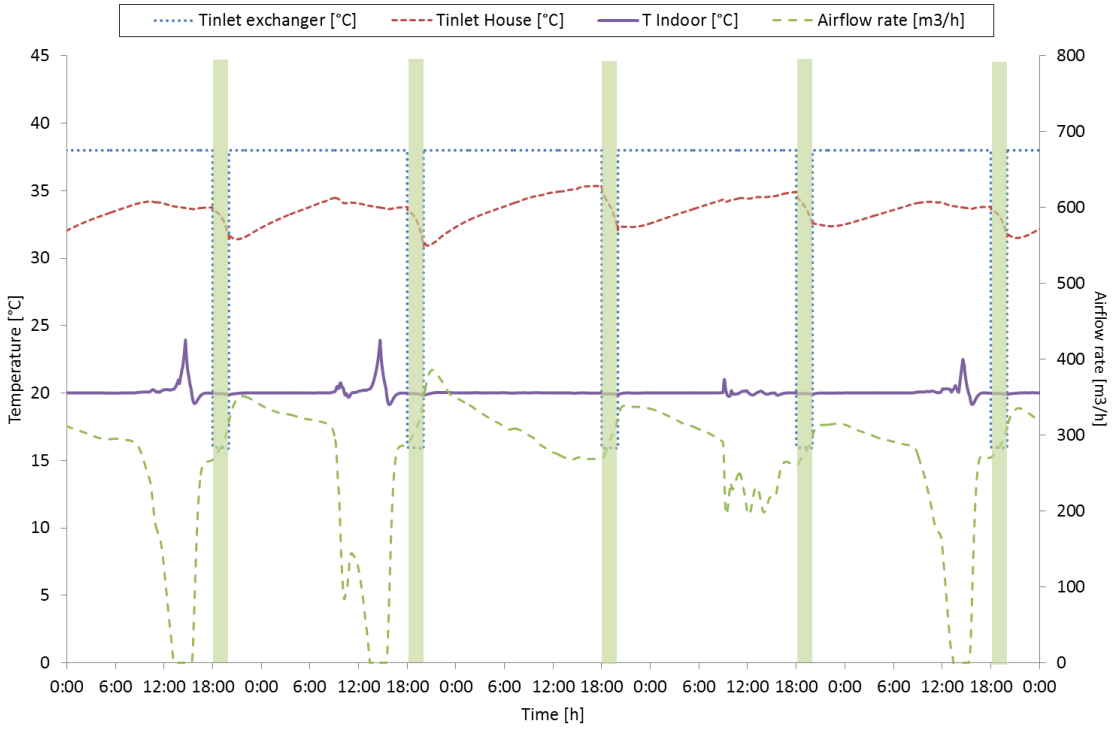

Figure 5.30: Performance of the heat exchanger, days 3-8, case 64, inlet exchanger air temperature=38°C, inlet house air temperature= outlet exchanger –4°C, simple load shifting scenario, second optimization approach

As with the first optimization approach, the monthly energy consumption and electricity bill are calculated for each of the presented cases; they are demonstrated in table 5.16.

Configuration	Inlet air exchanger temperature (°C)	Discharge Inlet air exchanger temperature (°C)	Monthly energy consumption (KWh)	Monthly electricity bill (€)	Load shifting	Thermal comfort
Conventional heating	-	-	652,23	86,10	×	✓
1	44	Indoor	832,06	110,27	✓	×
29	44	Indoor	814,98	107,03	✓	×
38	38	Indoor	820,79	106,19	✓	✓
38	44	Indoor -4	858,71	111,22	✓	✓
64	38	Indoor -4	829,19	108,39	✓	✓

Table 5.16: Monthly performance of the tested configurations, simple load shifting scenario, second optimization approach

5.5.4 Night charging scenario

The tests presented in the previous subsection provided us with two configurations able to satisfy the criteria of load shifting and acceptable indoor air conditions. These two configurations were used to reproduce the night charging scenario and the occupancy scenario, as presented in the first optimization approach.

Concerning the night charging scenario, two modifications were made in the operation of the system: the load shifting period was reduced to two hours (18:00-20:00) and conventional heating was used between 20:00 and 22:00. Table 5.17 summarizes the operation of the system for the configurations of the second optimization approach.

	Time				
	00:00-6:00	06:00-18:00	18:00-20:00	20:00-22:00	22:00-00:00
Inlet exchanger air temperature	38°C	Indoor air temperature	Indoor air temperature	Indoor air temperature	38°C
Airflow rate exchanger	PID on temperature	0	PID on temperature	0	PID on temperature
Inlet house air	Exchanger	Indoor air	Exchanger	Exchanger	Exchanger

temperature	outlet	temperature	outlet	outlet	outlet
Airflow rate house	Same as exchanger	0	Same as exchanger	0	Same as exchanger
Conventional heating	No	Yes	No	Yes	No

Table 5.17: Night charging operation description, second optimization approach

Case 38 was initially tested with an inlet exchanger air temperature of 44°C during the charging of the exchanger. When the unit was not charged, a heat recovery system was considered to provide the inlet exchanger air at a temperature according to equation 5.1. Results are presented in figure 5.31. The decreased PCM quantity and the longer conservation period (from the end of charging until the beginning of discharging) led to an important involuntary discharge of the unit. As a result, indoor air temperature decreased during the load shifting period.

In view of this fact, we decided to reduce the heat losses of the heat exchanger to the surrounding environment by a factor of 30%. In fact the heat exchanger model includes a heat loss factor that depends on the exterior structure and surface of the unit. Even though special caution was given for an efficient insulation of the heat exchanger, the experimental nature of its conception (openings for temperature sensors, coupling with the experimental platform etc) resulted in non-negligible heat losses. These losses seem to play an important role when the exchanger must be maintained at a charged state for a long period as they lead to involuntary discharge of the unit.

The last test was then repeated for a better insulated version of the heat exchanger. Figure 5.32 illustrates the performance of the unit for the night charging scenario under such conditions. The outlet exchanger air temperature decreases at a lower rate during the conservation period and the indoor temperature presents smaller variations.

Furthermore, the 64th case was tested under the same scenario and conditions. As for the 34th case, the performance of the unit with the initial insulation was not sufficient for a stable indoor air temperature (figure 5.33). The modification of this parameter demonstrated a better and adequate performance, as can be seen in figure 5.34.

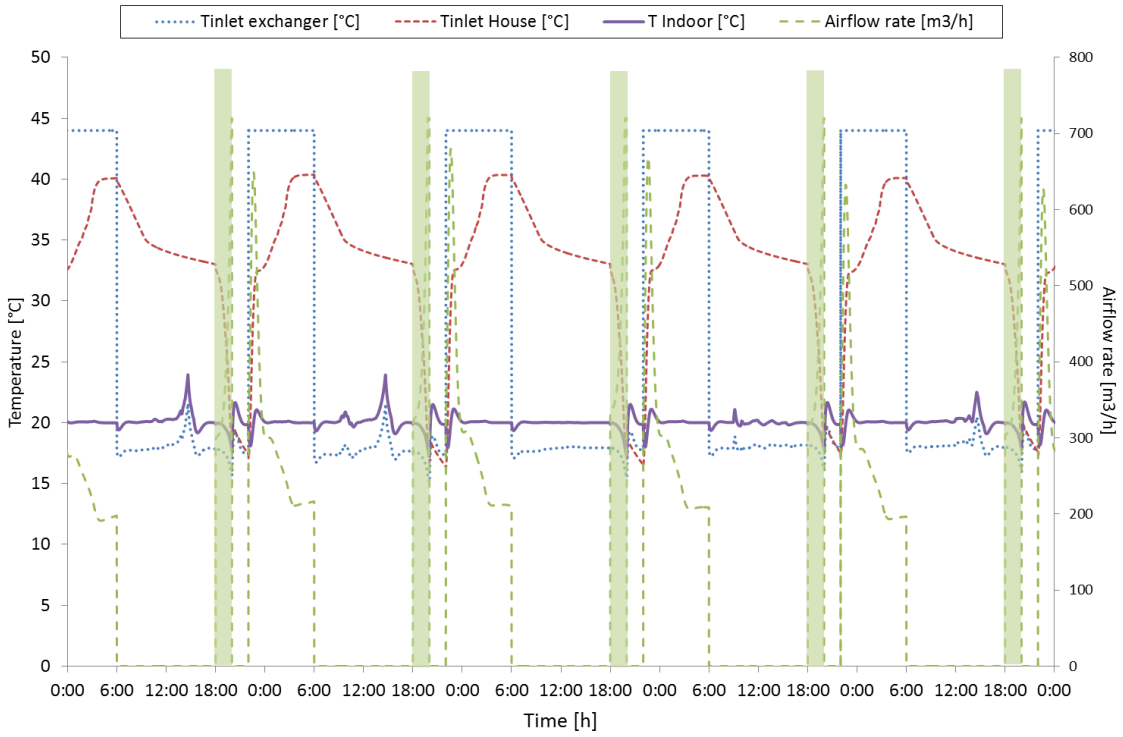

Figure 5.31: Performance of the heat exchanger, days 3-8, case 38, inlet exchanger air temperature=44°C, inlet house air temperature= outlet exchanger –4°C, simple load shifting scenario, second optimization approach

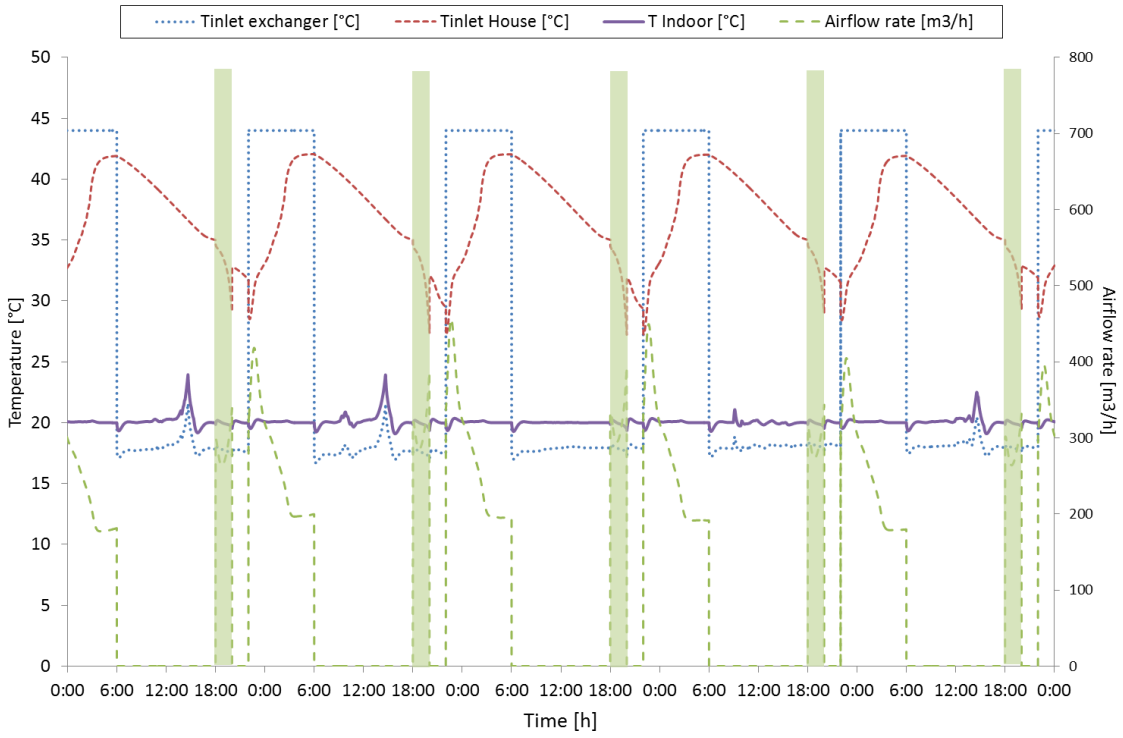

Figure 5.32: Performance of the heat exchanger, days 3-8, case 38, inlet exchanger air temperature=44°C, ameliorated insulation, night charging scenario, second optimization approach

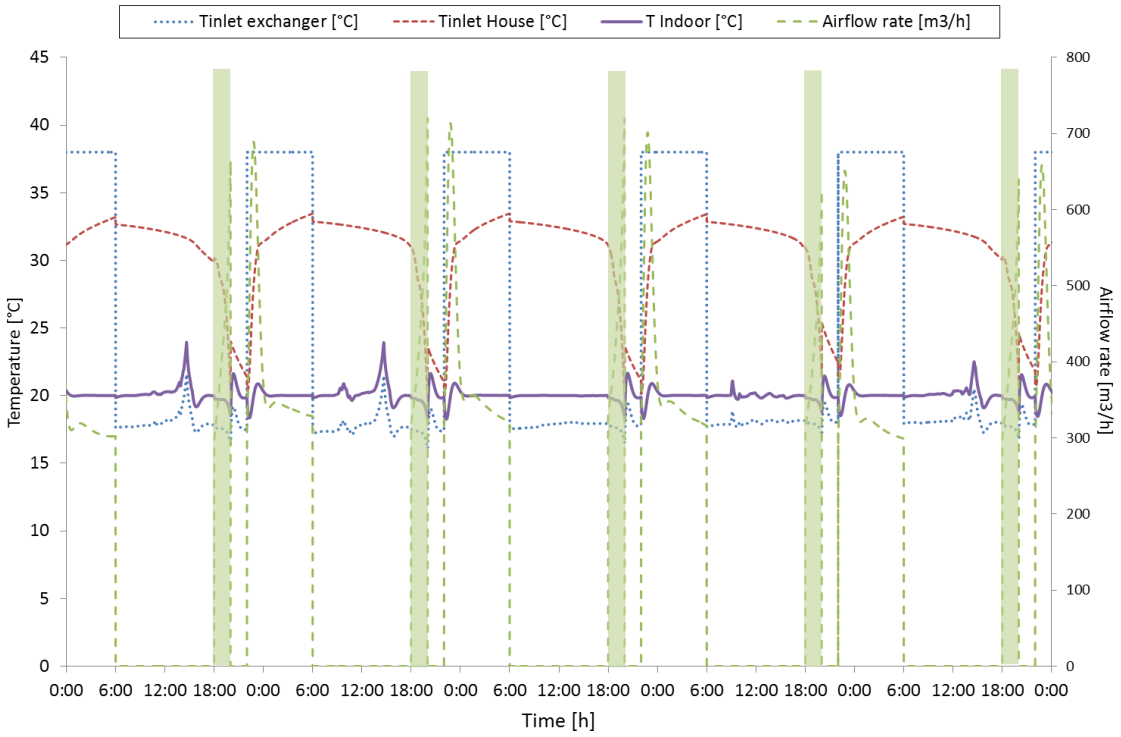

Figure 5.33: Performance of the heat exchanger, days 3-8, case 64, inlet exchanger air temperature=38°C, initial insulation, night charging scenario, second optimization approach

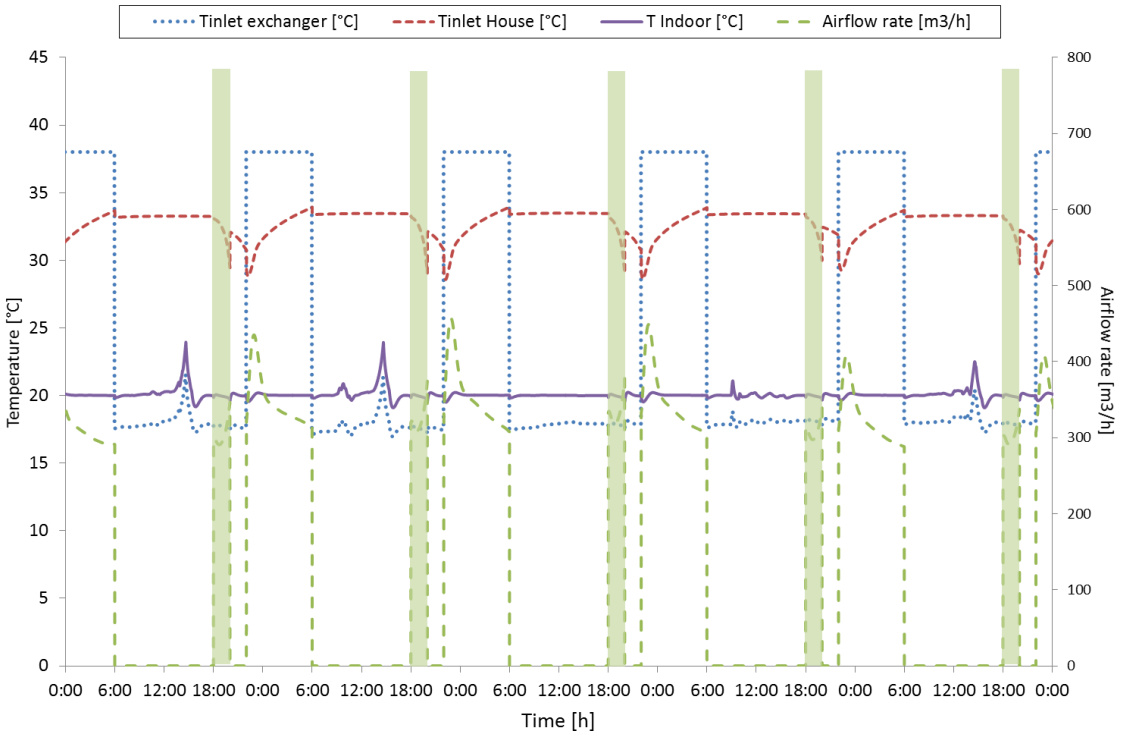

Figure 5.34: Performance of the heat exchanger, days 3-8, case 64, inlet exchanger air temperature=38°C, ameliorated insulation, night charging scenario, second optimization approach

Table 5.18 illustrates the energy consumption and subsequent electricity bill over the tested period. As expected, configurations presenting better insulation led to lower consumption and prices.

Configuration	Inlet air exchanger temperature (°C)	Insulation	Monthly energy consumption (KWh)	Monthly electricity bill (€)	Load shifting	Thermal comfort
Conventional heating	-	-	652,23	86,10	×	✓
38	44	Initial	821,10	101,16	✓	×
38	44	Ameliorated	747,88	93,09	✓	✓
64	38	Initial	793,32	98,27	✓	~×
64	38	Ameliorated	731,71	91,51	✓	✓

Table 5.18: Monthly performance of the tested configurations, night charging scenario, second optimization approach

5.5.5 Occupancy scenario

The occupancy scenario was reproduced in order to test the performance of configurations 34 and 64. The occupants presence was simulated according to the weekly program as presented in figure 5.20. The system is considered to operate similarly to the first optimization approach (subsection 5.4.7.2), with the difference of a shorter load shifting period. Table 5.19 summarizes this operation. As with the first optimization approach, the presence of occupants necessitates a heat recovery system and a heat exchanger bypass unit; it also involves heat gains from each person.

	Time				
	00:00-6:00	06:00-18:00	18:00-20:00	20:00-22:00	22:00-00:00
Inlet exchanger air temperature	38°C	Indoor air temperature	Indoor air temperature	Indoor air temperature	38°C
Airflow rate exchanger	PID on temperature	0	PID on temperature	0	PID on temperature
Inlet house air temperature	Exchanger outlet	Indoor air temperature	Exchanger outlet	Indoor air temperature	Exchanger outlet

Airflow rate house	Same as exchanger	PID on CO2	Same as exchanger	PID on CO2	Same as exchanger
Conventional heating	No	Yes	No	Yes	No

Table 5.19: Occupancy scenario operation description, second optimization approach

Configuration 38 was tested for initial (figure 5.35) and ameliorated (figure 5.36) thermal insulation conditions. Both presented an adequate performance, even though the former led to a small indoor temperature decrease at the end of the load shifting period.

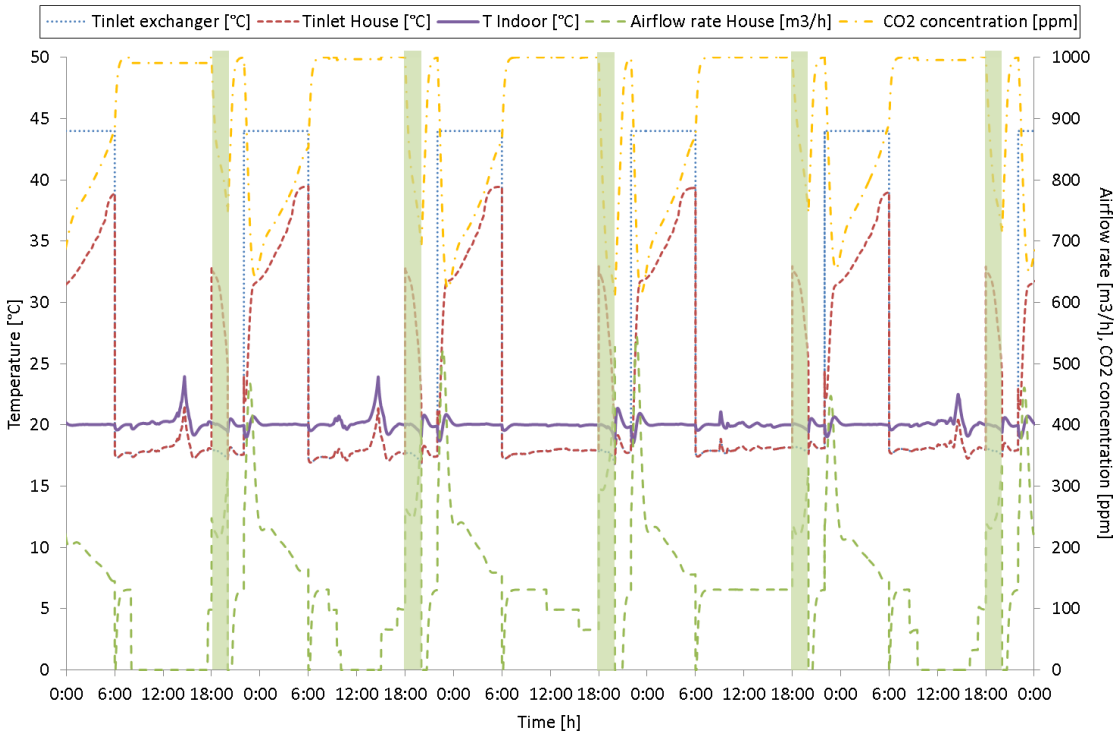

Figure 5.35: Performance of the heat exchanger, days 3-8, case 38, inlet exchanger air temperature=44°C, initial insulation, occupancy scenario, second optimization approach

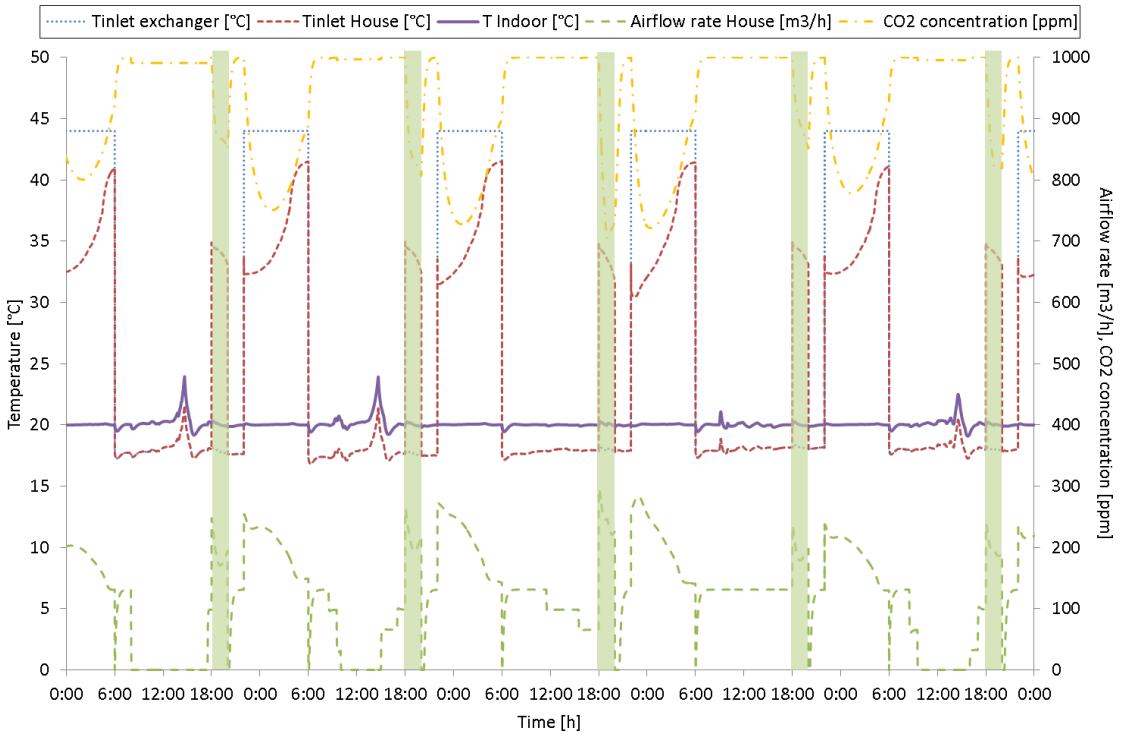

Figure 5.36: Performance of the heat exchanger, days 3-8, case 38, inlet exchanger air temperature=44°C, ameliorated insulation, occupancy scenario, second optimization approach

Lastly, configuration 64 was also tested for the occupancy scenario, under different conditions. Results are presented I in the following figures:

- Figure 5.37, inlet exchanger air temperature during charging period 38°C and initial insulation
- Figure 5.38, inlet exchanger air temperature during charging period 38°C and ameliorated insulation
- Figure 5.39, inlet exchanger air temperature during charging period 40°C and initial insulation
- Figure 5.40, inlet exchanger air temperature during charging period 40°C and ameliorated insulation

Apart from the first case, the tested configurations managed to maintain a stable indoor temperature during the discharge of the heat exchanger.

Table 5.20 presents the monthly electricity consumption and price for the tested period. Lower inlet exchanger air temperature values and better insulation led to lower consumption (and a lower electricity bill) while fulfilling the goals of the operation of the system.

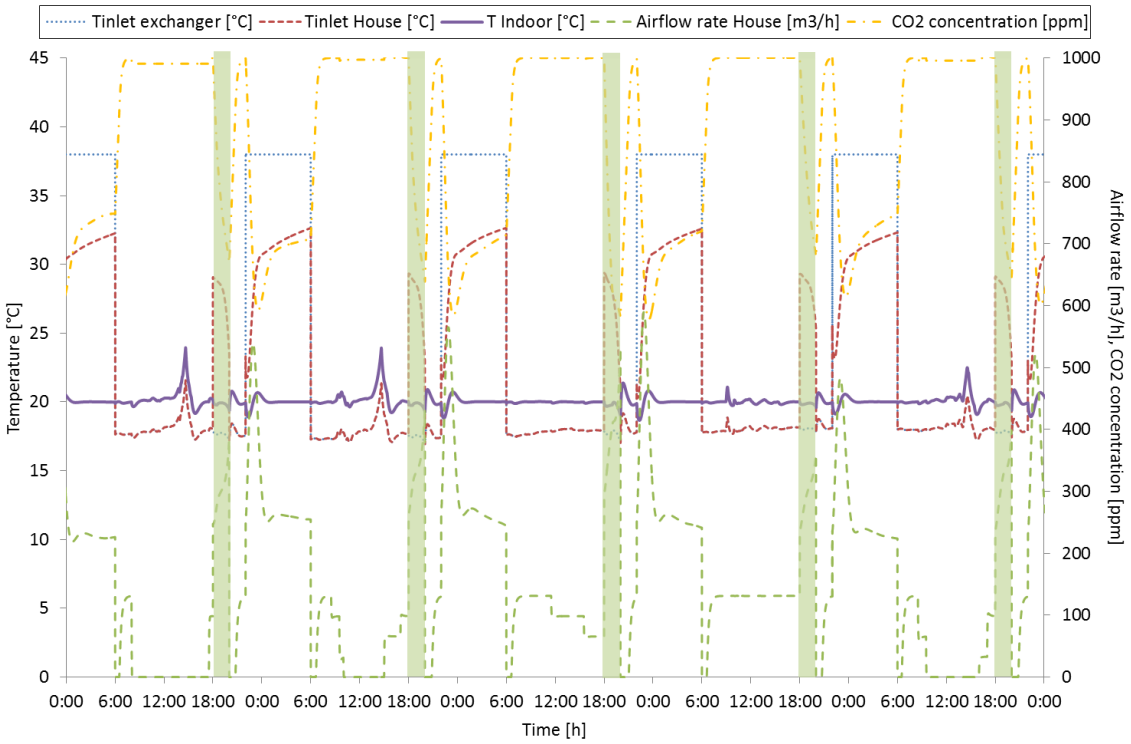

Figure 5.37: Performance of the heat exchanger, days 3-8, case 64, inlet exchanger air temperature=38°C, initial insulation, occupancy scenario, second optimization approach

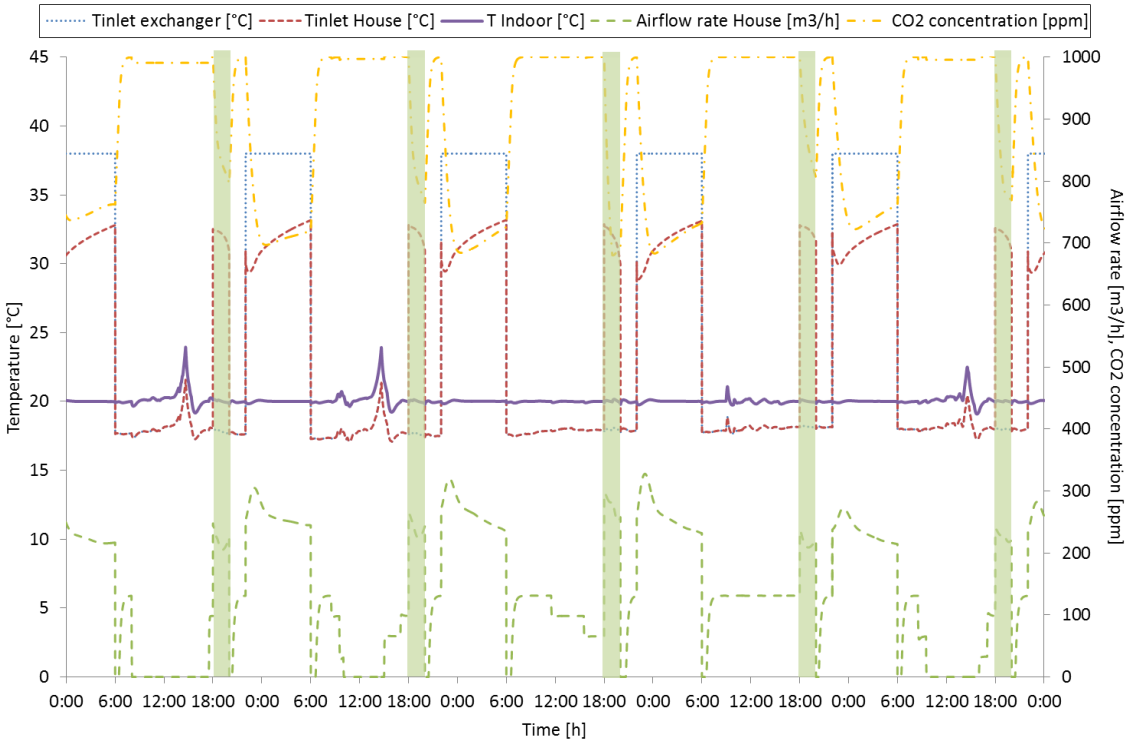

Figure 5.38: Performance of the heat exchanger, days 3-8, case 64, inlet exchanger air temperature=38°C, ameliorated insulation, occupancy scenario, second optimization approach

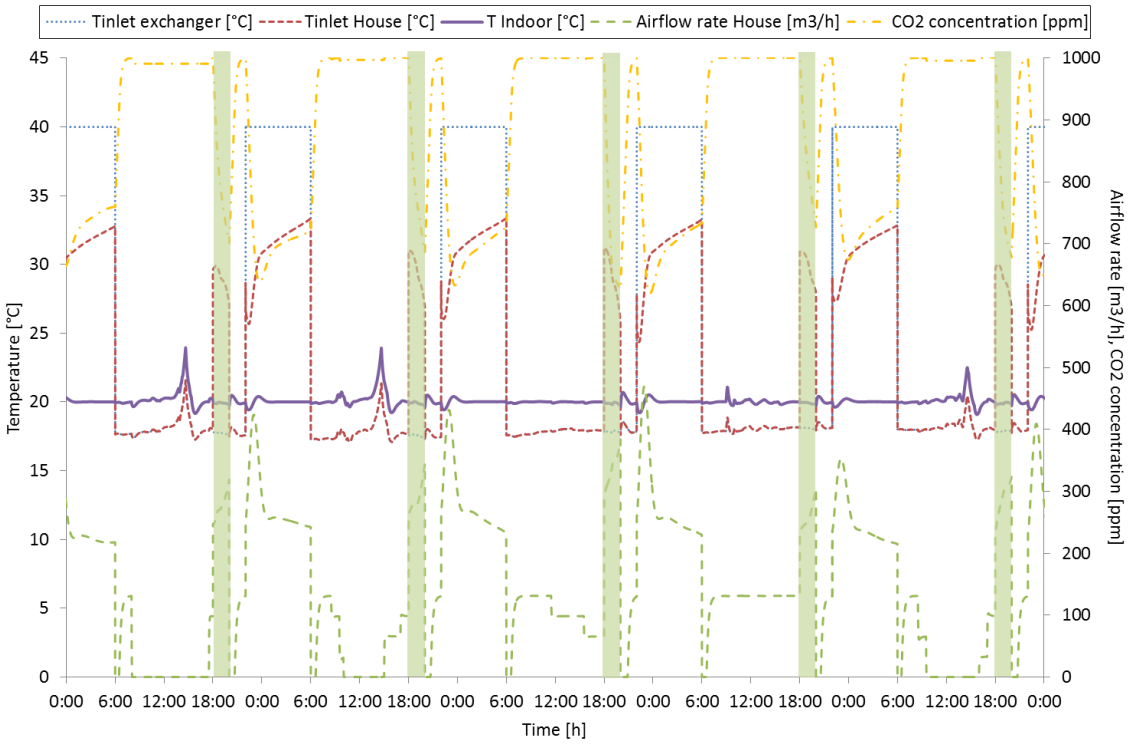

Figure 5.39: Performance of the heat exchanger, days 3-8, case 64, inlet exchanger air temperature=40°C, initial insulation, occupancy scenario, second optimization approach

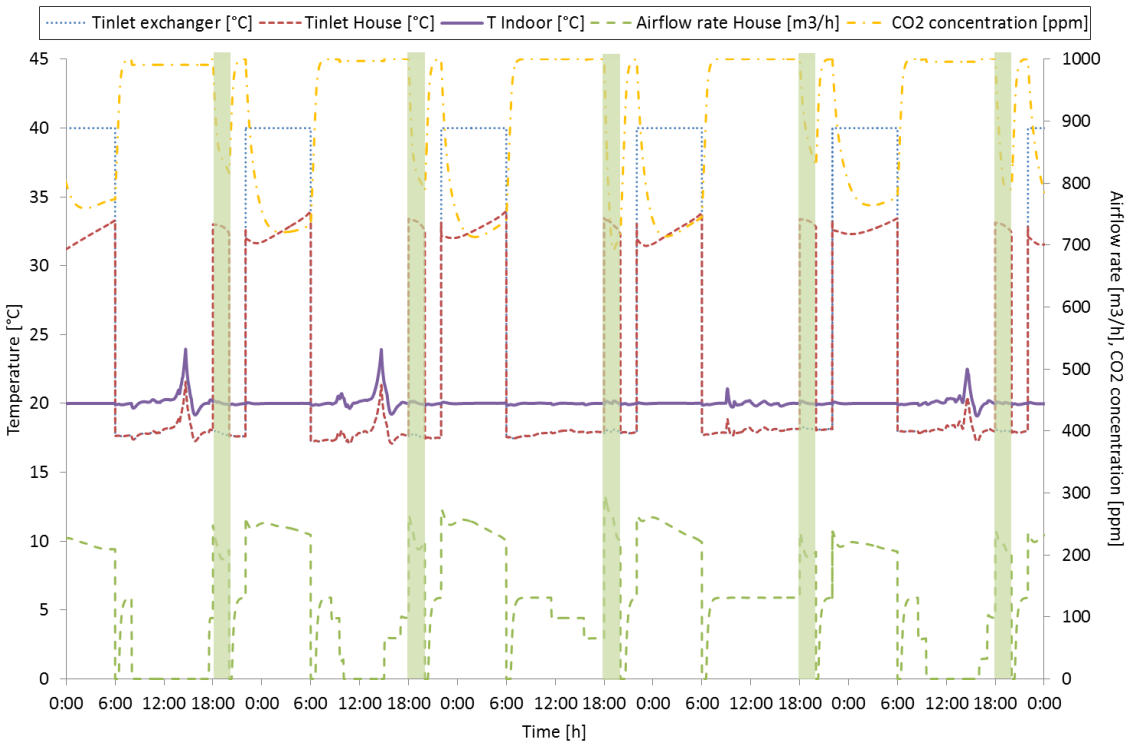

Figure 5.40: Performance of the heat exchanger, days 3-8, case 64, inlet exchanger air temperature=40°C, ameliorated insulation, occupancy scenario, second optimization approach

Configuration	Inlet air exchanger temperature (°C)	Insulation	Monthly energy consumption (KWh)	Monthly electricity bill (€)	Load shifting	Thermal comfort	Indoor air quality
Conventional heating	-		469,86	62,44	×	✓	✓
38	44	Initial	601,79	74,05	✓	~×	✓
38	44	Ameliorated	539,23	67,10	✓	✓	✓
64	38	Initial	571,31	71,00	✓	~✓	✓
64	38	Ameliorated	514,72	64,88	✓	✓	✓
64	40	Initial	578,80	71,69	✓	~×	✓
64	40	Ameliorated	527,28	66,12	✓	✓	✓

Table 5.20: Monthly performance of the tested configurations, occupancy scenario, second optimization approach

5.6 Conclusions of the second approach

The second optimization approach permitted us to overcome the limitations of the first one and to demonstrate the efficient operation of the system for the selected scenarios. A smaller and lighter exchanger was able to provide good indoor thermal and air quality conditions.

Even though the second approach's optimized configurations are manually defined (in fact, we didn't use metaheuristic methods such as genetic algorithms), their performances are sufficient. Indeed, as an example configuration 64 and 38 meet all indoor air conditions criteria while providing necessary load shifting with up to 10% energy consumption compared to the initial optimization approach. It is also important to stress the fact that those performances are not airflow rate and inlet temperature dependent.

In addition to the demonstration of the performances and capacities of the optimized configurations, the performed simulations also lead to several conclusions related to PCM thickness, PCM thermal proprieties and exchanger geometry that can be capitalized on when establishing design recommendations.

Conclusive summary and future work

Conclusive summary and future work

Synopsis

The research performed in this PhD dissertation was mainly motivated by the peak power problem observed in France during the late afternoon winter period. As these peaks are highly related to electrical heating, the objective of our work was initially to conceive and develop reliable numerical and experimental tools based on thermal storage technology and secondly to use these tools in order to develop efficient control strategies based on load shifting solutions.

The experimental part of the study consisted in the design and construction of a PCM-Air heat exchanger as the main element of the experimental platform and the place where thermal storage occurs in latent form. The heat storage system is composed of a set of PCM (paraffin) plates, embedded in the exchanger and integrated in a ventilation system. The initially observed drawback of PCM leakage was overcome with the construction of a second exchanger possessing a more rigorous structure. The unit was characterized and coupled to an experimental test cell (Hybcell), in which preliminary strategies were implemented, focusing on load shifting and maintenance of comfortable indoor conditions. The characterization results as well as the Hybcell tests which were carried out demonstrated the applicability of the proposed system but limitations were revealed, mostly concerning the time needed for the charging and discharging of the exchanger.

This observation along with the advantages of numerical studies (less time and money consuming) led to the development of a bidimensional numerical model with the purpose of reproducing the behavior of the heat exchanger. The model uses several methods and techniques, including the heat balance approach, the apparent heat capacity and the finite difference method in order to successfully represent the phase change process and the general operation of the system. The importance of the heat capacity values was revealed and further investigation of this parameter led to the creation of adequate curves according to the considered position of the PCM plate. Numerical and experimental results were confronted in order to calibrate and validate the model. Following this, the model was coupled to an existing building model in order to test the performance of the heat exchanger concerning load shifting, thermal comfort and indoor air quality through different scenarios.

Two optimization approaches were considered and numerically explored to overcome the limitations of the initial performance of the heat exchanger. The first one investigated the impact of the modification of the geometry of the unit when coupled to the building. Three configurations were selected and tested on a low energy building for a one month period. The benefits of the proposed system were demonstrated for scenarios presenting increasing difficulty: simple load shifting, night charging of the unit and lastly operation during the presence of the occupants. Electrical consumption was shifted from peak to off peak hours without affecting the thermal comfort and the air quality. Even though the final monthly power consumption was increased, the night charging of the unit allowed the operation of the system during hours with advantageous tariffs and the final electricity cost was reduced. Nevertheless, this approach demonstrated some disadvantages concerning the required PCM mass, the volume of the exchanger and the increased time which was needed for the charging of the unit.

This led to the second optimization approach which in addition to the geometry of the heat exchanger also investigated the PCM properties. Density, specific heat and conductivity values were modified, seeking the configurations with minimum charging time and maximum energy storage. The optimized versions of the unit were classified according to charging time and a one hour gain was observed for the same energy storage. In the end, the scenarios tested with the results of the first optimization approach were reproduced and we were able to obtain an efficient system with the initial PCM mass which performs load shifting while maintaining comfortable thermal and air quality conditions.

Perspectives

In this dissertation, the applicability and the benefits of latent heat storage technology were demonstrated through the numerical and experimental study of a PCM-Air heat exchanger, integrated in the ventilation system. Several fields can be investigated as a continuity of this work.

First of all, the controllers used for the operation of the system can be upgraded to more advanced ones, such as those using fuzzy logic. These controllers can offer a more adapted approach to the needs of the study and present smaller variations and more efficient results. Additionally, predictive tools can be integrated in the system's control/command interface. These tools may focus on the weather conditions or the presence of occupants in order to anticipate the heating needs of the building and adjust the operation of the system accordingly. Depending on the predicted needs, different energy storage levels can be decided, leading to a low, moderate or full charge of the heat exchanger. Metaheuristic methods such as genetic algorithms can also be used in the optimization study providing a different but more efficient approach.

Furthermore, the efficiency of the proposed system can be tested for different building properties and structure. The modification of the inertia or thermal insulation of the building may constitute examples of such a study. A more detailed design of the building with the separation of zones according to the occupants' usage and needs can be also studied.

The robustness of the proposed numerical solutions can be tested in an in-situ experimentation, whether in an experimental house equipped with all the necessary instrumentation or a real life dwelling with occupants who would understand the operation of the system. The latter case would necessitate a wider investigation of the impact of the integration of the system in an inhabited environment, focusing on fire hazards and potential PCM odor diffusion.

The study of the system can be extended to summer conditions in order to take advantage of night cooling concept technology, either experimentally or numerically. In the first case, the macroencapsulation choice of containment and the rigid structure of the second heat exchanger would allow a relatively easy replacement of the current paraffin with one more adapted to summer conditions (mostly one with a different melting range, maybe a different energy storage capacity). In the second case, the adaption to summer conditions would be performed through the modification of the PCM properties in the numerical model. Osterman et al. are currently studying a similar heat exchanger configuration with a PCM which may satisfy both winter and summer climates. It would be

interesting to see whether their results can contribute to this field and verify the efficiency of the proposed unit with the tools we developed.

Lastly, even though this study focused on the peak power issue, thermal storage technology can be coupled to other existing innovative technologies such as renewable energy resources, smart grids, living walls, etc. In that way, the benefits of each domain can be combined and offer wider and more efficient solutions to the operation of the built environment.

Texte de synthèse (français)

Texte de synthèse (français)

Optimisation numérique et expérimentale de stratégies d'effacement énergétique

Nikolaos Stathopoulos, 2015

Mots clés:

Bâtiment, Energie, Effacement énergétique, Stratégies de contrôle, Matériaux à changement de phase, Stockage thermique, Échangeur Thermique, Simulation thermique, Confort thermique, Qualité de l'air intérieur

Contexte

Le changement climatique dû à l'activité humaine, la raréfaction des ressources fossiles, les chocs pétroliers, l'augmentation de la population mondiale et urbaine constituent une liste alarmante de questions qui nécessitent des débats sérieux, de prise de décisions rigoureuses et des solutions innovantes. Plusieurs accords politiques ont déjà été mis en pratique aux niveaux nationaux et internationaux et d'autres initiatives sont en cours de préparation pour l'avenir, ce qui reflète une préoccupation mondiale ainsi qu'une nécessité d'agir croissante.

Prenant en compte ces considérations, le secteur du bâtiment joue un rôle clé, car il constitue à travers le monde l'un des principaux contributeurs en ce qui concerne la consommation d'énergie et les émissions de gaz à effet de serre. Compte tenu de ces faits, les politiques européennes et françaises envisagent d'imposer des réglementations des bâtiments à énergie zéro ou même à énergie positive dans un avenir proche. Deux problèmes principaux doivent être dépassés en ce qui concerne ces objectifs: l'intermittence des énergies renouvelables et les variations quotidiennes ou saisonnières de la consommation d'énergie. Plusieurs recherches ont été effectuées concernant le stockage de l'énergie, ce qui prouve que ce domaine peut fournir des applications pertinentes en réponse à ces inconvénients.

En général, la France fait face aux défis énoncés ci-dessus, mais elle présente également une particularité spécifique: des demandes de puissance de pointe élevées. Ces pics sont principalement rencontrés en fin d'après-midi en période d'hiver et sont fortement liés au chauffage électrique. Un projet a été élaboré sous l'égide et le financement de l'Agence Nationale de la Recherche, visant à développer un échangeur de chaleur MCP-Air couplé à une pompe à chaleur, comme une solution technique à la demande d'électricité augmentée au cours du créneau 18: 00-20: 00. Les partenaires du projet comprennent quatre unités de recherche (LGCB, CETHIL, ARMINES - CEP et EDF R & D) et un partenaire industriel (RIBO).

Objectifs et approche

C'est dans ce contexte que cette thèse vise à étudier le potentiel d'un échangeur de chaleur MCP-Air et propose des stratégies d'effacement de consommation électrique sans dégrader le confort thermique et la qualité de l'air intérieur.

L'idée générale est de développer un échangeur de chaleur intégré dans un système de ventilation, dans lequel une quantité suffisante de chaleur est stockée afin de remplacer l'utilisation du chauffage électrique pendant la période de de pointe. Trois objectifs majeurs ont été identifiés:

• Le développement des outils expérimentaux et numériques qui permettront l'élaboration, l'essai et l'évaluation des stratégies de contrôle;

• L'optimisation de la performance de l'échangeur de chaleur;

• L'élaboration des stratégies d'effacement pour différents scénarios.

L'approche qui a été suivie pour atteindre ces objectifs est un processus rétroactif sur la base de deux outils: un expérimental et un numérique. Un échangeur de chaleur MCP-Air a été conçu, construit, instrumenté, caractérisé et couplé à une cellule de test expérimental. En parallèle, un modèle numérique a été développé en utilisant l'approche de capacité thermique apparente et la méthode des différences finies. Le modèle a été calé et validé à l'aide des données expérimentales et suite à cela il a été couplé à un modèle de bâtiment. Une étude d'optimisation a été réalisée se focalisant sur la géométrie de l'échangeur et les propriétés du MCP pour obtenir des périodes de charge / décharge plus rapides avec un effet minimal sur l'énergie stockée. Enfin, la version optimisée de l'échangeur a été utilisé pour l'élaboration de stratégies de contrôle.

Chapitre 1 : Contexte énergétique et bâtiment

Pendant près d'un demi-siècle les questions liées à l'énergie ont acquis un intérêt croissant au sein des sociétés du monde entier en raison de leur importance économique et environnementale. Cette la prise de conscience mondiale est reflétée sur un nombre important d'accords signés entre plusieurs pays à travers le monde, visant à réduire la consommation d'énergie et de gaz à effet de serre (GES). La pierre angulaire de ces efforts a été le Protocole de Kyoto (Nations Unies, 1998). En ce qui concerne l'Union Européenne, le «paquet climat et énergie» (Commission européenne, 2008) a été adoptée en Décembre 2008, mettant l'accent sur les réductions d'émissions, augmentation de la production d'énergie renouvelable et l'efficacité énergétique.

En France, la nouvelle Loi sur la réglementation thermique (RT 2020, actuellement en discussion) va introduire le concept de bâtiments à énergie positive (BEPOS). Elle visera à diviser la consommation d'énergie par quatre et obliger tous les nouveaux bâtiments à atteindre les normes BEPOS.

Milieu bâti: un gros consommateur d'énergie

Un des facteurs les plus influençant quand il s'agit du domaine de l'énergie est le Bâtiment: selon l'Agence Internationale de l'Energie les bâtiments représentent environ 40% de la consommation d'énergie primaire parmi ses 29 pays membres. En outre, il est estimé (UNEP SBCI, 2009) que les

bâtiments contribuent de 33% aux émissions mondiales de GES, principalement en raison de l'utilisation de combustibles fossiles au cours de la phase opérationnelle. Ces chiffres montrent clairement l'impact environnemental significatif des bâtiments et le rôle clé qu'ils peuvent jouer dans la réduction de la consommation d'énergie et les émissions de GES.

La France n'est pas une exception par rapport à la situation européenne et internationale car ce secteur représente une part importante de la consommation d'énergie et des émissions de GES (ADEME, 2013, a, b). Plus précisément, le secteur du logement et du tertiaire sont responsable du 44% de la consommation finale d'énergie, 20% des émissions de GES et 22% des émissions de CO2. L'électricité est la principale source d'énergie des bâtiments français représentant 37% de la consommation finale, suivis par le gaz (32%), l'huile (16%), le renouvelable / déchets (15%) et le charbon (0,4%).

En 2012, le secteur résidentiel compte 33,4 millions de maisons, d'où 27,8 millions sont des résidences principales. L'électricité et le gaz sont les deux principales sources d'énergie du secteur résidentiel. Près des 2/3 de la consommation d'énergie est utilisée pour les besoins de chauffage, suivie par l'usage spécifique (PC, de séchage, de la télévision et d'autres appareils) (19,5%), l'eau chaude (12,1 %) et la cuisson (7%).

Le pourcentage d'utilisation du chauffage électrique dans le logement neuf atteint près de 75% des cas en 2008. La dernière. En outre, selon certaines estimations Négawatt (2009), le chauffage électrique atteint une consommation annuelle de 60 TWh, un nombre qui représente 27% de la consommation totale d'électricité du secteur résidentiel et de 12,3% de la consommation annuelle totale d'électricité en France.

Pour les 15 dernières années, la consommation électrique en France a présenté des pics de consommation électrique croissants. Pour la première fois, le seuil symbolique de 100.000 MW a été dépassé au cours de la vague de froid de Février 2012. En outre, selon RTE (RTE, 2012, a), l'augmentation de ces pics est plus rapide et plus dynamique que l'augmentation annuelle de la consommation électrique. Les valeurs maximales sont principalement observées pendant les heures de fin d'après-midi de la période d'hiver (19:00). Ces pics constituent le résultat de la fin des activités tertiaires, des besoins accrus de transport public et du démarrage des activités domestiques du soir. Un des facteurs les plus influents de ce phénomène est le chauffage électrique. Par ailleurs, RTE souligne la forte dépendance de la consommation électrique sur les valeurs de la température extérieure, en particulier pendant l'hiver.

Le terme thermo-sensibilité est appliqué pour décrire ce phénomène, avec une hausse de 2300 MW de la consommation par augmentation d'un degré Celsius de la température pendant l'hiver 2012. Cette valeur présente une croissance de 35% par rapport à celle de 2001/2002. Ce phénomène est beaucoup plus visible en France que dans les autres pays européens, car il représente près de la moitié de la thermo-sensibilité totale observée en Europe.

L'ampleur de la demande de puissance en heures de pointe a des conséquences économiques, environnementales et sociales importantes. Le système de gestion de l'énergie française est confronté à des difficultés croissantes pour répondre à de tels événements, car il repose en grande partie sur les centrales nucléaires, présentant des taux de production essentiellement constants de 63,130 MW, couvrant 77% de la consommation totale d'énergie (RTE, 2014). En conséquence, la France a à faire

appel à d'autres moyens de production d'énergie et / ou à s'adresser à des pays voisins pour importer. Dans les deux cas l'utilisation de combustibles fossiles est généralement impliquée, conduisant à une augmentation des émissions de CO2.

De plus, la période de pic de consommation électrique représente un pourcentage relativement faible de la consommation annuelle totale. Néanmoins, des investissements surdimensionnés importants doivent être réalisés sont pratiquement pas utilisés pour la plus grande partie de l'année. Ces coûts sont également susceptibles d'être répercutés sur les consommateurs, et plus particulièrement à la partie fixe de la facture électrique qui correspond au développement des infrastructures. Ce résultat pénalise surtout les petits consommateurs individuels, c'est-à-dire les ménages précaires. Les factures croissantes peuvent contribuer à la précarité énergétique des ménages à faible revenu qui ne peuvent pas se permettre un logement bien isolé ou d'un budget énergétique plus élevé.

Chapitre 2 Stockage d'énergie, MCP et application intégrées dans le système de ventilation

Comme indiqué précédemment, le bâtiment est l'un des principaux contributeurs en ce qui concerne la consommation d'énergie et les émissions de GES. En même temps, la population mondiale augmente et devrait se élever à 9,6 milliards d'ici 2050 (ONU, 2013). Un pourcentage croissant de la population vivra dans les villes, ce qui indique que les paysages urbains de haute densité seront également augmentés dans l'avenir. Une des conséquences de ce fait sera l'intensification de l'effet et de l'Îlot de chaleur et de pollution urbaine qui peut influencer négativement les taux de mortalité et les maladies liées à la chaleur (Haja et al., 2002). En effet, la vague de chaleur de l'été 2003 a été directement liée à 70,000 décès dans les pays européens (15.000 décès en France uniquement) (Robine et al., 2008).

Compte tenu de ces faits, la nécessité pour une gestion énergétique du bâtiment plus efficace semble essentielle, le remplacement des sources d'énergie conventionnelles par des ressources renouvelables étant une perspective très prometteuse. Néanmoins, l'intégration des ressources renouvelables dans le bâtiment présente quelques inconvénients, la difficulté principale étant la variabilité et l'intermittence de leur disponibilité (notamment concernant l'énergie éolienne et solaire).

En outre, comme présentés dans la partie précédente, les variations journalières et saisonnières de la consommation énergétique conduisent à des pics de consommations inquiétants et ont tendance à devenir un problème important pour les compagnies d'énergie, la France étant l'un des pays les plus touchés en Europe.

Dans ces conditions, le stockage d'énergie (energy storage - ES) peut jouer un rôle clé dans les bâtiments à efficacité énergétique en fournissant de nombreuses solutions concernant l'intermittentes des ressources renouvelables, tout en conservant un environnement intérieur confortable. En outre, il peut contribuer à la sécurité de l'approvisionnement en énergie, à l'élaboration des stratégies de contrôle avancées (associé à des smart grids) et l'augmentation de l'inertie. Le stockage thermique peut être effectué par divers procédés : thermiques, mécaniques, électromagnétiques, chimiques et biologiques.

Certains d'entre eux offrent un stockage d'énergie seulement à court terme et d'autres peuvent fournir un stockage à long terme.

Stockage thermique

Le stockage d'énergie thermique permet l'utilisation d'une certaine quantité de chaleur à une période ultérieure avec un décalage horaire, quotidienne ou même saisonnier. Ce stockage peut être atteint grâce à trois méthodes principales: le stockage de chaleur sensible, stockage de chaleur latente et stockage de chaleur chimique.

Le stockage de chaleur sensible se produit dans un milieu où le changement de température reste dans une plage fixe et sans changement de phase. Au contraire le stockage de chaleur sous fore latente se produit lorsque le support de stockage subit un changement de phase, de l'état solide à l'état liquide (généralement), ou de liquide à gaz ou de solide à gaz, et vice versa. La chaleur stockée est utilisé pour le changement de phase, ce qui permet d'obtenir une capacité de stockage beaucoup plus élevé et une plage de température de fonctionnement plus étroite par rapport aux systèmes de chaleur sensible.

Enfin, le stockage de chaleur chimique est basé sur l'énergie libérée et absorbée au cours de la rupture et la formation de liaisons moléculaires pour des réactions chimiques complètement réversibles.

Matériaux à changement de phase

Les matériaux à changement de phase (MCP) constituent l'un des principaux éléments des systèmes de stockage de chaleur latente. Le processus de changement de phase et le stockage de l'énergie latente subséquente leur permet de stocker des quantités importantes de chaleur dans un petit volume et dans une plage de température spécifique. Dans la plupart des applications à base de MCP du bâtiment, le changement de phase solide-liquide est préféré en raison de la faible variation de volume par rapport aux transformations gaz-liquide ou gaz-solide.

Plusieurs critères existent pour la classification des MCP en fonction de leur composition chimique, leur température de fusion, leur chaleur latente de fusion, etc. La catégorisation la plus fréquente les divise en trois groupes: organiques, inorganiques et eutectiques. Un grand nombre de matériaux ont été utilisées comme MCP et étudié dans des applications de stockage thermique, y compris les sels hydratés, les paraffine, les acides gras et les eutectiques de composés organiques et non-organiques.

Le confinement des MCP est un sujet très important dans dispositif de stockage thermique car elle est liée au processus de transfert de chaleur et la rigidité générale de la structure de l'application. Comme les MCP présentent une faible conductivité thermique, un confinement adéquat peut aider surmonter cet inconvénient, par exemple en fournissant une surface d'échange élevée par rapport au volume ou en ayant une faible épaisseur de stockage. Comme indiqué précédemment, des solutions de confinement mal-adaptés peuvent conduire à la corrosion et / ou des fuites du MCP, en rendant l'équipement non opérationnel. Plusieurs techniques sont proposées pour le confinement adéquat des MCP, y compris la macroencapsulation, la microencapsulation, l'incorporation directe et l'immersion.

Applications de MCP dans le bâtiment

Plusieurs applications utilisant des MCP ont déjà été étudiées dans le domaine du bâtiment ; elles peuvent être divisées en deux grandes catégories, les applications passives et les applications passives.

Les systèmes passifs

Dans les systèmes passifs le MCP est incorporé dans des composants spécifiques du bâtiment, visant à plusieurs objectifs: augmenter l'inertie thermique, minimiser l'utilisation des dispositifs mécaniques de chauffage / refroidissement, abaisser la fluctuation de la température intérieure et préserver le confort de l'occupant. Des exemples de telles applications sont les suivants : MCP en plaques de plâtre et panneaux muraux, MCP en béton, MCP en briques, MCP en plancher et plafond panneaux et MCP en vitre et voltes d'ombrages.

Les systèmes actifs

Les applications actives de MCP constituent une technologie améliorée pour l'utilisation du stockage thermique dans les bâtiments. Contrairement aux applications passives, le stockage thermique peut être activé par un système mécanique supplémentaire (ventilateurs, pompes, etc), en améliorant de cette façon les performances de transfert de chaleur et permettant le stockage ou le déstockage de chaleur / froid sur demande. Ces applications peuvent être utilisées pour des intervalles de temps spécifiques et sont capable de corréler les besoins avec les fournitures d'énergie.

Des exemples de telle technologie peuvent être trouvés dans les systèmes de ventilation ou des plafonds/planchers radiants.

MCP intégré dans des systèmes de ventilation

Dans ces types de systèmes, la chaleur est stockée dans un dispositif spécifique (échangeur de chaleur), thermiquement isolé du reste du bâtiment et utilisé uniquement sur demande et non pas automatiquement.

Les systèmes de stockage de chaleur latente sont généralement composées de quatre éléments de base:
• L'échangeur de chaleur qui contient le MCP macroencapsulé ou microencapsulé; c'est la composante principale du système et le lieu où la chaleur est stockée sous forme latente (et sensible).
• un circuit qui permet l'écoulement du fluide de transfert de chaleur (principalement l'air, parfois l'eau).
• une source de chaleur électrique ou solaire qui est utilisé pour chauffer ce fluide.
• un ventilateur ou une pompe qui régule le débit du fluide circulant dans le système.
En plus de ces éléments, différents capteurs sont généralement installés dans différentes parties du système afin de surveiller la température de l'air à l'entrée / sortie, la température du MCP, le flux d'air, etc.

Les avantages de cette technologie peuvent être résumés comme suit:

- ✓ stockage de grandes quantités d'énergie par unité de masse qui permet une variation de température plus faible (amélioration du confort thermique)

- ✓ L'utilisation de l'énergie produite à partir du solaire et de la chaleur des déchets qui vient de procédés exothermiques
- ✓ L'utilisation de l'énergie à prix faible pendant les périodes hors pointe pour le stockage et la restitution de cette énergie à des moments où les pleins tarifs sont appliqués.
- ✓ L'utilisation des systèmes de ventilation à taille réduite et le fonctionnement plus efficace

En conclusion, dans cette partie on a voulu présenter les solutions proposées par le stockage d'énergie en focalisant sur le stockage thermique sous forme latente. La prochaine partie est consacrée à la description du développement d'un tel outil : un échangeur de chaleur MCP-Air.

Chapitre 3 Elaboration d'un échangeur thermique

En association avec le projet Stock Air un besoin spécifique a été identifié: le développement d'un dispositif expérimental qui permet de stocker une quantité de chaleur suffisante pour remplacer la consommation de chauffage électrique en heure de pointe.

Plus précisément, l'application a été conçue pour un logement de faible énergie, de manière qu'il puisse être facilement intégré dans un système de ventilation et être en mesure de fournir une puissance de 2 kW sur une période de deux heures, ce qui correspond à la fin d'après-midi (18: 00-20: 00) ou le pic de demande de puissance est observé.

Ces objectifs ont conduit à certains facteurs de conception, parfois contradictoires entre eux :

- Petit volume (pour l'intégration dans le système de ventilation)
- stockage d'énergie suffisant pour satisfaire la nécessité 4kWh
- plage de température de fonctionnement spécifique
- transfert de chaleur élevé pour un processus de stockage / déstockage rapide
- structure rigide pour un confinement de MCP durable

Les considérations ci-dessus ont conduit à la nécessité du développement d'un échangeur de chaleur MCP-Air. Une analyse a été effectuée par le laboratoire EDF Matériaux et Mécanique des Composants (partenaire du projet Stock Air), comparant les propriétés de différents matériaux qui pourraient convenir à l'unité proposée. La paraffine Microtek 37D a été choisie en raison de ses propriétés avantageuses (tableau 1). En particulier, il présente une plage de température de fusion / solidification d'environ 37 ° C, une dilatation de 10% entre les phases et une chaleur latente de fusion de 230 kJ / kg.

Etat	Densité ($kg.m^{-3}$)	Conductivité thermique ($W.m^{-1}K^{-1}$)	Capacité spécifique ($kJ.kg^{-1}K^{-1}$)	Chaleur latente ($kJ.kg^{-1}$)	Plage de température de fusion (°C)
Solide	870	0.24	2.36	230	33 - 39,6

Liquide	779	0.18	2.45	226.8	35,5 - 30,3

Tableau 1 : Propriétés de la paraffine Microtek 37D

L'échangeur a été conçu de manière à pouvoir être intégré dans un système ventilation (plenum, faux plafond. A cet égard, sa taille devait être modeste et a été établi comme suit: 1,05m de longueur, 0,80m de largeur et 0,25m de hauteur.

La paraffine est macro-encapsulé dans 34 règles de maçon en aluminium, (1x0,10x0,018) m de dimension et ayant des ouvertures aux deux extrémités (figure 1). Les règles ont été sélectionnées à cause de la valeur élevée de la conductivité thermique de l'aluminium d'une part et leur prix relativement faible et leurs facilités d'accès, d'autre part. La paraffine a été insérée sous forme liquide et les plaques ont été scellées à l'aide des morceaux en bois et une colle élastique. Les plaques ont été assemblées par deux, puis placés parallèlement l'une à l'autre. Des mesures de poids ont été effectuées avant et après l'encapsulation de la paraffine, de manière à obtenir la masse exacte du MCP. Le résultat a été un total de 31,44 kg de MCP.

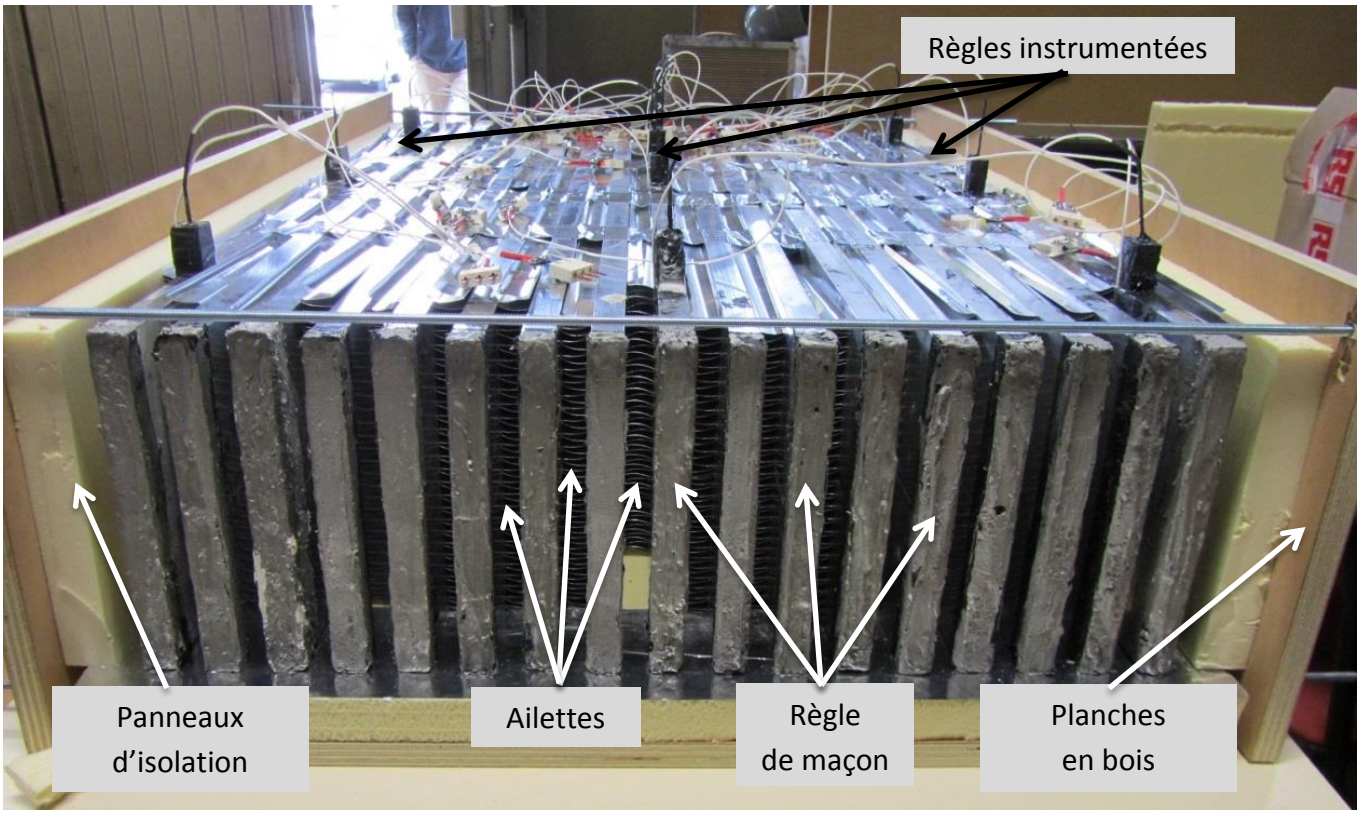

Figure 1 : L'échangeur en phase de construction

Des ailettes en aluminium, 0,019m d'épaisseur, ont été introduites entre les plaques pour augmenter l'échange thermique. Trois des plaques ont été équipées avec des composants supplémentaires qui ont été utilisés pour introduire des capteurs de température à des profondeurs variables à l'intérieur du MCP, en trois parties différentes des plaques: entrée, milieu et sortie. Des capteurs de température ont également été installés sur la surface extérieure de chaque plaque aux mêmes points. Des panneaux de

polystyrène encerclent les règles afin de les isoler thermiquement du milieu environnant. Enfin, des planches de bois ont été utilisées pour assembler le tout en assurant la stabilité de la structure.

L'utilisation de l'échangeur de chaleur a nécessité la construction d'une plate-forme composé de deux ventilateurs centrifuges, deux résistances chauffantes (1KW chacun), un diffuseur d'air et un collecteur d'air, plusieurs tuyaux de ventilation et raccords pour interconnecter les éléments précédents. La plate-forme expérimental développé assure la circulation et le chauffage de l'air à travers l'échangeur dans des conditions souhaités (température et débit d'air) et est utilisé pour coupler l'échangeur avec une pièce ou un bâtiment.

Un système de contrôle commande a été aussi nécessaire. Ce système est composé d'une chaîne de composants qui sont utilisés pour l'observation des propriétés thermiques, l'acquisition de données et le contrôle de la température et le débit d'air. Plusieurs capteurs ont été installés dans différentes parties de la plate-forme et l'échangeur de chaleur, ce qui permet de surveiller l'état de l'air et du MCP. Plus précisément, des capteurs de température et d'humidité relative ont été installés avant et après l'échangeur afin de mesurer les propriétés de l'air à l'entrée et la sortie. Le logiciel LabVIEW a été utilisé pour l'acquisition des données et le contrôle des dispositifs de la plate-forme expérimentale. L'interface développée permet une surveillance directe des propriétés de l'air et du MCP, l'automatisation des tests de caractérisation et l'élaboration de stratégies de contrôle.

Couplage avec une cellule expérimentale

La plate-forme expérimentale a été couplé avec une cellule d'essai expérimental appelé Hybcell, situé dans le campus d'ENTPE à Lyon, France (El Mankibi, 2003). Hybcell fait 5,1 m de long, 3,5 m de large, 2,9 m de haut et représente un bureau ou une petite salle de réunion. L'échangeur de chaleur est placé à l'extérieur de la cellule Hybcell et a été couplé à son système de ventilation mécanique. Le logiciel développé pour contrôle de l'échangeur a été fusionné avec le logiciel existant de l'Hybcell pour un fonctionnement simultané du système. Le couplage a été réalisé afin d'évaluer la performance de l'échangeur de chaleur dans des conditions réelles et d'élaborer des stratégies de contrôle.

Étude de caractérisation

Plusieurs tests de vérification et de caractérisation ont été réalisées pour différents débits d'air, visant à:

- Confirmer le bon fonctionnement des différents composants de la plate-forme expérimentale
- Confirmer le bon fonctionnement de l'interface d'acquisition-contrôle-commande
- Obtenir un profil du fonctionnement de l'échangeur pour différents débits d'air
- Vérifier l'uniformité du flux d'air entre les plaques
- Vérifier la répétabilité des phases de charge / décharge
- Acquérir des données expérimentales fiables pour la validation du modèle numérique

Fuite de MCP

Malgré les efforts de confinement étanche du MCP, des fuites ont été observées sur les bouchons en bois. La fuite a probablement été provoquée par la pression qui a été créé au cours du changement de phase et la dilatation du MCP. La quantité de MCP fuit n'était pas important, mais le problème devait

être résolu car ça pourrait conduire à une nouvelle détérioration de l'échangeur et le manque de connaissance de la quantité de MCP réel dans les plaques.

Compte tenu de ces faits, l'élaboration de nouvelles plaques a été décidée. Les nouvelles plaques ont été fabriquées par une usine métallurgique à l'aide du procédé d'extrusion. Le matériau utilisé était une fois de plus l'aluminium. Les plaques ont deux ouvertures pour le remplissage du MCP et l'évacuation de la pression provoquée par la dilatation entre les phases solide et liquide. Leurs dimensions étaient les mêmes que les règles de maçon: (1x0,10x0,018) m.

Résultats des tests de caractérisation

Comme indiqué précédemment, l'étude de caractérisation a été réalisée afin d'obtenir un profil complet du fonctionnement de l'échangeur et d'obtenir les données expérimentales nécessaires qui permettront de valider le modèle numérique.

Un protocole a été établi et peut être décrit comme suit:

• Test de deux configurations différentes: avec et sans ailettes

• Réalisation d'un cycle thermique complet avec une température d'entrée d'air de 44°C pendant le stockage et 26°C pendant la phase de déstockage

• Variation de valeurs du débit d'air de 100 à 500 m3 / h

• augmentation du débit d'air sur un pas de 100 m3 / h

Les résultats obtenus pour les tests avec ailettes sont présentés aux figures suivantes.

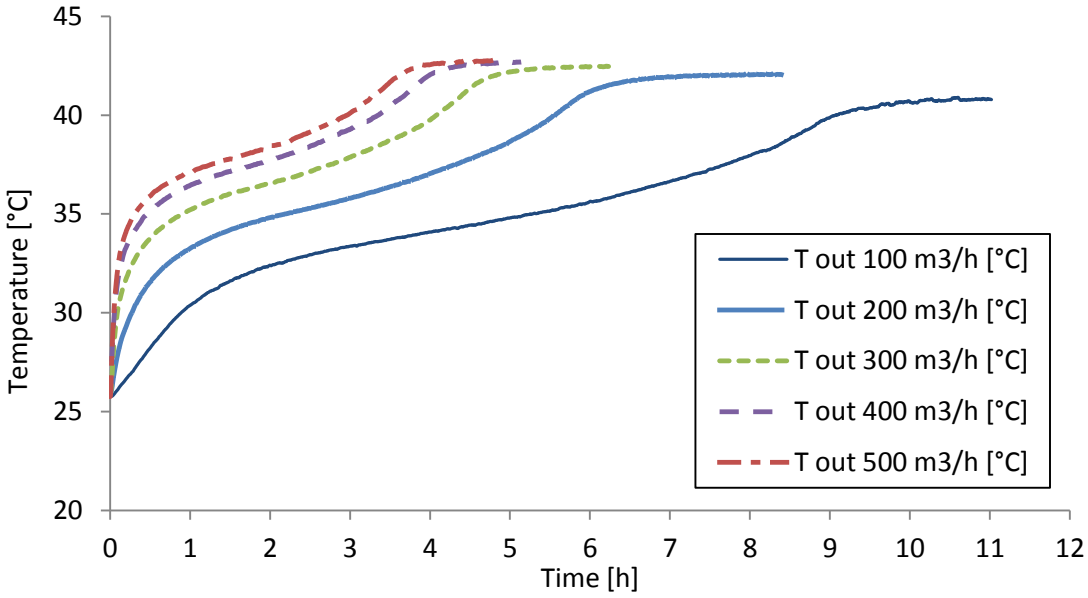

Figure 2: Résultats de la caractérisation de l'échangeur: température de l'air à la sortie, charge

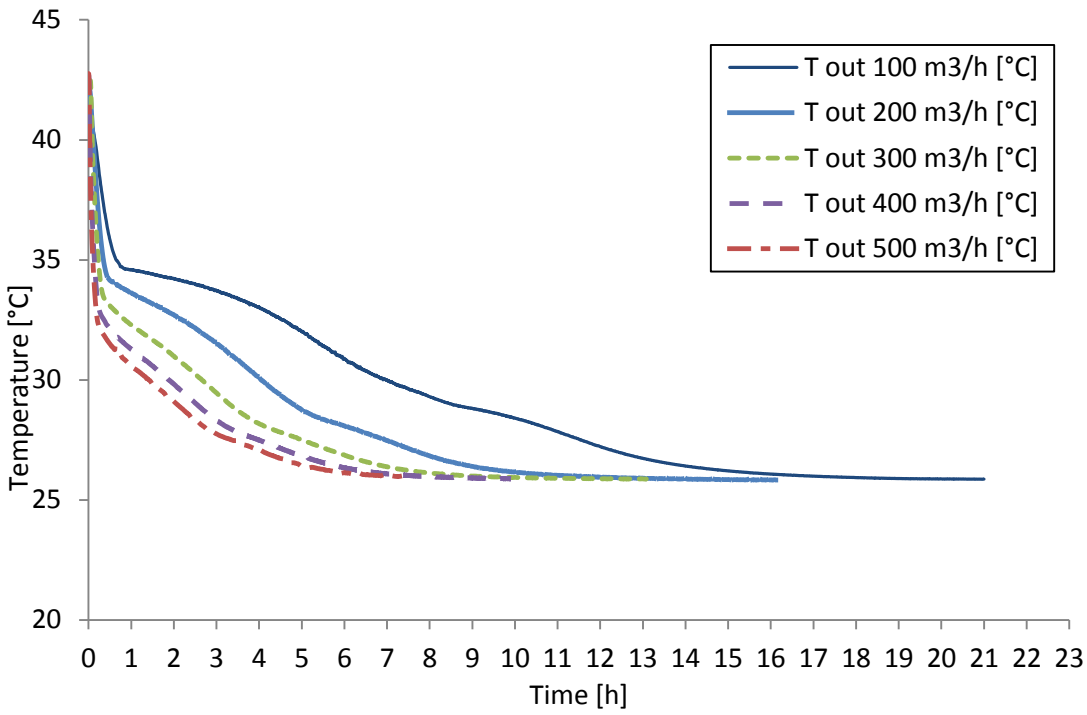

Figure 3: Résultats de la caractérisation de l'échangeur: température de l'air à la sortie, décharge

Discussion des résultats de caractérisation

Les figures 2 et 3 présentent l'évolution de la température d'air à la sortie de l'échangeur pendant la charge et la décharge du dispositif pour cinq débits différents. Bien que le transfert de chaleur soit accéléré par la présence d'ailettes, une période de temps importante est toujours nécessaire pour charger ou décharger complètement l'échangeur. Pour le débit le plus faible l'intervalle nécessaire a été 11 heures pour le stockage et 18 heures pour le déstockage. Cela peut être inquiétant surtout pour le processus de déstockage, car la barrière de deux heures (au cours de laquelle la demande de puissance de pointe se produit) est largement dépassée. D'autre part un débit d'air élevé peut détériorer le confort des occupants. Les taux élevés de flux d'air peuvent aussi provoquer une surchauffe de la résidence au cours de la phase de stockage.

Les résultats de caractérisation nous ont donné un aperçu du comportement du dispositif pour deux configurations différentes et des débits d'air variant. En outre, des données expérimentales fiables ont été obtenues pour le processus de calibrage et la validation du modèle numérique.

Chapitre 4 Elaboration d'un modèle numérique

Les modèles numériques sont des outils puissants qui peuvent aider à surmonter les limites des études expérimentales (temps et argent). Dans cette optique, le développement d'un modèle qui simule le comportement de l'échangeur était nécessaire. Le modèle devrait être à la fois rapide et précis dans la reproduction des résultats expérimentaux et faciliter le couplage avec un modèle existant de bâtiment pour le développement des stratégies d'optimisation et de contrôle.

Ainsi, un modèle numérique bidimensionnel a été créé dans un environnement Matlab / Simulink, en utilisant la méthode du bilan de chaleur et la méthode de la capacité thermique apparente. Pour la représentation numérique de l'échangeur, trois principaux médiums ont été choisi: l'air, le conteneur (aluminium) et le MCP. La moitié de l'épaisseur de la couche d'air expérimental et de l'épaisseur de la couche de MCP sont prises en compte dans l'étude numérique, étant donné que, par symétrie, les résultats peuvent être étendus à l'autre moitié (où s'appliquent des conditions similaires).

Chaque couche a ensuite été discrétisé en n régions égales (nœuds) de longueur dx = L / n, où L est la longueur totale de l'échangeur (figure 4).

De plus, la couche de MCP a été discrétisé transversalement en m nœuds, afin d'offrir la possibilité d'un traitement plus approfondi du milieu où le changement de phase se produit. Les résistances thermiques sont formulées entre les nœuds, avec différents coefficients utilisés pour les nœuds d'entrée et de sortie. La température de l'air à l'entrée de l'échangeur et le débit d'air sont introduits pour chaque pas de temps.

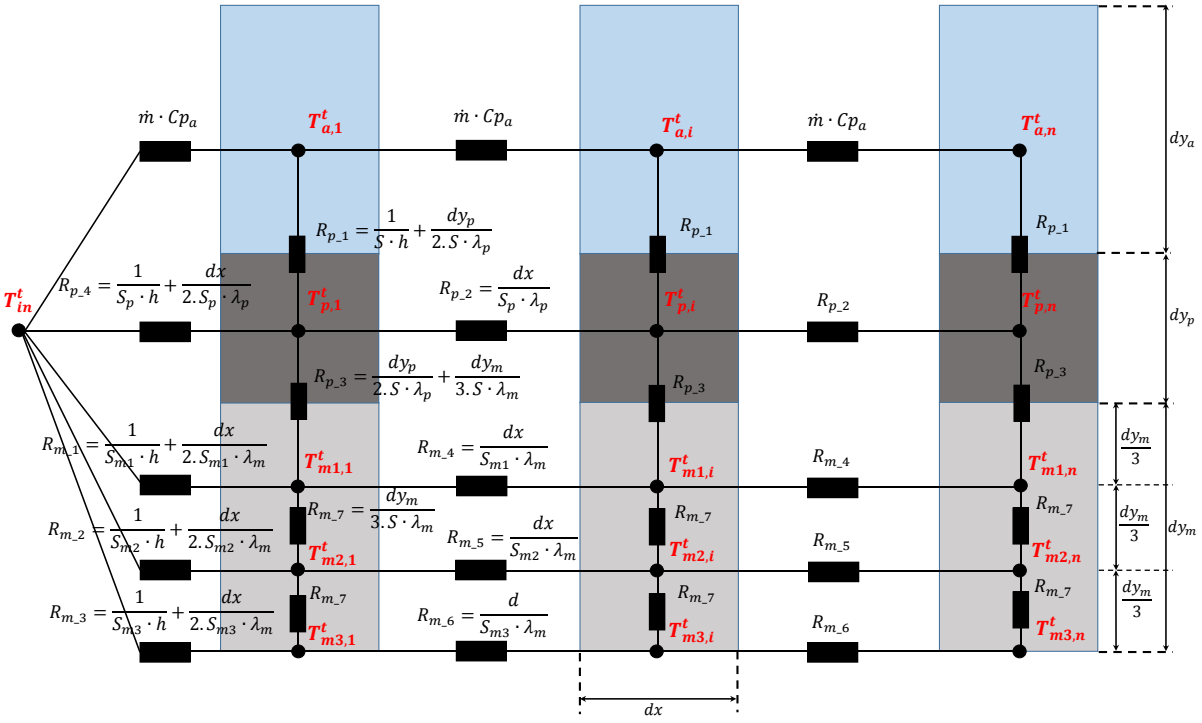

Figure 4 : Discrétisation nodale des couches considérées

La température moyenne $\overline{T} = \frac{T^t + T^{t-dt}}{2}$ est introduite et le bilan thermique est formulé pour chaque couche de la façon suivante:

Couche d'air:

$$T^{t-dt}_{a,i} = \left(1 + \frac{\dot{m}.dt}{2.\rho_a.V_a} + \frac{h.S.dt}{2.\rho_a.Cp_a.V_a}\right).\overline{T_{a,\iota}} - \frac{\dot{m}.dt}{2.\rho_a.V_a}.\overline{T_{a,\iota-1}} - \frac{h.S.dt}{2.\rho_a.Cp_a.V_a}.\overline{T_{p,\iota}}$$

Couche d'aluminium:

$$T_{p,i}^{t-dt} = \left[1 + \left(\frac{dt}{2.\rho_p.Cp_p.V_p}\right).\left(\frac{1}{R_{p_1}} + \frac{2}{R_{p_2}} + \frac{1}{R_{p_3}}\right)\right].\overline{T_{p,\iota}} - \frac{dt}{2.\rho_p.Cp_p.V_p.R_{p_2}}.\left(\overline{T_{p,\iota-1}} + \overline{T_{p,\iota+1}}\right) - \frac{dt}{2.\rho_p.Cp_p.V_p.R_{p_1}}.\overline{T_{a,\iota}} - \frac{dt}{2.\rho_p.Cp_p.V_p.R_{p_3}}.\overline{T_{m1,\iota}}$$

Couche de MCP:

$$T_{mj,i}^{t-dt} = \left[1 + \left(\frac{dt}{2.\rho_m.Cp_m.V_{m1}}\right).\left(\frac{1}{R_{p\_3}} + \frac{2}{R_{m\_4}} + \frac{1}{R_{m\_7}}\right)\right].\overline{T_{mJ,\iota}} - \frac{dt}{2.\rho_m.Cp_m.V_{m1}.R_{m\_4}}.\left(\overline{T_{m1,\iota-1}} + \overline{T_{mJ,\iota+1}}\right) - \frac{dt}{2.\rho_m.Cp_m.V_{m1}.R_{p\_3}}.\overline{T_{p,\iota}} - \frac{dt}{2.\rho_m.Cp_m.V_{m1}.R_{m\_7}}.\overline{T_{m(J+1),\iota}}$$

La température de l'air, de l'aluminium et du MCP sont calculées à chaque pas de temps, en utilisant la température à l'entrée et les températures calculées au pas de temps précédents. Le système d'équations résultantes est ensuite écrit sous une forme de matrice, ce qui conduit à l'équation finale:

$$\bar{T} = A^{-1}.\left(T^{t-dt} - B\right)$$

Ou $\bar{T}$ est une matrice contenant les valeurs moyennes de la température pour les couches d'air, d'aluminium et de MCP, A est la matrice contenant les coefficients de résistance thermique, T^{t-dt}) est une matrice les valeurs de température pour les trois couches au pas de temps précédent et B est un matrice contenant des valeurs de température initiale pour les trois couches. Enfin, les valeurs de température pour les trois couches sont calculées par l'équation suivante:

$$T^t = 2.\bar{T} - T^{t-dt}$$

Calibrage du modèle et importance de la capacité spécifique du MCP

Les résultats numériques initiaux ont été promettant, mais pas assez satisfaisant, quand comparé aux résultats expérimentaux. Après le calibrage de divers facteurs, l'importance des valeurs de la capacité thermique spécifique (Cp) du MCP a été observée. Dans un premier temps, le modèle utilisait les valeurs obtenues par le laboratoire d'EDF en utilisant la méthode DSC. Certaines études (Albright et al., Annexe 17 de l'AIE) concluent que le processus de DSC peut fournir des données et que les données fournis de cette méthode dépendent de la vitesse de chauffage/refroidissement du matériaux investigué.

Cela nous a conduits à la création de courbes de chaleur spécifique adéquates. L'idée initiale était de créer un triangle pointant vers la valeur de température de changement de phase. Compte tenu des deux pics observés sur les données de la DSC, un second pic a également été introduit dans la courbe pour la phase de refroidissement. En outre, il a été décidé de formulé trois courbes différentes selon la section de MCP considéré (entrée, intermédiaire et de sortie).

La figure 5 présente les résultats expérimentaux et numériques pour l'évolution de la température du MCP au milieu de l'échangeur pour trois débits différents. La non-linéarité de l'évolution de la température pendant les changements de phase est reproduite, y compris les deux pics qui se manifestent pendant la phase de solidification (reliée aux propriétés intrinsèques de la paraffine). Dans l'ensemble, le modèle développé parvient à simuler avec précision le comportement de tel qu'observé à travers la plate-forme expérimentale et est considéré comme validé.

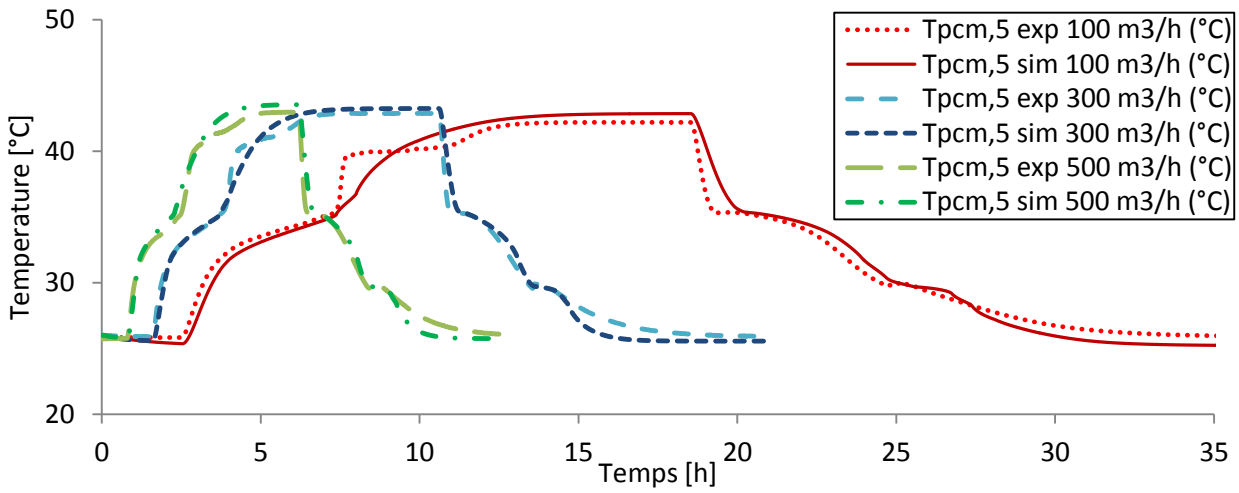

Figure 5: Résultats numériques et expérimentaux pour la température du MCP au nœud 5, débit de 100, 300 and 500 m3/h

Chapitre 5: Optimisation de l'échangeur et élaboration des stratégies de contrôle

Afin d'évaluer la performance de l'échangeur et le tester dans différents scénarios d'opération, un bâtiment a été conçu numériquement, en utilisant le modèle Hybcell 1.2. Il s'agit d'un modèle développé au laboratoire LGCB / ENTPE, sous l'environnement Matlab / Simulink en couplant un modèle thermique et un modèle d'écoulement de l'air sous pression.

Le bâtiment conçu est un local monozone de 80m^2 ayant une forme rectangulaire (10 m de long, 8 m de large et 3m de haut). Les murs sud, est et ouest ont deux fenêtres de 2.5mx1.5. Les propriétés des murs et des fenêtres ont été définies de manière à correspondre à une maison à faible énergie. Les données météorologiques ont été acquises en utilisant la station IDMP située au campus de l'ENTPE (Dumortier) et correspondent aux conditions climatiques Vaulx-en-Velin pour l'année 2013.

Des tests numériques ont été effectués pour le mois de janvier 2013, en utilisant l'échangeur à sa forme initiale. Plusieurs configurations ont été testées (température à l'entrée de l'échangeur et période de décharge) sans pour autant pouvoir satisfaire les critères d'effacement énergétique et de confort thermique.

Première approche d'optimisation

Le couplage numérique entre échangeur et bâtiment ont confirmé les observations expérimentales concernant un stockage d'énergie limitée et un temps de charge se produise. La première approche d'optimisation de l'échangeur consistait en l'utilisation du modèle développé pour modifier certains paramètres du dispositif. Plus précisément, les paramètres étudiés concernent les dimensions de l'unité, telles que la hauteur des trois couches considérées, PCM, l'air et de l'aluminium (dz), l'épaisseur de la couche de PCM (dym) et l'épaisseur de la couche d'air (dya).

Trois paramètres ont été introduits dans le modèle numérique en tant que facteurs de multiplication des paramètres en question. La hauteur a été multipliée par 1, 1,5 et 2, l'épaisseur de la couche de PCM a été multipliée par 1, 2, 3 et 4 et l'épaisseur de la couche d'air a été multipliée par 1, 2, 3 et 4.

Un total de 48 configurations a été produit et testé pour une période de 4 jours, choisie pour des raisons de rapidité. Trois critères ont été établis: déplacement de la charge de pointe, consommation mensuelle minimum et maintien du confort thermique. Une diminution de 0,5 ° C de la température intérieure du bâtiment a été tolérée.

Conception et essaie de trois scénarios

Suite à l'investigation des résultats obtenus, trois configurations ont été sélectionnées car elles remplissaient les critères établis. La première utilise plus de MCP, ayant ainsi un plus grand volume, mais consomme moins d'énergie. La seconde et troisième ont moins de MCP, mais consomment plus d'énergie. Toutes les trois, offrent différents points d'intérêt et ont été choisies pour tester le système de 'échangeur de chaleur + bâtiment' à travers différents scénarios.

Effacement énergétique simple

Le premier scénario avait comme but de vérifier la bonne opération de l'échangeur (déplacement de charge et maintien du confort thermique) pendant une période de temps plus longue ainsi que de calculer la consommation d'énergie et la facture d'électricité à la fin du mois.

Lors de ce scenario, la charge de l'échangeur s'effectuait entre 22h00-16h00 et la décharge au cours d'une période de six heures (16: 00-22: 00). La température de l'air à l'entrée de l'échangeur a été réglée à 38°C et le débit d'air est régulé par un contrôleur PID. Pour les trois configurations choisies, le système a réussi à maintenir la température de l'air ambiant à 20°C pendant toute la période d'essai.

Charge nocturne de l'échangeur

Une observation plus détaillée des besoins énergétiques de la maison montre que dans certains cas le chauffage n'est pas nécessaire pendant la journée. En effet, selon les conditions climatiques extérieures (principalement gains solaires) la puissance nécessaire diminue ou devient même zéro à partir de 10h00 à 16h00. Cette observation nous a conduit à la création d'un scénario de charge nocturne. Dans ce cas, l'échangeur est chargé pendant la nuit, à partir de 22h00 pour se terminer à 6h00 du matin. Jusqu'au début de la période de décharge du dispositif (16:00) un chauffage conventionnel est utilisé, si nécessaire. Cela permet de profiter des tarifs de nuit moins chères que EDF propose.

Les trois configurations ont été testées et ont réussi à fournir de bons résultats, mais avec une température d'air à l'entrée de l'échangeur augmenté. Même si la consommation d'énergie a été augmentée en utilisant l'échangeur, une diminution du coût final est observée car l'échangeur est chargé pendant la nuit.

Occupation et qualité de l'air intérieur

Enfin, un troisième et dernier scénario a été testé en introduisant la présence d'une famille de quatre personnes au modèle du bâtiment. La simulation d'occupation provoque deux changements importants par rapport aux deux scénarios précédents: le dégagement de chaleur et de CO_2 par chaque occupant. La

concentration de CO2 augmentée étant liée à des problèmes de santé (somnolence, maux de tête, léthargie) et des niveaux de productivité plus faibles (Siskos et al., 2001) une limite de 1000ppm a été établie pour cette valeur, selon les standards de ASHRAE.

Un système de ventilation plus avancé a été conçu pour ce scénario. Plus précisément une ventilation à double flux est considéré chauffer l'air frais entrant. De cette façon, l'air utilisé pour ventiler la maison est plus chaude que l'air extérieur et non polluée en CO_2. En outre, un by-pass a également été considéré, ce qui signifie que l'air entrant peut circuler à travers l'échangeur de chaleur air-PCM ou être injecté directement dans la maison. Cela permet le renouvellement de l'air intérieur sans affecter l'état de charge de l'échangeur. La charge nocturne est maintenue pour ce scénario également.

Le système optimisé proposé a réussi à offrir des conditions acceptables intérieures (confort thermique et QAI) pour les trois configurations, avec une augmentation de la température d'air à l'entrée de l'échangeur. Le débit d'air de l'échangeur est principalement défini par le contrôleur de la QAI mais cela n'a pas interféré avec la charge de l'échangeur de chaleur ou de la température de l'air intérieur. Les besoins de chauffage ont été réduits lorsque les occupants étaient présents dans la maison.

Conclusions de la première approche d'optimisation

La première démarche d'optimisation a été basée sur une étude de modification des dimensions de l'échangeur de chaleur et de la performance de l'unité lorsqu'il est couplé à une maison, concernant le déplacement de la charge, le confort thermique et la QAI.

Nous avons pu démontrer les avantages de l'unité optimisée selon différents scénarios. Cependant, la première approche d'optimisation a présenté certaines limites concernant la quantité de MCP utilisée, le volume du dispositif et la période nécessaire pour la charge longue.

Deuxième approche d'optimisation

Les limites de la première approche d'optimisation ont démontré la nécessité d'une seconde étude d'optimisation de l'échangeur, se concentrant sur le temps nécessaire pour la charge et l'énergie stockée durant cette période. Cette fois-ci, outre la modification des dimensions du dispositif, les propriétés du MCP ont également été modifié.

Les paramètres de dimensions ont été modifiés de manière à ne pas changer la quantité totale de PCM. Par exemple, une diminution de l'épaisseur de la couche de MCP résulte à une augmentation proportionnelle de la hauteur ou la longueur de la même couche (et respectivement de l'échangeur).

En ce qui concerne les propriétés de MCP, les paramètres modifiés étaient la conductivité, la densité et la chaleur spécifique. Enfin, la conductivité du conteneur a également été étudiée. Diffèrent MCP ont été examinés et une plage de valeurs a été proposé pour chaque propriété. Le même processus a été effectué pour le récipient, en investiguant la conductivité des matériaux divers (cuivre, l'acier, etc.). En conséquence, trois nouvelles valeurs pour chaque propriété ont été testées selon la plage établie.

Les tests d'optimisation ont été réalisés sous l'environnement Matlab pour une charge et décharge complète ; un critère d'arrêt a été établi pour la fin de ce processus. Pour chacune des trois configurations de dimensions différentes, la combinaison de toutes les valeurs possibles des propriétés du MCP a conduit à un total de 243 cas testés.

Des tests pour trois débits différents ont été réalisés (100, 300 et 500 m3/h) et les résultats ont été classés en fonction de la durée minimale pour le stockage ou déstockage de chaleur. Enfin, des simulations ont été réalisées pour la dimension initiale de l'échangeur, tout en modifiant les valeurs des propriétés de PCM. Toutes les configurations combinées un total de 4860 simulations a été réalisée.

Une partie des résultats est présentée au tableau 2 ; il s'agit des configurations qui ont été testées pour les scénarios mentionnés précédemment.

Classifi-cation	Conducti-vité MCP	Densité MCP	Capacité spécifique MCP	Conducti-vité du containe ur	Epaisseur (m)	Longueur (m)	Auteur (m)	Temps (h)	Energie (KWh)
1	4	0,9	0,7	0,5	0,006	0,1231	0,2216	3,35	2721,2
28	4	1,4	0,7	0,5	0,006	0,1231	0,2216	4,86	4050,71
38	3	0,9	1,25	0,5	0,006	0,1231	0,2216	5,5	4606,99
64	4	0,9	1,5	0,5	0,006	0,1231	0,2216	6,4	5447

Tableau 2: Classification des résultats obtenus pour le chargement de l'unité selon la durée de chargement plus rapide, taux de 300m3 / h de débit d'air

Une tendance a été détectée pour toutes les conditions de test différents (charge / décharge, débits différents), même si de petites variations existent : les configurations positionnées aux premières places sont celles avec des valeurs de chaleur spécifique et de densité plus petites, de couche de MCP plus mince et des valeurs de conductivité plus grandes.

La comparaison entre la forme initiale et les versions optimisées de l'échangeur montre une charge plus rapide du dispositif pour la même quantité de chaleur stockée. Les versions optimisées présentent une diminution d'une heure du temps nécessaire pour la charge.

Les résultats de la deuxième étude d'optimisation nous ont fourni une grande liste de configurations, chacune présentant des avantages et des inconvénients pour notre cas d'étude. Les scénarios qui ont été testés avec les résultats de la première approche d'optimisation ont été reproduits en utilisant les configurations récemment obtenus.

Effacement simple, deuxième approche d'optimisation

L'un des objectifs de la deuxième approche était de réduire la période d'effacement afin de mieux se conformer au problème du pic de consommation observé en France. Le même scénario s'est donc

reproduit, en modifiant toutefois la période d'effacement à 18: 00-20: 00 et en testant les configurations obtenues avec la deuxième approche.

La première configuration testée est celle qui a présenté la charge la plus rapide (cas 1, tableau 2). Cette configuration a été testée pour diverses valeurs de la température de l'air à l'entrée de l'échangeur. La configuration n'a pas fourni de résultats satisfaisants, car la température de l'air intérieur a diminué pendant la période de déplacement de la charge. Un second test a été réalisé, en utilisant la configuration 28 (tableau 2) vu que c'est la configuration présentant une augmentation significative de la quantité d'énergie stockée. Cette configuration a aussi été testée pour des températures de l'air augmentées, mais aucun d'entre elles n'a réussi à maintenir une température de l'air intérieur stable pendant la période d'effacement.

Après l'insuffisance des deux premiers cas, la configuration 38 a été testée. Elle correspond à la configuration nécessitant le même temps pour une charge complète que la version initiale de l'échangeur. L'énergie stockée augmentée de cette configuration a permis un fonctionnement efficace du système.

Nous avons ensuite voulu tester les performances de cette configuration avec un scénario plus difficile. Comme décrit dans le scénario d'occupation de la première étude d'optimisation, en cas de présence humaine l'air intérieur ne peut plus être réinjecté dans la maison, car il est considéré être pollué. Afin de surmonter cet obstacle un système de récupération de chaleur a été utilisé, fournissant de l'air à une température inférieure à celle à l'intérieur. Cette fois, nous avons testé cette option, mais à une condition plus difficile: la température de l'air à l''entrée de l'échangeur pendant la période d'effacement a été prise comme la valeur de la température de l'air intérieur moins 4 °C. Le test de la 38ème configuration dans de telles conditions a montré qu'une augmentation de la température de l'air au cours de la période de pic était nécessaire afin d'obtenir des conditions de confort thermique stables.

Enfin, une configuration présentant un stockage d'énergie encore plus élevé a été testé (cas 64, tableau 2). Cette configuration a réussi à fournir un fonctionnement efficace du système avec une température, même avec une température d'air à l'entrée de 38°C de l'air pendant le processus de charge et une température intérieure moins 4 °C au cours de la décharge.

Charge nocturne, deuxième approche d'optimisation

Les tests présentés dans le paragraphe précédent nous ont fourni avec deux configurations capables de satisfaire les critères de déplacement de la charge et des conditions intérieures acceptables. Ces deux configurations ont été utilisées pour reproduire le scénario de charge nocturne.

Deux modifications ont été apportées dans le fonctionnement du système: la période d'effacement a été réduite à deux heures (18: 00-20: 00) et un chauffage classique a été utilisé de 20 :00 à 22:00.

Le cas 38 a d'abord été testé avec une température d'air à l'entrée de l'échangeur de 44 °C pendant la charge de l'échangeur. La diminution de la quantité de MCP et la durée de conservation plus longue ont conduit à une décharge involontaire importante de l'appareil. En conséquence, la température de l'air intérieur a diminué pendant la période de décharge. Compte tenu de ce fait, nous avons décidé de

réduire les pertes de chaleur de l'échangeur par un facteur de 30%. Le dernier essai a ensuite été répété pour une version mieux isolé de l'échangeur de chaleur. La température de l'air de l'échangeur de sortie diminue à un rythme plus faible pendant la période de conservation et la température intérieure présente des variations plus petites.

En outre, le cas 64 a été testé pour le même scénario et conditions. Comme pour le cas 34, la performance de l'appareil avec l'isolation initiale n'était pas suffisante pour une température de l'air intérieur stable. La modification de ce paramètre a démontré une meilleure performance.

Occupation et QAI, deuxième approche d'optimisation

Le scénario d'occupation a été reproduit dans le but de tester les performances des configurations 34 et 64. Le système est considéré fonctionner de manière similaire à la première approche d'optimisation, à la différence d'une période de transfert de charge plus courte. Comme pour la première approche d'optimisation, la présence d'occupants nécessite un système de récupération de chaleur et un système by-pass de l'échangeur; elle implique également des gains de chaque personne de chaleur.

La configuration 38 a été testée pour des conditions d'isolation thermique initiales et améliorées. Les deux ont présentées une performance adéquate, même si le premier cas conduit à une légère baisse de la température intérieure à la fin de la période d'effacement. La figure 6 présente la performance du système pour le dernier cas, en zoomant sur les jours 3 à 8, où les besoins énergétiques sont élevés.

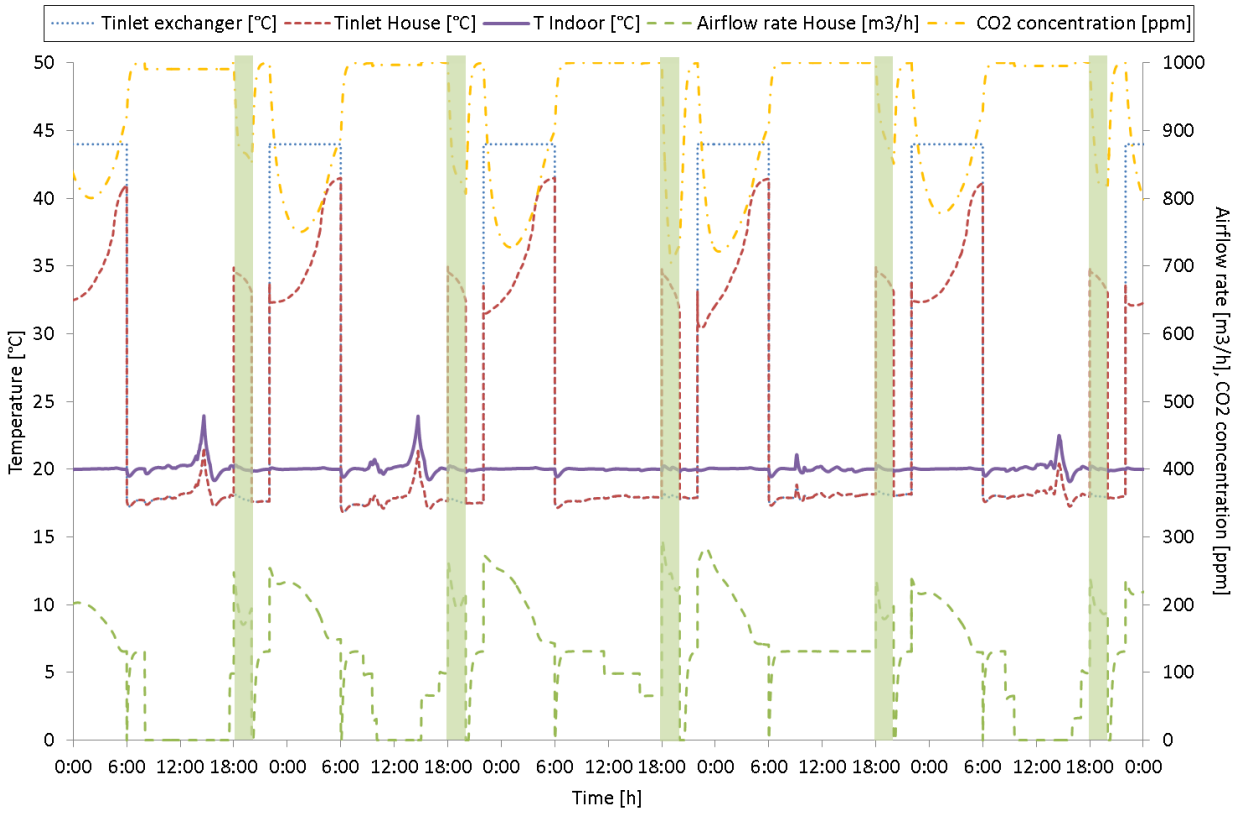

Figure 6 : Performance de l'échangeur, jours3-8, 38 cas, dernier cas

Enfin, la configuration 64 a également été testée pour le scénario d'occupation, pour une température de l'air à l'entrée de 38°C et de 40°C et pour une isolation initiale et améliorée. Mis à part le premier cas (38°C et isolation initiale), les configurations testées ont réussi à maintenir une température stable à l'intérieur pendant la décharge de l'échangeur.

Conclusions et perspectives

Synopsis

La recherche effectuée lors de cette thèse a été principalement motivée par le problème de la pointe électrique observé en France au cours de l'hiver en fin d'après-midi. Comme ces pics sont fortement liés à chauffage électrique, l'objectif de notre travail était d'une part de concevoir et de développer des outils numériques et expérimentaux fiables, basés sur la technologie de stockage thermique et d'autre part d'utiliser ces outils afin de développer des stratégies de contrôle efficaces, basées sur des solutions de déplacement de la charge.

La partie expérimentale de l'étude a consisté à la conception et la construction d'un échangeur de chaleur MCP-Air comme le principal élément de la plate-forme expérimentale et l'endroit où le stockage thermique a lieu sous forme latente. Le système de stockage de chaleur est composé d'un ensemble de plaques MCP (paraffine), calées dans l'échangeur et intégrées dans un système de ventilation. L'inconvénient initialement observé de la fuite MCP a été surmonté par la construction d'un deuxième échangeur possédant une structure plus rigoureuse. Les résultats de la caractérisation ont démontré l'applicabilité du système proposé mais ont aussi révélés des limites, surtout en ce qui concerne le temps nécessaire pour la charge et la décharge de l'échangeur.

Cette observation a conduit au développement d'un modèle numérique bidimensionnel dans le but de reproduire le comportement de l'échangeur. Le modèle utilise plusieurs méthodes et techniques, y compris l'approche du bilan thermique, la capacité thermique apparente et la méthode des différences finies afin de représenter avec succès le processus de changement de phase et le fonctionnement général du système. L'importance des valeurs de capacité de chaleur a été révélée et une enquête plus approfondie de ce paramètre a conduit à la création de courbes adéquates en fonction de la position considérée de la plaque de MCP. Résultats numériques et expérimentaux ont été confrontés afin de calibrer et valider le modèle. Suite à cela, le modèle a été couplé à un modèle de bâtiment existant afin de tester les performances de l'échangeur à propos de l'effacement énergétique, le confort thermique et la qualité de l'air intérieur lors des différents scénarios.

Deux approches d'optimisation ont été considérées et numériquement exploitées pour surmonter les limites de la performance initiale de l'échangeur. La première a examiné l'impact de la modification de la géométrie du dispositif lorsque celui est couplé à l'immeuble. Trois configurations ont été sélectionnées et testées sur un bâtiment à basse énergie pour une période d'un mois. Les avantages du système proposé ont été démontrées pour des scénarios présentant une difficulté croissante: déplacement de la charge simple, charge du dispositif pendant la nuit et enfin fonctionnement pendant la présence des occupants. La consommation électrique a été déplacée des heures pleines aux heures creuses sans affecter le confort thermique et la qualité de l'air. Bien que la consommation d'énergie finale mensuelle

a été augmentée, la charge nocturne de l'unité a permis le fonctionnement du système pendant les heures avec des tarifs avantageux, conduisant à un coût d'électricité final réduit. Néanmoins, cette approche a montré certains inconvénients concernant la masse de MCP utilisée, le volume de l'échangeur et le temps élevé pour la charge du dispositif.

Cela a conduit à la seconde approche d'optimisation qui, en plus de la géométrie de l'échangeur a également étudié les propriétés du MCP. Densité, chaleur spécifique et conductivité ont été modifiées, en cherchant les configurations avec un temps de charge minimum et stockage d'énergie maximum. Les versions optimisées du dispositif ont été classées selon la durée de charge et un gain d'une heure a été observé pour le même stockage d'énergie. À la fin, les scénarios testés avec les résultats de la première approche d'optimisation ont été reproduits et nous avons pu obtenir un système efficace avec une masse de MCP initiale, capable d'effectuer l'effacement souhaité tout en maintenant des conditions thermiques et qualité d'air confortables.

Perspectives

Dans cette thèse, l'applicabilité et les avantages de la technologie de stockage de chaleur latente ont été démontrés par l'étude numérique et expérimentale d'un échangeur de chaleur MCP-Air, intégré dans un système de ventilation. Plusieurs domaines peuvent être examinés comme une continuité de ce travail.

Tout d'abord, des contrôleurs avancés peuvent être utilisés pour le fonctionnement du système, tels que ceux utilisant la logique floue. Ces contrôleurs peuvent offrir une approche plus adaptée aux besoins de l'étude, présenter des variations inferieures et des résultats meilleurs. En outre, des outils prédictifs peuvent être intégrés dans le système contrôle / commande du système. Ces outils peuvent se focaliser sur les conditions météorologiques ou la présence des occupants afin d'anticiper les besoins de chauffage du bâtiment et ajuster le fonctionnement du système en conséquence. Selon les besoins prévus, les niveaux de stockage d'énergie différents peuvent être décidées, conduisant à une charge faible, modérée ou complète de l'échangeur. Des méthodes Metaheuristic tels que les algorithmes génétiques peuvent également être utilisées dans l'étude d'optimisation fournissant une approche différente, mais plus efficace.

En outre, l'efficacité du système proposé peut être testée pour des propriétés différentes du bâtiment. La modification de l'inertie ou de l'isolation thermique du bâtiment peuvent constituer des exemples d'une telle étude. Une conception plus détaillée de l'immeuble avec la séparation des zones selon l'utilisation et les besoins des occupants peut également être étudié.

La robustesse des solutions numériques proposées peut être testée dans une expérimentation in situ, que ce soit dans une maison expérimentale ou une habitation réelle avec des occupants qui comprennent le fonctionnement du système. Le dernier cas nécessiterait une enquête plus large de l'impact de l'intégration du système dans un environnement habité, mettant l'accent sur les risques d'incendie et la diffusion de l'odeur du MCP.

L'étude du système peut être étendue à des conditions estivales afin de profiter concept du refroidissement nocturne, soit par voie expérimentale soit numériquement. Dans le premier cas, le choix de macroencapsulation et de la structure rigide du second échangeur de chaleur peut permettre un

remplacement relativement facile de la paraffine utilisée avec un MCP plus adapté aux conditions d'été (essentiellement un MCP avec une plage de température de fusion différente, peut-être une capacité de stockage d'énergie différent). Dans le second cas, l'adaptation à des conditions estivales sera effectuée par la modification des propriétés du MCP dans le modèle numérique. Osterman et al. sont en train d'étudier une configuration d'échangeur similaire avec un MCP qui peut satisfaire les deux climats : hivernal et estival. Il serait intéressant de voir si leurs résultats peuvent contribuer à ce domaine et de vérifier l'efficacité d'un tel dispositif avec les outils que nous avons développés.

Enfin, même si cette étude a porté sur la question des pics de consommation, la technologie de stockage thermique peut être couplé à d'autres technologies innovantes existants tels que les énergies renouvelables, les smart grids, les murs vivants, etc. De cette façon, les avantages de chaque domaine peuvent être combinés afin d'obtenir des solutions plus larges et plus efficaces en ce qui concerne le fonctionnement du bâtiment.

References

References

Abedin A., Rosen M. (2011). A Critical Review of Thermochemical Energy Storage Systems. *The Open Renewable Energy Journa*l, 4, 42-46

ADEME. (2013, a) Bâtiment, Chiffres Clés

ADEME. (2013, b) Climat, air et énergie

ADEME & RTE. (2007), Le contenu en CO2 du kWh électrique: Avantages comparés du contenu marginal et du contenu par usages sur la base de l'historique

Albright LD (1990) Environment control for animals and plants. ASAE Textbook, 4. American Society of Agricultural Engineers, Michigan, St. Joseph

Arkar C., Medved S., (2005). Influence of accuracy of thermal property data of a phase change material on the result of a numerical model of a packed bed latent heat storage with spheres, Thermochimica Acta, 438, 192-201

Arkar A., Vidrih B., Medved S. (2006). Efficiency of free cooling using latent heat storage integrated into the ventilation system of a low energy building, *International Journal of Refrigeration*, 30, 134-143

ASHRAE. (2013). Ventilation for Acceptable Indoor Air Quality (ANSI Approved), Guidelines in ASHRAE Standard 62.1-2013, Appendix B, Summary of Selected Air Quality

Baetens R., Jelle B. P., Gustavsen A. (2010). Phase change materials for building applications: A state-of-the-art review. *Energy and Buildings*, 42, 1361-1368

Borderon J. (2012). Integration des materiaux à changement de phase comme systeme de régulation dynamique en rénovation thermique, *PhD thesis*, ENTPE France

Cabeza L.F., Castell A., Barreneche C., de Gracia A., Fernández A.I. (2011). Materials used as PCM in thermal energy storage in buildings: A review. *Renewable and Sustainable Energy Reviews,* 15, 1675-1695

Cabeza L., Mehling H. (2008). Heat and cold storage with PCM: An up to date introduction into basics and applications, Springer , Handbook

Chen H., Cong T.N., Yang W., Tan C., Li Y., Ding Y. (2009). Progress in electrical energy storage system: A critical review. *Progress in Natural Science,* 19, 291-312

Dolado P., Lazaro A., Marin J.M., Zalba B. (2011). Characterization of melting and solidification in a real-scale PCM-air heat exchanger: Experimental results and empirical model, *Renewable Energy*, 36, 2906-2917

Dumortier D. (2003). Lumière naturelle et rayonnement solaire - Mesures au sol et estimations á partir d'images satellites - Développement de services Web pour l'éclairage naturel des bâtiments, Thèse d'habilitation, INSA- Univ. Claude Bernard Lyon 1, Septembre 2003. http://idmp.entpe.fr/vaulx/index.htm.

Dutil Y., Rousse D. R., Ben Salah N., Lassue S., Zalewski L., (2011). A review on phase-change materials: Mathematical modeling and simulations, Renewable and Sustainable Energy Reviews, 15, 112-130

El Mankibi M. (2003). Development and evaluation of experimental and numerical control strategies for hybrid ventilation, PhD Thesis, INSA Lyon

European Comission. (2002). Energy Performance of Buildings Directive (Directive 2002/91/EC)

European Commission. (2008). A strategy for smart, sustainable and inclusive growth

European Commission. (2011). Energy Roadmap 2050

Farid M., Khudhair A., Razack S., Al-Hallaj S. (2004). A review on phase change energy storage: materials and applications. *Energy Conversion and Management,* 45, 1597-1615

Fernandes D., Pitié F., Cáceres G., Baeyens J. (2012). Thermal energy storage: "How previous findings determine current research priorities" *Energy,* 39, 246-257

Hadjieva, M., Kanev S., Argirov J. (1992). Thermophysical properties of some paraffins applicable to thermal energy storage. *Solar Energy Materials and Solar Cells*, 27, 181-187

Hajat S., Kovats R.S., Atkinson R.W. & Haines A. (2002). Impact of hot temperatures on death in London: a time series approach. *Journal of Epidemiology and Community Health*, 56, 367-372

Hale D.V., Hoover M.J., O'Neill M.J. (1971). Phase change materials hand book. Alabaa: Marshal Space Flight Center.

Heim D., Clarke J.A. (2004). Numerical modelling and thermal simulation of PCM–gypsum composites with ESP-r, Energy and Buildings, 36, 795-805

Hu H., Argyropoulos S., (1996). Mathematical modelling of solidification and melting: a review, Modelling and Simulation in Materials Science and Engineering, 4, 371-396.

Idelsohn S., Storti M., Crivelli L. (1994). Numerical methods in phase-change problems, Archives of Computational Methods in Engineering, 1, 49-74.

IEA. Annex 17. (2005). Advanced Thermal Energy Storage through Phase Change Materials and Chemical Reactions – Feasibility Studies and Demonstration projects, Final report.

IEA. Annex 23. (2013). Applying Energy Storage in Ultra-low Energy Buildings, Final report.

IEA Task 32. (2005). Thermal energy storage for solar and low energy buildings. Handbook

IEA. (2008). Energy efficiency requirements in building codes, energy efficiency policies or new buildings, IEA Information paper

INSEE. (2011). La précarité énergétique : avoir froid ou dépenser trop pour se chauffer

INSEE. (2012). Bilan énergétique 2012

Khudhair A. M., Farid M. (2003). A review on energy conservation in building applications with thermal storage by latent heat using phase change materials. *Energy Conversion and Management,* 45, 263-275

Lamberg P., Sirén K. (2003). Approximate analytical model for solidification in a finite PCM storage with internal fins, Applied Mathematical Modelling, 7, 491-513

Lazaro A., Dolado P., Marín J.M., Zalba B. (2009). PCM–air heat exchangers for free-cooling applications in buildings: Experimental results of two real-scale prototypes, *Energy Conversion and Management*, 50, 439-443

Lin K., Zhang Y., Di H., Yang R. (2007). Study of an electrical heating system with ductless air supply and shape-stabilized PCM for thermal storage, *Energy Conversion and Management,* 48, 2016-2024

Mackenzie J.A., Robertson M.L. (2002). A moving mesh method for the solution of the one-dimensional phase-field equations. Comput Phys, 181, 526–44.

MEDDE. (2006). Actualisation 2006 du Plan Climat 2004-2012

MEDDE. (2009). La première loi du Grenelle

MEDDE. (2010). Loi Grenelle 2

MEDDTL. (2010). Bilan énergétique de la France rapport du SOeS

Mitchell S. L., Myers T. G. (2012). Application of heat balance integral methods to one-dimensional phase change problems, International Journal of Differential Equations

Nagano K., Takeda S., Mochida T., Shikamura K. (2004). Thermal characteristics of a direct heat exchange system between granules with phase change material and air, *Applied Thermal Engineering,* 24, 2131-2144

Nedjar B. (2002). An enthalpy-based finite element method for nonlinear heat problems involving phase change, *Comput Struct,* 80, 9–21.

NégaWatt. (2009). La pointe d'électricité en France … zéro pointé !, Dossier de Presse

Osterman E., Butala V., Stritih U. (2013). Room Heat Exchanger with PCM as a Thermal Accumulation for Heating and Cooling of Buildings. *Conference: CLIMA 2013 – 11th REHVA world congress and the 8th international conference on IAQVEC*

Parameshwaran R., Kalaiselvam S., Harikrishnan S., Elayaperumal A. (2012). Sustainable thermal energy storage technologies for buildings: A review, *Renewable and Sustainable Energy Reviews,* 16, 2394-2433

Pasupathy A., Velraj R., Seeniraj R.V. (2008). Phase change material-based building architecture for thermal management in residential and commercial establishments, *Renewable and Sustainable Energy Reviews*, 12, 39-64

Pomianowski M., Heiselberg P., Zhang Y. (2013). Review of thermal energy storage technologies based on PCM application in buildings, *Energy and Buildings,* 67, 56-69

Robine J.-M., Cheung S.L., Le Roy S., Van Oyen H., Griffith C., Michel J.-P. (2008). Death toll exceeded 70,000 in Europe during the summer of 2003. *Comptes Rendus Biologies*,331, 171-178

Rolph W.D. and Bathe K. J. (1982). An efficient algorithm for analysis of nonlinear heat transfer with phase changes, Int. J. Numer. Meth. Eng., 18, 119–34

RTE. éCO2mix. www.rte-france.com/lienrapide/eco2mix

RTE. (2012, a). Bilan électrique

RTE. (2012, b). La vague de froid de février

RTE. (2013).Bilan électrique

RTE. (2014). Memo

Salyer IO, Sircar AK. (1990). Phase change materials for heating and cooling of residential buildings and other applications. *Proceedings of 25th Intersociety Energy Conversion Engineering Conference*, 236-43.

Sharma A., Tyagi V.V., Chen C.R., Buddhi D. (2009). Review on thermal energy storage with phase change materials and applications, *Renewable and Sustainable Energy Reviews,* 13, 318-345

Siskos P. A., Bouba K. E., Stroubou A.P. (2001). Determination of Selected Pollutants and Measurement of Physical Parameters for the Evaluation of Indoor Air Quality in School Buildings in Athens, Greece. Indoor and Built Environment, 10, (3-4), pp185-192.

Soares N., Costa J.J., Gaspar A.R., Santos P. (2013). Review of passive PCM latent heat thermal energy storage systems towards buildings' energy efficiency, *Energy and Buildings,* 59, 82-103

Turnpenny J.R., Etheridge D.W., Reay D.A. (2001). Novel ventilation system for reducing air conditioning in buildings. Part II: testing of the prototype, *Applied Thermal Energy*, 21, 1203-1217

UN. (2013). World population projected to reach 9.6 billion by 2050 with most growth in developing regions, Press release

UNEP SBCI. (2009). Buildings and climate change, Summary for decision makers

United Nations. (1998). Kyoto protocol to the United Nations framework convention on climate change

Verma P., Varun, Singal S.K. (2008). Review of mathematical modeling on latent heat thermal energy storage systems using phase-change material, Renewable and Sustainable Energy Reviews, 12, 999-1031

Voller V.R., Swenson J.B., Kim W., Paola C. (2006). An enthalpy method for moving boundary problems on the earth's surface. International Journal of Numerical Methods for Heat & Fluid Flow, 16, 641 - 54.

Voller V.R. and Swaminathan C.R. (1991). General source-based method for solidification phase change Numer. Heat Transfer, 19, 175–89

Zalba B., Marın J.M., Cabeza L., Mehling H. (2003). Review on thermal energy storage with phase change: materials, heat transfer analysis and applications, Applied Thermal Engineering, 23, 251-283

Zalba B., Marin J.M., Cabeza L.F., Melhing H. (2004). Free-cooling of buildings with phase change materials, *International Journal of Refrigeration*, 27, 839-849

Zhou D., Zhao C.Y., Tian Y. (2012). Review on thermal energy storage with phase change materials (PCMs) in building applications, *Applied Energy*, 92, 593-605

Appendices

Appendices

Appendix A1

Second optimization approach, charging of the unit, airflow rate of 300 m^3/h

lmpc	rmcp	cpmcp	lalu	dym	dx	dz	time	energy
4	0,9	0,7	0,5	0,001188	0,12309149	0,22156468	3,35	2721,19836
3	0,9	0,7	0,5	0,001188	0,12309149	0,22156468	3,36666667	2725,61476
2	0,9	0,7	0,5	0,001188	0,12309149	0,22156468	3,4	2729,82398
4	0,9	0,7	1,3	0,001188	0,12309149	0,22156468	3,49722222	2751,40226
3	0,9	0,7	1,3	0,001188	0,12309149	0,22156468	3,51111111	2753,56008
4	0,9	0,7	1,6	0,001188	0,12309149	0,22156468	3,53888889	2758,53639
2	0,9	0,7	1,3	0,001188	0,12309149	0,22156468	3,54166667	2756,04927
3	0,9	0,7	1,6	0,001188	0,12309149	0,22156468	3,55277778	2760,61904
2	0,9	0,7	1,6	0,001188	0,12309149	0,22156468	3,58333333	2762,71056
4	0,9	0,7	0,5	0,002394	0,086711	0,15607979	3,93888889	2387,76575
3	0,9	0,7	0,5	0,002394	0,086711	0,15607979	4,00277778	2394,54682
4	0,9	0,7	1,3	0,002394	0,086711	0,15607979	4,02777778	2396,99669
4	0,9	0,7	1,6	0,002394	0,086711	0,15607979	4,05	2398,51691
3	0,9	0,7	1,3	0,002394	0,086711	0,15607979	4,08888889	2402,4226
3	0,9	0,7	1,6	0,002394	0,086711	0,15607979	4,11388889	2404,59515
2	0,9	0,7	0,5	0,002394	0,086711	0,15607979	4,13333333	2400,4828
2	0,9	0,7	1,3	0,002394	0,086711	0,15607979	4,21111111	2406,52146
2	0,9	0,7	1,6	0,002394	0,086711	0,15607979	4,23611111	2408,47018
4	0,9	0,7	0,5	0,002988	0,07761505	0,13970709	4,26388889	2311,23413
4	0,9	0,7	1,3	0,002988	0,07761505	0,13970709	4,33055556	2316,96383
4	0,9	0,7	1,6	0,002988	0,07761505	0,13970709	4,34722222	2317,87191
3	0,9	0,7	0,5	0,002988	0,07761505	0,13970709	4,36388889	2321,57141
3	0,9	0,7	1,3	0,002988	0,07761505	0,13970709	4,425	2325,73186
3	0,9	0,7	1,6	0,002988	0,07761505	0,13970709	4,44166667	2326,65494
2	0,9	0,7	0,5	0,002988	0,07761505	0,13970709	4,56111111	2329,97805
2	0,9	0,7	1,3	0,002988	0,07761505	0,13970709	4,61666667	2332,9001
2	0,9	0,7	1,6	0,002988	0,07761505	0,13970709	4,63333333	2333,54911
4	1,4	0,7	0,5	0,001188	0,12309149	0,22156468	4,85277778	4050,70151
3	1,4	0,7	0,5	0,001188	0,12309149	0,22156468	4,87777778	4056,91827
2	1,4	0,7	0,5	0,001188	0,12309149	0,22156468	4,93333333	4064,83634
4	1,4	0,7	1,3	0,001188	0,12309149	0,22156468	5,03333333	4087,50912
3	1,4	0,7	1,3	0,001188	0,12309149	0,22156468	5,05833333	4091,67517
4	1,4	0,7	1,6	0,001188	0,12309149	0,22156468	5,08611111	4096,05619

2	1,4	0,7	1,3	0,001188	0,12309149	0,22156468	5,10555556	4094,99408
3	1,4	0,7	1,6	0,001188	0,12309149	0,22156468	5,11111111	4100,16537
2	1,4	0,7	1,6	0,001188	0,12309149	0,22156468	5,15555556	4102,45887
4	0,9	1,25	0,5	0,001188	0,12309149	0,22156468	5,46388889	4598,92341
3	0,9	1,25	0,5	0,001188	0,12309149	0,22156468	5,49444444	4606,98771
2	0,9	1,25	0,5	0,001188	0,12309149	0,22156468	5,55555556	4615,18585
4	0,9	1,25	1,3	0,001188	0,12309149	0,22156468	5,65833333	4638,48075
3	0,9	1,25	1,3	0,001188	0,12309149	0,22156468	5,68333333	4642,09215
4	0,9	1,25	1,6	0,001188	0,12309149	0,22156468	5,71388889	4647,34073
2	0,9	1,25	1,3	0,001188	0,12309149	0,22156468	5,73611111	4645,70143
3	0,9	1,25	1,6	0,001188	0,12309149	0,22156468	5,73888889	4650,96486
4	1,4	0,7	0,5	0,002394	0,086711	0,15607979	5,73888889	3607,85736
2	0,9	1,25	1,6	0,001188	0,12309149	0,22156468	5,79166667	4654,40806
3	1,4	0,7	0,5	0,002394	0,086711	0,15607979	5,83611111	3617,58412
4	1,4	0,7	1,3	0,002394	0,086711	0,15607979	5,84444444	3618,15316
4	1,4	0,7	1,6	0,002394	0,086711	0,15607979	5,875	3620,30233
3	1,4	0,7	1,3	0,002394	0,086711	0,15607979	5,93611111	3626,06128
3	1,4	0,7	1,6	0,002394	0,086711	0,15607979	5,96388889	3627,55253
2	1,4	0,7	0,5	0,002394	0,086711	0,15607979	6,03333333	3626,18948
2	1,4	0,7	1,3	0,002394	0,086711	0,15607979	6,11944444	3631,32663
4	1,84	0,7	0,5	0,001188	0,12309149	0,22156468	6,14444444	5213,86618
2	1,4	0,7	1,6	0,002394	0,086711	0,15607979	6,14722222	3632,89575
3	1,84	0,7	0,5	0,001188	0,12309149	0,22156468	6,18055556	5222,87072
4	1,4	0,7	0,5	0,002988	0,07761505	0,13970709	6,21111111	3502,54953
2	1,84	0,7	0,5	0,001188	0,12309149	0,22156468	6,25	5232,20026
4	1,4	0,7	1,3	0,002988	0,07761505	0,13970709	6,28611111	3508,12827
4	1,4	0,7	1,6	0,002988	0,07761505	0,13970709	6,30833333	3509,2345
4	1,84	0,7	1,3	0,001188	0,12309149	0,22156468	6,34722222	5254,48461
3	1,4	0,7	0,5	0,002988	0,07761505	0,13970709	6,35833333	3516,68712
3	1,84	0,7	1,3	0,001188	0,12309149	0,22156468	6,37777778	5259,18909
4	0,9	1,5	0,5	0,001188	0,12309149	0,22156468	6,4	5446,99531
4	1,84	0,7	1,6	0,001188	0,12309149	0,22156468	6,40833333	5264,20843
3	1,4	0,7	1,3	0,002988	0,07761505	0,13970709	6,425	3520,34817
3	1,84	0,7	1,6	0,001188	0,12309149	0,22156468	6,43611111	5268,13726
2	1,84	0,7	1,3	0,001188	0,12309149	0,22156468	6,43888889	5263,55835
3	0,9	1,5	0,5	0,001188	0,12309149	0,22156468	6,43888889	5456,68106
3	1,4	0,7	1,6	0,002988	0,07761505	0,13970709	6,44722222	3521,20711
4	0,9	1,25	0,5	0,002394	0,086711	0,15607979	6,46388889	4110,6699
2	1,84	0,7	1,6	0,001188	0,12309149	0,22156468	6,49722222	5272,01883
2	0,9	1,5	0,5	0,001188	0,12309149	0,22156468	6,51388889	5467,08696
4	0,9	1,25	1,3	0,002394	0,086711	0,15607979	6,57222222	4120,72458
3	0,9	1,25	0,5	0,002394	0,086711	0,15607979	6,575	4121,79014
4	0,9	1,25	1,6	0,002394	0,086711	0,15607979	6,60555556	4123,07835

4	0,9	1,5	1,3	0,001188	0,12309149	0,22156468	6,60833333	5488,70004
3	0,9	1,5	1,3	0,001188	0,12309149	0,22156468	6,63888889	5493,25458
2	1,4	0,7	0,5	0,002988	0,07761505	0,13970709	6,64722222	3527,70537
4	0,9	1,5	1,6	0,001188	0,12309149	0,22156468	6,66944444	5498,28612
3	0,9	1,25	1,3	0,002394	0,086711	0,15607979	6,675	4129,47134
3	0,9	1,5	1,6	0,001188	0,12309149	0,22156468	6,7	5502,80612
2	1,4	0,7	1,3	0,002988	0,07761505	0,13970709	6,70277778	3528,83147
2	0,9	1,5	1,3	0,001188	0,12309149	0,22156468	6,70555556	5498,49131
3	0,9	1,25	1,6	0,002394	0,086711	0,15607979	6,70555556	4131,2026
2	1,4	0,7	1,6	0,002988	0,07761505	0,13970709	6,72222222	3529,28282
2	0,9	1,5	1,6	0,001188	0,12309149	0,22156468	6,76388889	5506,89779
2	0,9	1,25	0,5	0,002394	0,086711	0,15607979	6,79444444	4130,44066
2	0,9	1,25	1,3	0,002394	0,086711	0,15607979	6,88333333	4135,35944
2	0,9	1,25	1,6	0,002394	0,086711	0,15607979	6,91111111	4136,48876
4	0,9	1,25	0,5	0,002988	0,07761505	0,13970709	6,99166667	3993,29705
4	0,9	1,25	1,3	0,002988	0,07761505	0,13970709	7,06666667	3998,39045
4	0,9	1,25	1,6	0,002988	0,07761505	0,13970709	7,09166667	3999,58447
3	0,9	1,25	0,5	0,002988	0,07761505	0,13970709	7,15555556	4008,70851
3	0,9	1,25	1,3	0,002988	0,07761505	0,13970709	7,225	4011,93412
3	0,9	1,25	1,6	0,002988	0,07761505	0,13970709	7,24722222	4012,64634
4	1,84	0,7	0,5	0,002394	0,086711	0,15607979	7,26666667	4674,22742
4	1,84	0,7	1,3	0,002394	0,086711	0,15607979	7,37777778	4684,22791
3	1,84	0,7	0,5	0,002394	0,086711	0,15607979	7,39166667	4686,43293
4	1,84	0,7	1,6	0,002394	0,086711	0,15607979	7,41111111	4686,22201
2	0,9	1,25	0,5	0,002988	0,07761505	0,13970709	7,48055556	4020,43838
3	1,84	0,7	1,3	0,002394	0,086711	0,15607979	7,49444444	4693,88355
3	1,84	0,7	1,6	0,002394	0,086711	0,15607979	7,52777778	4695,69876
2	0,9	1,25	1,3	0,002988	0,07761505	0,13970709	7,53611111	4020,80681
2	0,9	1,25	1,6	0,002988	0,07761505	0,13970709	7,55555556	4021,09391
4	0,9	1,5	0,5	0,002394	0,086711	0,15607979	7,56944444	4888,28128
2	1,84	0,7	0,5	0,002394	0,086711	0,15607979	7,63888889	4696,05309
4	0,9	1,5	1,3	0,002394	0,086711	0,15607979	7,68333333	4898,25756
3	0,9	1,5	0,5	0,002394	0,086711	0,15607979	7,7	4901,04107
4	0,9	1,5	1,6	0,002394	0,086711	0,15607979	7,71666667	4900,25579
2	1,84	0,7	1,3	0,002394	0,086711	0,15607979	7,72777778	4699,85581
2	1,84	0,7	1,6	0,002394	0,086711	0,15607979	7,75555556	4700,78033
3	0,9	1,5	1,3	0,002394	0,086711	0,15607979	7,80277778	4908,05003
3	0,9	1,5	1,6	0,002394	0,086711	0,15607979	7,83611111	4909,67171
4	1,84	0,7	0,5	0,002988	0,07761505	0,13970709	7,85555556	4543,26531
4	1,84	0,7	1,3	0,002988	0,07761505	0,13970709	7,93055556	4548,01756
4	1,84	0,7	1,6	0,002988	0,07761505	0,13970709	7,95277778	4548,68275
2	0,9	1,5	0,5	0,002394	0,086711	0,15607979	7,95555556	4910,57914
3	1,84	0,7	0,5	0,002988	0,07761505	0,13970709	8,03888889	4560,12143

4	1,4	1,25	0,5	0,001188	0,12309149	0,22156468	8,04166667	6949,08416
2	0,9	1,5	1,3	0,002394	0,086711	0,15607979	8,04444444	4914,05378
2	0,9	1,5	1,6	0,002394	0,086711	0,15607979	8,07222222	4914,78516
3	1,4	1,25	0,5	0,001188	0,12309149	0,22156468	8,09166667	6961,59089
3	1,84	0,7	1,3	0,002988	0,07761505	0,13970709	8,10555556	4562,43607
3	1,84	0,7	1,6	0,002988	0,07761505	0,13970709	8,12777778	4562,86473
4	0,9	1,5	0,5	0,002988	0,07761505	0,13970709	8,17777778	4751,75024
2	1,4	1,25	0,5	0,001188	0,12309149	0,22156468	8,18611111	6974,27212
4	0,9	1,5	1,3	0,002988	0,07761505	0,13970709	8,25555556	4756,54444
4	1,4	1,25	1,3	0,001188	0,12309149	0,22156468	8,26944444	6993,70274
4	0,9	1,5	1,6	0,002988	0,07761505	0,13970709	8,27777778	4757,23395
3	1,4	1,25	1,3	0,001188	0,12309149	0,22156468	8,30833333	6999,52193
4	1,4	1,25	1,6	0,001188	0,12309149	0,22156468	8,33611111	7003,25793
3	0,9	1,5	0,5	0,002988	0,07761505	0,13970709	8,36944444	4769,29835
3	1,4	1,25	1,6	0,001188	0,12309149	0,22156468	8,375	7008,94283
2	1,4	1,25	1,3	0,001188	0,12309149	0,22156468	8,39166667	7005,80709
2	1,84	0,7	0,5	0,002988	0,07761505	0,13970709	8,40277778	4572,57321
3	0,9	1,5	1,3	0,002988	0,07761505	0,13970709	8,43888889	4771,65522
2	1,4	1,25	1,6	0,001188	0,12309149	0,22156468	8,45555556	7013,99007
2	1,84	0,7	1,3	0,002988	0,07761505	0,13970709	8,45555556	4571,77863
3	0,9	1,5	1,6	0,002988	0,07761505	0,13970709	8,45833333	4771,65745
2	1,84	0,7	1,6	0,002988	0,07761505	0,13970709	8,475	4571,80027
2	0,9	1,5	0,5	0,002988	0,07761505	0,13970709	8,74722222	4781,84169
2	0,9	1,5	1,3	0,002988	0,07761505	0,13970709	8,8	4780,80501
2	0,9	1,5	1,6	0,002988	0,07761505	0,13970709	8,81944444	4780,58098
4	1,4	1,5	0,5	0,001188	0,12309149	0,22156468	9,45555556	8258,17535
4	1,4	1,25	0,5	0,002394	0,086711	0,15607979	9,48611111	6264,13865
3	1,4	1,5	0,5	0,001188	0,12309149	0,22156468	9,51388889	8272,79346
4	1,4	1,25	1,3	0,002394	0,086711	0,15607979	9,6	6272,75807
2	1,4	1,5	0,5	0,001188	0,12309149	0,22156468	9,62777778	8288,12379
4	1,4	1,25	1,6	0,002394	0,086711	0,15607979	9,63333333	6273,8938
3	1,4	1,25	0,5	0,002394	0,086711	0,15607979	9,64722222	6279,39634
4	1,4	1,5	1,3	0,001188	0,12309149	0,22156468	9,69444444	8303,86193
3	1,4	1,5	1,3	0,001188	0,12309149	0,22156468	9,74166667	8311,04883
3	1,4	1,25	1,3	0,002394	0,086711	0,15607979	9,75	6284,12702
4	1,4	1,5	1,6	0,001188	0,12309149	0,22156468	9,76388889	8313,21971
3	1,4	1,25	1,6	0,002394	0,086711	0,15607979	9,78333333	6285,05994
3	1,4	1,5	1,6	0,001188	0,12309149	0,22156468	9,81111111	8319,69698
2	1,4	1,5	1,3	0,001188	0,12309149	0,22156468	9,83888889	8317,75922
2	1,4	1,5	1,6	0,001188	0,12309149	0,22156468	9,90555556	8325,19696
2	1,4	1,25	0,5	0,002394	0,086711	0,15607979	9,96944444	6290,28675
2	1,4	1,25	1,3	0,002394	0,086711	0,15607979	10,0527778	6290,47023
2	1,4	1,25	1,6	0,002394	0,086711	0,15607979	10,0777778	6289,95409

4	1,4	1,25	0,5	0,002988	0,07761505	0,13970709	10,2277778	6093,41045
4	1,84	1,25	0,5	0,001188	0,12309149	0,22156468	10,2555556	9004,16912
4	1,4	1,25	1,3	0,002988	0,07761505	0,13970709	10,3	6096,17448
3	1,84	1,25	0,5	0,001188	0,12309149	0,22156468	10,3194444	9020,21704
4	1,4	1,25	1,6	0,002988	0,07761505	0,13970709	10,3222222	6096,05825
2	1,84	1,25	0,5	0,001188	0,12309149	0,22156468	10,4444444	9037,23226
3	1,4	1,25	0,5	0,002988	0,07761505	0,13970709	10,4666667	6114,26025
4	1,84	1,25	1,3	0,001188	0,12309149	0,22156468	10,4972222	9049,7159
3	1,4	1,25	1,3	0,002988	0,07761505	0,13970709	10,5277778	6113,71451
3	1,4	1,25	1,6	0,002988	0,07761505	0,13970709	10,5472222	6113,03966
3	1,84	1,25	1,3	0,001188	0,12309149	0,22156468	10,55	9057,88272
4	1,84	1,25	1,6	0,001188	0,12309149	0,22156468	10,5694444	9058,89005
3	1,84	1,25	1,6	0,001188	0,12309149	0,22156468	10,6194444	9065,84701
2	1,84	1,25	1,3	0,001188	0,12309149	0,22156468	10,6555556	9064,91632
2	1,84	1,25	1,6	0,001188	0,12309149	0,22156468	10,7222222	9071,602
2	1,4	1,25	0,5	0,002988	0,07761505	0,13970709	10,9333333	6127,55713
2	1,4	1,25	1,3	0,002988	0,07761505	0,13970709	10,975	6122,72854
2	1,4	1,25	1,6	0,002988	0,07761505	0,13970709	10,9916667	6121,50923
4	1,4	1,5	0,5	0,002394	0,086711	0,15607979	11,1222222	7462,43613
4	1,4	1,5	1,3	0,002394	0,086711	0,15607979	11,2305556	7468,59522
4	1,4	1,5	1,6	0,002394	0,086711	0,15607979	11,2638889	7469,02378
3	1,4	1,5	0,5	0,002394	0,086711	0,15607979	11,3111111	7479,50027
3	1,4	1,5	1,3	0,002394	0,086711	0,15607979	11,4083333	7481,67481
3	1,4	1,5	1,6	0,002394	0,086711	0,15607979	11,4388889	7481,53538
2	1,4	1,5	0,5	0,002394	0,086711	0,15607979	11,6861111	7491,14228
2	1,4	1,5	1,3	0,002394	0,086711	0,15607979	11,7583333	7487,32971
2	1,4	1,5	1,6	0,002394	0,086711	0,15607979	11,7833333	7485,98325
4	1,4	1,5	0,5	0,002988	0,07761505	0,13970709	11,9722222	7261,24408
4	1,4	1,5	1,3	0,002988	0,07761505	0,13970709	12,0333333	7261,21851
4	1,84	1,25	0,5	0,002394	0,086711	0,15607979	12,0416667	8144,87025
4	1,4	1,5	1,6	0,002988	0,07761505	0,13970709	12,0555556	7260,43604
4	1,84	1,5	0,5	0,001188	0,12309149	0,22156468	12,0777778	10716,0106
4	1,84	1,25	1,3	0,002394	0,086711	0,15607979	12,1472222	8149,52749
3	1,84	1,5	0,5	0,001188	0,12309149	0,22156468	12,1555556	10735,4403
4	1,84	1,25	1,6	0,002394	0,086711	0,15607979	12,1805556	8149,62355
3	1,84	1,25	0,5	0,002394	0,086711	0,15607979	12,2472222	8163,34754
3	1,4	1,5	0,5	0,002988	0,07761505	0,13970709	12,25	7284,50148
3	1,4	1,5	1,3	0,002988	0,07761505	0,13970709	12,2972222	7280,38398
2	1,84	1,5	0,5	0,001188	0,12309149	0,22156468	12,3	10754,6024
3	1,4	1,5	1,6	0,002988	0,07761505	0,13970709	12,3166667	7279,1252
4	1,84	1,5	1,3	0,001188	0,12309149	0,22156468	12,3222222	10759,8732
3	1,84	1,25	1,3	0,002394	0,086711	0,15607979	12,3388889	8163,43481
3	1,84	1,25	1,6	0,002394	0,086711	0,15607979	12,3694444	8162,65375

3	1,84	1,5	1,3	0,001188	0,12309149	0,22156468	12,3861111	10769,7757
4	1,84	1,5	1,6	0,001188	0,12309149	0,22156468	12,3972222	10768,404
3	1,84	1,5	1,6	0,001188	0,12309149	0,22156468	12,4583333	10776,5384
2	1,84	1,5	1,3	0,001188	0,12309149	0,22156468	12,5111111	10778,1158
2	1,84	1,5	1,6	0,001188	0,12309149	0,22156468	12,5805556	10783,3378
2	1,84	1,25	0,5	0,002394	0,086711	0,15607979	12,65	8174,76938
2	1,84	1,25	1,3	0,002394	0,086711	0,15607979	12,7166667	8168,67644
2	1,84	1,25	1,6	0,002394	0,086711	0,15607979	12,7388889	8166,55374
2	1,4	1,5	0,5	0,002988	0,07761505	0,13970709	12,7888889	7297,52668
2	1,4	1,5	1,3	0,002988	0,07761505	0,13970709	12,8166667	7288,82411
2	1,4	1,5	1,6	0,002988	0,07761505	0,13970709	12,8277778	7286,20058
4	1,84	1,25	0,5	0,002988	0,07761505	0,13970709	12,95	7926,03738
4	1,84	1,25	1,3	0,002988	0,07761505	0,13970709	13,0055556	7924,42165
4	1,84	1,25	1,6	0,002988	0,07761505	0,13970709	13,025	7923,08943
3	1,84	1,25	0,5	0,002988	0,07761505	0,13970709	13,25	7950,77035
3	1,84	1,25	1,3	0,002988	0,07761505	0,13970709	13,2888889	7944,44086
3	1,84	1,25	1,6	0,002988	0,07761505	0,13970709	13,3055556	7942,404
2	1,84	1,25	0,5	0,002988	0,07761505	0,13970709	13,8305556	7963,49843
2	1,84	1,25	1,3	0,002988	0,07761505	0,13970709	13,8472222	7952,08359
2	1,84	1,25	1,6	0,002988	0,07761505	0,13970709	13,8583333	7948,87702
4	1,84	1,5	0,5	0,002394	0,086711	0,15607979	14,1222222	9709,04488
4	1,84	1,5	1,3	0,002394	0,086711	0,15607979	14,2138889	9709,58873
4	1,84	1,5	1,6	0,002394	0,086711	0,15607979	14,2472222	9708,5047
3	1,84	1,5	0,5	0,002394	0,086711	0,15607979	14,3666667	9730,64245
3	1,84	1,5	1,3	0,002394	0,086711	0,15607979	14,4388889	9725,07053
3	1,84	1,5	1,6	0,002394	0,086711	0,15607979	14,4666667	9722,76414
2	1,84	1,5	0,5	0,002394	0,086711	0,15607979	14,8333333	9741,86014
2	1,84	1,5	1,3	0,002394	0,086711	0,15607979	14,8777778	9729,10751
2	1,84	1,5	1,6	0,002394	0,086711	0,15607979	14,8972222	9725,27614
4	1,84	1,5	0,5	0,002988	0,07761505	0,13970709	15,1583333	9449,59214
4	1,84	1,5	1,3	0,002988	0,07761505	0,13970709	15,1944444	9443,34098
4	1,84	1,5	1,6	0,002988	0,07761505	0,13970709	15,2111111	9440,69964
3	1,84	1,5	0,5	0,002988	0,07761505	0,13970709	15,5055556	9476,69797
3	1,84	1,5	1,3	0,002988	0,07761505	0,13970709	15,525	9465,23566
3	1,84	1,5	1,6	0,002988	0,07761505	0,13970709	15,5361111	9461,39965
2	1,84	1,5	1,3	0,002988	0,07761505	0,13970709	16,1666667	9470,034
2	1,84	1,5	1,6	0,002988	0,07761505	0,13970709	16,1722222	9465,10446
2	1,84	1,5	0,5	0,002988	0,07761505	0,13970709	16,175	9487,94705

Appendix A2

Second optimization approach, charging of the unit, airflow rate of 500 m^3/h

lmpc	rmcp	cpmcp	lalu	dym	dx	dz	time	energy
2	0,9	0,7	0,5	0,001188	0,1	0,27272727	2,77777778	2652,65696
2	0,9	0,7	1,3	0,001188	0,1	0,27272727	2,77777778	2650,77826
2	0,9	0,7	1,6	0,001188	0,1	0,27272727	2,77777778	2649,91746
3	0,9	0,7	0,5	0,001188	0,1	0,27272727	2,77777778	2657,71478
3	0,9	0,7	1,3	0,001188	0,1	0,27272727	2,77777778	2657,57411
3	0,9	0,7	1,6	0,001188	0,1	0,27272727	2,77777778	2656,69384
4	0,9	0,7	0,5	0,001188	0,1	0,27272727	2,77777778	2657,55059
4	0,9	0,7	1,3	0,001188	0,1	0,27272727	2,77777778	2659,44246
4	0,9	0,7	1,6	0,001188	0,1	0,27272727	2,77777778	2659,19077
4	0,9	0,7	0,5	0,002394	0,1	0,13533835	2,84444444	2297,15087
4	0,9	0,7	1,3	0,002394	0,1	0,13533835	2,87777778	2302,05838
4	0,9	0,7	1,6	0,002394	0,1	0,13533835	2,88611111	2302,69499
3	0,9	0,7	0,5	0,002394	0,1	0,13533835	2,91388889	2298,39692
3	0,9	0,7	1,3	0,002394	0,1	0,13533835	2,94166667	2301,85971
3	0,9	0,7	1,6	0,002394	0,1	0,13533835	2,95277778	2303,30612
2	0,9	0,7	0,5	0,002394	0,1	0,13533835	3,05	2300,30655
2	0,9	0,7	1,3	0,002394	0,1	0,13533835	3,07777778	2302,91553
2	0,9	0,7	1,6	0,002394	0,1	0,13533835	3,08611111	2303,4191
4	0,9	0,7	0,5	0,002988	0,1	0,10843373	3,15555556	2241,58036
4	0,9	0,7	1,3	0,002988	0,1	0,10843373	3,175	2244,4303
4	0,9	0,7	1,6	0,002988	0,1	0,10843373	3,18055556	2244,94781
3	0,9	0,7	0,5	0,002988	0,1	0,10843373	3,25833333	2242,83665
3	0,9	0,7	1,3	0,002988	0,1	0,10843373	3,275	2244,48023
3	0,9	0,7	1,6	0,002988	0,1	0,10843373	3,28055556	2244,86963
4	1,4	0,7	0,5	0,001188	0,1	0,27272727	3,29166667	3798,73377
3	1,4	0,7	0,5	0,001188	0,1	0,27272727	3,31944444	3803,74429
2	1,4	0,7	0,5	0,001188	0,1	0,27272727	3,37222222	3808,03264
4	1,4	0,7	1,3	0,001188	0,1	0,27272727	3,40833333	3826,35389
3	1,4	0,7	1,3	0,001188	0,1	0,27272727	3,43333333	3828,70642
4	1,4	0,7	1,6	0,001188	0,1	0,27272727	3,44166667	3832,02752
2	0,9	0,7	0,5	0,002988	0,1	0,10843373	3,46111111	2244,93795
3	1,4	0,7	1,6	0,001188	0,1	0,27272727	3,46388889	3833,6793
2	0,9	0,7	1,3	0,002988	0,1	0,10843373	3,47777778	2246,14602
2	0,9	0,7	1,6	0,002988	0,1	0,10843373	3,48055556	2246,06458
2	1,4	0,7	1,3	0,001188	0,1	0,27272727	3,48055556	3829,04145
2	1,4	0,7	1,6	0,001188	0,1	0,27272727	3,51388889	3834,77381

4	0,9	1,25	0,5	0,001188	0,1	0,27272727	3,69722222	4312,92006
3	0,9	1,25	0,5	0,001188	0,1	0,27272727	3,73055556	4319,58132
2	0,9	1,25	0,5	0,001188	0,1	0,27272727	3,79166667	4324,47423
4	0,9	1,25	1,3	0,001188	0,1	0,27272727	3,82222222	4342,86512
3	0,9	1,25	1,3	0,001188	0,1	0,27272727	3,85	4345,41077
4	0,9	1,25	1,6	0,001188	0,1	0,27272727	3,85833333	4349,61005
3	0,9	1,25	1,6	0,001188	0,1	0,27272727	3,88611111	4352,13607
2	0,9	1,25	1,3	0,001188	0,1	0,27272727	3,90555556	4345,99048
2	0,9	1,25	1,6	0,001188	0,1	0,27272727	3,94166667	4352,15727
4	1,4	0,7	0,5	0,002394	0,1	0,13533835	4,13888889	3474,97549
4	1,84	0,7	0,5	0,001188	0,1	0,27272727	4,15	4890,49067
4	1,4	0,7	1,3	0,002394	0,1	0,13533835	4,17777778	3481,12649
3	1,84	0,7	0,5	0,001188	0,1	0,27272727	4,18611111	4897,60958
4	1,4	0,7	1,6	0,002394	0,1	0,13533835	4,18888889	3482,31804
3	1,4	0,7	0,5	0,002394	0,1	0,13533835	4,23888889	3476,24521
2	1,84	0,7	0,5	0,001188	0,1	0,27272727	4,25555556	4903,18792
3	1,4	0,7	1,3	0,002394	0,1	0,13533835	4,27222222	3480,39153
3	1,4	0,7	1,6	0,002394	0,1	0,13533835	4,28333333	3481,26915
4	1,84	0,7	1,3	0,001188	0,1	0,27272727	4,28333333	4922,40357
3	1,84	0,7	1,3	0,001188	0,1	0,27272727	4,31666667	4926,15827
4	0,9	1,5	0,5	0,001188	0,1	0,27272727	4,32222222	5110,03849
4	1,84	0,7	1,6	0,001188	0,1	0,27272727	4,32222222	4930,08034
3	1,84	0,7	1,6	0,001188	0,1	0,27272727	4,35277778	4931,68595
3	0,9	1,5	0,5	0,001188	0,1	0,27272727	4,35833333	5117,14647
2	1,84	0,7	1,3	0,001188	0,1	0,27272727	4,37777778	4926,19369
2	1,84	0,7	1,6	0,001188	0,1	0,27272727	4,41666667	4932,78832
2	0,9	1,5	0,5	0,001188	0,1	0,27272727	4,43333333	5123,80573
2	1,4	0,7	0,5	0,002394	0,1	0,13533835	4,44166667	3477,88567
4	0,9	1,5	1,3	0,001188	0,1	0,27272727	4,45833333	5142,90452
2	1,4	0,7	1,3	0,002394	0,1	0,13533835	4,46944444	3480,17953
2	1,4	0,7	1,6	0,002394	0,1	0,13533835	4,47777778	3480,45039
3	0,9	1,5	1,3	0,001188	0,1	0,27272727	4,49166667	5146,16609
4	0,9	1,5	1,6	0,001188	0,1	0,27272727	4,49722222	5150,07163
3	0,9	1,5	1,6	0,001188	0,1	0,27272727	4,52777778	5151,71636
2	0,9	1,5	1,3	0,001188	0,1	0,27272727	4,55555556	5146,38655
4	1,4	0,7	0,5	0,002988	0,1	0,10843373	4,59166667	3400,24208
2	0,9	1,5	1,6	0,001188	0,1	0,27272727	4,59444444	5152,56389
4	1,4	0,7	1,3	0,002988	0,1	0,10843373	4,61388889	3403,67686
4	1,4	0,7	1,6	0,002988	0,1	0,10843373	4,61944444	3404,11737
4	0,9	1,25	0,5	0,002394	0,1	0,13533835	4,65833333	3960,72893
4	0,9	1,25	1,3	0,002394	0,1	0,13533835	4,69722222	3967,05781
4	0,9	1,25	1,6	0,002394	0,1	0,13533835	4,70833333	3967,88735
3	1,4	0,7	0,5	0,002988	0,1	0,10843373	4,73888889	3400,71996

3	1,4	0,7	1,3	0,002988	0,1	0,10843373	4,75833333	3402,6233
3	1,4	0,7	1,6	0,002988	0,1	0,10843373	4,76388889	3403,0023
3	0,9	1,25	0,5	0,002394	0,1	0,13533835	4,77222222	3962,05683
3	0,9	1,25	1,3	0,002394	0,1	0,13533835	4,80555556	3965,9977
3	0,9	1,25	1,6	0,002394	0,1	0,13533835	4,81666667	3967,04463
2	0,9	1,25	0,5	0,002394	0,1	0,13533835	5	3963,38216
2	0,9	1,25	1,3	0,002394	0,1	0,13533835	5,02777778	3965,25705
2	0,9	1,25	1,6	0,002394	0,1	0,13533835	5,03611111	3965,32725
2	1,4	0,7	0,5	0,002988	0,1	0,10843373	5,03611111	3402,28399
2	1,4	0,7	1,3	0,002988	0,1	0,10843373	5,05	3402,62404
2	1,4	0,7	1,6	0,002988	0,1	0,10843373	5,05277778	3402,28419
4	0,9	1,25	0,5	0,002988	0,1	0,10843373	5,16666667	3878,1797
4	0,9	1,25	1,3	0,002988	0,1	0,10843373	5,18888889	3881,58296
4	0,9	1,25	1,6	0,002988	0,1	0,10843373	5,19444444	3882,03391
4	1,84	0,7	0,5	0,002394	0,1	0,13533835	5,23333333	4505,68973
4	1,84	0,7	1,3	0,002394	0,1	0,13533835	5,27222222	4511,97751
4	1,84	0,7	1,6	0,002394	0,1	0,13533835	5,28611111	4513,07564
3	0,9	1,25	0,5	0,002988	0,1	0,10843373	5,33333333	3878,13632
3	0,9	1,25	1,3	0,002988	0,1	0,10843373	5,35	3879,84163
3	0,9	1,25	1,6	0,002988	0,1	0,10843373	5,35833333	3880,33085
3	1,84	0,7	0,5	0,002394	0,1	0,13533835	5,36111111	4506,59043
3	1,84	0,7	1,3	0,002394	0,1	0,13533835	5,39722222	4511,06983
3	1,84	0,7	1,6	0,002394	0,1	0,13533835	5,40833333	4511,83396
4	1,4	1,25	0,5	0,001188	0,1	0,27272727	5,40833333	6521,70627
4	0,9	1,5	0,5	0,002394	0,1	0,13533835	5,45	4712,47137
3	1,4	1,25	0,5	0,001188	0,1	0,27272727	5,45555556	6530,50169
4	0,9	1,5	1,3	0,002394	0,1	0,13533835	5,48888889	4719,05417
4	0,9	1,5	1,6	0,002394	0,1	0,13533835	5,50277778	4720,12432
2	1,4	1,25	0,5	0,001188	0,1	0,27272727	5,55	6538,35181
4	1,4	1,25	1,3	0,001188	0,1	0,27272727	5,56111111	6558,92123
3	0,9	1,5	0,5	0,002394	0,1	0,13533835	5,58333333	4713,64829
3	1,4	1,25	1,3	0,001188	0,1	0,27272727	5,60277778	6562,29054
4	1,4	1,25	1,6	0,001188	0,1	0,27272727	5,60555556	6566,55232
2	1,84	0,7	0,5	0,002394	0,1	0,13533835	5,61388889	4507,22906
3	0,9	1,5	1,3	0,002394	0,1	0,13533835	5,61666667	4717,45088
3	0,9	1,5	1,6	0,002394	0,1	0,13533835	5,62777778	4718,43615
2	1,84	0,7	1,3	0,002394	0,1	0,13533835	5,64166667	4508,66433
3	1,4	1,25	1,6	0,001188	0,1	0,27272727	5,64722222	6569,80242
2	1,84	0,7	1,6	0,002394	0,1	0,13533835	5,65	4508,84129
2	0,9	1,25	0,5	0,002988	0,1	0,10843373	5,66388889	3878,82182
2	0,9	1,25	1,3	0,002988	0,1	0,10843373	5,675	3878,65161
2	0,9	1,25	1,6	0,002988	0,1	0,10843373	5,68055556	3878,58602
2	1,4	1,25	1,3	0,001188	0,1	0,27272727	5,68611111	6563,2407

2	1,4	1,25	1,6	0,001188	0,1	0,27272727	5,72777778	6569,45829
4	1,84	0,7	0,5	0,002988	0,1	0,10843373	5,8	4413,60578
4	1,84	0,7	1,3	0,002988	0,1	0,10843373	5,82222222	4417,07301
4	1,84	0,7	1,6	0,002988	0,1	0,10843373	5,82777778	4417,44077
2	0,9	1,5	0,5	0,002394	0,1	0,13533835	5,84722222	4713,92802
2	0,9	1,5	1,3	0,002394	0,1	0,13533835	5,875	4715,47289
2	0,9	1,5	1,6	0,002394	0,1	0,13533835	5,88333333	4715,44348
3	1,84	0,7	0,5	0,002988	0,1	0,10843373	5,98888889	4413,44952
3	1,84	0,7	1,3	0,002988	0,1	0,10843373	6,00555556	4415,09335
3	1,84	0,7	1,6	0,002988	0,1	0,10843373	6,01111111	4415,16633
4	0,9	1,5	0,5	0,002988	0,1	0,10843373	6,03888889	4617,09293
4	0,9	1,5	1,3	0,002988	0,1	0,10843373	6,06111111	4620,65591
4	0,9	1,5	1,6	0,002988	0,1	0,10843373	6,06666667	4620,86291
3	0,9	1,5	0,5	0,002988	0,1	0,10843373	6,23333333	4616,56781
3	0,9	1,5	1,3	0,002988	0,1	0,10843373	6,25	4618,01217
3	0,9	1,5	1,6	0,002988	0,1	0,10843373	6,25555556	4617,99126
4	1,4	1,5	0,5	0,001188	0,1	0,27272727	6,34166667	7752,31255
2	1,84	0,7	0,5	0,002988	0,1	0,10843373	6,35555556	4412,71416
2	1,84	0,7	1,3	0,002988	0,1	0,10843373	6,36666667	4412,25405
2	1,84	0,7	1,6	0,002988	0,1	0,10843373	6,37222222	4412,13227
3	1,4	1,5	0,5	0,001188	0,1	0,27272727	6,39722222	7763,03201
4	1,4	1,5	1,3	0,001188	0,1	0,27272727	6,50555556	7792,28819
2	1,4	1,5	0,5	0,001188	0,1	0,27272727	6,50833333	7771,92779
3	1,4	1,5	1,3	0,001188	0,1	0,27272727	6,55555556	7796,81354
4	1,4	1,5	1,6	0,001188	0,1	0,27272727	6,55555556	7801,16673
3	1,4	1,5	1,6	0,001188	0,1	0,27272727	6,60277778	7804,08651
2	0,9	1,5	0,5	0,002988	0,1	0,10843373	6,61666667	4615,48864
2	0,9	1,5	1,3	0,002988	0,1	0,10843373	6,625	4614,69971
2	0,9	1,5	1,6	0,002988	0,1	0,10843373	6,63055556	4614,47557
2	1,4	1,5	1,3	0,001188	0,1	0,27272727	6,65555556	7798,07605
2	1,4	1,5	1,6	0,001188	0,1	0,27272727	6,69722222	7802,81378
4	1,4	1,25	0,5	0,002394	0,1	0,13533835	6,81944444	6043,41988
4	1,4	1,25	1,3	0,002394	0,1	0,13533835	6,86111111	6050,42461
4	1,84	1,25	0,5	0,001188	0,1	0,27272727	6,86944444	8454,55952
4	1,4	1,25	1,6	0,002394	0,1	0,13533835	6,87222222	6051,42002
3	1,84	1,25	0,5	0,001188	0,1	0,27272727	6,93055556	8466,1779
3	1,4	1,25	0,5	0,002394	0,1	0,13533835	6,98611111	6044,05921
3	1,4	1,25	1,3	0,002394	0,1	0,13533835	7,01944444	6047,81139
3	1,4	1,25	1,6	0,002394	0,1	0,13533835	7,03055556	6048,15874
4	1,84	1,25	1,3	0,001188	0,1	0,27272727	7,03888889	8495,65541
2	1,84	1,25	0,5	0,001188	0,1	0,27272727	7,05	8475,37019
4	1,84	1,25	1,6	0,001188	0,1	0,27272727	7,08888889	8503,95478
3	1,84	1,25	1,3	0,001188	0,1	0,27272727	7,09166667	8500,10212

3	1,84	1,25	1,6	0,001188	0,1	0,27272727	7,14166667	8507,72452
2	1,84	1,25	1,3	0,001188	0,1	0,27272727	7,2	8501,14332
2	1,84	1,25	1,6	0,001188	0,1	0,27272727	7,24444444	8506,72323
2	1,4	1,25	0,5	0,002394	0,1	0,13533835	7,31111111	6042,03562
2	1,4	1,25	1,3	0,002394	0,1	0,13533835	7,33611111	6042,4716
2	1,4	1,25	1,6	0,002394	0,1	0,13533835	7,34444444	6042,28252
4	1,4	1,25	0,5	0,002988	0,1	0,10843373	7,54722222	5925,35247
4	1,4	1,25	1,3	0,002988	0,1	0,10843373	7,56388889	5928,17518
4	1,4	1,25	1,6	0,002988	0,1	0,10843373	7,56944444	5928,21262
3	1,4	1,25	0,5	0,002988	0,1	0,10843373	7,78611111	5922,78945
3	1,4	1,25	1,3	0,002988	0,1	0,10843373	7,79722222	5923,29805
3	1,4	1,25	1,6	0,002988	0,1	0,10843373	7,80277778	5923,1298
4	1,4	1,5	0,5	0,002394	0,1	0,13533835	7,98888889	7203,8837
4	1,4	1,5	1,3	0,002394	0,1	0,13533835	8,02777778	7210,59919
4	1,4	1,5	1,6	0,002394	0,1	0,13533835	8,03888889	7211,25557
4	1,84	1,5	0,5	0,001188	0,1	0,27272727	8,06666667	10064,9833
3	1,84	1,5	0,5	0,001188	0,1	0,27272727	8,13888889	10078,2364
3	1,4	1,5	0,5	0,002394	0,1	0,13533835	8,18055556	7203,24892
3	1,4	1,5	1,3	0,002394	0,1	0,13533835	8,21111111	7206,25418
3	1,4	1,5	1,6	0,002394	0,1	0,13533835	8,21944444	7205,84496
4	1,84	1,5	1,3	0,001188	0,1	0,27272727	8,24444444	10107,774
2	1,4	1,25	0,5	0,002988	0,1	0,10843373	8,25555556	5918,01625
2	1,4	1,25	1,3	0,002988	0,1	0,10843373	8,25833333	5915,73063
2	1,4	1,25	1,6	0,002988	0,1	0,10843373	8,26111111	5915,00691
2	1,84	1,5	0,5	0,001188	0,1	0,27272727	8,28055556	10089,3286
4	1,84	1,5	1,6	0,001188	0,1	0,27272727	8,29722222	10115,8437
3	1,84	1,5	1,3	0,001188	0,1	0,27272727	8,30833333	10113,1569
3	1,84	1,5	1,6	0,001188	0,1	0,27272727	8,35833333	10119,6491
2	1,84	1,5	1,3	0,001188	0,1	0,27272727	8,43333333	10113,3529
2	1,84	1,5	1,6	0,001188	0,1	0,27272727	8,48055556	10118,6898
2	1,4	1,5	0,5	0,002394	0,1	0,13533835	8,55555556	7198,58705
2	1,4	1,5	1,3	0,002394	0,1	0,13533835	8,575	7197,54877
2	1,4	1,5	1,6	0,002394	0,1	0,13533835	8,58333333	7196,94797
4	1,84	1,25	0,5	0,002394	0,1	0,13533835	8,64444444	7864,92581
4	1,84	1,25	1,3	0,002394	0,1	0,13533835	8,68055556	7871,16873
4	1,84	1,25	1,6	0,002394	0,1	0,13533835	8,69166667	7871,52753
4	1,4	1,5	0,5	0,002988	0,1	0,10843373	8,82777778	7064,48212
4	1,4	1,5	1,3	0,002988	0,1	0,10843373	8,83888889	7066,86546
4	1,4	1,5	1,6	0,002988	0,1	0,10843373	8,84444444	7066,84694
3	1,84	1,25	0,5	0,002394	0,1	0,13533835	8,85	7863,6224
3	1,84	1,25	1,3	0,002394	0,1	0,13533835	8,87777778	7865,94696
3	1,84	1,25	1,6	0,002394	0,1	0,13533835	8,88888889	7865,98675
3	1,4	1,5	0,5	0,002988	0,1	0,10843373	9,10277778	7059,89598

3	1,4	1,5	1,3	0,002988	0,1	0,10843373	9,10833333	7059,47154
3	1,4	1,5	1,6	0,002988	0,1	0,10843373	9,11111111	7058,64561
2	1,84	1,25	0,5	0,002394	0,1	0,13533835	9,25555556	7857,63485
2	1,84	1,25	1,3	0,002394	0,1	0,13533835	9,27222222	7855,74676
2	1,84	1,25	1,6	0,002394	0,1	0,13533835	9,27777778	7854,5519
4	1,84	1,25	0,5	0,002988	0,1	0,10843373	9,54444444	7713,58268
4	1,84	1,25	1,3	0,002988	0,1	0,10843373	9,55277778	7715,4173
4	1,84	1,25	1,6	0,002988	0,1	0,10843373	9,55833333	7715,18256
2	1,4	1,5	0,5	0,002988	0,1	0,10843373	9,64166667	7050,93943
2	1,4	1,5	1,3	0,002988	0,1	0,10843373	9,64166667	7047,6122
2	1,4	1,5	1,6	0,002988	0,1	0,10843373	9,64166667	7046,14729
3	1,84	1,25	0,5	0,002988	0,1	0,10843373	9,83888889	7707,42289
3	1,84	1,25	1,3	0,002988	0,1	0,10843373	9,84444444	7706,71445
3	1,84	1,25	1,6	0,002988	0,1	0,10843373	9,84444444	7705,33047
4	1,84	1,5	0,5	0,002394	0,1	0,13533835	10,1277778	9381,25959
4	1,84	1,5	1,3	0,002394	0,1	0,13533835	10,1583333	9386,92146
4	1,84	1,5	1,6	0,002394	0,1	0,13533835	10,1694444	9386,90955
3	1,84	1,5	0,5	0,002394	0,1	0,13533835	10,3666667	9378,49963
3	1,84	1,5	1,3	0,002394	0,1	0,13533835	10,3861111	9379,08604
3	1,84	1,5	1,6	0,002394	0,1	0,13533835	10,3944444	9378,18158
2	1,84	1,25	1,6	0,002988	0,1	0,10843373	10,4111111	7689,65971
2	1,84	1,25	1,3	0,002988	0,1	0,10843373	10,4138889	7691,59712
2	1,84	1,25	0,5	0,002988	0,1	0,10843373	10,4194444	7696,07868
2	1,84	1,5	0,5	0,002394	0,1	0,13533835	10,8333333	9368,2032
2	1,84	1,5	1,3	0,002394	0,1	0,13533835	10,8416667	9363,94453
2	1,84	1,5	1,6	0,002394	0,1	0,13533835	10,8444444	9361,94171
4	1,84	1,5	0,5	0,002988	0,1	0,10843373	11,1611111	9201,27505
4	1,84	1,5	1,3	0,002988	0,1	0,10843373	11,1638889	9202,27661
4	1,84	1,5	1,6	0,002988	0,1	0,10843373	11,1638889	9201,11213
3	1,84	1,5	1,6	0,002988	0,1	0,10843373	11,4944444	9187,2467
3	1,84	1,5	1,3	0,002988	0,1	0,10843373	11,4972222	9189,28268
3	1,84	1,5	0,5	0,002988	0,1	0,10843373	11,5027778	9191,96386
2	1,84	1,5	1,6	0,002988	0,1	0,10843373	12,1472222	9163,99594
2	1,84	1,5	1,3	0,002988	0,1	0,10843373	12,15	9166,30838
2	1,84	1,5	0,5	0,002988	0,1	0,10843373	12,1638889	9172,94647

Appendix A3

Second optimization approach, discharging of the unit, airflow rate of 300m^3/h

lmpc	rmcp	cpmcp	lalu	dym	dx	dz	time	energy
4	0,9	0,7	0,5	0,001188	0,12309149	0,22156468	3,91944444	-2974,7809
3	0,9	0,7	0,5	0,001188	0,12309149	0,22156468	3,94166667	-2981,09273
2	0,9	0,7	0,5	0,001188	0,12309149	0,22156468	3,99444444	-2991,65713
4	0,9	0,7	1,3	0,001188	0,12309149	0,22156468	4,09166667	-2964,45559
3	0,9	0,7	1,3	0,001188	0,12309149	0,22156468	4,11388889	-2968,85148
4	0,9	0,7	1,6	0,001188	0,12309149	0,22156468	4,14166667	-2960,38531
2	0,9	0,7	1,3	0,001188	0,12309149	0,22156468	4,16111111	-2977,55192
3	0,9	0,7	1,6	0,001188	0,12309149	0,22156468	4,16388889	-2964,68235
2	0,9	0,7	1,6	0,001188	0,12309149	0,22156468	4,21111111	-2972,31006
4	0,9	0,7	0,5	0,002394	0,086711	0,15607979	4,88888889	-3063,37966
3	0,9	0,7	0,5	0,002394	0,086711	0,15607979	4,975	-3071,34117
4	0,9	0,7	1,3	0,002394	0,086711	0,15607979	4,98611111	-3054,64353
4	0,9	0,7	1,6	0,002394	0,086711	0,15607979	5,00833333	-3051,57547
3	0,9	0,7	1,3	0,002394	0,086711	0,15607979	5,06666667	-3062,88894
3	0,9	0,7	1,6	0,002394	0,086711	0,15607979	5,09444444	-3059,55128
2	0,9	0,7	0,5	0,002394	0,086711	0,15607979	5,15555556	-3089,7016
2	0,9	0,7	1,3	0,002394	0,086711	0,15607979	5,23888889	-3081,29751
2	0,9	0,7	1,6	0,002394	0,086711	0,15607979	5,26666667	-3078,45007
4	0,9	0,7	0,5	0,002988	0,07761505	0,13970709	5,40555556	-3125,2794
4	0,9	0,7	1,3	0,002988	0,07761505	0,13970709	5,45	-3091,73517
4	0,9	0,7	1,6	0,002988	0,07761505	0,13970709	5,46944444	-3086,25521
3	0,9	0,7	0,5	0,002988	0,07761505	0,13970709	5,53333333	-3129,92443
3	0,9	0,7	1,3	0,002988	0,07761505	0,13970709	5,6	-3122,83928
3	0,9	0,7	1,6	0,002988	0,07761505	0,13970709	5,61666667	-3118,31445
4	1,4	0,7	0,5	0,001188	0,12309149	0,22156468	5,68055556	-4548,40605
3	1,4	0,7	0,5	0,001188	0,12309149	0,22156468	5,71944444	-4559,31239
2	0,9	0,7	0,5	0,002988	0,07761505	0,13970709	5,78611111	-3138,12985
2	1,4	0,7	0,5	0,001188	0,12309149	0,22156468	5,79722222	-4573,52334
2	0,9	0,7	1,3	0,002988	0,07761505	0,13970709	5,84166667	-3131,16335
2	0,9	0,7	1,6	0,002988	0,07761505	0,13970709	5,85833333	-3128,66041
4	1,4	0,7	1,3	0,001188	0,12309149	0,22156468	5,89166667	-4522,19295
3	1,4	0,7	1,3	0,001188	0,12309149	0,22156468	5,92777778	-4530,54487
4	1,4	0,7	1,6	0,001188	0,12309149	0,22156468	5,95555556	-4515,54206
3	1,4	0,7	1,6	0,001188	0,12309149	0,22156468	6,00277778	-4535,74419
2	1,4	0,7	1,3	0,001188	0,12309149	0,22156468	6,01111111	-4555,77202
2	1,4	0,7	1,6	0,001188	0,12309149	0,22156468	6,07222222	-4548,59365

4	0,9	1,25	0,5	0,001188	0,12309149	0,22156468	6,39444444	-5201,36131
3	0,9	1,25	0,5	0,001188	0,12309149	0,22156468	6,43888889	-5214,16343
2	0,9	1,25	0,5	0,001188	0,12309149	0,22156468	6,52777778	-5231,34885
4	0,9	1,25	1,3	0,001188	0,12309149	0,22156468	6,63333333	-5188,97068
3	0,9	1,25	1,3	0,001188	0,12309149	0,22156468	6,675	-5196,14476
4	0,9	1,25	1,6	0,001188	0,12309149	0,22156468	6,69166667	-5164,94176
3	0,9	1,25	1,6	0,001188	0,12309149	0,22156468	6,74444444	-5188,46104
2	0,9	1,25	1,3	0,001188	0,12309149	0,22156468	6,75555556	-5211,4364
2	0,9	1,25	1,6	0,001188	0,12309149	0,22156468	6,825	-5202,97265
4	1,4	0,7	0,5	0,002394	0,086711	0,15607979	7,14444444	-4730,36923
4	1,84	0,7	0,5	0,001188	0,12309149	0,22156468	7,18611111	-5936,63692
3	1,84	0,7	0,5	0,001188	0,12309149	0,22156468	7,23611111	-5949,97794
4	1,4	0,7	1,3	0,002394	0,086711	0,15607979	7,25555556	-4717,87529
3	1,4	0,7	0,5	0,002394	0,086711	0,15607979	7,275	-4743,56754
4	1,4	0,7	1,6	0,002394	0,086711	0,15607979	7,28611111	-4712,8617
2	1,84	0,7	0,5	0,001188	0,12309149	0,22156468	7,33888889	-5971,24182
3	1,4	0,7	1,3	0,002394	0,086711	0,15607979	7,38055556	-4731,32377
3	1,4	0,7	1,6	0,002394	0,086711	0,15607979	7,41388889	-4726,48666
4	1,84	0,7	1,3	0,001188	0,12309149	0,22156468	7,43055556	-5904,35165
4	0,9	1,5	0,5	0,001188	0,12309149	0,22156468	7,48333333	-6216,60601
3	1,84	0,7	1,3	0,001188	0,12309149	0,22156468	7,48888889	-5931,94794
4	1,84	0,7	1,6	0,001188	0,12309149	0,22156468	7,51944444	-5914,71331
3	0,9	1,5	0,5	0,001188	0,12309149	0,22156468	7,53888889	-6230,61353
2	1,4	0,7	0,5	0,002394	0,086711	0,15607979	7,54166667	-4772,83479
3	1,84	0,7	1,6	0,001188	0,12309149	0,22156468	7,56388889	-5923,32
2	1,84	0,7	1,3	0,001188	0,12309149	0,22156468	7,58333333	-5948,42244
2	1,4	0,7	1,3	0,002394	0,086711	0,15607979	7,63888889	-4760,89583
2	0,9	1,5	0,5	0,001188	0,12309149	0,22156468	7,64722222	-6252,99955
2	1,84	0,7	1,6	0,001188	0,12309149	0,22156468	7,65555556	-5940,15956
2	1,4	0,7	1,6	0,002394	0,086711	0,15607979	7,66944444	-4755,96669
4	0,9	1,5	1,3	0,001188	0,12309149	0,22156468	7,75	-6202,317
3	0,9	1,5	1,3	0,001188	0,12309149	0,22156468	7,79722222	-6211,8767
4	0,9	1,5	1,6	0,001188	0,12309149	0,22156468	7,82777778	-6194,0755
3	0,9	1,5	1,6	0,001188	0,12309149	0,22156468	7,87222222	-6203,2592
2	0,9	1,5	1,3	0,001188	0,12309149	0,22156468	7,89444444	-6229,38989
4	1,4	0,7	0,5	0,002988	0,07761505	0,13970709	7,90833333	-4834,69264
4	1,4	0,7	1,3	0,002988	0,07761505	0,13970709	7,93888889	-4782,83947
4	1,4	0,7	1,6	0,002988	0,07761505	0,13970709	7,95555556	-4775,65031
2	0,9	1,5	1,6	0,001188	0,12309149	0,22156468	7,96944444	-6220,29034
4	0,9	1,25	0,5	0,002394	0,086711	0,15607979	8,05	-5421,64828
3	1,4	0,7	0,5	0,002988	0,07761505	0,13970709	8,09444444	-4843,13282
3	1,4	0,7	1,3	0,002988	0,07761505	0,13970709	8,16111111	-4833,24914
4	0,9	1,25	1,3	0,002394	0,086711	0,15607979	8,16388889	-5407,43367

3	1,4	0,7	1,6	0,002988	0,07761505	0,13970709	8,17777778	-4826,20947
3	0,9	1,25	0,5	0,002394	0,086711	0,15607979	8,2	-5436,75244
4	0,9	1,25	1,6	0,002394	0,086711	0,15607979	8,2	-5401,73498
3	0,9	1,25	1,3	0,002394	0,086711	0,15607979	8,30833333	-5423,22737
3	0,9	1,25	1,6	0,002394	0,086711	0,15607979	8,34166667	-5417,9278
2	1,4	0,7	0,5	0,002988	0,07761505	0,13970709	8,46388889	-4856,63355
2	0,9	1,25	0,5	0,002394	0,086711	0,15607979	8,49722222	-5470,91324
2	1,4	0,7	1,3	0,002988	0,07761505	0,13970709	8,52222222	-4846,6232
2	1,4	0,7	1,6	0,002988	0,07761505	0,13970709	8,54166667	-4842,90627
2	0,9	1,25	1,3	0,002394	0,086711	0,15607979	8,6	-5457,03298
2	0,9	1,25	1,6	0,002394	0,086711	0,15607979	8,63055556	-5452,23391
4	0,9	1,25	0,5	0,002988	0,07761505	0,13970709	8,90833333	-5543,64335
4	0,9	1,25	1,3	0,002988	0,07761505	0,13970709	8,93055556	-5484,43143
4	0,9	1,25	1,6	0,002988	0,07761505	0,13970709	8,95	-5475,73028
4	1,84	0,7	0,5	0,002394	0,086711	0,15607979	9,05277778	-6198,87405
3	0,9	1,25	0,5	0,002988	0,07761505	0,13970709	9,11944444	-5553,54834
4	1,84	0,7	1,3	0,002394	0,086711	0,15607979	9,16944444	-6183,07806
3	0,9	1,25	1,3	0,002988	0,07761505	0,13970709	9,18611111	-5542,52362
3	0,9	1,25	1,6	0,002988	0,07761505	0,13970709	9,20277778	-5534,39844
4	1,84	0,7	1,6	0,002394	0,086711	0,15607979	9,20555556	-6176,95597
3	1,84	0,7	0,5	0,002394	0,086711	0,15607979	9,21944444	-6217,28023
3	1,84	0,7	1,3	0,002394	0,086711	0,15607979	9,33055556	-6201,76329
3	1,84	0,7	1,6	0,002394	0,086711	0,15607979	9,36666667	-6195,25985
4	1,4	1,25	0,5	0,001188	0,12309149	0,22156468	9,38611111	-8023,68156
4	0,9	1,5	0,5	0,002394	0,086711	0,15607979	9,43055556	-6494,91765
3	1,4	1,25	0,5	0,001188	0,12309149	0,22156468	9,45555556	-8042,01043
2	0,9	1,25	0,5	0,002988	0,07761505	0,13970709	9,53055556	-5569,00142
4	0,9	1,5	1,3	0,002394	0,086711	0,15607979	9,54722222	-6478,04616
2	1,84	0,7	0,5	0,002394	0,086711	0,15607979	9,55555556	-6256,09172
4	0,9	1,5	1,6	0,002394	0,086711	0,15607979	9,58333333	-6471,6788
2	0,9	1,25	1,3	0,002988	0,07761505	0,13970709	9,59166667	-5557,50505
2	1,4	1,25	0,5	0,001188	0,12309149	0,22156468	9,59166667	-8070,47498
3	0,9	1,5	0,5	0,002394	0,086711	0,15607979	9,60277778	-6514,16138
2	0,9	1,25	1,6	0,002988	0,07761505	0,13970709	9,61111111	-5553,50749
2	1,84	0,7	1,3	0,002394	0,086711	0,15607979	9,66111111	-6240,6533
4	1,4	1,25	1,3	0,001188	0,12309149	0,22156468	9,68611111	-8007,87751
2	1,84	0,7	1,6	0,002394	0,086711	0,15607979	9,69166667	-6235,03267
3	0,9	1,5	1,3	0,002394	0,086711	0,15607979	9,71666667	-6497,60622
3	1,4	1,25	1,3	0,001188	0,12309149	0,22156468	9,74722222	-8020,1588
3	0,9	1,5	1,6	0,002394	0,086711	0,15607979	9,75277778	-6491,22205
4	1,4	1,25	1,6	0,001188	0,12309149	0,22156468	9,775	-7997,42091
3	1,4	1,25	1,6	0,001188	0,12309149	0,22156468	9,83333333	-8009,5579
2	1,4	1,25	1,3	0,001188	0,12309149	0,22156468	9,86944444	-8043,12848

2	0,9	1,5	0,5	0,002394	0,086711	0,15607979	9,95555556	-6554,73422
2	1,4	1,25	1,6	0,001188	0,12309149	0,22156468	9,95555556	-8032,15336
4	1,84	0,7	0,5	0,002988	0,07761505	0,13970709	10,0138889	-6339,88187
4	1,84	0,7	1,3	0,002988	0,07761505	0,13970709	10,0277778	-6272,51466
4	1,84	0,7	1,6	0,002988	0,07761505	0,13970709	10,0472222	-6262,83474
2	0,9	1,5	1,3	0,002394	0,086711	0,15607979	10,0583333	-6538,39308
2	0,9	1,5	1,6	0,002394	0,086711	0,15607979	10,0916667	-6532,66739
3	1,84	0,7	0,5	0,002988	0,07761505	0,13970709	10,2527778	-6352,57326
3	1,84	0,7	1,3	0,002988	0,07761505	0,13970709	10,3166667	-6339,74141
3	1,84	0,7	1,6	0,002988	0,07761505	0,13970709	10,3333333	-6330,59429
4	0,9	1,5	0,5	0,002988	0,07761505	0,13970709	10,4305556	-6643,01845
4	0,9	1,5	1,3	0,002988	0,07761505	0,13970709	10,4416667	-6572,0766
4	0,9	1,5	1,6	0,002988	0,07761505	0,13970709	10,4583333	-6562,17127
3	0,9	1,5	0,5	0,002988	0,07761505	0,13970709	10,6777778	-6656,25798
2	1,84	0,7	0,5	0,002988	0,07761505	0,13970709	10,7138889	-6370,01191
3	0,9	1,5	1,3	0,002988	0,07761505	0,13970709	10,7416667	-6642,99847
3	0,9	1,5	1,6	0,002988	0,07761505	0,13970709	10,7583333	-6633,31805
2	1,84	0,7	1,3	0,002988	0,07761505	0,13970709	10,7694444	-6356,92114
2	1,84	0,7	1,6	0,002988	0,07761505	0,13970709	10,7888889	-6352,47933
4	1,4	1,5	0,5	0,001188	0,12309149	0,22156468	11,0138889	-9607,36581
3	1,4	1,5	0,5	0,001188	0,12309149	0,22156468	11,0972222	-9629,46461
2	0,9	1,5	0,5	0,002988	0,07761505	0,13970709	11,1555556	-6674,78505
2	0,9	1,5	1,3	0,002988	0,07761505	0,13970709	11,2138889	-6661,113
2	0,9	1,5	1,6	0,002988	0,07761505	0,13970709	11,2333333	-6656,15094
2	1,4	1,5	0,5	0,001188	0,12309149	0,22156468	11,2583333	-9664,02832
4	1,4	1,5	1,3	0,001188	0,12309149	0,22156468	11,3416667	-9589,81897
3	1,4	1,5	1,3	0,001188	0,12309149	0,22156468	11,4138889	-9604,67213
4	1,4	1,5	1,6	0,001188	0,12309149	0,22156468	11,4361111	-9578,42333
3	1,4	1,5	1,6	0,001188	0,12309149	0,22156468	11,5083333	-9592,64
2	1,4	1,5	1,3	0,001188	0,12309149	0,22156468	11,5611111	-9632,70401
2	1,4	1,5	1,6	0,001188	0,12309149	0,22156468	11,6527778	-9619,99087
4	1,4	1,25	0,5	0,002394	0,086711	0,15607979	11,8166667	-8403,98365
4	1,84	1,25	0,5	0,001188	0,12309149	0,22156468	11,9333333	-10512,7649
4	1,4	1,25	1,3	0,002394	0,086711	0,15607979	11,9361111	-8382,76701
4	1,4	1,25	1,6	0,002394	0,086711	0,15607979	11,975	-8374,2116
3	1,84	1,25	0,5	0,001188	0,12309149	0,22156468	12,025	-10536,8005
3	1,4	1,25	0,5	0,002394	0,086711	0,15607979	12,0333333	-8429,28955
3	1,4	1,25	1,3	0,002394	0,086711	0,15607979	12,15	-8408,65273
3	1,4	1,25	1,6	0,002394	0,086711	0,15607979	12,1861111	-8400,0314
2	1,84	1,25	0,5	0,001188	0,12309149	0,22156468	12,2	-10574,847
4	1,84	1,25	1,3	0,001188	0,12309149	0,22156468	12,275	-10494,416
3	1,84	1,25	1,3	0,001188	0,12309149	0,22156468	12,3527778	-10511,2957
4	1,84	1,25	1,6	0,001188	0,12309149	0,22156468	12,3722222	-10482,1696

3	1,84	1,25	1,6	0,001188	0,12309149	0,22156468	12,45	-10498,0664
2	1,4	1,25	0,5	0,002394	0,086711	0,15607979	12,475	-8482,25713
2	1,84	1,25	1,3	0,001188	0,12309149	0,22156468	12,5111111	-10541,9188
2	1,4	1,25	1,3	0,002394	0,086711	0,15607979	12,5777778	-8461,49647
2	1,84	1,25	1,6	0,001188	0,12309149	0,22156468	12,6055556	-10528,2802
2	1,4	1,25	1,6	0,002394	0,086711	0,15607979	12,6111111	-8454,25178
4	1,4	1,25	1,3	0,002988	0,07761505	0,13970709	13,0416667	-8506,12802
4	1,4	1,25	0,5	0,002988	0,07761505	0,13970709	13,0555556	-8597,9813
4	1,4	1,25	1,6	0,002988	0,07761505	0,13970709	13,0555556	-8493,0437
3	1,4	1,25	0,5	0,002988	0,07761505	0,13970709	13,3583333	-8616,30551
3	1,4	1,25	1,3	0,002988	0,07761505	0,13970709	13,4194444	-8599,1181
3	1,4	1,25	1,6	0,002988	0,07761505	0,13970709	13,4333333	-8586,46367
4	1,4	1,5	0,5	0,002394	0,086711	0,15607979	13,8444444	-10075,0118
2	1,4	1,25	0,5	0,002988	0,07761505	0,13970709	13,9583333	-8640,01596
4	1,4	1,5	1,3	0,002394	0,086711	0,15607979	13,9666667	-10049,4301
4	1,4	1,5	1,6	0,002394	0,086711	0,15607979	14,0027778	-10039,0953
2	1,4	1,25	1,3	0,002988	0,07761505	0,13970709	14,0055556	-8622,32299
4	1,84	1,5	0,5	0,001188	0,12309149	0,22156468	14,0194444	-12597,6701
2	1,4	1,25	1,6	0,002988	0,07761505	0,13970709	14,0222222	-8616,01189
3	1,4	1,5	0,5	0,002394	0,086711	0,15607979	14,1027778	-10105,8864
3	1,84	1,5	0,5	0,001188	0,12309149	0,22156468	14,1277778	-12626,4135
3	1,4	1,5	1,3	0,002394	0,086711	0,15607979	14,2166667	-10080,6771
3	1,4	1,5	1,6	0,002394	0,086711	0,15607979	14,25	-10070,97
2	1,84	1,5	0,5	0,001188	0,12309149	0,22156468	14,3333333	-12672,3076
4	1,84	1,5	1,3	0,001188	0,12309149	0,22156468	14,3833333	-12577,7672
3	1,84	1,5	1,3	0,001188	0,12309149	0,22156468	14,4777778	-12597,7669
4	1,84	1,5	1,6	0,001188	0,12309149	0,22156468	14,4916667	-12563,4509
3	1,84	1,5	1,6	0,001188	0,12309149	0,22156468	14,5833333	-12582,6163
2	1,4	1,5	0,5	0,002394	0,086711	0,15607979	14,6166667	-10169,2595
2	1,84	1,5	1,3	0,001188	0,12309149	0,22156468	14,6666667	-12634,7477
2	1,4	1,5	1,3	0,002394	0,086711	0,15607979	14,7166667	-10144,7826
2	1,4	1,5	1,6	0,002394	0,086711	0,15607979	14,75	-10135,7156
2	1,84	1,5	1,6	0,001188	0,12309149	0,22156468	14,7666667	-12618,9175
4	1,84	1,25	0,5	0,002394	0,086711	0,15607979	14,9861111	-11029,9263
4	1,84	1,25	1,3	0,002394	0,086711	0,15607979	15,1055556	-11001,7894
4	1,84	1,25	1,6	0,002394	0,086711	0,15607979	15,1416667	-10990,5955
4	1,4	1,5	1,3	0,002988	0,07761505	0,13970709	15,2472222	-10197,4247
4	1,4	1,5	1,6	0,002988	0,07761505	0,13970709	15,2583333	-10181,9163
3	1,84	1,25	0,5	0,002394	0,086711	0,15607979	15,2638889	-11063,8186
4	1,4	1,5	0,5	0,002988	0,07761505	0,13970709	15,2805556	-10308,1528
3	1,84	1,25	1,3	0,002394	0,086711	0,15607979	15,375	-11036,2148
3	1,84	1,25	1,6	0,002394	0,086711	0,15607979	15,4083333	-11025,4326
3	1,4	1,5	0,5	0,002988	0,07761505	0,13970709	15,6388889	-10330,6373

3	1,4	1,5	1,3	0,002988	0,07761505	0,13970709	15,6888889	-10309,8244
3	1,4	1,5	1,6	0,002988	0,07761505	0,13970709	15,7	-10294,4252
2	1,84	1,25	0,5	0,002394	0,086711	0,15607979	15,8222222	-11133,2077
2	1,84	1,25	1,3	0,002394	0,086711	0,15607979	15,9166667	-11106,3695
2	1,84	1,25	1,6	0,002394	0,086711	0,15607979	15,9472222	-11096,4327
2	1,4	1,5	0,5	0,002988	0,07761505	0,13970709	16,3361111	-10358,7345
2	1,4	1,5	1,3	0,002988	0,07761505	0,13970709	16,3722222	-10337,1393
2	1,4	1,5	1,6	0,002988	0,07761505	0,13970709	16,3861111	-10329,5302
4	1,84	1,25	1,3	0,002988	0,07761505	0,13970709	16,4833333	-11163,3968
4	1,84	1,25	1,6	0,002988	0,07761505	0,13970709	16,4916667	-11146,1165
4	1,84	1,25	0,5	0,002988	0,07761505	0,13970709	16,5305556	-11284,9315
3	1,84	1,25	0,5	0,002988	0,07761505	0,13970709	16,9194444	-11309,6749
3	1,84	1,25	1,3	0,002988	0,07761505	0,13970709	16,9611111	-11286,5617
3	1,84	1,25	1,6	0,002988	0,07761505	0,13970709	16,9694444	-11269,7812
4	1,84	1,5	0,5	0,002394	0,086711	0,15607979	17,5666667	-13225,5845
2	1,84	1,25	0,5	0,002988	0,07761505	0,13970709	17,6694444	-11340,2478
4	1,84	1,5	1,3	0,002394	0,086711	0,15607979	17,6722222	-13191,2466
2	1,84	1,25	1,3	0,002988	0,07761505	0,13970709	17,6972222	-11316,3782
2	1,84	1,25	1,6	0,002988	0,07761505	0,13970709	17,7083333	-11308,0772
4	1,84	1,5	1,6	0,002394	0,086711	0,15607979	17,7083333	-13177,7069
3	1,84	1,5	0,5	0,002394	0,086711	0,15607979	17,8916667	-13266,6061
3	1,84	1,5	1,3	0,002394	0,086711	0,15607979	17,9888889	-13233,1213
3	1,84	1,5	1,6	0,002394	0,086711	0,15607979	18,0222222	-13220,0325
2	1,84	1,5	0,5	0,002394	0,086711	0,15607979	18,5388889	-13349,851
2	1,84	1,5	1,3	0,002394	0,086711	0,15607979	18,6222222	-13316,9857
2	1,84	1,5	1,6	0,002394	0,086711	0,15607979	18,65	-13305,1019
4	1,84	1,5	1,3	0,002988	0,07761505	0,13970709	19,2666667	-13382,9083
4	1,84	1,5	1,6	0,002988	0,07761505	0,13970709	19,2666667	-13361,9197
4	1,84	1,5	0,5	0,002988	0,07761505	0,13970709	19,3527778	-13529,7808
3	1,84	1,5	0,5	0,002988	0,07761505	0,13970709	19,8027778	-13560,1758
3	1,84	1,5	1,3	0,002988	0,07761505	0,13970709	19,825	-13531,5647
3	1,84	1,5	1,6	0,002988	0,07761505	0,13970709	19,8277778	-13511,0897
2	1,84	1,5	0,5	0,002988	0,07761505	0,13970709	20,6694444	-13595,9078
2	1,84	1,5	1,3	0,002988	0,07761505	0,13970709	20,6777778	-13566,3011
2	1,84	1,5	1,6	0,002988	0,07761505	0,13970709	20,6833333	-13555,9734

Appendix A4

Second optimization approach, discharging of the unit, airflow rate of 500m^3/h

lmpc	rmcp	cpmcp	lalu	dym	dx	dz	time	energy
3	0,9	0,7	0,5	0,001188	0,15151515	0,18	2,77777778	-3129,93354
4	0,9	0,7	0,5	0,001188	0,15151515	0,18	2,77777778	-3117,60215
4	0,9	0,7	1,3	0,001188	0,15151515	0,18	2,78333333	-3126,97305
2	0,9	0,7	0,5	0,001188	0,15151515	0,18	2,80277778	-3146,56144
4	0,9	0,7	1,6	0,001188	0,15151515	0,18	2,80277778	-3125,29714
3	0,9	0,7	1,3	0,001188	0,15151515	0,18	2,80833333	-3133,43984
3	0,9	0,7	1,6	0,001188	0,15151515	0,18	2,82777778	-3134,06485
2	0,9	0,7	1,3	0,001188	0,15151515	0,18	2,86111111	-3146,67889
2	0,9	0,7	1,6	0,001188	0,15151515	0,18	2,88055556	-3146,353
4	0,9	0,7	0,5	0,002394	0,07518797	0,18	3,61944444	-3162,91918
4	0,9	0,7	1,3	0,002394	0,07518797	0,18	3,66666667	-3158,52281
4	0,9	0,7	1,6	0,002394	0,07518797	0,18	3,68055556	-3156,53257
3	0,9	0,7	0,5	0,002394	0,07518797	0,18	3,70833333	-3174,46447
3	0,9	0,7	1,3	0,002394	0,07518797	0,18	3,75	-3170,39114
3	0,9	0,7	1,6	0,002394	0,07518797	0,18	3,76388889	-3168,57539
2	0,9	0,7	0,5	0,002394	0,07518797	0,18	3,89166667	-3200,68513
2	0,9	0,7	1,3	0,002394	0,07518797	0,18	3,92777778	-3195,89855
2	0,9	0,7	1,6	0,002394	0,07518797	0,18	3,93888889	-3194,06827
4	1,4	0,7	0,5	0,001188	0,15151515	0,18	3,94444444	-4766,54194
3	1,4	0,7	0,5	0,001188	0,15151515	0,18	3,98888889	-4781,06113
4	1,4	0,7	1,3	0,001188	0,15151515	0,18	4,02777778	-4773,34584
4	1,4	0,7	1,6	0,001188	0,15151515	0,18	4,05277778	-4771,62075
3	1,4	0,7	1,3	0,001188	0,15151515	0,18	4,06666667	-4784,34603
2	1,4	0,7	0,5	0,001188	0,15151515	0,18	4,07222222	-4805,04764
3	1,4	0,7	1,6	0,001188	0,15151515	0,18	4,09166667	-4783,43324
2	1,4	0,7	1,3	0,001188	0,15151515	0,18	4,14444444	-4802,72616
2	1,4	0,7	1,6	0,001188	0,15151515	0,18	4,16944444	-4803,03879
4	0,9	0,7	1,6	0,002988	0,06024096	0,18	4,3	-3416,18088
4	0,9	0,7	1,3	0,002988	0,06024096	0,18	4,30555556	-3428,87344
3	0,9	0,7	0,5	0,002988	0,06024096	0,18	4,33055556	-3359,65644
3	0,9	0,7	1,3	0,002988	0,06024096	0,18	4,33333333	-3329,41802
3	0,9	0,7	1,6	0,002988	0,06024096	0,18	4,33888889	-3324,10109
4	0,9	1,25	0,5	0,001188	0,15151515	0,18	4,44166667	-5448,35467
2	0,9	0,7	0,5	0,002988	0,06024096	0,18	4,475	-3253,53777
3	0,9	1,25	0,5	0,001188	0,15151515	0,18	4,49166667	-5464,58815
2	0,9	0,7	1,3	0,002988	0,06024096	0,18	4,50555556	-3249,50488

2	0,9	0,7	1,6	0,002988	0,06024096	0,18	4,50833333	-3248,37371
4	0,9	1,25	1,3	0,001188	0,15151515	0,18	4,52777778	-5454,76553
4	0,9	1,25	1,6	0,001188	0,15151515	0,18	4,55555556	-5455,29759
3	0,9	1,25	1,3	0,001188	0,15151515	0,18	4,575	-5469,68741
2	0,9	1,25	0,5	0,001188	0,15151515	0,18	4,58611111	-5491,39319
3	0,9	1,25	1,6	0,001188	0,15151515	0,18	4,6	-5467,67968
2	0,9	1,25	1,3	0,001188	0,15151515	0,18	4,66388889	-5491,47961
4	0,9	0,7	0,5	0,002988	0,06024096	0,18	4,66388889	-3630,77828
2	0,9	1,25	1,6	0,001188	0,15151515	0,18	4,68888889	-5489,19899
4	1,84	0,7	0,5	0,001188	0,15151515	0,18	4,99166667	-6213,90236
3	1,84	0,7	0,5	0,001188	0,15151515	0,18	5,05	-6234,84716
4	1,84	0,7	1,3	0,001188	0,15151515	0,18	5,08611111	-6223,84718
4	1,84	0,7	1,6	0,001188	0,15151515	0,18	5,11666667	-6221,74528
3	1,84	0,7	1,3	0,001188	0,15151515	0,18	5,13888889	-6239,49298
2	1,84	0,7	0,5	0,001188	0,15151515	0,18	5,15555556	-6263,851
3	1,84	0,7	1,6	0,001188	0,15151515	0,18	5,16666667	-6238,10351
4	0,9	1,5	0,5	0,001188	0,15151515	0,18	5,2	-6506,95097
2	1,84	0,7	1,3	0,001188	0,15151515	0,18	5,23888889	-6264,41417
3	0,9	1,5	0,5	0,001188	0,15151515	0,18	5,25833333	-6527,4394
2	1,84	0,7	1,6	0,001188	0,15151515	0,18	5,26388889	-6261,74967
4	1,4	0,7	0,5	0,002394	0,07518797	0,18	5,28333333	-4879,73679
4	0,9	1,5	1,3	0,001188	0,15151515	0,18	5,29722222	-6516,03897
4	0,9	1,5	1,6	0,001188	0,15151515	0,18	5,32777778	-6514,71781
4	1,4	0,7	1,3	0,002394	0,07518797	0,18	5,33055556	-4872,69686
4	1,4	0,7	1,6	0,002394	0,07518797	0,18	5,34722222	-4868,60783
3	0,9	1,5	1,3	0,001188	0,15151515	0,18	5,35	-6531,30231
2	0,9	1,5	0,5	0,001188	0,15151515	0,18	5,37222222	-6557,52067
3	0,9	1,5	1,6	0,001188	0,15151515	0,18	5,38055556	-6530,06002
3	1,4	0,7	0,5	0,002394	0,07518797	0,18	5,41666667	-4897,73858
2	0,9	1,5	1,3	0,001188	0,15151515	0,18	5,45555556	-6558,33842
3	1,4	0,7	1,3	0,002394	0,07518797	0,18	5,46111111	-4891,01815
3	1,4	0,7	1,6	0,002394	0,07518797	0,18	5,475	-4888,16894
2	0,9	1,5	1,6	0,001188	0,15151515	0,18	5,48333333	-6556,85575
2	1,4	0,7	0,5	0,002394	0,07518797	0,18	5,68055556	-4936,99707
2	1,4	0,7	1,3	0,002394	0,07518797	0,18	5,72222222	-4930,0881
2	1,4	0,7	1,6	0,002394	0,07518797	0,18	5,73611111	-4927,55112
4	0,9	1,25	0,5	0,002394	0,07518797	0,18	5,95	-5590,97266
4	0,9	1,25	1,3	0,002394	0,07518797	0,18	6	-5583,19768
4	0,9	1,25	1,6	0,002394	0,07518797	0,18	6,01388889	-5578,40541
3	0,9	1,25	0,5	0,002394	0,07518797	0,18	6,1	-5611,61731
3	0,9	1,25	1,3	0,002394	0,07518797	0,18	6,14444444	-5604,48033
3	0,9	1,25	1,6	0,002394	0,07518797	0,18	6,16111111	-5600,83649
4	1,4	0,7	1,6	0,002988	0,06024096	0,18	6,27777778	-5277,19241

4	1,4	0,7	1,3	0,002988	0,06024096	0,18	6,28333333	-5295,8924
3	1,4	0,7	1,6	0,002988	0,06024096	0,18	6,31388889	-5136,98108
3	1,4	0,7	1,3	0,002988	0,06024096	0,18	6,31944444	-5145,08515
3	1,4	0,7	0,5	0,002988	0,06024096	0,18	6,32777778	-5191,41966
2	0,9	1,25	0,5	0,002394	0,07518797	0,18	6,39722222	-5657,01625
2	0,9	1,25	1,3	0,002394	0,07518797	0,18	6,43888889	-5649,14673
2	0,9	1,25	1,6	0,002394	0,07518797	0,18	6,45277778	-5646,25564
4	1,4	1,25	0,5	0,001188	0,15151515	0,18	6,52222222	-8388,98985
2	1,4	0,7	0,5	0,002988	0,06024096	0,18	6,53333333	-5028,11131
2	1,4	0,7	1,3	0,002988	0,06024096	0,18	6,55	-5023,50983
2	1,4	0,7	1,6	0,002988	0,06024096	0,18	6,55833333	-5021,43612
3	1,4	1,25	0,5	0,001188	0,15151515	0,18	6,59722222	-8417,41976
4	1,4	1,25	1,3	0,001188	0,15151515	0,18	6,63333333	-8401,73555
4	1,4	1,25	1,6	0,001188	0,15151515	0,18	6,66666667	-8401,71645
4	1,84	0,7	0,5	0,002394	0,07518797	0,18	6,68611111	-6390,93608
3	1,4	1,25	1,3	0,001188	0,15151515	0,18	6,70277778	-8423,38137
3	1,4	1,25	1,6	0,001188	0,15151515	0,18	6,73333333	-8420,13347
4	1,84	0,7	1,3	0,002394	0,07518797	0,18	6,73611111	-6381,42098
2	1,4	1,25	0,5	0,001188	0,15151515	0,18	6,73888889	-8458,0561
4	1,84	0,7	1,6	0,002394	0,07518797	0,18	6,75277778	-6376,08946
2	1,4	1,25	1,3	0,001188	0,15151515	0,18	6,83333333	-8457,08357
4	1,4	0,7	0,5	0,002988	0,06024096	0,18	6,83333333	-5606,13224
3	1,84	0,7	0,5	0,002394	0,07518797	0,18	6,85277778	-6414,51635
2	1,4	1,25	1,6	0,001188	0,15151515	0,18	6,86388889	-8455,10851
3	1,84	0,7	1,3	0,002394	0,07518797	0,18	6,9	-6406,35681
3	1,84	0,7	1,6	0,002394	0,07518797	0,18	6,91666667	-6402,22575
4	0,9	1,5	0,5	0,002394	0,07518797	0,18	6,96388889	-6695,22083
4	0,9	1,5	1,3	0,002394	0,07518797	0,18	7,01388889	-6684,80986
4	0,9	1,5	1,6	0,002394	0,07518797	0,18	7,03055556	-6679,54269
4	0,9	1,25	1,6	0,002988	0,06024096	0,18	7,05833333	-6048,73136
4	0,9	1,25	1,3	0,002988	0,06024096	0,18	7,07777778	-6069,88252
3	0,9	1,25	1,3	0,002988	0,06024096	0,18	7,10277778	-5897,27061
3	0,9	1,25	1,6	0,002988	0,06024096	0,18	7,10555556	-5887,84693
3	0,9	1,25	0,5	0,002988	0,06024096	0,18	7,12777778	-5950,47458
3	0,9	1,5	0,5	0,002394	0,07518797	0,18	7,13333333	-6719,94171
3	0,9	1,5	1,3	0,002394	0,07518797	0,18	7,18611111	-6711,41992
2	1,84	0,7	0,5	0,002394	0,07518797	0,18	7,18888889	-6466,33241
3	0,9	1,5	1,6	0,002394	0,07518797	0,18	7,2	-6707,62335
2	1,84	0,7	1,3	0,002394	0,07518797	0,18	7,23055556	-6457,59803
2	1,84	0,7	1,6	0,002394	0,07518797	0,18	7,24722222	-6454,00424
2	0,9	1,25	0,5	0,002988	0,06024096	0,18	7,35277778	-5763,48962
2	0,9	1,25	1,3	0,002988	0,06024096	0,18	7,36944444	-5758,28181
2	0,9	1,25	1,6	0,002988	0,06024096	0,18	7,37777778	-5755,87458

2	0,9	1,5	0,5	0,002394	0,07518797	0,18	7,48611111	-6774,25411
2	0,9	1,5	1,3	0,002394	0,07518797	0,18	7,53055556	-6765,2466
2	0,9	1,5	1,6	0,002394	0,07518797	0,18	7,54444444	-6761,38768
4	1,4	1,5	0,5	0,001188	0,15151515	0,18	7,65833333	-10038,9453
4	0,9	1,25	0,5	0,002988	0,06024096	0,18	7,70277778	-6424,53316
3	1,4	1,5	0,5	0,001188	0,15151515	0,18	7,74444444	-10070,5118
4	1,4	1,5	1,3	0,001188	0,15151515	0,18	7,77777778	-10054,6101
4	1,4	1,5	1,6	0,001188	0,15151515	0,18	7,81388889	-10053,5856
3	1,4	1,5	1,3	0,001188	0,15151515	0,18	7,85833333	-10079,5573
3	1,4	1,5	1,6	0,001188	0,15151515	0,18	7,89444444	-10077,4039
2	1,4	1,5	0,5	0,001188	0,15151515	0,18	7,91111111	-10121,1586
4	1,84	0,7	1,6	0,002988	0,06024096	0,18	7,91944444	-6915,37649
4	1,84	0,7	1,3	0,002988	0,06024096	0,18	7,93611111	-6940,05595
3	1,84	0,7	1,3	0,002988	0,06024096	0,18	7,975	-6743,30766
3	1,84	0,7	1,6	0,002988	0,06024096	0,18	7,975	-6732,22627
3	1,84	0,7	0,5	0,002988	0,06024096	0,18	8,00833333	-6803,24566
2	1,4	1,5	1,3	0,001188	0,15151515	0,18	8,01388889	-10120,6285
2	1,4	1,5	1,6	0,001188	0,15151515	0,18	8,04722222	-10117,1854
4	0,9	1,5	1,6	0,002988	0,06024096	0,18	8,24444444	-7244,53921
2	1,84	0,7	0,5	0,002988	0,06024096	0,18	8,25	-6590,45196
4	0,9	1,5	1,3	0,002988	0,06024096	0,18	8,26111111	-7270,67955
2	1,84	0,7	1,3	0,002988	0,06024096	0,18	8,27222222	-6583,83976
2	1,84	0,7	1,6	0,002988	0,06024096	0,18	8,28055556	-6581,55647
4	1,84	1,25	0,5	0,001188	0,15151515	0,18	8,29722222	-10981,7975
3	0,9	1,5	1,3	0,002988	0,06024096	0,18	8,30277778	-7064,92127
3	0,9	1,5	1,6	0,002988	0,06024096	0,18	8,30277778	-7053,36702
3	0,9	1,5	0,5	0,002988	0,06024096	0,18	8,34166667	-7127,6522
3	1,84	1,25	0,5	0,001188	0,15151515	0,18	8,39166667	-11017,8049
4	1,84	1,25	1,3	0,001188	0,15151515	0,18	8,425	-10999,6922
4	1,84	1,25	1,6	0,001188	0,15151515	0,18	8,46111111	-10998,2796
3	1,84	1,25	1,3	0,001188	0,15151515	0,18	8,51111111	-11026,7906
3	1,84	1,25	1,6	0,001188	0,15151515	0,18	8,54722222	-11023,8214
2	1,84	1,25	0,5	0,001188	0,15151515	0,18	8,57222222	-11071,1797
2	0,9	1,5	0,5	0,002988	0,06024096	0,18	8,58888889	-6904,58534
2	0,9	1,5	1,3	0,002988	0,06024096	0,18	8,61111111	-6898,20074
2	0,9	1,5	1,6	0,002988	0,06024096	0,18	8,61944444	-6895,54209
4	1,84	0,7	0,5	0,002988	0,06024096	0,18	8,66388889	-7344,87647
2	1,84	1,25	1,3	0,001188	0,15151515	0,18	8,68055556	-11071,6085
2	1,84	1,25	1,6	0,001188	0,15151515	0,18	8,71388889	-11068,2429
4	1,4	1,25	0,5	0,002394	0,07518797	0,18	8,71388889	-8658,04044
4	1,4	1,25	1,3	0,002394	0,07518797	0,18	8,76388889	-8644,74857
4	1,4	1,25	1,6	0,002394	0,07518797	0,18	8,78055556	-8638,19515
3	1,4	1,25	0,5	0,002394	0,07518797	0,18	8,93055556	-8691,21662

3	1,4	1,25	1,3	0,002394	0,07518797	0,18	8,97777778	-8679,93997
3	1,4	1,25	1,6	0,002394	0,07518797	0,18	8,99444444	-8674,58473
4	0,9	1,5	0,5	0,002988	0,06024096	0,18	9,02222222	-7694,57105
2	1,4	1,25	0,5	0,002394	0,07518797	0,18	9,36666667	-8760,41284
2	1,4	1,25	1,3	0,002394	0,07518797	0,18	9,40833333	-8748,49103
2	1,4	1,25	1,6	0,002394	0,07518797	0,18	9,42222222	-8744,07388
4	1,84	1,5	0,5	0,001188	0,15151515	0,18	9,75	-13151,2103
3	1,84	1,5	0,5	0,001188	0,15151515	0,18	9,86111111	-13194,5724
4	1,84	1,5	1,3	0,001188	0,15151515	0,18	9,88611111	-13173,3027
4	1,84	1,5	1,6	0,001188	0,15151515	0,18	9,92777778	-13171,812
3	1,84	1,5	1,3	0,001188	0,15151515	0,18	9,98888889	-13206,0402
3	1,84	1,5	1,6	0,001188	0,15151515	0,18	10,0277778	-13203,1162
2	1,84	1,5	0,5	0,001188	0,15151515	0,18	10,075	-13259,6935
2	1,84	1,5	1,3	0,001188	0,15151515	0,18	10,1861111	-13260,0892
4	1,4	1,5	0,5	0,002394	0,07518797	0,18	10,2	-10375,4283
2	1,84	1,5	1,6	0,001188	0,15151515	0,18	10,2222222	-13256,28
4	1,4	1,5	1,3	0,002394	0,07518797	0,18	10,25	-10359,6977
4	1,4	1,5	1,6	0,002394	0,07518797	0,18	10,2666667	-10351,155
4	1,4	1,25	1,6	0,002988	0,06024096	0,18	10,3	-9370,36699
4	1,4	1,25	1,3	0,002988	0,06024096	0,18	10,325	-9403,21138
3	1,4	1,25	1,3	0,002988	0,06024096	0,18	10,3666667	-9138,62869
3	1,4	1,25	1,6	0,002988	0,06024096	0,18	10,3666667	-9123,94439
3	1,4	1,25	0,5	0,002988	0,06024096	0,18	10,4194444	-9220,31224
3	1,4	1,5	0,5	0,002394	0,07518797	0,18	10,4555556	-10415,0279
3	1,4	1,5	1,3	0,002394	0,07518797	0,18	10,5027778	-10401,5529
3	1,4	1,5	1,6	0,002394	0,07518797	0,18	10,5166667	-10395,6095
2	1,4	1,25	0,5	0,002988	0,06024096	0,18	10,7305556	-8932,14078
2	1,4	1,25	1,3	0,002988	0,06024096	0,18	10,7444444	-8923,39488
2	1,4	1,25	1,6	0,002988	0,06024096	0,18	10,75	-8919,67375
2	1,4	1,5	0,5	0,002394	0,07518797	0,18	10,9638889	-10497,961
2	1,4	1,5	1,3	0,002394	0,07518797	0,18	11,0027778	-10484,1584
2	1,4	1,5	1,6	0,002394	0,07518797	0,18	11,0166667	-10478,2959
4	1,84	1,25	0,5	0,002394	0,07518797	0,18	11,0361111	-11356,4427
4	1,84	1,25	1,3	0,002394	0,07518797	0,18	11,0833333	-11338,8645
4	1,84	1,25	1,6	0,002394	0,07518797	0,18	11,0972222	-11329,9206
4	1,4	1,25	0,5	0,002988	0,06024096	0,18	11,2805556	-9950,17668
3	1,84	1,25	0,5	0,002394	0,07518797	0,18	11,3111111	-11400,3951
3	1,84	1,25	1,3	0,002394	0,07518797	0,18	11,3555556	-11385,408
3	1,84	1,25	1,6	0,002394	0,07518797	0,18	11,3694444	-11378,8597
2	1,84	1,25	0,5	0,002394	0,07518797	0,18	11,8611111	-11490,8977
2	1,84	1,25	1,3	0,002394	0,07518797	0,18	11,8944444	-11475,0229
2	1,84	1,25	1,6	0,002394	0,07518797	0,18	11,9083333	-11469,1808
4	1,4	1,5	1,6	0,002988	0,06024096	0,18	12,0416667	-11228,386

4	1,4	1,5	1,3	0,002988	0,06024096	0,18	12,075	-11267,8209
3	1,4	1,5	1,6	0,002988	0,06024096	0,18	12,1138889	-10933,7838
3	1,4	1,5	1,3	0,002988	0,06024096	0,18	12,1166667	-10951,4469
3	1,4	1,5	0,5	0,002988	0,06024096	0,18	12,1861111	-11049,6876
2	1,4	1,5	0,5	0,002988	0,06024096	0,18	12,5416667	-10703,9369
2	1,4	1,5	1,3	0,002988	0,06024096	0,18	12,55	-10693,5219
2	1,4	1,5	1,6	0,002988	0,06024096	0,18	12,5527778	-10689,2042
4	1,84	1,5	0,5	0,002394	0,07518797	0,18	12,9222222	-13612,2248
4	1,84	1,5	1,3	0,002394	0,07518797	0,18	12,9638889	-13590,7128
4	1,84	1,5	1,6	0,002394	0,07518797	0,18	12,975	-13579,6697
4	1,84	1,25	1,6	0,002988	0,06024096	0,18	13,0194444	-12289,389
4	1,84	1,25	1,3	0,002988	0,06024096	0,18	13,0527778	-12332,2952
3	1,84	1,25	1,6	0,002988	0,06024096	0,18	13,0888889	-11967,0763
3	1,84	1,25	1,3	0,002988	0,06024096	0,18	13,0972222	-11986,5012
3	1,84	1,25	0,5	0,002988	0,06024096	0,18	13,1777778	-12094,2554
4	1,4	1,5	0,5	0,002988	0,06024096	0,18	13,2055556	-11922,3368
3	1,84	1,5	0,5	0,002394	0,07518797	0,18	13,2416667	-13665,1638
3	1,84	1,5	1,3	0,002394	0,07518797	0,18	13,2805556	-13647,0099
3	1,84	1,5	1,6	0,002394	0,07518797	0,18	13,2916667	-13638,7362
2	1,84	1,25	0,5	0,002988	0,06024096	0,18	13,5555556	-11715,5714
2	1,84	1,25	1,3	0,002988	0,06024096	0,18	13,5583333	-11704,2406
2	1,84	1,25	1,6	0,002988	0,06024096	0,18	13,5611111	-11699,4572
2	1,84	1,5	0,5	0,002394	0,07518797	0,18	13,8805556	-13773,1141
2	1,84	1,5	1,3	0,002394	0,07518797	0,18	13,9083333	-13753,747
2	1,84	1,5	1,6	0,002394	0,07518797	0,18	13,9194444	-13746,3786
4	1,84	1,25	0,5	0,002988	0,06024096	0,18	14,2861111	-13048,4652
4	1,84	1,5	1,6	0,002988	0,06024096	0,18	15,2138889	-14726,7405
4	1,84	1,5	1,3	0,002988	0,06024096	0,18	15,2583333	-14778,2241
3	1,84	1,5	1,6	0,002988	0,06024096	0,18	15,2888889	-14341,4416
3	1,84	1,5	1,3	0,002988	0,06024096	0,18	15,3	-14364,7637
3	1,84	1,5	0,5	0,002988	0,06024096	0,18	15,4083333	-14494,2783
2	1,84	1,5	1,3	0,002988	0,06024096	0,18	15,825	-14025,1578
2	1,84	1,5	1,6	0,002988	0,06024096	0,18	15,8277778	-14019,0778
2	1,84	1,5	0,5	0,002988	0,06024096	0,18	15,8333333	-14039,118
4	1,84	1,5	0,5	0,002988	0,06024096	0,18	16,7166667	-15635,2295